

New OFDM Schemes Based on Orthogonal Transforms for Mobile Communications Systems



Hussein Abdullah Leftah Al-Sodani

School of Electrical and Electronic Engineering

Newcastle University, Newcastle upon Tyne, UK.

A thesis submitted for the degree of

Doctor of Philosophy

May 2013

Declaration

I declare that this thesis is my own work and it has not been previously submitted, either by me or by anyone else, for a degree or diploma at any educational institute, school or university. To the best of my knowledge, this thesis does not contain any previously published work, except where another person's work used has been cited and included in the list of references.

Hussein Abdullah Leftah Al-Sodani

To my loving parents, my Father and my Mother

To whom I respect and love.

With all my love

The more original the discovery, the more obvious it seems afterward.

-Arthur Koestler

*I wish I could be more moderate in my desires. But I can't, so there is
no rest.*

-John Muir, 1826

*Sure I am that this day we are masters of our fate that the task which
has been set before us is not above our strength; that its pangs and toils
are not beyond my endurance. As long as we have faith in our own
cause and an unconquerable will to win, victory will not be denied us.*

-Winston Churchill

Acknowledgements

In the name of Allah, the Beneficent, the Merciful

After almost four years of work in cold and warm, long and short days, by the GOD well, this research project has been completed. Firstly, Praise and Gratitude be to Allah for his mercy that he surrounded me with, for giving me the strength and health during the days of study, so that this dissertation can be finished accordingly. Secondly, I wish to express my gratitude to my supervisor, Professor Said Boussakta, for his continuous advice, support and encouragement throughout this research. It is a pleasure to thank our lovely school receptionist, Deborah Alexander, and postgraduate research coordinator, Mrs Gill Webber for their assistant in numerous ways.

I would like to offer my deepest regards and blessing to all those who supported me in any respect during the completion of this project; I would also like to thank my parents, Mum and Dad for their encouragement, as without their enthusiasm and patient the journey would have been much more difficult. I would also like to thank all the PhD students in the school that their friendship and company made life enjoyable at the university. Also, to my friends in the UK and Iraq, I thank you all for the companionship that made this journey much easier.

I would also like to thank my sponsor, the Ministry of Higher Education and Scientific Research (MOHSR), Iraq and to the Iraqi cultural attach-London for supporting me financially during my study in England.

Abstract

In this thesis, two new orthogonal frequency division multiplexing (OFDM) systems are presented. The first scheme proposes a new OFDM system transceiver based on the C-transform, which is termed C-OFDM. Over multipath channels, the C-OFDM achieves 10 dB signal-to-noise ratio (SNR) gain at 10^{-4} bit-error-rate (BER), in comparison to the OFDM that based on the discrete cosine transform (DCT-OFDM) and the conventional OFDM schemes. It also reduces the peak-to-average power ratio (PAPR) of the OFDM signal by about 1 dB and in some cases up to 3 dB. In the second scheme, a new fast, orthogonal \mathbf{X} -transform is produced. The proposed \mathbf{X} -transform is then used in a new OFDM named X-OFDM to greatly reduce the complexity, the PAPR and the BER. The proposed scheme achieves around 15 dB SNR gain in comparison to the conventional OFDM at 10^{-4} BER and reduces the average PAPR (over 10^5 OFDM symbol) by about 6 dB for $N = 1024$ subcarriers. Furthermore, in this study, the \mathbf{X} -transform is utilized to produce a new Alamouti space-time OFDM (ST-OFDM). The proposed ST-X-OFDM scheme reduces the transmitter complexity and achieves important SNR gain over the conventional ST-OFDM systems. The BER performance of the proposed schemes in the presence of solid-state power amplifiers (SSPAs) is also investigated analytically and by simulation. It shows that the X-OFDM is resilient to the SSPAs nonlinear distortion whereas the C-OFDM may lead to BER impairment in the presence of the SSPA. Furthermore, a coding technique to mitigate the sensitivity of the C-OFDM scheme to the SSPA is also proposed in this study.

In this research, mathematical models for the proposed C-OFDM, X-OFDM and ST-X-OFDM, which tightly match the simulation results over a diverse range of transmission scenarios and mapping schemes,

are also derived. In addition, the BER performance of the proposed C-OFDM and X-OFDM schemes in the presence of the carrier frequency offset (CFO), with and without frequency synchronization algorithm, are also investigated. The proposed C-OFDM and X-OFDM schemes are more sensitive to the CFO than the conventional schemes. However, when frequency synchronization algorithm is used, both the proposed schemes retain their significant BER improvement in comparison to the conventional schemes.

Contents

Nomenclature	xix
List of Symbols	xxii
1 Introduction	1
1.1 Literature Review	1
1.2 Multicarrier Modulation (MCM)	2
1.3 OFDM Scheme	3
1.4 Drawbacks of OFDM Systems	5
1.5 Related works	6
1.5.1 DCT-OFDM System	6
1.5.2 Unitary precoded DFT-OFDM System	7
1.5.3 Alamouti ST-OFDM	8
1.5.4 PAPR Reduction of the UP-OFDM	9
1.6 Aim of the Thesis	10
1.7 Contributions of the Thesis	11
1.7.1 C-OFDM Systems	11
1.7.2 X-OFDM Systems	11
1.7.3 Alamouti ST-X-OFDM System	12
1.7.4 PAPR of Unitary Precoded OFDM system	12
1.8 Thesis Outline	12
1.9 List of Publications and Awards	14
2 Orthogonal Frequency Division Multiplexing: Fundamentals	15
2.1 Introduction to the OFDM Systems	15
2.2 Multipath Propagation	17
2.3 The OFDM system model and Definitions	19

2.3.1	Digital Mapper/De-mapper	19
2.3.2	IFFT/FFT Transforms	21
2.3.3	Guard Interval	24
2.3.3.1	Cyclic Extension of OFDM Symbols	24
2.3.3.2	Zero-Padding of OFDM Symbols	27
2.4	DCT-OFDM system model	29
2.5	Theoretical BER of the OFDM	29
2.5.1	Zero Forcing (ZF) Equalizer	30
2.5.2	Minimum Mean-Square-Error (MMSE) Equalizer	31
2.6	Up/Down Converters	33
2.7	Peak-to-average power ratio (PAPR)	34
2.8	Sensitivity to the Carrier Frequency Offset (CFO)	35
2.9	Conclusion	38
3	Novel Efficient OFDM Systems Based on Trigonometric Trans-	
	forms	40
3.1	Introduction	40
3.2	WHT-Precoded DCT-OFDM system	41
3.3	C Transform Based OFDM System	44
3.4	Transmission Analysis	48
3.5	Peak-to-average power ratio (PAPR)	54
3.6	System Performance in the Presence of the CFO	56
3.7	Computational Complexity Analysis	56
3.7.1	The C -Transform	57
3.7.2	Discrete Cosine Transform (DCT)	60
3.7.3	WHT-DCT	60
3.7.4	Fast Fourier Transform (FFT)	61
3.8	Wire-line Applications of the Proposed Schemes	62
3.9	Simulation Results And Discussion	63
3.9.1	PAPR Reduction	64
3.9.2	BER Performance	65
3.9.2.1	BER performance over AWGN Channel	65
3.9.2.2	BER Performance over Wireless Multipath Channel	65
3.9.2.3	BER Performance In the Presence of the CFO	67

3.9.3	BER Performance over wire-line channel	69
3.10	Conclusion	71
4	Efficient OFDM System Based on New X-Transform for PAPR Reduction and Diversity Enhancement	73
4.1	Introduction	73
4.2	X-Transform and X-OFDM System	75
4.3	Theoretical Analysis of the BER Performance Over Multipath Channels	78
4.3.1	Zero-Forcing Equalizer	80
4.3.2	Minimum Mean-Square-Error Equalizer	82
4.4	X-OFDM with Zero-Padding (ZP)	85
4.5	Complexity Analysis and Comparison	88
4.5.1	The X Transform	88
4.5.2	Fast Fourier Transform (FFT)	89
4.5.3	Fast Hartley-Fourier Transform (FHT-FFT)	89
4.5.4	Transmitter Complexities	90
4.5.5	Receiver Complexities	91
4.5.6	Complexity of X-OFDM versus C-OFDM	91
4.5.7	Complexity of X-OFDM Versus SC-FDE	92
4.6	CFO Effects on BER Performance Over Multipath Channels	92
4.7	Simulation results and discussions	94
4.7.1	PAPR of the Proposed Scheme	94
4.7.2	BER Performance	97
4.7.2.1	Over Multipath Channels	97
4.7.2.2	In the Presence of CFO	98
4.7.2.3	Coded and Coded-Interleaved Systems	101
4.8	Conclusion	101
5	Low Complexity X-OFDM System for STBC Diversity Enhancement Over Frequency-Selective Fading Channels	105
5.1	Introduction	105
5.2	Proposed System	106
5.3	Reducing Transmitter Complexity	108
5.4	Two Transmit Antennas and One Receive Antenna (2×1)	109

5.4.1	Zero-Forcing (ZF) Equalizer	112
5.4.2	Minimum Mean-Square-Error (MMSE) Equalizer	115
5.5	Two Transmit and Two Receive Antennas (2×2)	118
5.6	Complexity analysis	121
5.6.1	\mathbf{X} Transform	121
5.6.2	ST-OFDM	122
5.6.3	UP-ST-OFDM	122
5.6.3.1	WHT precoder	122
5.6.3.2	DHT precoder	122
5.7	Simulation results and discussions	123
5.7.1	BER Performance Over Multipath Channels	124
5.8	Conclusion	125
6	BER Performance of Unitary Precoded OFDM Systems in the Presence of SSPA	130
6.1	Introduction	130
6.2	PAPR of the C-OFDM System	131
6.3	PAPR of Unitary precoded OFDM Systems	132
6.4	SSPA Model	133
6.5	Transmission performance of the C-OFDM in the presence of the SSPA	135
6.6	Results and Discussions of the C-OFDM System	137
6.6.1	Over AWGN Channel	138
6.6.2	Over Multipath Channels	138
6.7	Coded C-OFDM System in the Presence of the SSPA	140
6.8	Performance Analysis of the UP-OFDM in the Presence of the SSPA	145
6.9	Results and Discussions	148
6.9.1	Over AWGN Channel	148
6.9.2	Over Multipath Channels	149
6.9.3	Coded UP-OFDM over the Multipath Channel	151
6.10	Conclusion	156
7	Conclusion and Future Work	157
7.1	Conclusion	157
7.2	Future Work	159

A Submitted Paper to IEEE Transactions on Communications [84]	161
References	188

List of Figures

1.1	Evolution of the OFDM system.	4
2.1	Multipath phenomena in wireless channels	17
2.2	Tapped delay line	18
2.3	Frequency-time variations of the ITU channel (a: Pedestrian B and b: Vehicular A).	20
2.4	Block diagram of discrete baseband model of OFDM system.	21
2.5	Orthogonal basis of the OFDM symbol	23
2.6	Cyclic prefix extension.	25
2.7	Zero-Padding guard interval.	28
2.8	DCT-OFDM system block diagram.	29
2.9	BER performance of the conventional OFDM system for the QPSK and the 16-QAM constellations over the ITU pedestrian B channel in comparison to the performance over the AWGN channel; theoretically and by simulation.	33
2.10	PAPR performance of the conventional OFDM for $N = 128, 256, 512$ and 1024, using (a: 16-QAM modulation and b: QPSK modulation).	36
2.11	PAPR performance of the DCT-OFDM for $N = 128, 256, 512$ and 1024, using (a: 16-QAM modulation and b: QPSK modulation).	37
2.12	BER performance of the conventional OFDM system in the presence of the CFO.	39
3.1	Proposed WHT-DCT-OFDM system block diagram.	42
3.2	Power spectral densities of the DFT, the DCT and the WHT-IDCT OFDM systems.	43
3.3	C-OFDM system block diagram when complex signalling format is used.	45

3.4	System block diagram in the presence of the CFO cancellation algorithm.	57
3.5	Butterfly structure of BDS transforms.	58
3.6	Butterflies of the C -transform:(a) C-transform butterfly, (b) Modified C -transform butterfly.	58
3.7	Transmitter block diagram of the DFT-DMT system.	63
3.8	Transmitter block diagram of the C-DMT system.	63
3.9	PAPR performance of the proposed C-OFDM, DCT-OFDM and the conventional DFT-OFDM systems using the 16-QAM modulation format, the DCT-OFDM and DFT-OFDM systems having the same graphs.	64
3.10	BER of the proposed C-OFDM , DCT-OFDM and DFT-OFDM systems over AWGN channel. All have the same graphs.	66
3.11	BER performance of the proposed C-OFDM, DCT-OFDM and DFT-OFDM systems over the ITU Pedestrian B channel and for the QPSK modulation, theory and simulation are in good agreement.	67
3.12	BER performance of the proposed C-OFDM, DCT-OFDM and DFT-OFDM systems over the ITU Pedestrian B channel and for the 16-QAM modulation, theory and simulation are in good agreement.	68
3.13	BER performance of the proposed C-OFDM, DCT-OFDM and DFT-OFDM systems over the ITU Vehicular A channel and for the QPSK modulation, theory and simulation are in good agreement.	68
3.14	BER performance of the proposed C-OFDM, DCT-OFDM and DFT-OFDM systems over ITU Vehicular A channel and for the 16-QAM modulation, theory and simulation are in good agreement.	69
3.15	BER performance for the proposed C-OFDM, DCT-OFDM and the DFT-OFDM systems over the ITU vehicular class A channel and CFO=0.03, 0.06 and 0.1 and 16-QAM modulation format.	70
3.16	BER performance for the proposed C-OFDM, DCT-OFDM and the DFT-OFDM systems over the ITU vehicular class A channel and CFO=2.628 when the QPSK and the 16-QAM modulation formats are used.	70

3.17 BER performance for the proposed C-DMT, DCT-DMT and DFT-DMT systems for the BPSK modulation formats; simulation and theory results are in marvellous agreement.	71
4.1 Schematic diagram of the proposed \mathbf{X} -transform.	75
4.2 Proposed X-OFDM system block diagram.	79
4.3 Block diagram of the X-OFDM scheme with ZP	85
4.4 Basic unit of \mathbf{X} transform.	89
4.5 Power in OFDM signal (a) the conventional system and (b) the proposed system.	95
4.6 PAPR performance of the proposed X-OFDM, SC-FDE, WHT-OFDM and the conventional OFDM systems, using 16-QAM modulation and $N = 1024$	96
4.7 BER performance of the proposed X-OFDM, OFDM and SC-FDE systems for QPSK and 16-QAM modulations over ITU pedestrian B channel and MMSE detection.	98
4.8 BER performance of the proposed X-OFDM, OFDM and SC-FDE systems for QPSK and 16-QAM modulations over ITU vehicular A channel and MMSE detection.	99
4.9 BER performance of the proposed X-OFDM, SC-FDE and the OFDM systems for QPSK and 16-QAM modulations over ITU pedestrian B channel and ZF detection.	99
4.10 BER performance of the proposed X-OFDM, SC-FDE and the OFDM systems for QPSK and 16-QAM modulations over ITU vehicular A channel and ZF detection.	100
4.11 BER performance for the proposed X-OFDM and the OFDM systems over ITU pedestrian class B channel and CFO=0.02, 0.035 and 0.05 and 16-QAM modulation.	101
4.12 BER performance for the proposed X-OFDM and the OFDM systems over ITU pedestrian class B channel and CFO=0.01, 0.015 and 0.02 and 64-QAM modulation.	102

4.13 BER performance for the proposed X-OFDM, DFT-OFDM and SC-OFDM systems over ITU pedestrian class B channel and CFO=3.42 when 16-QAM modulation format and *M&M* synchronization algorithm are employed. 102

4.14 BER performance of coded proposed X-OFDM and coded OFDM systems for QPSK and 16-QAM modulations over ITU pedestrian B channel. 103

4.15 BER performance of coded proposed X-OFDM and coded OFDM systems for QPSK and 16-QAM modulations over ITU vehicular A channel. 103

4.16 BER performance of coded-interleaved X-OFDM, coded-interleaved SC-FDE and coded-interleaved OFDM systems versus uncoded systems for 16-QAM modulation over ITU vehicular A channel. 104

5.1 Proposed Alamouti ST-X-OFDM system block diagram. 106

5.2 Two transmit antennas and two receive antennas. 118

5.3 BER performance of the proposed ST-X-OFDM and the conventional ST-OFDM systems over pedestrian B channel model, MMSE detection and 16-QAM modulation format. 125

5.4 BER performance of the proposed ST-X-OFDM and the conventional ST-OFDM over pedestrian B channel model, MMSE detection and QPSK modulation format. 126

5.5 BER performance of the proposed ST-X-OFDM and the conventional ST-OFDM systems over vehicular A channel model, MMSE detection and the 16-QAM modulation. 126

5.6 BER performance of the proposed ST-X-OFDM and the conventional ST-OFDM systems over vehicular A channel model, MMSE detection and the QPSK modulation. 127

5.7 BER performance of the proposed ST-X-OFDM and the conventional ST-OFDM systems over pedestrian B channel model, ZF detection and the 16-QAM modulation. 127

5.8 BER performance of the proposed ST-X-OFDM and the conventional ST-OFDM systems over pedestrian B channel model, ZF detection and the QPSK modulation. 128

5.9	BER performance of the proposed ST-X-OFDM and the conventional ST-OFDM systems over vehicular A channel model, ZF detection and the 16-QAM modulation.	128
5.10	BER performance of the proposed ST-X-OFDM and the conventional ST-OFDM systems over vehicular A channel model, ZF detection and the QPSK modulation.	129
6.1	PAPR performance of the conventional OFDM and UP-OFDM systems with precoder matrix WHT, DCT, DHT (X-OFDM) and the DFT (SC-FDE), using the 16-QAM modulation and $N = 1024$	133
6.2	Nonlinear characteristics of the SSPA	134
6.3	Effect of the IBO on the spectrum of the OFDM signal using the SSPA with $N=1024$	135
6.4	BER performance of the C-OFDM, DCT-OFDM and the conventional OFDM systems of the QPSK and 16-QAM modulations with the SSPA of (IBO=7dB) over the AWGN channel.	139
6.5	BER performance of the C-OFDM, DCT-OFDM and the conventional OFDM systems of the QPSK and 16-QAM modulations with the SSPA of (IBO=5dB) over the AWGN channel.	139
6.6	BER performance of the C-OFDM, DCT-OFDM and the conventional OFDM systems of the QPSK and 16-QAM modulations with the SSPA of (IBO=3dB) over the AWGN channel.	140
6.7	BER performance of the C-OFDM, DCT-OFDM, and DFT-OFDM of the 16-QAM and the QPSK modulations with SSPA of IBO=7 dB over the ITU channel (a: pedestrian B and b: vehicular A).	141
6.8	BER performance of the C-OFDM, DCT-OFDM, and DFT-OFDM of the 16-QAM and the QPSK modulations with SSPA of IBO=5 dB over the ITU channel (a: pedestrian B and b: vehicular A).	142
6.9	BER performance of the C-OFDM, DCT-OFDM, and DFT-OFDM of the 16-QAM and the QPSK modulations with SSPA of IBO=3 dB over the ITU channel (a: pedestrian B and b: vehicular A).	143

6.10 BER performances of uncoded/coded proposed C-OFDM, DCT-OFDM and DFT-OFDM systems in the presence of SSPA over ITU class A vehicular channel for 16-QAM modulation formats (a: IBO=5 dB and b: IBO=3 dB). 144

6.11 BER performance of the DFT (SC-FDE), DHT (X-OFDM), DCT, WHT precoded OFDM and the conventional OFDM for the 16-QAM modulation with the SSPA (IBO=7 dB) over the AWGN channel. . . 149

6.12 BER performance of the DFT (SC-FDE), DHT (X-OFDM), DCT, WHT precoded OFDM and the conventional OFDM for the 16-QAM modulation with the SSPA (IBO=5 dB) over the AWGN channel. . . 150

6.13 BER performance of the DFT (SC-FDE), DHT (X-OFDM), DCT, WHT precoded OFDM and the conventional OFDM for the 16-QAM modulation with the SSPA (IBO=3 dB) over the AWGN channel. . . 150

6.14 BER performance of the DFT (SC-FDE), DHT (X-OFDM), DCT, WHT precoded OFDM and the conventional OFDM for the 16-QAM modulation with the SSPA of IBO=7 dB over the ITU channel (a: Pedestrian B and b: Vehicular A). 152

6.15 BER performance of the DFT (SC-FDE), DHT (X-OFDM), DCT, WHT precoded OFDM and the conventional OFDM for the 16-QAM modulation with the SSPA of IBO=5 dB over the ITU channel (a: Pedestrian B and b: Vehicular A). 153

6.16 BER performance of the DFT (SC-FDE), DHT (X-OFDM), DCT, WHT precoded OFDM and the conventional OFDM for the 16-QAM modulation with the SSPA of IBO=3 dB over the ITU channel (a: Pedestrian B and b: Vehicular A). 154

6.17 BER performances of the coded DFT (SC-FDE), DHT (X-OFDM), DCT, WHT precoded OFDM and the conventional OFDM for the 16-QAM modulation with the SSPA over the ITU class A vehicular channel for the 16-QAM modulation (a: IBO=5 dB and b: IBO=3 dB). 155

List of Tables

2.1	System parameters for simulations.	32
3.1	Comparison of Real Arithmetic Operations for the Proposed C Transform, DCT, WHT-DCT and FFT Transforms Under Complex Constellation Consideration.	61
3.2	Total number of real operations.	62
3.3	Comparison of real arithmetic operations of the proposed CT, the DCT and the FFT based-DMT systems.	63
3.4	System parameters for simulations.	65
4.1	Comparison based on real arithmetic operations of transmitter of the proposed X-OFDM and the conventional OFDM based on single butterfly implementation.	90
4.2	Comparison based on real arithmetic operations of the receiver of the proposed X-OFDM and the conventional OFDM systems based on single butterfly implementation.	91
4.3	System parameters for simulations.	96
5.1	Comparison based on real arithmetic operations of the X-transform and other transforms that used in the ST-OFDM.	123
5.2	System parameters for simulations.	123

Nomenclature

Acronyms

ADSL	Asynchronous Digital Subcarrier Loop
AM/AM	Amplitude Modulation/Amplitude Modulation
AM/PM	Amplitude Modulation/Phase Modulation
AWGN	Additive White Gaussian Noise
BDS	Block Diagonal Structure
BER	Bit Error Rate
BPSK	Binary Phase Shift Keying
BRO	Bit Reverse Order
BW	Bandwidth
CA	Complex Addition
CCDF	Cumulative Distribution Function
CFO	Carrier Frequency Offset
CIR	Channel Impulse Response
CM	Complex Multiplication
CP	Cyclic Prefix
CSI	Channel State Information
CT	C Transform

DCT	Discrete Cosine Transform
DFT	Discrete Fourier Transform
DHT	Discrete Hartley Transform
DMT	Discrete Multi-tone
FEC	Forward Error Correction
FFT	Fast Fourier Transform
FHT	Fast Hartley Transform
GRO	Gray Reverse Order
HPA	High Power Amplifier
IBI	Inter-Block Interference
IBO	Input Back-Off
ICI	Inter-Carrier Interference
IDCT	Inverse DCT
IDFT	Inverse DFT
IFFT	Inverse FFT
ISI	Intersymbol Interference
ITU	International Telecommunication Union
IXT	Inverse X Transform
MCM	Multicarrier Modulation
MIMO	Multiple Input Multiple Output
MMSE	Minimum Mean-square-error
OFDM	Orthogonal Frequency Division Multiplexing
P/S	Parallel-to-Serial

PAM	Pulse Amplitude Modulation
PAPR	Peak to Average Power Ratio
PSD	Power Spectrum Density
QAM	Quadrature Amplitude Modulation
QPSK	Quadrature Phase Shift Keying
RA	Real Addition
RM	Real Multiplaiication
RO	Real Operation
S/P	Serial-to-Parallel
SNR	Signal-to-Noise Ratio
SSPA	Solid State Power Amplifier
SVD	Singular Value Decomposition
UP-OFDM	Unitary Precoded OFDM
US	Uncorrelated Scattering
WiMAX	Worldwide Interoperability for Microwave Access
XT	X Transform
ZF	Zero Forcing

List of Symbols

N	Number of subcarriers
Δf	Frequency spacing between subcarriers of OFDM signal
\mathbf{d}	Signal constellations sequence
S_n	Information symbol of \mathbf{d}
\mathbf{S}	Data symbol vector of \mathbf{d}
\hat{S}_n	Detected data symbol vector
$\hat{\mathbf{S}}$	Detected information symbol
M	Modulation order
\mathbf{B}	Binary data matrix
$\hat{\mathbf{B}}$	Estimated binary data
k	Index on transmitted symbols
n	Index on input symbols
s_k	OFDM samples of \mathbf{S}
\mathbf{s}	OFDM symbol vector
y_k	The k_{th} sample of the received signal
\mathbf{y}	Received OFDM symbol vector
u_k	The OFDM samples of \mathbf{s} after adding the guard interval
\mathbf{u}	OFDM symbol after adding the guard interval
r_k	Frequency-domain samples of \mathbf{r}
\mathbf{r}	Frequency-domain samples of \mathbf{r}
\mathbf{q}	The received signal vector before channel equalization
q_n	The n_{th} sample of the vector \mathbf{q}
q_n^{MMSE}	The n_{th} sample of the vector \mathbf{q} in the case of the MMSE equalizer
q_n^{ZF}	The n_{th} sample of the vector \mathbf{q} in the case of the ZF equalizer
τ_m	Maximum channel delay
τ_p	Delay time of the signal which passes through the path p

$\delta(x)$	Chronicle delta
$(.)^T$	Transpose operation
$(.)^{-1}$	Inverse matrix
$(.)^{\mathbb{H}}$	Hermitian transpose matrix
$(.)^*$	Conjugate
$L + 1$	Number of taps in multipath channel
$ \cdot $	Absolute value of a complex variable
$\mathbf{F}^{\mathbb{H}}$	Normalised $N \times N$ IFFT matrix
\mathbf{F}	Normalised $N \times N$ FFT matrix
$j^2 = -1$	Imaginary unit
$\log_2(x)$	Logarithm x for the base 2
BW	Transmission bandwidth
N_g	Guard interval length
N_t	Total OFDM signal's length $N_t = N + N_g$
T_s	Time duration of the useful part of the OFDM symbol
T_g	Time duration of the guard interval
T	Time duration of the transmitted OFDM symbol ($T = T_s + T_g$)
f_s	Sampling frequency
e^x	Exponential operation
\otimes	Convolution operation
P_e^{M-PSK}	BER of the PSK modulation of order M
P_e^{M-QAM}	BER of the QAM modulation of order M
P_e^{QPSK}	BER of the QOSK modulation
P_e^{16-QAM}	BER of the 16-QAM modulation
$Q(x)$	The Q-function
m_b	Number of bits per each data symbol ($m_b = \log_2 M$)
μ	The number of nearest neighbours signal points
μ_{QPSK}	The number of nearest neighbours signal points in the QPSK modulation $\mu_{QPSK} = 2$
μ_{16-QAM}	The number of nearest neighbours signal points in the 16-QAM modulation $\mu_{QPSK} = 3$
β_m	The SNR at the receiver
β_i^{ZF}	The SNR at the i_{th} sunchannel in the case of ZF equalizer
β_i^{MMSE}	The SNR at the i_{th} sunchannel in the case of MMSE equalizer

χ_n	The MMSE equalizer
γ_b	SNR per bit for each subcarrier
γ_s	SNR per symbol
e_n^{ZF}	Error signal in the case of ZF equalizer
e_n^{MMSE}	Error signal in the case of MMSE equalizer
\mathcal{P}_n^{ZF}	Noise power at the receiver in the case of ZF equalizer
\mathcal{P}_n^{MMSE}	Noise power at the receiver in the case of MMSE equalizer
\mathcal{P}_s^{MMSE}	Signal power at the receiver in the case of MMSE equalizer
Υ	Diagonal CFO matrix
$\bar{\mathbf{H}}$	A diagonal matrix, its diagonal elements are the frequency domain representation of the channel impulse response
Π	The ICI matrix
Ψ_{cp}^T	Expression to add the CP sequence
Ψ_{cp}^R	Expression to discard the CP sequence
Ψ_{zp}^T	Expression to add the ZP sequence
Ψ_{zp}^R	Expression to discard the CP sequence
H_n	Frequency response of the channel impulse response $H_n = \sum_{l=0}^{L-1} h_l e^{-j\frac{2\pi nl}{N}}$
\mathbf{H}_{Cir}	Channel circulant matrix
\mathbf{H}	Channel tall matrix
$b \leq a$	b less than or equal a
\neq	Not equal
\mathbf{v}	The AWGN noise vector
v_k	Noise k_{th} samples of \mathbf{v}
Ω	The FFT of the AWGN
Ω_n	the n_{th} sample of Ω
σ_v^2	Noise variance
ξ_n	The amplified noise part ($\xi_n = \frac{\Omega_n}{H_n}$)
$\hat{\xi}_i$	DHT transformation of ξ_n
$E\{\cdot\}$	Expected value
$A(\cdot)$	AM/AM conversion of the nonlinear amplifier
$\phi(\cdot)$	AM/PM conversion of the nonlinear amplifier
P_{max}	Maximum (saturation) power of the amplifier
P_{av}	Average power of the amplifier

A_s	is the amplifier input saturation voltage
\wp	is a parameter which controls the transition smoothness from linear region to saturation region
η	is the amplifier attenuation on the useful part
$\bar{\mathbf{v}}$	is the distortion part of the output signal
$\hat{\mathbf{u}}$	The amplified replica of \mathbf{u}
R_b	Data rate
c	Speed of light
f_c	Carrier frequency
λ	Wavelength of the signal
$\text{Re}\{\cdot\}$	Real part of a complex variable
$\text{Im}\{\cdot\}$	Imaginary part of a complex variable
\simeq	approximately equal
\mathbf{H}_0	Channel convolutional Toeplitz matrix
$\mathbf{\Lambda}$	A diagonal matrix, its diagonal elements are the square roots of the eigenvalues of $\mathbf{H}_0^{\text{H}}\mathbf{H}_0$
\mathbf{V}	A matrix its columns are the eigenvectors of $\mathbf{H}_0^{\text{H}}\mathbf{H}_0$
\mathbf{U}	A matrix its columns are the eigenvectors of $\mathbf{H}_0\mathbf{H}_0^{\text{H}}$
λ_i	Is the i_{th} element of the diagonal of $\mathbf{\Lambda}$
$\mathbf{\Delta}$	Matrices combination, $\mathbf{X}\Psi_{zp}^T\mathbf{V}$
$\bar{\mathbf{\Delta}}$	Matrices combination $\mathbf{V}^{\text{H}}\Psi_{zp}\mathbf{X}^{\text{H}}$
tr	Trace operation
\mathbf{I}_N	Identity matrix on dimension N
$\mathbf{\Theta}_1$	$\mathbf{\Theta}_1 = \left[\mathbf{\Lambda}^{\text{H}} \left(\mathbf{\Lambda}\mathbf{\Lambda}^{\text{H}} + \frac{1}{\gamma_s}\mathbf{I}_{N_t} \right)^{-1} \mathbf{\Lambda} \right]$
$\mathbf{\Theta}_2$	$\mathbf{\Theta}_2 = \left[\mathbf{\Lambda}^{\text{H}} \left(\mathbf{\Lambda}\mathbf{\Lambda}^{\text{H}} + \frac{1}{\gamma_s}\mathbf{I}_{N_t} \right)^{-1} \mathbf{\Lambda} - \mathbf{I}_{N_t} \right]$
$\mathbf{\Theta}_3$	$\mathbf{\Theta}_3 = \mathbf{\Lambda}^{\text{H}} \left(\mathbf{\Lambda}\mathbf{\Lambda}^{\text{H}} + \frac{1}{\gamma_s}\mathbf{I}_{N_t} \right)^{-1}$
$\mathbf{\Theta}_{4i}$	$\mathbf{\Theta}_{4i} = \text{diag}\left(\frac{1}{\gamma_s \lambda_i ^2+1}\right)$
R_A	Number of real additions
R_M	Number of real multiplications
C_A	Number of complex additions
C_M	Number of complex multiplications
R_O	Total number of real operations
E_b/N_0	Energy per bit-to-noise ratio

\mathbf{R}_S	Covariance matrix
$h_l^{(m,n)}$	channel impulse response between the m_{th} transmit antenna and n_{th} receive antenna
$\mathbf{h}^{(m,n)}$	diagonal matrix of FFT of $h_l^{(m,n)}$
Σ	$\Sigma_n = H_n^{(1)} ^2 + H_n^{(2)} ^2$
Σ'_n	$\Sigma'_n = H_n^{(1,1)} ^2 + H_n^{(2,1)} ^2 + H_n^{(1,2)} ^2 + H_n^{(2,2)} ^2$
\tilde{h}	Channel impulse response
\mathbf{W}	WHT matrix
\mathbf{D}	DCT matrix
\mathbf{A}	DHT matrix
\odot	point-by-point product
\otimes	The Kronecker product
$\mathbf{\Gamma}$	Gray reverse order matrix
$\mathbf{\Phi}$	Bit reverse order matrix
$\hat{\mathbf{D}}$	Matrices combination ($\hat{\mathbf{D}} = \mathbf{\Gamma}\mathbf{D}^T\mathbf{\Phi}$)
\hat{D}_{kn}	k_{th}, n_{th} element of $\hat{\mathbf{D}}$
\mathbf{G}^{ZF}	ZF equalizer matrix
\mathbf{G}^{MMSE}	MMSE equalizer matrix
E_s	Symbol energy
ϵ	CFO normalized to the subcarriers spacing
$\hat{\epsilon}$	estimated ϵ

Chapter 1

Introduction

1.1 Literature Review

Communications, in general, whether wireless, wire-line, analogue or digital, refer to accessing information reliably to the receiver side. Wireless communications ensure connectivity without the need for fixed wire-line cable connection which enable data to be reached anywhere and at any time. The first wireless transmission was demonstrated in December 1902 when Guglielmo Marconi sent a signal across the Atlantic from North America. Since that time, wireless communications, either analogue or digital, have continued to develop rapidly as the demand for high data rate increases.

In digital communications, the input information symbols, which are drawn from specific digital modulator, are mapped into waveforms for transmission. At the receiver side the received signal is mapped back into digital symbols, the link between the transmitted and the received signals being termed the communication channel. Different types of wireless communication channel provide different kinds of distortion and noise. Over ideal channels scenario, the transmitted and the received signals are in perfect match. Such ideal channels, however, do not exist in reality where the signal is scattered, diffracted and deflected before reaching the receiver. Thus, the received signal is considered to be a superposition of many incoherent signals that belong to the same original one but with different time delay. The channel is also characterized by its bandwidth which is defined as a measure of the width of a range of frequencies that can pass through the corresponding channel.

As any communication system where a channel causes a performance-limited

impairment, the modulation technique must be chosen carefully to cope with the channel-made distortions and to handle the interference successfully. Intersymbol interference (ISI) is considered one of the major obstacles to the design of a reliable modulation scheme that is convenient for high data rate transmission. In conventional single carrier systems, this interference is mitigated by equalizers. As higher the data rate is, the more complex the equalizers are, where the symbol time becomes smaller and the equalizer needs more taps to handle the delay spread of the channel. This problem is especially considerable when the channel spreads relative to the symbol time are significantly large.

To efficiently use the available bandwidth, a frequency division multiplexing (FDM) technique was adopted. In this technique, relatively low data rate signals can be transmitted over wide bandwidth channel using a detached carrier frequency for each signal. To avoid the overlap between adjacent signals, the carrier frequencies should be separated far apart by sufficiently empty spectral regions. This also facilitates the detection process of each signal at the receiver side. However, these empty spectral regions are still considered as wasted regions as no active signals are carried on these frequency intervals.

To overcome such problems of the ISI and empty spectral region, the pioneer was orthogonal frequency division multiplexing (OFDM) technique which was first proposed in 1966 by Chang [1]. It is a transmission technique that uses multicarrier (MC) technology where the data symbols are distributed over several subcarrier frequencies with overlapped spectra and transfers the impulse response of the frequency selective multipath channel into parallel decoupled flat fading subchannels, each corresponding to the specific subcarrier. Despite the overlapping spectra of the OFDM subcarriers, the data symbols can be recovered without any interference. This may sounds like a miracle; however, this is achieved as a consequence of the orthogonality of the base functions of Fourier series.

1.2 Multicarrier Modulation (MCM)

Multicarrier modulation (MCM) has received growing interest in the last few decades because of its ability in mitigating time dispersion of the multipath channels and efficiently using of the transmission bandwidth [2]. In multicarrier schemes, the

data is modulated at relatively low data rates, about 0.1 of the coherence time and transmitted in parallel over several narrow subchannels which come from the division of the transmission bandwidth. The symbol time on each subchannel is extended N times, where N is the number of active subchannels. Hence, the channel dispersion does not introduce severe impairment as each subchannel experiences a flat response in frequency domain. An example of MCM systems is the OFDM which is a special case of the MCM technology where all the carriers are orthogonal.

1.3 OFDM Scheme

Fig. 1.1 shows the OFDM evolution among the time. The OFDM system was first proposed by Chang in 1966 [1] to mitigate the effects of the multipath channel without losing data rate. In 1971, Weinstein and Ebert [3] showed that the multicarrier systems and in particular the OFDM systems can be accomplished using a discrete Fourier transform (DFT) as a modulation scheme.

The OFDM is a multicarrier transmission technique that spreads the data symbols over orthogonal subcarriers with overlapped spectra. Since that time, the OFDM suffered from ISI problems until 1980 when the cyclic prefix (CP) was introduced by A. Peled and A. Ruiz [4] to reduce the equalization complexity and avoid the problem of the ISI in OFDM systems. The CP is the last N_g samples of each OFDM symbol, must be no less than maximum access delay of the multipath channel, are appended to the beginning of the same OFDM symbol. The success of using the CP in the OFDM systems to mitigate the effects of the ISI encouraged communication engineers to consider the OFDM technology for practical applications. Consequently, in 1985, Cimini of Bell Labs proposed the OFDM technology for mobile communications [5]. It follows that, in 1987, Alard and Lassalle [6] considered the use of the OFDM transmission for broadcasting and for digital audio broadcasting (DAB) systems [7]. Several years later, the success of DAB motivated the communication engineers to produce a digital video broadcasting (DVB) system [8]. Regarding the application in wire-line communication, the pioneer was by Cioffi and others at Stanford [9] who explored the potential of using the OFDM as a modulation scheme in discrete multi-tone (DMT) modulation and digital subcarrier loop (DSL) applications. Four years later, in 1995, the approach of using multiple

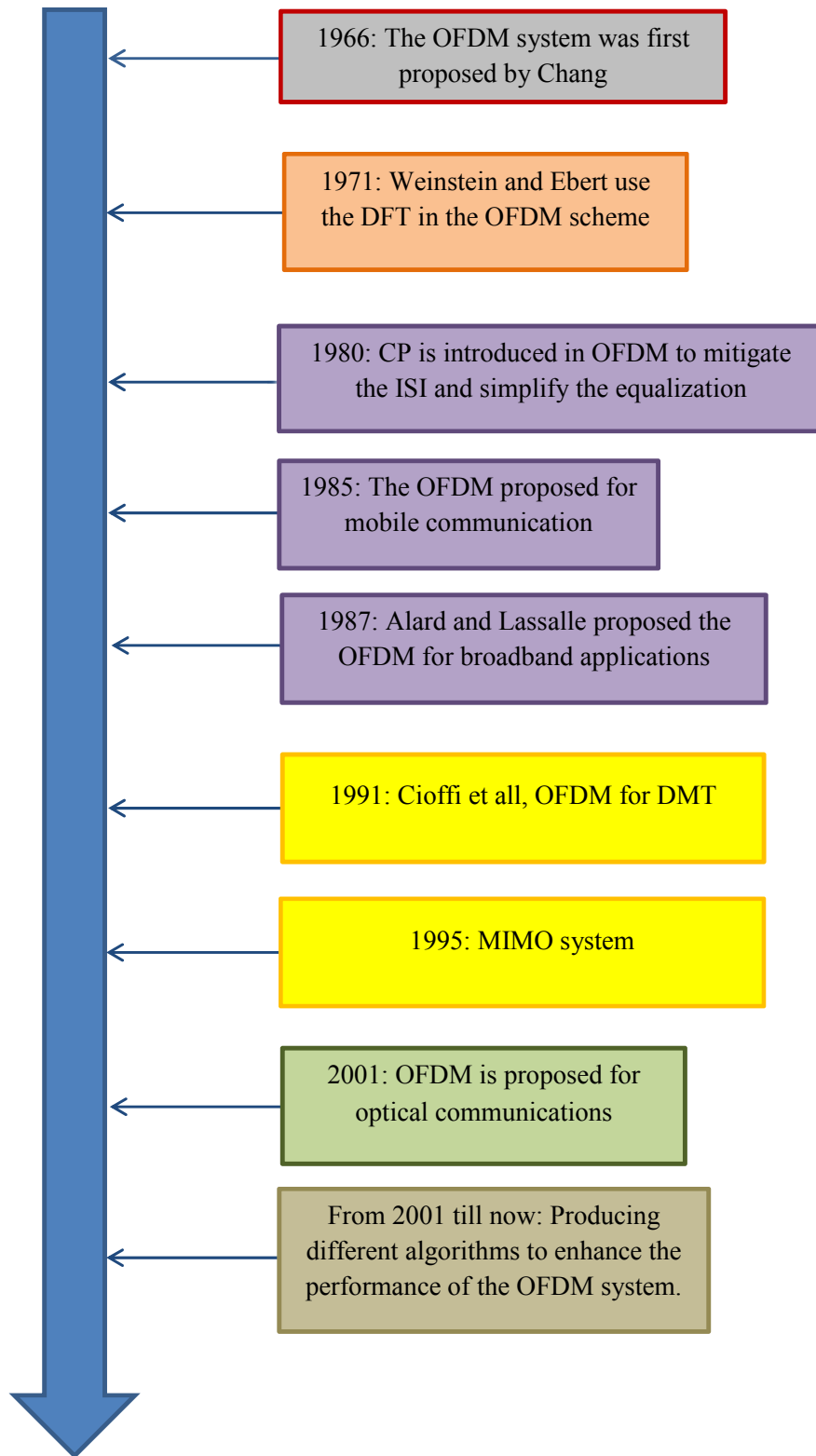


Figure 1.1: Evolution of the OFDM system.

input-multiple output (MIMO) to exploit the channel capacity was proposed [10].

Applications of the OFDM in optical communications have been developed over the last two decades being first proposed by Hui in 2001 [11]. These applications include optical wireless communications [12] and [13], optical fibre with single mode [14] and [15], multi-mode optical fibre [16] and [17] and plastic optical fibre [18]. However, the optical OFDM systems are beyond the scope of this thesis.

In 1990, the mobile phone was so expensive with only 11 million subscribers around the world while its cost decreased rapidly and the number of subscribers rose to 2 billion in 2005. More and more, OFDM has been adopted as standard not only for wireless communications such as wireless local area network (WLAN), IEEE 802.11a/g/n, metropolitan area networks (IEEE 802.16a), the European standard HIPERLAN/2 (High Performance Local Area Network, Type 2) [19] and WiMAX [20] and [21], but also for wire-line communications such as asymmetric digital sub-carrier loop (ADSL) which is well-known as discrete multi-tone modulation (DMT) [22] and power line communication [23], [24].

1.4 Drawbacks of OFDM Systems

Despite the success of the conventional OFDM system in many fields of applications and standards, it has serious challenges.

- Signal diversity provided by the OFDM system is still not adequate to mitigate the dispersive effects of severe hostile channels. This can be attributed to the whole bit-error-rate (BER) performance is dominated by the subcarrier with the smallest signal-to-noise ratio (SNR) leading to a poor performance over channels with narrowband deep notches spectral.
- The high peak-to-average power ratio (PAPR) is considered one of the major obstacles to the design of a reliable OFDM system. The PAPR of the OFDM signal sometimes force the high power amplifier (HPA) to work in the nonlinear region leading to clipping in the OFDM signal. The clipping distortion that is produced by the HPA may have severe performance-limiting impairment on the OFDM systems. The higher the PAPR is, the wider linear range of the HPA is required, which is costly.

- As the subcarriers spacing is relatively low, the OFDM system is sensitive to carrier frequency offset (CFO) which breaks the orthogonality of subcarriers and introduce inter-carrier interference (ICI). This problem will be addressed in more detail in Chapter Two.
- Working on the aforementioned problems required further added complexity to the OFDM system which might significantly affects the development progress toward the next generation in mobile communications.

1.5 Related works

1.5.1 DCT-OFDM System

Recently, there has been growing interest in MCM based on OFDM that adopts the DFT [25], [26], [27] and [28]. More recently, there has been significant attention towards the OFDM that is based on discrete cosine transform (DCT) [29] and [30] which has been found appealing [31], [32], [33] and [34]. This is because the peculiar characteristics of the DCT as a real transform with low computational complexity. In literature, [35] proposed the use of the DCT in the DMT systems, when the input data are real, to avoid the Hermitian constraint on the input data. This is unachievable in the case of the DFT based DMT as the DFT of a real data is complex. More recently, [36] demonstrated the application of the DCT in the DMT systems and it has been found attractive. However, more efficient DMT system and wireless OFDM system that exploits the potential channel capacity is crucial for modern digital communications.

In fact, BER performance of both the DCT-OFDM and the conventional OFDM are usually channel-limited performance. For example, over the additive white Gaussian noise (AWGN) channel, possible improvement from 10^{-3} to 10^{-4} in BER performance can be achieved by increasing the signal-to-noise ratio (SNR) by just around 1 dB. However, achieving the same improvement over multipath fading channel counterpart such as the international telecommunication union (ITU) channel required around 8 dB enhancement in the SNR. In practice, this improvement should not be achieved by increasing the transmit power or adding costly equipments as it hinders the high speed wireless communications which are crucially demanded for future

multimedia communications.

Large number of techniques have been developed to mitigate the detrimental effect of frequency-selective multipath fading channels in wireless communications including; power allocation, and channel independent precoders [37] and [38]. Though the power allocation technique seems theoretically effective, it suffers from two practically major drawbacks. The first problem is that the high dynamic power range at the transmitter to attain the instantaneous channel requirements demands a costly power amplifier. The second is the high complexity as requiring a link to feed the channel information from the transmitter to the receiver where channel state information (CSI) must be available at the transmitter. Channel independent precoder such as the Walsh-Hadamard transform (WHT) has been utilized in the OFDM systems to either improve the BER performance [39] or reduce the PAPR [40]. However, the proposed scheme inherits the properties of the DFT-OFDM not the popular properties of the DCT-OFDM that are mentioned in [35].

1.5.2 Unitary precoded DFT-OFDM System

MCM based on OFDM system has received a remarkable attention in the last two decades, [41] and [42], because of its peculiar characteristics with bandwidth efficiency and immunity against multipath fading channels. Therefore, this modulation is widely adopted in wireless broadband communications systems as well as wire-line communications such as the ADSL technology and a power line communications (PLC) [43] and [44].

The OFDM system that is based on the FFT as a modulation scheme cannot exploit the full diversity of the multipath channel as the BER performance is dominated by the subcarrier with the small SNR, [45] and [46], leading to a poor performance over channels with narrowband deep notches spectral. Furthermore, its high PAPR is one of the major problems in the OFDM systems. As a result, several techniques have been proposed to reduce the high PAPR within the OFDM systems including amplitude clipping and filtering, partial transmit sequence (PTS) and selective-mapping (SLM) [47] and [48]. Their complexity, however, is relatively high as only one of several generated sequences is used for transmission. On the other hand, some research have been conducted with the aim to improve the transmission of OFDM systems by using discrete Hartley transform (DHT) [49],[50], [51],

[52] and [53], DCT [54], and [31] or a precoder. The technique of using different unitary transforms as a channel independent precoder to improve the BER performance of OFDM systems was also discussed in [37]. Further investigation regarding the WHT precoded OFDM showed that it improves the BER performance, [55] and [39], and reduce the PAPR [40]. The PAPR reduction, however, is still poor and has relatively high complexity.

On the other hand, DFT precoded OFDM, which is well known as single carrier frequency domain equalizer (SC-FDE) with a cyclic prefix [45], [56] and [57], is considered as one of the solutions to improve the BER and reduce the PAPR. It achieves better BER performance and has a much lower PAPR than the conventional OFDM, and low complexity where a single one-tap equalizer could be applied which is exactly the same as that one used in the conventional OFDM. However, unlike the OFDM systems, the SC-FDE system is not a multiplexing scheme as the information symbols pass to the channel directly without being processed by any transform or multiplexed with other information symbols. Therefore, the fast fading channel with rapid change in the impulse response can have direct impact on SC-FDE performance as it will be shown later in the current chapter.

1.5.3 Alamouti ST-OFDM

In any reliable communication system to stand as good candidate to meet the demanding of recent development in wireless broadband communications, its resilience to frequency-selective multipath channels and the ISI must be confirmed [58] and [59]. Antenna diversity has received a noticeable attention in the last decade as a practical powerful technique in mitigating the deleterious effects of multipath channels [60], [61] and [62]. However, the ISI was the main concern as the ISI free condition is only guaranteed when the communication channel is flat fading.

In broadband communications, the transmit diversity adopting Alamouti space-time block coding (STBC) scheme [63] has been implemented in blocks and embedded with the OFDM system to produce a structure commonly known as ST-OFDM [64], [65] and [66]. It has been shown that the resulted system is much better than the conventional OFDM system where it utilizes the advantages of the OFDM and the STBC systems to produce an efficient ST-OFDM system in avoiding the ISI and enhancing the diversity [67] and [68]. Furthermore, a plethora of research has

been conducted showing that the transceiver of the ST-OFDM can be more robust to multipath channels if it is combined with a properly designed precoder [69], [70], [71], [72], [73] [74] and [75].

The approaches in [69]-[71] exploit the knowledge of the channel state information (CSI) at the transmitter to design the required precoder. However, this kind of precoders requires a feedback link from the receiver to the transmitter which reduces the system throughput and demands more complexity. In [72]-[73], a unitary precoder design with limited feedback for achieving high spectral efficiency was presented. In [74] and more recently in [75], the authors presented a precoded ST-OFDM where the CSI is not known at the transmitter. The approach in [74] utilized a filter-bank (polynomial) precoders for mitigation of ISI and blind equalization for multiple-input/ multiple-output (MIMO) transmission. On the other hand, the approach in [75] is considerably complex as it requires two additional complex precoders hardware or four times the complexity of the real unitary precoders at the transmitter. This is because one of these precoders is used for processing real part while the other for the imaginary part of the complex symbol at each transmitter branch.

1.5.4 PAPR Reduction of the UP-OFDM

With increased reliance on broadband communications that adopt the OFDM as a modulation scheme, new techniques are constantly being developed to improve the OFDM transmission [70]. As the OFDM signal comes from a superposition of many data symbols, this OFDM signal might have high PAPR [76].

The PAPR is considered one of the drawbacks of the OFDM system as it can cause a significant degradation in the BER performance in the presence of nonlinear distortion produced by extensive solid-state power amplifiers (SSPAs) [77]. To overcome such a problem, research has been conducted to present different PAPR reduction techniques, such as using a unitary channel independent precoder in the OFDM system [55], [78] and [79], and this is the main scope of the current chapter.

The use of unitary channel independent precoders in the OFDM systems (UP-OFDM) presents an attractive approach design for a reliable communication system [37]. An attractive feature of the UP-OFDM systems is to provide a way to exploit the available channel capacity by increasing the diversity of the transmitted signal

and reducing the PAPR. One of the suggested unitary transforms for precoding OFDM systems is the WHT, and this transform was found to enhance the diversity of the transmitted OFDM signal and reduce the PAPR [55]. The use of the DCT as a precoder in the OFDM systems to reduce the PAPR was investigated and found to be feasible [78], where it achieved better PAPR reduction than the WHT precoded OFDM. More recently, the DHT precoded OFDM [79], which combined to \mathbf{X} -transform, has been found to achieve better PAPR reduction than the DCT precoded OFDM.

On the other hand, the DFT precoded OFDM system [80] which is well-known as SC-FDE [57], is one of the solutions to improve the BER and reduce the PAPR.

The reduction in the PAPR does not usually mean an advantage in the OFDM system as some PAPR reduction techniques might lead to BER performance degradation [81]. It can be noted that all the advantages of the UP-OFDM systems are futile unless their performance improvement in the presence of the SSPA is confirmed. This chapter explains that nonlinear distortion due to the SSPA can sometimes have a severe effect on the UP-OFDM systems. It clearly shows that, although some precoders can reduce the PAPR of the OFDM system, their performance in the presence of the SSPA is worse than the conventional OFDM without precoder. In addition, coding technique to mitigate the sensitivity of the UP-OFDM system to the nonlinear distortion is proposed.

1.6 Aim of the Thesis

The work toward the next generation in mobile communications requires an efficient modulation scheme that significantly mitigates the effects of multipath channels. The performance improvement of the OFDM scheme should not be at the cost of increasing the signal power, increasing the complexity and/or sacrificing the bandwidth. The achievement of enhancing the transmitted signal diversity and/or reducing the PAPR is usually at the cost of adding extra complexity and/or reducing the data rate. The motivation of this thesis is to achieve a compromise solution among signal diversity, complexity of the system, and the PAPR reduction. In other words, the aim of this thesis is to present OFDM systems based on orthogonal transforms resilience to multipath transmission, reduce the PAPR with reasonable

complexity.

1.7 Contributions of the Thesis

There are four main significant objectives for this thesis.

1.7.1 C-OFDM Systems

In the first objective, a novel OFDM system based on the DCT utilizing the WHT as a channel independent precoder is presented [82]. Firstly, the WHT and the DCT are presented separately to perform the OFDM modulation scheme. Secondly, for the sake of complexity reduction these two transforms, the WHT and the DCT are presented in single compact transform which is the **C**-transform (a method to obtain the DCT via the Hadamard transform) proposed in [83] is utilized to implement the OFDM scheme.

An exact mathematical model for the BER performance of the proposed C-OFDM over multipath channels is also derived in this thesis. The proposed scheme has the advantage of enhancing the OFDM signal diversity and ultimately more resilience to multipath channels. It achieves about 10 dB SNR gain at 10^{-4} BER and reduces the PAPR about 1 dB over the DCT-OFDM and the DFT-OFDM. Furthermore, as the WHT-DCT or **C**-transform are real transforms, the proposed system can avoid the Hermitian constrict condition on the input data when used for baseband transmission with real data modulation format. This will be elaborated in Chapter Three.

1.7.2 X-OFDM Systems

For the second objective, another novel OFDM system which is different in characteristics from the C-OFDM system is presented. In this system, a new low complexity **X**-transform which combines the effects of the DHT and the DFT transforms is proposed to produce a new OFDM system called X-OFDM [84] and [85]. The proposed X-OFDM system exploits the channel diversity and achieves significant SNR gain over the conventional OFDM system. It also enormously reduces the computational complexity and the PAPR. In this contribution the Morelli and Mengalli (M&M) CFO synchronization algorithm is modified to adapt it to the proposed X-OFDM

to enhance its performance in the presence of the CFO. This will be elaborated in Chapter Four.

1.7.3 Alamouti ST-X-OFDM System

The third objective of this thesis is to combine the effects of Alamouti STBC code and \mathbf{X} -transform to produce efficient ST-X-OFDM system. The proposed ST-X-OFDM scheme significantly reduces the transmitter complexity and achieves advantages of both Alamouti STBC scheme and X-OFDM without some of their disadvantages. Unlike the SISO X-OFDM where the ZF and single tap equalizer leads to a worse performance than conventional OFDM with ZF detection, the ZF detection has no deleterious effects on the proposed ST-X-OFDM.

1.7.4 PAPR of Unitary Precoded OFDM system

In the fourth objective of this thesis, the PAPR reduction and BER performance of the unitary precoded OFDM (UP-OFDM) with different unitary transforms in the presence of solid-state power amplifiers (SSPAs) are investigated. Although unitary precoders can reduce the PAPR, different precoders lead to different levels in the PAPR reduction. Therefore, analysis and simulation results show that the DFT and the DHT precoders (single carrier-frequency domain equalizer (SC-FDE) and X-OFDM) achieve significant BER improvement in the OFDM systems, even in the presence of the SSPA distortion. The simulation results also show that the DCT and the WHT can lead to BER impairment in the presence of the SSPA. Furthermore, a coding technique is proposed in this thesis to mitigate the sensitivity of the UP-OFDM schemes to the SSPA nonlinearity [86]. Simulation results also reveal that the coded UP-OFDM approximately matched the performance of all the unitary precoders.

1.8 Thesis Outline

This thesis is organised as follows:

Chapter Two lay out the mathematical dimensions of the OFDM system, its challenges and solutions. It describes two types of OFDM systems, DFT-OFDM and DCT-OFDM. This chapter also gives a detailed analysis to the use of guard

interval, represented by the CP and the ZP, to mitigate the effects of the ISI between successive OFDM symbols. It also explains the concept of the PAPR in the OFDM system and the effects of CFO on the OFDM system performance.

In Chapter Three, new OFDM systems based on trigonometric transforms are presented. Mathematical analysis is first given for the proposed scheme. Mathematical analysis and exact BER formula for the proposed scheme, over multipath fading channels with zero-padding and MMSE detection, that tightly match the simulation results is also derived in this chapter. The ZP-C-OFDM system is more robust to frequency-selective multipath fading channels than both the ZP-DCT-OFDM and ZP-DFT-OFDM systems thanks to the **C**-transform combining the effects of the WHT and the DCT transforms, hence, increases the transmitted signal diversity. Subsequently, this chapter presents the complexity analysis of the **C**-transform and compared to the DCT, WHT-DCT and FFT. Simulation results in the standards context of the ITU pedestrian and vehicular channel models is also presented at the end of this chapter followed by the conclusions.

Chapter Four presents an improved OFDM system with very low complexity **X**-transform which is efficiently resilient to multipath transmission and huge reduction in the PAPR. It first introduces the new **X** transform and its computational complexity. It follows that, theoretical analysis of the BER performance of the proposed X-OFDM system over a multipath fading channels for the ZF and MMSE detection is introduced. Simulation results and discussions are then presented followed by the conclusions.

Application of the proposed X-OFDM in MIMO systems with the ZF and the MMSE equalizers are presented mathematically and by computer simulation in Chapter Five. The proposed system module is first presented, followed by the BER analysis of the proposed system with two transmit antennas and one receive antennas over multipath frequency-selective channels. The complexity analysis of the transmitter's transforms is mentioned and compared to other multicarrier precoders. Simulation results and conclusions are then drawn at the end of this chapter.

Investigation and giving comparison and solutions of BER performance of the C-OFDM and the X-OFDM systems in the presence of the SSPA is presented in Chapter Six. It first presents the PAPR of the C-OFDM and UP-OFDM system based on different unitary precoders. It also presents the SSPA model and demon-

strates its on the BER performance of the C-OFDM and the UP-OFDM systems. Simulation results and discussion followed by chapter conclusions are finally presented at the end of this chapter.

Finally, our conclusions and future works are drawn in Chapter Seven.

1.9 List of Publications and Awards

Publications

1. H.A. Leftah and S. Boussakta, "Efficient Modulation Scheme for OFDM System with ZP and MMSE Equalizer", in *Proc. IEEE International Conference on Communications (ICC)*, 2013 1-5.
2. H.A. Leftah and S. Boussakta, "Precoded DCT-OFDM system for baseband and wireless transmission: Performance analysis and evaluation," *Wireless Telecommunications Symposium (WTS)*, 2012, pp.1-6, 18-20 April 2012.
3. H.A. Leftah and S. Boussakta, "Efficient coded DCT-OFDM system utilizing Walsh-Hadamard Transform," *Wireless Telecommunications Symposium (WTS)*, 2012, pp.1-5, 18-20 April 2012.
4. H.A. Leftah and S. Boussakta, "BER Performance of DCT Precoded DFT-OFDM System in Presence of HPA," *Annual Research Conference (ARC) 2012*, Newcastle University, 25-26th January 2012.
5. H.A. Leftah and S. Boussakta, "New DCT-OFDM System Utilizing Discrete Walsh-Hadamard Transform," *Postgraduate Conference (PGC) 2011*, Newcastle University, 26-27th January 2011.

Awards

1. I have been awarded best paper prize in Annual Research conference (ARC) that held in Newcastle University, 25-26th January 2012.
2. I have awarded imagination company prize for 3rd best paper and presentation of postgraduate conference (PGC) that held in Newcastle University, 26-27th January 2011.

Chapter 2

Orthogonal Frequency Division

Multiplexing: Fundamentals

The focus of this chapter is on the architecture and performance of the OFDM to highlight the strengths and weaknesses of the OFDM systems. Mathematical definitions for the features of OFDM are introduced. The guard interval, represented by either the CP or zero-padding (ZP), is explained in detail in this chapter. The chapter also demonstrates the effects of multipath fading channel on the BER performance of the OFDM systems. The concept of the PAPR of the OFDM signal is also explained and investigated. Furthermore, the impacts of the SSPAs and the carrier frequency offset (CFO) on the transmission performance are discussed. This chapter mainly describes a textbook knowledge about OFDM system and its structure, strengths and weaknesses.

2.1 Introduction to the OFDM Systems

The OFDM, as any other communication system, is mainly constructed from three parts; transmitter, receiver and the transmission channel (the media).

Transmission channel is the media that connects transmitter and receiver and it is a key-important determining the reliability of communication system. Despite the fact that the OFDM transfers the frequency-selective multipath fading channels into parallel decoupled flat fading subchannels, the BER performance of the OFDM is usually channel-limited performance. The symbols on significantly attenuated subchannels will be completely wiped out as it falls below the noise level.

The transmitter of the conventional OFDM system mainly comprises mapper and the IFFT. The IFFT modulates the data symbols and carry them on orthogonal subcarriers with overlapped spectra. Although the spectra of the individual subcarriers are overlapped, the data symbols can be completely recovered at the receiver without any interference from other subcarriers by using the FFT. This is a consequence of the orthogonality of the base functions of the Fourier series. It also transfers the impulse response of a frequency-selective multipath channel into parallel decoupled flat fading subchannels each corresponding to a specific subcarrier.

In the last two decades, there has been growing interest to the OFDM that adopts the DFT or its fast algorithm (FFT) counterpart as a modulation scheme [25], [26]. On the other hand, a plethora of research have been conducted with the aim of improving the OFDM scheme by replacing FFT by another unitary transform such as the DCT [29] and [30]. With the ability to mitigate the effects of multipath fading and the delay spread of radio channels, the OFDM has been adopted in many applications and standards, for instance, (IEEE 802.11a/g/n), metropolitan area networks (IEEE 802.16a) and high performance radio LAN (HIPERLAN/2) as well as wire-line digital communications systems, such as asymmetric digital subcarrier loop (ADSL) [22] and power line communications (PLC) [87].

The main reason that the OFDM has taken long time to prevail is the high signal processing complexity of the DFT. It has been turned from theory to practical after developing the FFT and the huge development revolution in the signal processing field. The ISI between the successive OFDM symbols can be removed by attaching a guard interval to the OFDM symbol. This guard can be either the CP or the ZP. In the case of the CP, a copy of the last few samples of the OFDM symbol, its length is larger than the channel impulse response, is attached to the beginning of the symbol. In other words, the OFDM symbol is cyclically extended. Whereas, in the case of ZP, the OFDM symbol is extended with zeros with a length larger than or equal to the maximum channel access delay.

The receiver usually performs the reverse of the transmitter operations and functions. In other words, the receiver removes the guard sequence, then processes the signal by the FFT and applies the de-mapper on the resulted signal.

2.2 Multipath Propagation

Different kinds of wireless channel produce different kinds of attenuations and ultimately different BER performance. Non-line-of-sight communications channels are characterized by multipath propagation where the received signal is the superposition of many radio signals that are reflected and arrive at the receiver at different time. In other words, the received signal is a superposition of different copies of the main transmitted signal with different delays and attenuations as shown in Fig. 2.1. Multipath channels, in general, can be modelled using a tapped delay line (TDL) as shown in Fig. 2.2; where $L + 1$ is the number of paths and each path shows a gain h_p where τ_p is the delay time of the signal which passes through the path p . It can be also noted from Fig. 2.2 that the received signal y_k is the transmitted signal after passing through the multipath channel and corrupted by the AWGN. The multipath channel impulse response is given as:

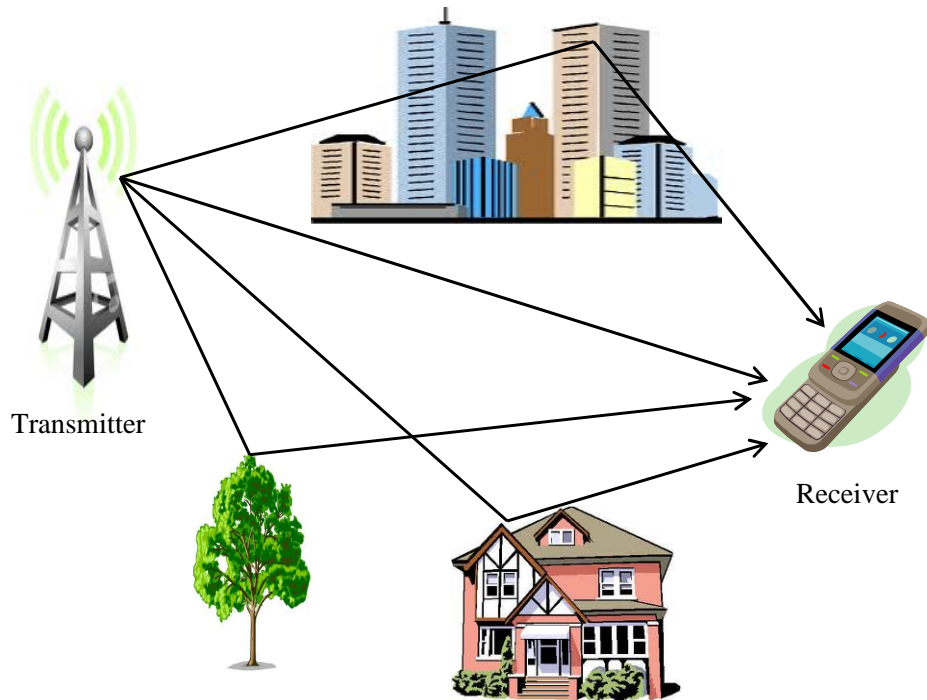


Figure 2.1: Multipath phenomena in wireless channels

$$\tilde{h}_k = \sum_{i=0}^L h_i \delta_{k-\tau_i}, \quad (2.1)$$

where h_i is the i^{th} path attenuation and δ_x is the chronicle delta, it is equal to 1 only when $x = 0$ and zero elsewhere. Owing to the interference between the reflected signals with each other and the direct one, ISI is produced causing signal latency

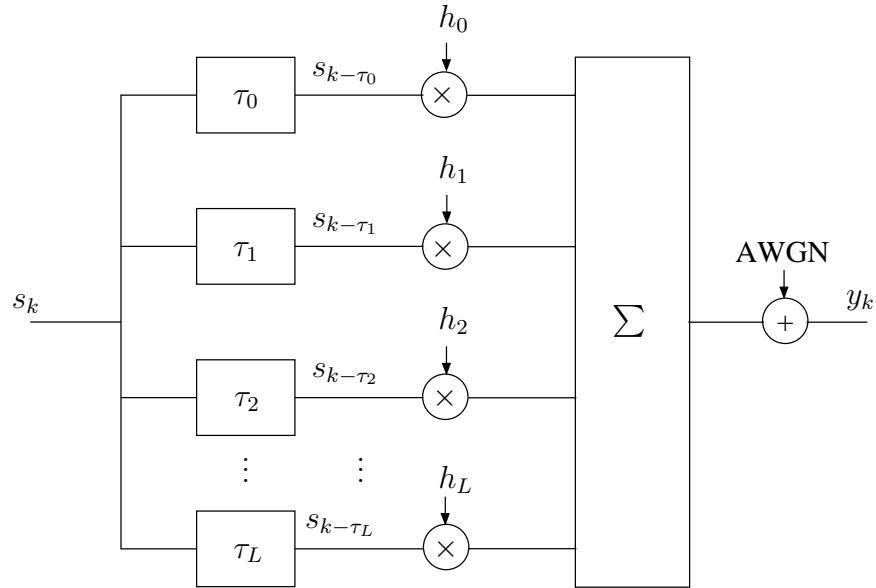


Figure 2.2: Tapped delay line

and significant degradation in communication system performance.

To mitigate this problem, the symbol duration T_s must be larger than the maximum channel delay τ_m ($\tau_m \ll T_s$). The delay spread depends on the environment around the transceiver. In outdoor scenarios, for instant, the ITU vehicular A channel, the maximum access delay is $2.51 \mu s$ and $3.7 \mu s$ for the case of pedestrian B channel. On the other side for indoors channels such as the HIPERLAN/2 channel model A, the maximum access delay is only $0.39 \mu s$.

The bit rate of the digital communication system is defined as

$$R_b = \log_2(M)T_s^{-1}, \quad (2.2)$$

where M is the constellation order. The data rate is 400 kbit/s for a symbol duration $T_s = 10 \mu s$ when 16-QAM modulation is used. This bit rate is reduced to half (200 kbit/s) when the symbol length is double in long ($T_s = 20 \mu s$). Thus, the ISI is eliminated in this case, however, at the cost of the bit rate.

Another drawback arisen from multipath phenomenon is the received signals of different access time interfere either constructively or destructively leading to fading. This fading can be deep in some frequencies of the signal spectrum leading to serious impairment in communication system performance.

To increase the data rate for a certain bandwidth $BW = T_s^{-1}$ for a given channel delay τ_m and mitigate the problem of frequency selectivity of channel fading, OFDM

is the solution. The OFDM splits up the high data rate signal, of period T_s , into N lower data rate signals, each of period NT_s , and sends them on N different subcarriers. Hence, for a given channel delay τ_m , there is no need to increase the symbol duration T_s to avoid the ISI as the OFDM extends the data period inherently to N times without affecting the bit rate.

The OFDM mitigates the effects of frequency-selective fading channels by transferring the impulse response of such a channel into several parallel decoupled subchannels each experiences flat fading. However, each subchannel or subcarrier will experience different level of this flat fading as shown in Figs. 2.3(a) and 2.3(b) for ITU channel pedestrian and vehicular models respectively. It can be seen from Figs. 2.3(a) and 2.3(b) that multipath channels have some deep fades on some subcarrier indexes and the position of these deep fades is changing from each OFDM frame to another, making all the subcarriers susceptible to such deep fade during the whole transmission.

OFDM can be considered as either a modulation or multiplexing technique that can be implemented efficiently by using the DFT or the FFT.

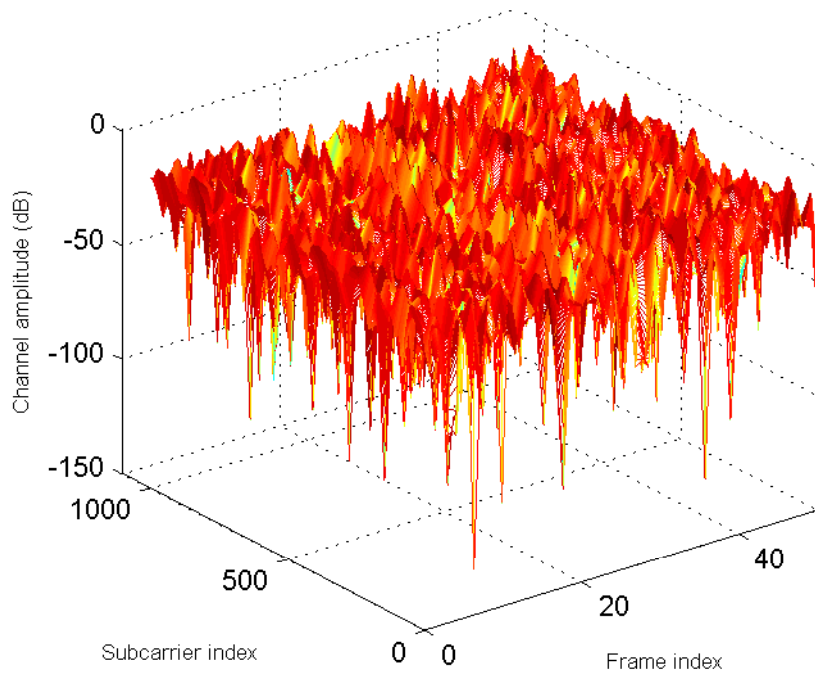
2.3 The OFDM system model and Definitions

The block diagram of the conventional OFDM system that based on the DFT (DFT-OFDM) is shown in Fig. 2.4. The main parts incorporated in this figure are:

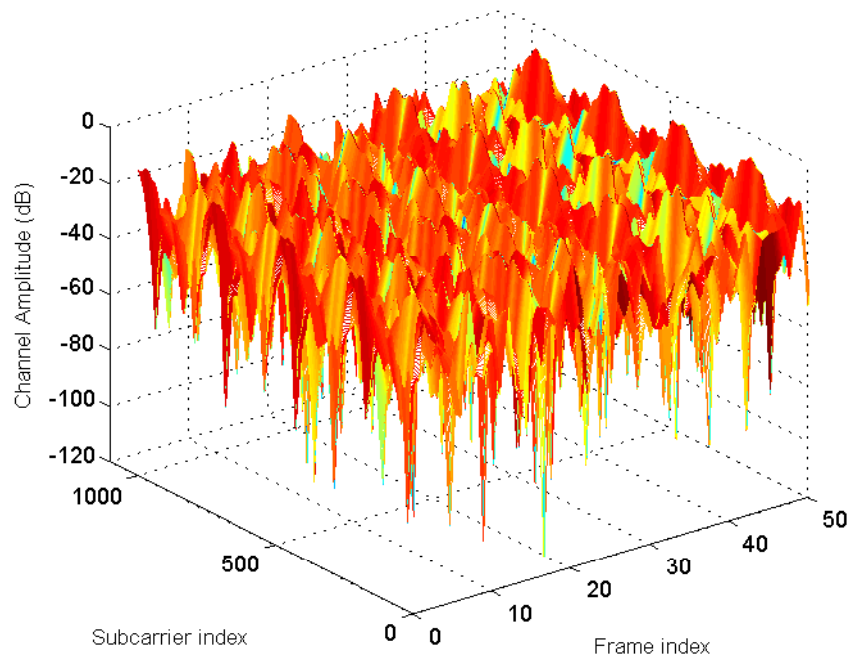
2.3.1 Digital Mapper/De-mapper

In digital communications, the information is assumed to be available in either binary form or analogue form after being sampled and quantized. For the case of analogue signal, it is first sampled with a sampling rate greater than or equal to the Nyquist rate, ($f_s \geq 2BW$), and then quantized each sample to its corresponding appropriate level to obtain the binary information.

There is an array of digital modulation schemes such as M-array phase shift keying (M-PSK) and M-array quadrature amplitude modulation (M-QAM). The slowest modulation scheme, which is sometimes called the simplest scheme, is the binary phase shift keying where $M = 2$ and only one binary data bit maps to a polar format of ± 1 (phase difference 180°). Quadrature phase-shift-keying (QPSK)



(a) Frequency-time variations of the ITU pedestrian B channel.



(b) Frequency-time variations of the ITU vehicular A channel.

Figure 2.3: Frequency-time variations of the ITU channel (a: Pedestrian B and b: Vehicular A).

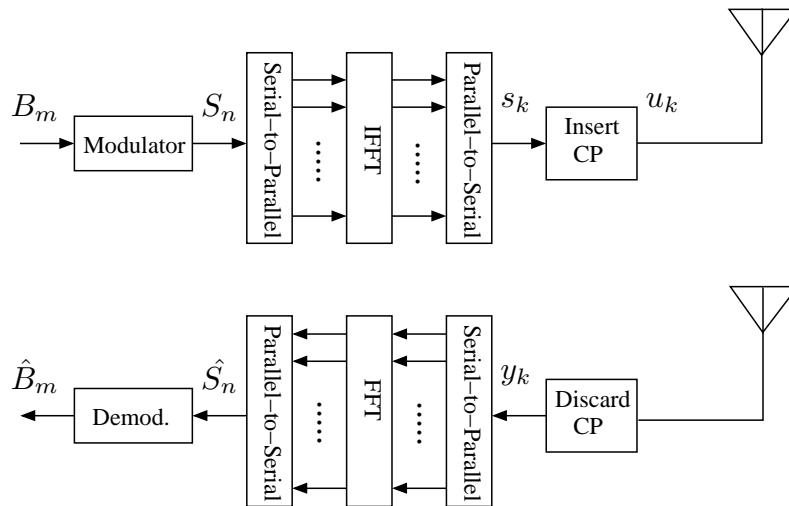


Figure 2.4: Block diagram of discrete baseband model of OFDM system.

is another scheme where $M = 4$, it maps each consecutive two bits to a symbol. Therefore, the QPSK constellation is two times faster in transferring data than the BPSK.

For the M-QAM, when $M = 16$, it is commonly called 16-QAM constellation. The 16-QAM constellation is more efficient in terms of bit rate as it packs more information bits into a symbol. It maps each four consecutive bits into a symbol taken from the 16-QAM alphabet. The bit rate of the 16-QAM constellation is two times higher than that of the QPSK and four times higher than that of the BPSK. In general, the faster the scheme, such as the 16-QAM, the more sophisticated in implementation and the more susceptible to error. Therefore, the modulation scheme should be chosen carefully to cope with the channel limitations.

2.3.2 IFFT/FFT Transforms

Although the fundamentals of the OFDM system are known since early sixties, the OFDM was not used as the standard for any digital communication system until 80s. This is because the enormous technology revolution in digital signal processing techniques in 80s that makes the design of modems much easier than the high complexity of the DFT. Coinciding with this technology revolution, the efficient FFT is adopted in the OFDM systems. An N -point DFT requires N^2 multiplications whereas it requires only $\frac{N}{2} \log_2 N$ multiplications for the case of the FFT counterpart. The modulation technique involves assembling the information symbols that drawn from specific constellation into parallel blocks of length N symbols. It follows

that an inverse FFT (IFFT) is performed on each block of this information symbols to generate the OFDM samples which are sent serially through the channel. At the receiver side, the received symbols are first serial-to-parallel (S/P) converted and then detected by the forward FFT.

The IFFT/FFT are used, respectively to modulate/demodulate the data symbols that are drawn from the modulator. They are also necessary to provide the orthogonal basis that carry the information symbols on overlapped subcarriers without being interfered.

The discrete-time complex-baseband block diagram of the conventional OFDM that based on the FFT is shown in Fig. 2.4. The binary data, \mathbf{B} , are first set in blocks for mapping as

$$\mathbf{B} = \begin{bmatrix} B_{1,0} & B_{1,1} & \cdots & B_{1,N-1} \\ B_{2,0} & B_{2,1} & \cdots & B_{2,N-1} \\ \vdots & \vdots & \ddots & \vdots \\ B_{m,0} & B_{m,1} & \cdots & B_{m,N-1} \end{bmatrix}, \quad (2.3)$$

where $B_{p,q} \in \{0, 1\}$. Each column in \mathbf{B} is mapped into one of $M \triangleq 2^m$ possible M -array phase-shift-keying (M-PSK) or M -array quadrature-amplitude-modulation (M-QAM) symbols using Gray mapping, to produce the information vector $\mathbf{S} = [S_0, S_1, \dots, S_{N-1}]^T$.

In OFDM systems, the information symbols which are statistically independent are carried on N subcarriers. Each adjacent subcarriers are mathematically orthogonal with 90-degree phase shift between them. Owing to the orthogonality principle of symbols carried on these subchannels, they can be overlapped without affects each one another. This in turns enables the OFDM to use the bandwidth efficiently. This overlapped spectrum is shown in Fig. 2.5.

The FFT within the structure of the OFDM systems is necessary to provide the orthogonal basis that carry the information symbols on overlapped subcarriers without interference between them. The information symbols, $\mathbf{S}^T = [S_0, S_1, \dots, S_{N-1}]$, are processed by the inverse DFT (IDFT) to produce the OFDM symbol as [88]

$$\mathbf{s} = \mathbf{F}^{\text{H}} \mathbf{S}, \quad (2.4)$$

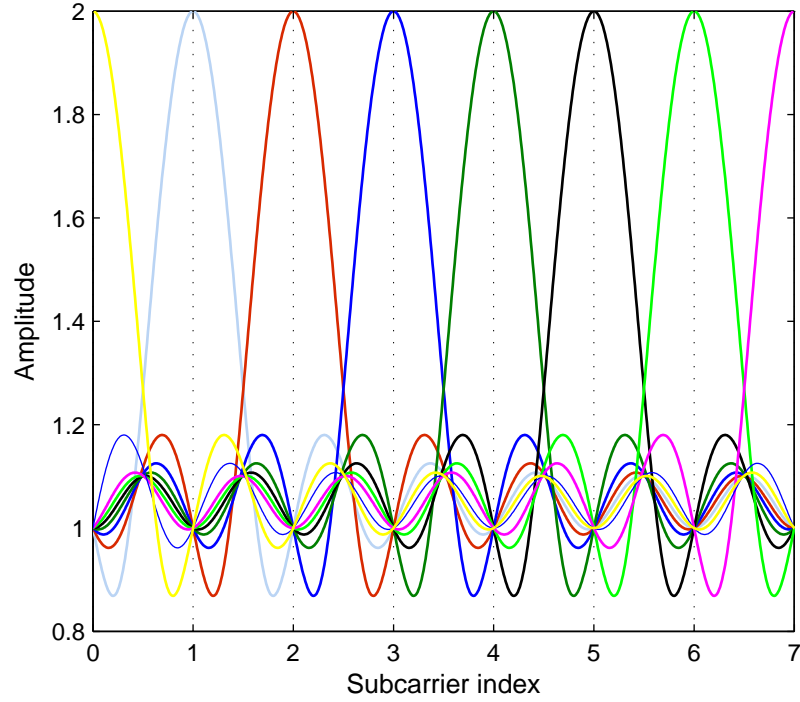


Figure 2.5: Orthogonal basis of the OFDM symbol

where \mathbf{F} is the normalised $N \times N$ FFT matrix and $(.)^{\text{H}}$ is the Hermitian conjugate. The elements of \mathbf{F} are defined as $F_{k,n} = (1/\sqrt{N}) \exp(-j2\pi kn/N)$, where k and n denote the row and column numbers $\{k, n\} = 0, 1, \dots, N-1$, respectively and the transformation \mathbf{F} of size $N \times N$ can be expressed as

$$\mathbf{F} = \frac{1}{\sqrt{N}} \begin{bmatrix} 1 & 1 & \dots & 1 \\ 1 & e^{-j2\pi/N} & \dots & e^{-j2\pi(N-1)/N} \\ \vdots & \vdots & \ddots & \vdots \\ 1 & e^{-j2\pi(N-1)/N} & \dots & e^{-j2\pi(N-1)(N-1)/N} \end{bmatrix}, \quad (2.5)$$

where $\mathbf{F}^{-1} = \mathbf{F}^H$. Consequently, the k^{th} sample in the sequence \mathbf{s} can be expressed as

$$s_k = \frac{1}{\sqrt{N}} \sum_{n=0}^{N-1} S_n e^{j\frac{2\pi kn}{N}}, \quad k = 0, 1, \dots, N-1. \quad (2.6)$$

where

$j^2 = -1$: is the imaginary unit,

k : index on transmitted symbols,

n : index on input symbols that drawn from specific digital modulator,

N : number of FFT points,

$T_s = \frac{N}{BW}$: useful symbol time and BW is the system transmission bandwidth,

$T_g = \frac{N_g}{BW}$: guard time,

$T = T_s + T_g = \frac{N + N_g}{BW}$: transmitted symbol time,

$\Delta f = \frac{BW}{N} = \frac{1}{T_s}$: subcarrier frequency spacing.

It is obvious from (2.6) that each data symbol S_n , is distributed over N different samples $\{s_k\}_{k=0}^{N-1}$ which are transmitted over N different flat fading subchannels as it will be explain later in the current chapter.

2.3.3 Guard Interval

Guard interval of length no less than the maximum excess delay of multipath propagation channel does not carry any information and it is discarded at the receiver side. It is efficient in mitigating the ISI between each successive OFDM symbols either by transmit samples of zero values or samples that copied from last part of OFDM symbol over this guard interval. This will be elaborated in next section.

2.3.3.1 Cyclic Extension of OFDM Symbols

A guard band interval which is commonly called the cyclic prefix (CP) is added to the time-domain signal after the parallel-to-serial conversion. The CP is a copy of the last N_g samples of the OFDM symbol, \mathbf{s} , appending them to the beginning of the IFFT output to form the time-domain OFDM symbol as

$$\mathbf{u} = [s_{N-N_g}, s_{N-N_g+1}, \dots, s_N, \mathbf{s}]. \quad (2.7)$$

The samples of \mathbf{u} are then sent sequentially through the channel where they experience fading before they arrive to the receiver.

In fact, the OFDM transfers a multipath fading channel into parallel decoupled flat fading subchannels by the mean of the CP. The CP changes the linear convolution of the signal with the channel to circular convolution and finally the property of circular convolution/multiplication is applicable which enables single one tap equalizer. It is simply the last N_g samples of the OFDM symbol, must be greater than or equal to the maximum excess delay of the multipath propagation

2.3 The OFDM system model and Definitions

channel, is appended to the beginning of the OFDM symbol as shown in Fig. 2.6. Mathematically, the resulting redundant signal is of length $N_t = N + N_g$, which can be expressed as

$$\mathbf{u} = \mathbf{\Psi}_{cp}^{Tr} \mathbf{s}, \quad (2.8)$$

where $\mathbf{\Psi}_{cp}^{Tr}$ is an $N_t \times N$ matrix and can be written as

$$\mathbf{\Psi}_{cp}^{Tr} = \begin{bmatrix} \mathbf{0}_{N_g \times (N-N_g)} & \mathbf{I}_{N_g} \\ & \mathbf{I}_N \end{bmatrix}. \quad (2.9)$$

The entries of the resulting redundant block are finally sent sequentially through

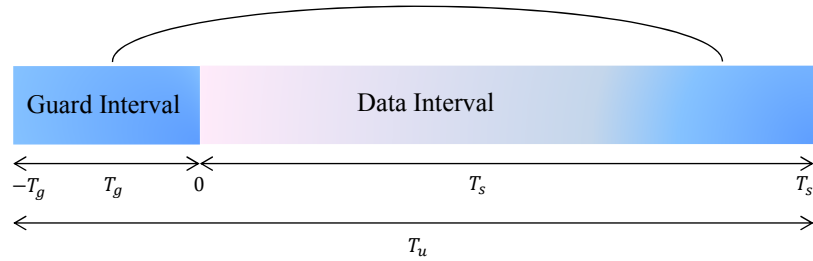


Figure 2.6: Cyclic prefix extension.

the channel. Assume that the channel is $L + 1$ taps channel. The received signal is the convolution of the transmitted signal \mathbf{u} with the channel impulse response \tilde{h} which can be written as

$$\begin{aligned} y_k &= [u_k \otimes \tilde{h}_k] + v_k, \\ &= \sum_{d=0}^L u_{k-d} h_d + v_k, \end{aligned} \quad (2.10)$$

where \otimes denotes the convolution operation and $\mathbf{v} = [v_0, v_1, \dots, v_{N-1}]^T$ are the additive white Gaussian noise (AWGN) samples which are independent and normally distributed random variables with zero-mean and variance $\sigma_v^2 = E\{|v_n|^2\}$, and $E\{\cdot\}$ denotes the expectation operation. Equation (2.10) can be written in a more expressive way in matrix form as

$$\begin{aligned} \mathbf{y} &= \mathbf{H}_0 \mathbf{u}, \\ &= \mathbf{H}_0 \mathbf{\Psi}_{cp}^{Tr} \mathbf{s}. \end{aligned} \quad (2.11)$$

In (2.11), \mathbf{H}_0 is a $N_t \times N_t$ channel convolutional Toeplitz matrix defined in [41] ,

2.3 The OFDM system model and Definitions

whose elements l^{th} $0 \leq l \leq N_t - 1$ row and p^{th} $0 \leq p \leq N_t - 1$ column are given as $H_0(l, p) = h(l - p)$ for $0 \leq (l - p) \leq L$ and $H_0(l, p) = 0$ otherwise. Thus its matrix can be written as

$$\mathbf{H}_0 = \begin{bmatrix} h_0 & 0 & 0 & 0 & \dots & \dots & 0 & 0 \\ h_1 & h_0 & 0 & 0 & \dots & \dots & 0 & 0 \\ \dots & h_1 & h_0 & 0 & \dots & \dots & 0 & 0 \\ \dots & \dots & h_1 & \dots & \dots & \dots & 0 & 0 \\ h_L & \dots \\ 0 & h_L & \dots & \dots & \dots & \dots & \dots & \dots \\ 0 & 0 & \dots & \dots & \dots & \dots & \dots & \dots \\ 0 & 0 & 0 & h_L & \dots & \dots & h_1 & h_0 \end{bmatrix}. \quad (2.12)$$

At the receiver side, this redundant sequence shall be removed to avoid the ISI as

$$\begin{aligned} \mathbf{q} &= \mathbf{F}\Psi_{cp}^R \mathbf{H}_0 \Psi_{cp}^{Tr} \mathbf{F}^H \mathbf{S}, \\ &= \mathbf{F}\mathbf{H}_{Cir} \mathbf{F}^H \mathbf{S}. \end{aligned} \quad (2.13)$$

In (2.13), Ψ_{cp}^R is a $N \times N_t$ matrix used to discard the cyclic extension at the receiver side and it can be written as

$$\Psi_{cp}^R = [\mathbf{0}_{N \times N_g} \quad \mathbf{I}_N], \quad (2.14)$$

and $\mathbf{H}_{Cir} = \Psi_{cp}^R \mathbf{H}_0 \Psi_{cp}^{Tr}$ is an $N \times N$ circulant matrix, can be written as

$$\mathbf{H}_{Cir} = \begin{bmatrix} h_0 & 0 & 0 & 0 & h_L & \dots & h_3 & h_2 & h_1 \\ h_1 & h_0 & 0 & 0 & 0 & h_L & \dots & h_3 & h_2 \\ h_2 & h_1 & h_0 & 0 & \dots & \dots & h_L & \dots & h_3 \\ \dots & \dots & h_1 & \dots & \dots & \dots & \dots & \dots & \dots \\ \dots & h_L \\ h_L & \dots & \dots & \dots & \dots & \dots & 0 & 0 & 0 \\ 0 & h_L & \dots & \dots & \dots & \dots & h_0 & 0 & 0 \\ 0 & 0 & \dots & \dots & \dots & \dots & h_1 & h_0 & 0 \\ 0 & 0 & 0 & h_L & \dots & \dots & h_2 & h_1 & h_0 \end{bmatrix}. \quad (2.15)$$

This means that the CP changes the linear convolution of the OFDM signal with the channel into circular convolution. Owing to the property of circular convolution in time domain is equal to the multiplication in frequency domain, $\mathbf{FH}_{Cir}\mathbf{F}^H$ is a diagonal matrix, its diagonal elements are the elements of the channel transfer function $H_n = \sum_{l=0}^{L-1} h_l e^{-j\frac{2\pi nl}{N}}$, ($0 \leq n \leq N - 1$). Subsequently, the received signal is a point-wise multiplication of the information symbols by channel transfer function and (2.13) can be rewritten as

$$q_n = H_n S_n + \Omega_n. \quad (2.16)$$

Consequently, the CP in the OFDM system has two folds advantage; firstly, it prevents the ISI when its length is greater than maximum channel delay. Secondly, it mitigates the ICI by transferring the multipath fading channel into parallel flat fading subchannels each corresponds to single individual subcarrier. However, the use of the CP in the OFDM system is not purely positive, it has notable drawback that the symbol s_k which is transmitted on the k^{th} subcarrier will be completely wiped out when the corresponding channel transfer function is zero $H_n = 0$ [89]. More recently, it has been suggested to replace the CP by ZP, where the OFDM signal as shown in Fig. 2.7. Unlike the non-zero CP, the ZP involves a zeros samples which are appended to the signal to be transmitted after the IFFT. The common features of CP-OFDM and ZP-OFDM transmission that both can completely avoid ISI and have the same spectral efficiency when the length of CP and ZP are equal. However, ZP system assures symbol recovery regardless of the channel zeros location whereas this property is unavailable in the case of the CP counterpart. In spite of the fact that the ZP-OFDM can achieve better BER performance than the CP-OFDM scheme, the complexity of the ZP-OFDM is higher than that of the CP-OFDM scheme.

2.3.3.2 Zero-Padding of OFDM Symbols

The ZP-OFDM scheme can sometimes achieve better BER performance than the CP-OFDM scheme [89] because the data symbols can be recovered regardless of the channel zero locations. The equalizer complexity of the OFDM with a ZP is higher than the complexity of the OFDM equalizer with a CP [90] in the case of a

2.3 The OFDM system model and Definitions

quasi-static channel where the channel equalization could be done in the frequency domain by simple one tap equalizer. The resulting redundant signal is of length $N_t = N + N_g$ and can be expressed as

$$\mathbf{u} = \mathbf{\Psi}_{zp} \mathbf{s}, \quad (2.17)$$

where $\mathbf{\Psi}_{zp}$ is an $N_t \times N$ matrix, which can be written as

$$\mathbf{\Psi}_{zp} = \begin{bmatrix} \mathbf{I}_N \\ \mathbf{0}_{N_g \times N} \end{bmatrix}. \quad (2.18)$$

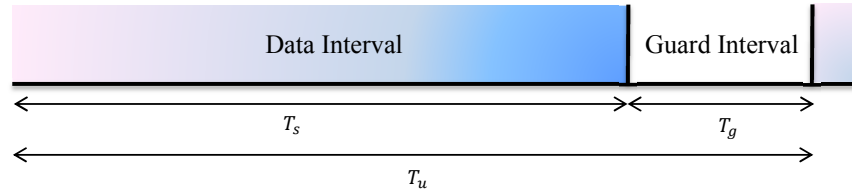


Figure 2.7: Zero-Padding guard interval.

The received signal at the receiver side can be written in matrix form as

$$\begin{aligned} \mathbf{y} &= \mathbf{H}_0 \mathbf{\Psi}_{zp} \mathbf{u}, \\ &= \mathbf{H} \mathbf{u}. \end{aligned} \quad (2.19)$$

In (2.19), $\mathbf{H} = \mathbf{H}_0 \mathbf{\Psi}_{zp}$ is an $N_t \times N$ matrix defined as [91]

$$\mathbf{H} = \begin{bmatrix} h_0 & 0 & 0 & 0 & \cdot & \cdot & 0 & 0 \\ h_1 & h_0 & 0 & 0 & \cdot & \cdot & 0 & 0 \\ \cdot & h_1 & h_0 & 0 & \cdot & \cdot & 0 & 0 \\ h_L & \cdot \\ 0 & h_L & \cdot & \cdot & h_1 & \cdot & \cdot & 0 \\ 0 & 0 & \cdot & \cdot & \cdot & \cdot & \cdot & h_0 \\ \cdot & \cdot \\ \cdot & h_L \end{bmatrix}. \quad (2.20)$$

The DFT is not the only transform that has been adopted in the OFDM systems to provide the orthogonal basis that carry the data symbols. Discrete cosine

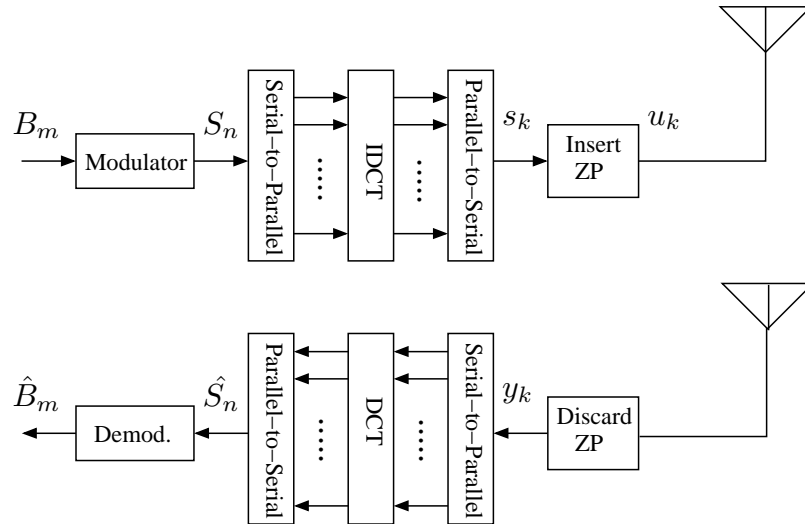


Figure 2.8: DCT-OFDM system block diagram.

transform (DCT) has also been suggested to implement the modulation scheme of the OFDM system.

Unlike the DFT-OFDM, the DCT-OFDM does not have circular convolution-multiplication property. Consequently, a CP as that one been applied to DFT-OFDM is inapplicable. One of the solutions was suggested by [29] by doubling the data, however, this sacrifices the bandwidth as half of the transmitted data are redundant data. Zero padding scheme is consider as one of the best solutions, it ensures symbol recovery regardless of channel zero locations and explore the full diversity of the OFDM signal.

2.4 DCT-OFDM system model

The DCT-OFDM system block diagram is shown in Fig. 2.8. The main difference between the DFT-OFDM and the DCT-OFDM systems is that, in the latter the IDCT/DCT are used for modulation/demodulation process instead of the IFFT/FFT. It can also be seeing from Fig. 2.8 that the zero-padding guard interval is used instead of the CP in the case of the DFT-OFDM.

2.5 Theoretical BER of the OFDM

From equation (2.16) it is clear that the information symbols that come from specific constellation are independently carried on decoupled subchannels with added

AWGN noise. Therefore, it can be said that each subchannel can be consider as an independent transmission scheme with its own SNR and BER. Therefore the overall BER of the DFT-OFDM can be given by averaging the BER for the individual subchannels [92] as follows

$$P_e^{M-PSK} = \frac{\mu}{m_b} \frac{1}{N} \sum_{m=0}^{N-1} Q \left(\sqrt{2\beta_m} \sin\left(\frac{\pi}{M}\right) \right), \quad (2.21)$$

and

$$P_e^{M-QAM} = \frac{4 - 2^{(2-m_b/2)}}{m_b} \frac{1}{N} \sum_{m=0}^{N-1} Q \left(\sqrt{\frac{3\beta_m}{M-1}} \right). \quad (2.22)$$

In (2.21) and (2.22), μ denotes the number of nearest neighbours signal points ($\mu_{QPSK} = 2$ and $\mu_{16-QAM} = 3$), M is the level on constellation and $m_b = \log_2 M$ represents the number of bits in each digitally encoded symbol, $Q(x)$ denotes the Q-function of x and β_m is the signal power, per symbol, to noise power ratio. In other words, by substituting the specific parameters that assigned to the QPSK and the 16-QAM, the BER is respectively given as

$$P_e^{QPSK} = \frac{1}{N} \sum_{m=1}^N Q \left(\sqrt{\beta_m} \right), \quad (2.23)$$

and

$$P_e^{16-QAM} = \frac{3}{4N} \sum_{m=1}^N Q \left(\sqrt{\frac{\beta_m}{5}} \right). \quad (2.24)$$

Therefore, to evaluate the BER performance of the OFDM system, the SNR (β_m), $m = 0, 1, 2, \dots, N - 1$, per each subchannel must be calculated. This can be achieve by several ways, such as linear equalizer, decision feedback equalizer, adaptive equalizer, zero-forcing (ZF) equalizer and minimum mean-square-error (MMSE) equalizer. During this thesis, we will consider the case of ZF and MMSE equalizers [93] as they are simple in implementation and can achieve good channel cancellation.

2.5.1 Zero Forcing (ZF) Equalizer

In the ZF case, the equalization is achieved by simply dividing each received symbol in (2.16) by the corresponding channel dependent factor H_n

$$q_n^{ZF} = s_n + \frac{\Omega_n}{H_n}. \quad (2.25)$$

The noise error signal is then calculated as the difference between the transmitted and the received data symbols, $e_n^{ZF} = q_n^{ZF} - S_n$ and the noise power per each subchannel can be given as

$$\mathcal{P}_n^{ZF} = \frac{\sigma_v^2}{|H_i|^2}. \quad (2.26)$$

Thus, the signal to noise ratio for each symbol will be given as

$$\beta_i^{ZF} = |H_i|^2 \gamma_s. \quad (2.27)$$

The average BER for the system is calculated by averaging the BER to the number of subchannels as follows

$$P_e^{QPSK} = \frac{1}{N} \sum_{i=0}^{N-1} Q(\sqrt{\gamma_s |H_i|^2}), \quad (2.28)$$

and

$$P_e^{16QAM} = \frac{3}{4N} \sum_{i=0}^{N-1} Q\left(\sqrt{\frac{\gamma_s |H_i|^2}{5}}\right). \quad (2.29)$$

2.5.2 Minimum Mean-Square-Error (MMSE) Equalizer

The MMSE equalizer, χ_n , is defined as

$$\begin{aligned} \chi_n &= \frac{E_s H_n^*}{E_s |H_n|^2 + \sigma_v^2}, \\ &= \frac{\gamma_s H_n^*}{1 + \gamma_s |H_n|^2}. \end{aligned} \quad (2.30)$$

It follows that the equalized signal is given as

$$q_n^{MMSE} = S_n H_n \chi_n + \Omega_n \chi_n. \quad (2.31)$$

$$q_n^{MMSE} = S_n \frac{\gamma_s |H_n|^2}{1 + \gamma_s |H_n|^2} + \Omega_n \chi_n. \quad (2.32)$$

The error signal is then calculated as the difference between the transmitted and the received data symbols, $e_n^{MMSE} = q_n^{MMSE} - S_n$, and can be written as

$$\begin{aligned} e_n^{MMSE} &= S_n H_n \chi_n - S_n + \Omega_n \chi_n, \\ &= [H_n \chi_n - 1] S_n + \Omega_n \chi_n. \end{aligned} \quad (2.33)$$

Table 2.1: System parameters for simulations.

System Item	Parameter
Modulation	QPSK and 16-QAM
Synchronisation	Complete
Antenna type	Perfect
Channel type	AWGN, ITU pedestrian B and ITU vehicular A
Equalisation	One-tap FDE
Number of Subcarriers (N)	1024
Duration of CP	$N/4$
Bandwidth	10MHz

In (2.33), $H_n \chi_n - 1 = \frac{-1}{1 + \gamma_s |H_n|^2}$. Thus (2.33) can be written as

$$e_n^{MMSE} = S_n \frac{-1}{1 + \gamma_s |H_n|^2} + \Omega_n \frac{\gamma_s H_n^*}{1 + \gamma_s |H_n|^2}. \quad (2.34)$$

As the data symbols and the AWGN are statistically independent, the noise power of the i^{th} subchannel is then expressed as

$$\begin{aligned} \mathcal{P}_{n_i}^{MMSE} &= E [|e_n^{MMSE}|^2], \\ &= \frac{E_s}{[1 + \gamma_s |H_i|^2]^2} + \frac{\sigma_v^2 \gamma_s^2 |H_i|^2}{[1 + \gamma_s |H_i|^2]^2}, \\ &= \frac{E_s}{[1 + \gamma_s |H_i|^2]^2} + \frac{E_s \gamma_s |H_i|^2}{[1 + \gamma_s |H_i|^2]^2}, \\ &= \frac{E_s}{1 + \gamma_s |H_i|^2}. \end{aligned} \quad (2.35)$$

The signal power $\mathcal{P}_{s_i}^{MMSE} = E [|q_n^{MMSE}|^2]$ and it is given as

$$\begin{aligned} \mathcal{P}_{s_i}^{MMSE} &= \frac{E_s \gamma_s^2 |H_i|^4}{[1 + \gamma_s |H_i|^2]^2} + \frac{E_s \gamma_s |H_i|^2}{[1 + \gamma_s |H_i|^2]^2}, \\ &= \frac{E_s \gamma_s |H_i|^2}{1 + \gamma_s |H_i|^2}. \end{aligned} \quad (2.36)$$

Then the SNR of the i^{th} subchannel $\beta_i^{MMSE} = \frac{\mathcal{P}_{s_i}^{MMSE}}{\mathcal{P}_{n_i}^{MMSE}}$ is then given as

$$\beta_i^{MMSE} = \gamma_s |H_i|^2. \quad (2.37)$$

It is obvious from (2.37) that the DFT-OFDM is very close in the BER performance for both the ZF and the MMSE detection.

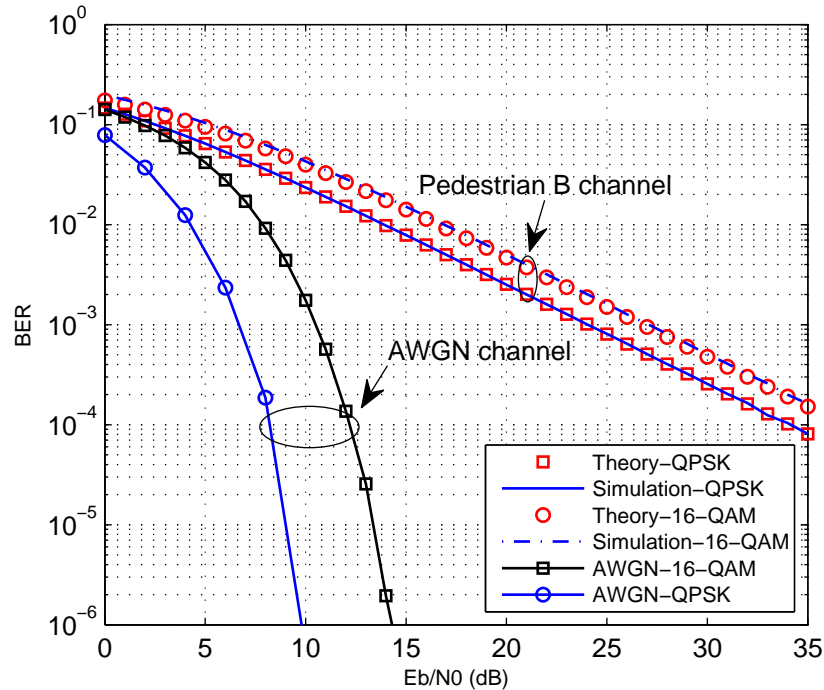


Figure 2.9: BER performance of the conventional OFDM system for the QPSK and the 16-QAM constellations over the ITU pedestrian B channel in comparison to the performance over the AWGN channel; theoretically and by simulation.

The BER performance of the conventional OFDM for the QPSK and the 16-QAM modulations over the AWGN channel and the ITU pedestrian B channel is shown in Fig. 2.9. The system parameters that used in our simulation is shown in Table 2.1. Theoretical results are obtained by using the formulas in (2.28) for the case of QPSK and (2.29) for the case of 16-QAM. It can be observed from Fig. 2.9 that although the OFDM transfers the multipath channel into flat-fading subchannels, it is still significantly affected by the type of the channel. We are aiming to improve the performance of OFDM over multipath channels to make it as close as possible to that over the AWGN channel. It is note worthy noting that in this thesis we usually stop at level of 10^{-4} BER as it requires very long time to simulate results that can come below this level.

2.6 Up/Down Converters

In digital communication, a carrier frequency that usually much greater than the signal bandwidth is used to carry the information signal from the transmitter side to the receiver side passing through the channel. The signal at the transmitter is

called baseband signal while it is up-converted to bandpass signal to be transmitted through the media, it follows that, at the receiver side, this passband signal is then down converted to base-band signal. In practise, the local oscillators that used to generate the carrier frequency for up and down conversion are not perfectly synchronized, hence, carrier frequency offset (CFO) which leads to significant performance impairment is generated within the OFDM system.

2.7 Peak-to-average power ratio (PAPR)

The PAPR in the transmitted signal of the OFDM systems is considered one of the main problems plaguing the OFDM systems, which arises from the addition of a large number of statistically independent symbols. Suppose the input data symbols S_m ($m = 0, 1, \dots, N - 1$) are statistically independent and identically distributed (i.i.d), i.e. the real part S_m^I and the imaginary part S_m^Q are uncorrelated and orthogonal. Then, based on the central limit theorem, when N is considerably large, the distribution of both S_m^I and S_m^Q approach Gaussian distribution with zero-mean [76], and its power is given as

$$E_s = \frac{1}{2}E [|S_m^I|^2 + |S_m^Q|^2], \quad (2.38)$$

where $E[s]$ represents the expected value of the random variable s . The basic cause of the high PAPR in the OFDM signal is the Gaussian signal distribution that arises due to the (IFFT, IDCT or ICT) operation. The PAPR for a given OFDM block can be written as

$$PAPR \{s_k\} = \frac{\max_{0 \leq k \leq N-1} |s_k|^2}{E [|s_k|^2]}, \quad (2.39)$$

where $\max_{0 \leq k \leq N-1}$ denotes the maximum instantaneous power ratio and $E [|s_k|^2]$ denotes the average power of the signal. In the case of the DFT-OFDM,

$$s_k = \frac{1}{\sqrt{N}} \sum_{m=0}^{N-1} S_m e^{j \frac{2\pi km}{N}} \quad (2.40)$$

then $\max_{0 \leq k \leq N-1} |x_k|^2 \leq N|x_k|_{max}^2$ and $E[|s_k|^2] = E[|S_m|^2]$ and the PAPR can be computed easily and upper bounded as

$$PAPR\{s_k\} \leq N \frac{|S_m|_{max}^2}{E[|S_m|^2]} \quad (2.41)$$

In (2.41), equality is attained at $k = 0$ where all the sub-symbols have the same phase. In particular, each of the N output samples from the IDCT or the IFFT operation involves the sum of N data symbols.

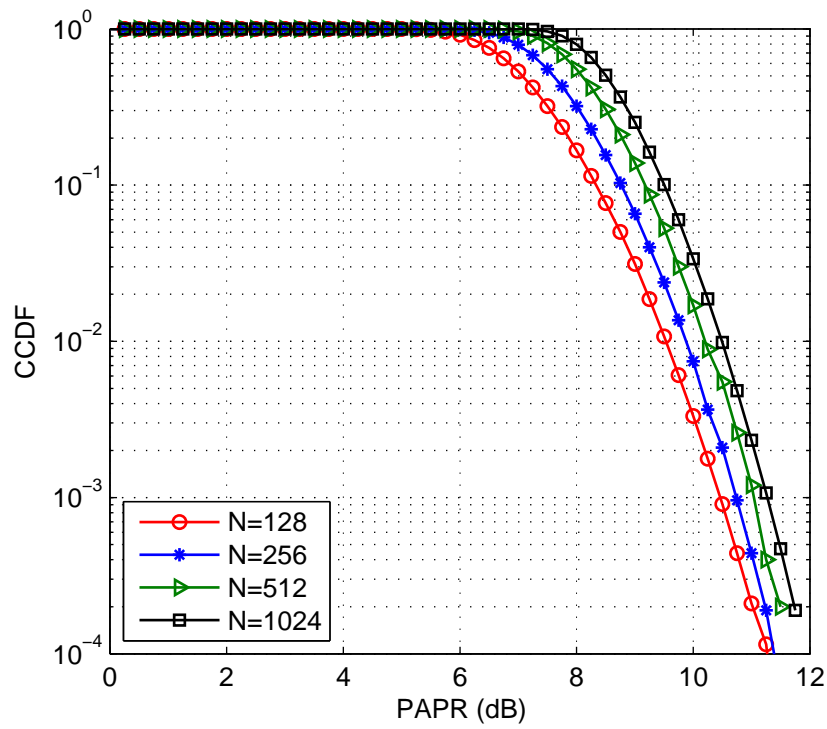
In order to have an awareness and intuitive view of the PAPR statistics, complementary cumulative density function (CCDF) was investigated for the conventional OFDM signal when the 16-QAM and QPSK modulations are used and different number of subcarriers as shown in Fig 2.10. Also to ensure the reliability of computer simulations, 100 000 OFDM frames were generated to obtain each PAPR value. It is observed from Figs. 2.10(a) and 2.10(b) that the PAPR proportional with the number of subcarriers where as large the number of subcarriers is, as high the PAPR of the OFDM signal.

For the case of the DCT-OFDM, the CCDF of the transmitted signal is shown in Figs. 2.11(a) and 2.11(b) for both the 16-QAM and the QPSK modulations. It can be seen from Fig. 2.11 that the PAPR of the DCT-OFDM system is the same of that of the conventional OFDM for the same number of subcarriers.

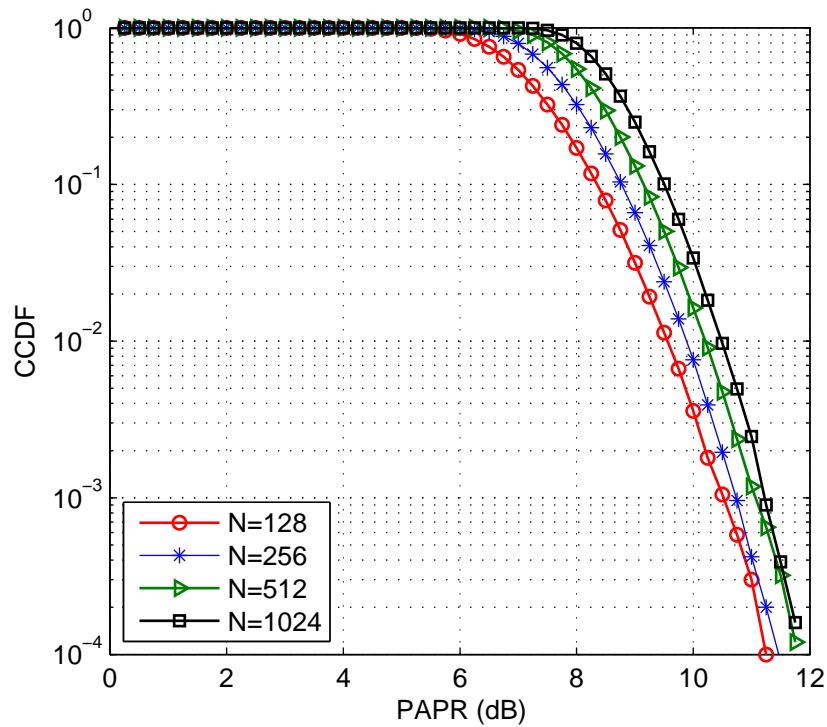
2.8 Sensitivity to the Carrier Frequency Offset (CFO)

Carrier frequency offset CFO that is caused by frequency mismatch of local oscillators has significant effects on the BER performance of OFDM systems as it produces inter-carrier interference (ICI) that destroys the orthogonality of the subcarriers [94] and [95]. As a result, it is so important to investigate the validity of the proposed system in the presence of CFO. The received signal at the receiver side in the presence of the CFO could be expressed by matrix form as

$$\begin{aligned} \mathbf{y} &= \mathbf{\Upsilon} \mathbf{H} \mathbf{s} + \mathbf{v}, \\ &= \mathbf{\Upsilon} \mathbf{H} \mathbf{F}^{\mathbb{H}} \mathbf{S} + \mathbf{v}. \end{aligned} \quad (2.42)$$

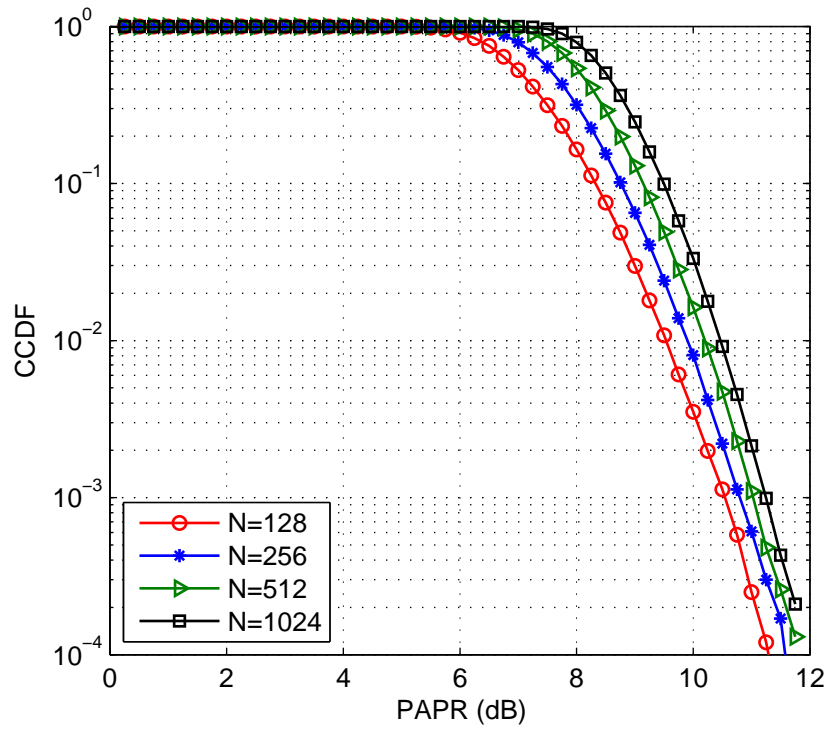


(a) 16-QAM.

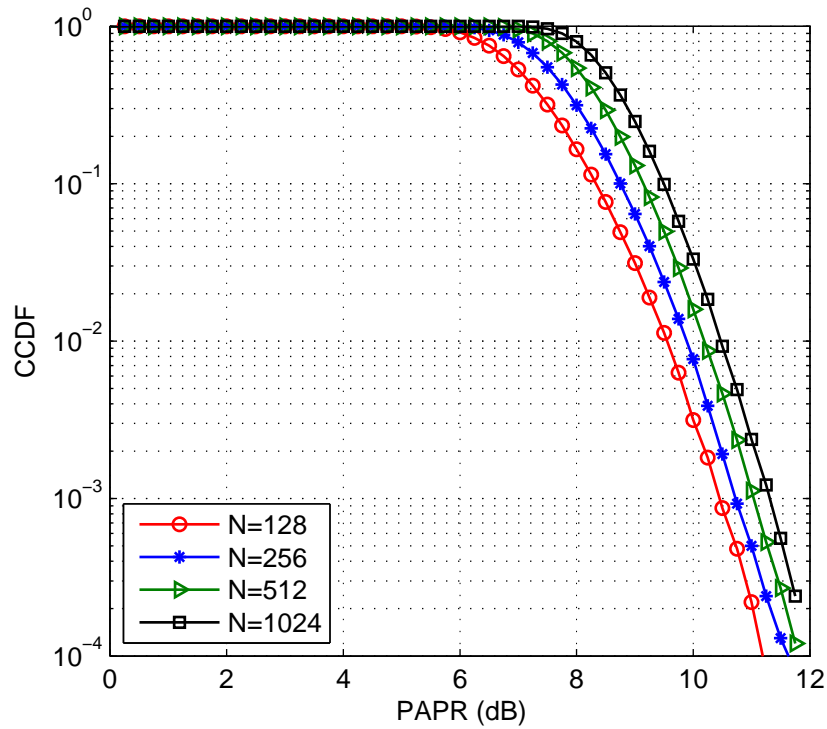


(b) QPSK.

Figure 2.10: PAPR performance of the conventional OFDM for $N = 128, 256, 512$ and 1024 , using (a: 16-QAM modulation and b: QPSK modulation).



(a) 16-QAM.



(b) QPSK.

Figure 2.11: PAPR performance of the DCT-OFDM for $N = 128, 256, 512$ and 1024 , using (a: 16-QAM modulation and b: QPSK modulation).

In (2.42), \mathbf{Y} is a diagonal matrix, the elements of the diagonal are given as $e^{j\frac{2\pi\epsilon(0:N-1)}{N}}$, ϵ is the CFO normalized to the subcarrier spacing, and \mathbf{H} is the channel matrix given in (2.15). Because of the CP, the channel matrix \mathbf{H} becomes a circulant matrix and it is diagonalized by pre and post multiplications by \mathbf{F}^{H} and \mathbf{F} . That the received signal after the DFT transformation can be written as

$$\begin{aligned}\mathbf{Y} &= \mathbf{F}\mathbf{Y}\mathbf{H}\mathbf{F}^{\text{H}}\mathbf{S} + \mathbf{F}\mathbf{v}, \\ &= \mathbf{F}\mathbf{Y}\mathbf{F}^{\text{H}}\mathbf{F}\mathbf{H}\mathbf{F}^{\text{H}}\mathbf{S} + \mathbf{\Omega}, \\ &= \mathbf{\Pi}\bar{\mathbf{H}}\mathbf{S} + \mathbf{\Omega}.\end{aligned}\tag{2.43}$$

where $\bar{\mathbf{H}} = \mathbf{F}\mathbf{H}\mathbf{F}^{\text{H}}$ is a diagonal matrix, its diagonal elements are the frequency domain representation of the channel impulse response, $H_n = \sum_{l=0}^{L-1} h_l e^{-j\frac{2\pi nl}{N}}$ and $\mathbf{\Pi} = \mathbf{F}\mathbf{Y}\mathbf{F}^{\text{H}}$ denotes the ICI matrix.

Fig. 2.12 shows the simulation results of the BER performance of the conventional OFDM system over ITU pedestrian B channel and in the presence of the CFO. It is obvious from Fig. 2.12 that the OFDM system is very sensitive to the CFO which some times consider as a type of Doppler shift as it cause rapid changes in the channel impulse response [31].

2.9 Conclusion

The mathematical dimensions of the OFDM system have been revealed in this chapter. Cyclic prefix (CP) or zero-padding (ZP) guard interval could be used in the OFDM systems to mitigate the effects of the ISI. Single-tap equalizer is applicable in the case of the CP whereas it is not applicable in the case of the ZP. It has also been shown that the performance of the OFDM system is sensitive to the type of channel, carrier frequency offset and the PAPR of the OFDM signal.

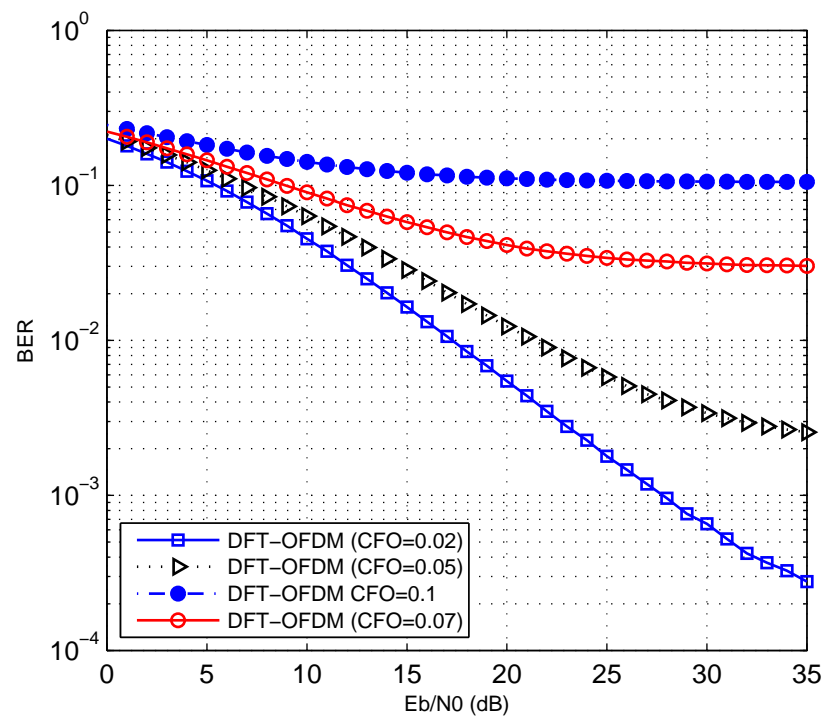


Figure 2.12: BER performance of the conventional OFDM system in the presence of the CFO.

Chapter 3

Novel Efficient OFDM Systems Based on Trigonometric Transforms

3.1 Introduction

DCT based OFDM system has proved itself as a possible alternative candidate to the conventional DFT based OFDM system. Hence, this chapter provides two new OFDM systems similar in principle but different in complexity. The two proposed OFDM systems are based on the DCT and utilize the WHT as a channel independent precoder. The first system employs the two transforms (WHT-DCT) separately as a cascading device. In the second scheme, a low computational complexity **C**-transform (a method of obtaining the DCT via the WHT) proposed in [83], is used in another OFDM system transceiver (C-OFDM). Although both the proposed OFDM schemes have the same significant diversity gain, their complexity is different. The emphasis will be on the C-OFDM as the other system obeys the same principle of the C-OFDM scheme.

The BER performance of the proposed C-OFDM system is evaluated by mathematics and simulation for different channel models, signal mappings, and under zero-padding and MMSE detection. The results are compared with that of the DCT based OFDM (DCT-OFDM) and the conventional OFDM, providing that, over multipath channels, the new C-OFDM system outperforms the OFDMs that are based on the DCT and the DFT. This can be attributed to the fact that the

information symbols are spread out over other subcarriers by the WHT, mitigating the deleterious effect of deep notches in the channel spectral. However, this phenomenon is not exhibited in the DFT-OFDM system and the DCT-OFDM system counterparts. The **C**-transform has also been found to reduce the PAPR of the OFDM signal without affecting the average value.

In contrast to the conventional OFDM system that based on the DFT, when real valued modulation such as binary-phase-shift keying (BPSK) or pulse-amplitude-modulation (PAM) is used, the C-OFDM system can avoid in-phase/quadrature phase (IQ) imbalance problems discussed in [96], which are considered one of the weaknesses in the DFT-OFDM systems. The new C-OFDM can also be used with complex valued constellation as it is considered in this chapter for the QPSK and the 16-QAM modulations.

3.2 WHT-Precoded DCT-OFDM system

The system block diagram of the proposed WHT-DCT-OFDM system is shown in Fig. 3.1. In order to ensure symbol recovery regardless of the channel zero locations in addition to reduce the intersymbol interference (ISI), zero padding (ZP) guard interval is used in our proposed scheme. MMSE detection is used at the receiver side to compensate for the channel effects. Complex modulation such as the 16-QAM or the QPSK is used where the WHT/DCT is used twice in the transmitter and receiver, one for the real part whilst the other is for the imaginary part of the complex information symbols. However, WHT-IDCT/DCT-IWHT blocks in the both transmitter and receiver should be used only once when a real modulation format such as the BPSK is used.

Fig. 3.2 shows the power spectral density (PSD) of the conventional OFDM, DCT-OFDM, and the WHT precoded DCT-OFDM systems all for the 16-QAM modulation. It is clear that both the DCT-OFDM and the WHT-DCT-OFDM systems have the same PSD shape.

Consider block-by-block transmission where each N data symbols are transmitted as a block. The binary data, b_n , are first mapped into complex modulated data symbols, $S_n = S_n^I + jS_n^Q$, using the M-QAM or the M-PSK modulation. These data symbols are serial-to-parallel (S/P) converted and then split into real and imaginary

parts. Each part is then passed through the same procedure to produce the OFDM signal. These symbols of length N is then processed by the WHT and this can be mathematically expressed as

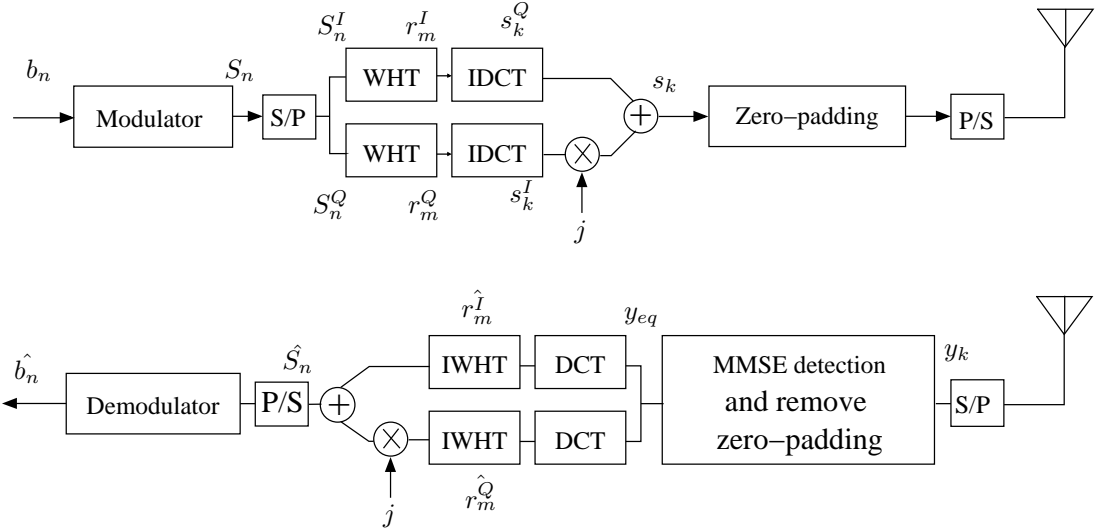


Figure 3.1: Proposed WHT-DCT-OFDM system block diagram.

$$r_m = \mathbf{W}_m \mathbf{S}, \quad (3.1)$$

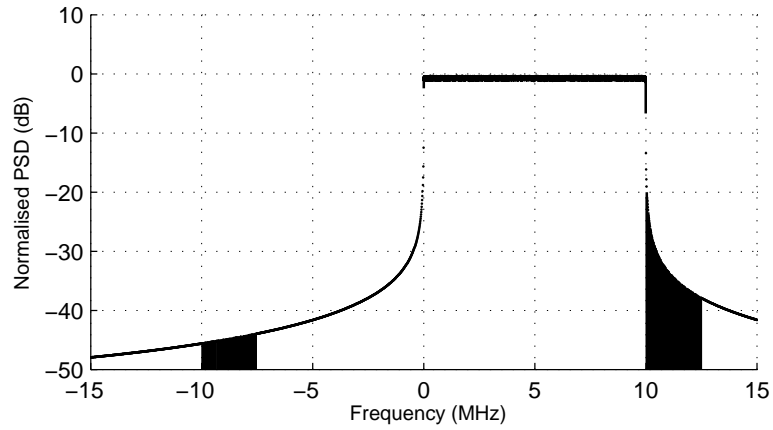
where \mathbf{W}_m denotes the m^{th} row of the Walsh-Hadamard matrix (\mathbf{W}) which is given, for $N = 8$, as

$$\mathbf{W}_8 = \begin{bmatrix} 1 & 1 & 1 & 1 & 1 & 1 & 1 & 1 \\ 1 & -1 & 1 & -1 & 1 & -1 & 1 & -1 \\ 1 & 1 & -1 & -1 & 1 & 1 & -1 & -1 \\ 1 & -1 & -1 & 1 & 1 & -1 & -1 & 1 \\ 1 & 1 & 1 & 1 & -1 & -1 & -1 & -1 \\ 1 & -1 & 1 & -1 & -1 & 1 & -1 & 1 \\ 1 & 1 & -1 & -1 & -1 & -1 & 1 & 1 \\ 1 & -1 & -1 & 1 & -1 & 1 & 1 & -1 \end{bmatrix}. \quad (3.2)$$

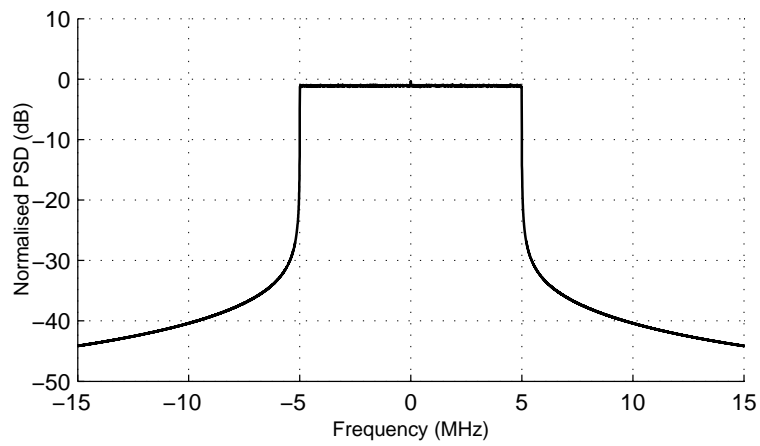
In matrix form, \mathbf{r} can be written as

$$\mathbf{r} = \mathbf{W} \mathbf{S}. \quad (3.3)$$

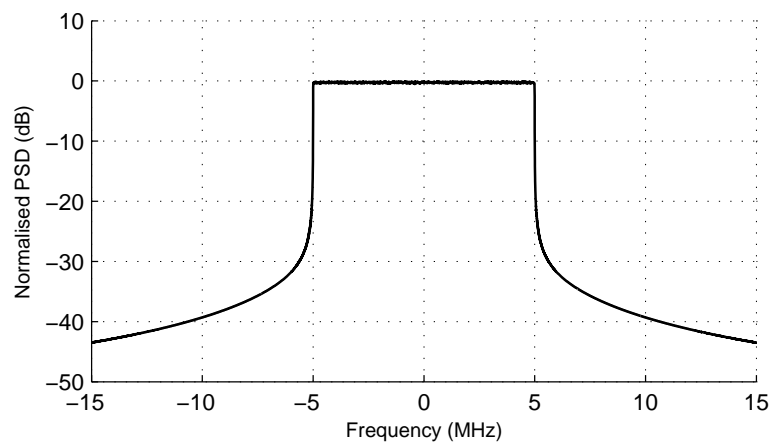
It follows that, these output samples modulate N different subcarriers using the



(a) Power spectral density of IFFT.



(b) Power spectral density of IDCT.



(c) Power spectral density of WHT-IDCT.

Figure 3.2: Power spectral densities of the DFT, the DCT and the WHT-IDCT OFDM systems.

IDCT as

$$s_k = \sqrt{\frac{2}{N}} \sum_{m=0}^{N-1} \alpha_m r_m \cos \left[\frac{\pi (2k+1)m}{2N} \right], \quad (3.4)$$

where α_m is equal to 1 only when $m = 0$ and equal to $\frac{1}{\sqrt{2}}$ otherwise. The signal \mathbf{s} can be rewritten in matrix form as

$$\begin{aligned} \mathbf{s}^I &= \mathbf{D}^T \mathbf{W} \mathbf{S}^I, \\ \mathbf{s}^Q &= \mathbf{D}^T \mathbf{W} \mathbf{S}^Q, \end{aligned} \quad (3.5)$$

where \mathbf{s} and \mathbf{S} are $N \times 1$ vectors, $(\cdot)^I$ and $(\cdot)^Q$ denote the real and imaginary components respectively, $(\cdot)^T$ is the transpose operation and \mathbf{D} is the DCT matrix. These real and imaginary parts are then made complex to generate the complex OFDM signal, $\mathbf{s} = \mathbf{s}^I + j\mathbf{s}^Q$, where $j = \sqrt{-1}$. To prevent the intersymbol interference (ISI), the OFDM signal is zero-padded with N_g samples, must be larger than or equal to the length of the channel (maximum channel delay). The resulting $N_t \times 1$ vector ($N_t = N + N_g$) is then given as

$$\mathbf{u}^I = \mathbf{\Psi}_{zp} \mathbf{s}^I, \quad (3.6)$$

where $\mathbf{\Psi}_{zp}$ was defined in (2.18) in chapter two as $\mathbf{\Psi}_{zp} = [\mathbf{I}_N \mathbf{0}_{N \times N_g}]^T$ is an $N_t \times N$ zero-padding matrix, \mathbf{I}_N is an N dimensions identity matrix and $\mathbf{0}_{N \times N_g}$ is an $N \times N_g$ zeros matrix. The entries of the resulting redundant block are finally sent sequentially through the channel. The complexity of the WHT-DCT can be reduced by using a transform known as **C**-transform which will be presented in the next section.

3.3 C Transform Based OFDM System

In this section, the **C**-transform (a unitary transform combines the effects of the WHT and the DCT) proposed in [83] is utilized in implementation of a novel OFDM system. The proposed C-OFDM scheme block diagram for complex data constellation is shown in Fig. 3.3. It shows that the zero-padding guard interval scheme is used instead of the conventional cyclic prefix (CP) together with an MMSE [31] detection to compensate for the channel effects. In this work, we are adopting the ITU pedestrian B and vehicular A channel models which vary form each OFDM

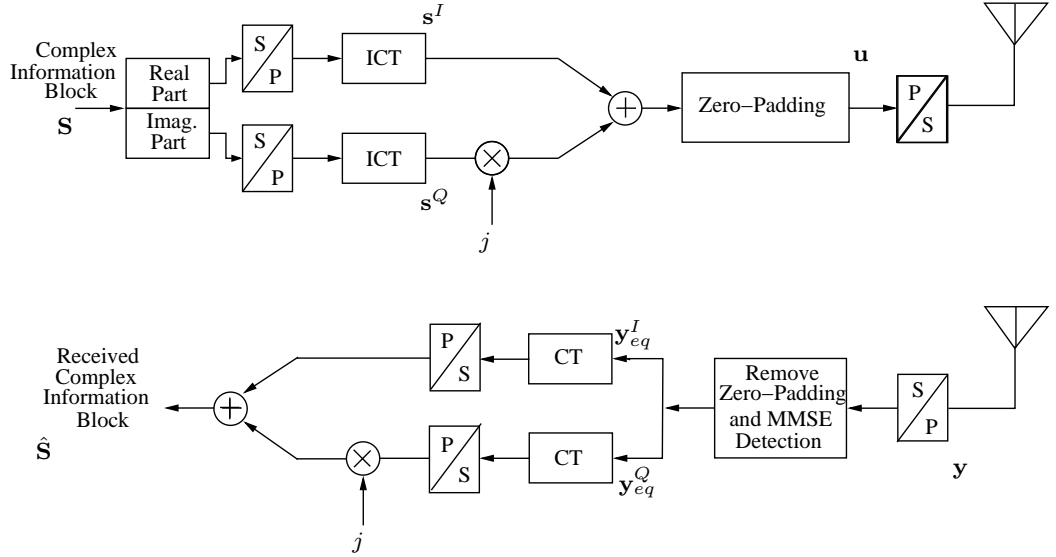


Figure 3.3: C-OFDM system block diagram when complex signalling format is used.

symbol to another whilst it is constant during each single OFDM symbol.

Based on the specific constellation format, the input data is first mapped into real or complex modulated symbols S_m , ($m = 0, 1, 2, \dots, N - 1$). We denote the block of data in a vector form as

$$\mathbf{S}^T = [S_0, S_1, \dots, S_{N-1}], \quad (3.7)$$

where \mathbf{S} is an $(N \times 1)$ vector represents the information symbols. These data symbols then modulate N different subcarriers by using inverse \mathbf{C} -transform (ICT) and the resulting samples would be expressed as: first, the data symbols that drawn from complex or real modulation format are transformed by the WHT transform as

$$r_n = \frac{1}{\sqrt{N}} \sum_{m=0}^{N-1} S_m (-1)^{\mu_{m,n}}, \quad (3.8)$$

where

$$\mu_{m,n} = \sum_{j=1}^{N_1} m_j \odot n_j. \quad (3.9)$$

In (3.9), $m_j \odot n_j$ denotes the j^{th} bit-by-bit product of the binary representation of the integers m_j and n_j (AND operation between the bits of the binary representation of m and n) while N_1 , is the number of binary digits in each index. Then these output samples modulate N different subcarriers as

$$s_k^{C-OFDM} = \frac{1}{\sqrt{N}} \sum_{n=0}^{N-1} r_n \hat{D}_{kn}. \quad (3.10)$$

Substitute r_n in (3.8) into (3.10) yields

$$s_k^{C-OFDM} = \frac{1}{N} \sum_{n=0}^{N-1} \sum_{m=0}^{N-1} S_m (-1)^{\mu_{m,n}} \hat{D}_{kn}. \quad (3.11)$$

In (3.11), \hat{D}_{kn} is the k^{th} row and n^{th} column element of the $\hat{\mathbf{D}}^T$ matrix and it is given as

$$\hat{\mathbf{D}} = \mathbf{\Gamma} \mathbf{D}^T \mathbf{\Phi}, \quad (3.12)$$

where $\mathbf{\Gamma}$ and $\mathbf{\Phi}$ are the Gray-reverse-order (GRO) matrix where each two successive values are differ in only one bit, and the bit-reverse-order (BRO) matrix respectively. It follows that, (3.11) can be written as

$$s_k^{C-OFDM} = \frac{1}{N} \sum_{m=0}^{N-1} S_m \sum_{n=0}^{N-1} (-1)^{\mu_{m,n}} \hat{D}_{kn} \quad (3.13a)$$

$$= \frac{1}{N} \sum_{m=0}^{N-1} S_m C_{km}, \quad (3.13b)$$

where $C_{km} = \sum_{n=0}^{N-1} (-1)^{\mu_{m,n}} \hat{D}_{kn}$ is the k^{th} row and m^{th} column element of the inverse \mathbf{C} -transform. In matrix form, (3.13b) can be written as

$$\mathbf{s}^{C-OFDM} = \hat{\mathbf{D}}^T \mathbf{W} \mathbf{S}, \quad (3.14a)$$

$$= \mathbf{C}^T \mathbf{S}, \quad (3.14b)$$

In (3.14b), \mathbf{s} is an $N \times 1$ vector represents the OFDM symbol and \mathbf{W}_N denotes the WHT matrix of order N . It is worth mentioning here that the GRO of the rows and BRO of the columns are applied to the \mathbf{D}^T to derive the fast algorithm for the ICT. Consequently, the $\hat{\mathbf{D}}^T$ can be written as a function of its lower order matrices as

$$\hat{\mathbf{D}}_N^T = \begin{bmatrix} \mathbf{J}_{\frac{N}{2}} & \mathbf{J}_{\frac{N}{2}} \\ \mathbf{K}_{\frac{N}{2}} & -\mathbf{K}_{\frac{N}{2}} \end{bmatrix}. \quad (3.15)$$

On the other hand, \mathbf{W} of size $N = 2^n$, where n is an integer, can be expressed as

$$\begin{aligned} \mathbf{W}_N &= \otimes_{i=1}^n \mathbf{W}_2, \\ &= \overbrace{\mathbf{W}_2 \otimes \mathbf{W}_2 \otimes \cdots \otimes \mathbf{W}_2}^n, \end{aligned} \quad (3.16)$$

where $\mathbf{W}_2 = \begin{bmatrix} 1 & 1 \\ 1 & -1 \end{bmatrix}$ is the WHT of size 2, and \otimes is the Kronecker product. Accordingly, the WHT matrix could be written in lower order matrices as

$$\mathbf{W}_N = \begin{bmatrix} \mathbf{W}_{\frac{N}{2}} & \mathbf{W}_{\frac{N}{2}} \\ \mathbf{W}_{\frac{N}{2}} & -\mathbf{W}_{\frac{N}{2}} \end{bmatrix}. \quad (3.17)$$

Therefore the ICT can be written as

$$\mathbf{C}_N = \begin{bmatrix} 2\mathbf{J}_{\frac{N}{2}}\mathbf{W}_{\frac{N}{2}} & 0 \\ 0 & 2\mathbf{K}_{\frac{N}{2}}\mathbf{W}_{\frac{N}{2}} \end{bmatrix}. \quad (3.18)$$

For clarity, the ICT matrix for $N = 8$ is shown in bellow:

$$\mathbf{C}_8^T = \begin{bmatrix} 1 & 0 & . & . & . & . & . & . \\ 0 & 1 & 0 & . & . & . & . & . \\ 0 & 0.9239 & 0.3827 & 0 & . & . & . & . \\ . & -0.3827 & 0.9239 & 0 & . & . & . & . \\ . & . & . & 0.9061 & -0.0747 & 0.3753 & 0.1802 & . \\ . & . & . & 0.2126 & 0.7682 & -0.5133 & 0.3182 & . \\ . & . & . & -0.3182 & 0.5133 & 0.7682 & 0.2126 & . \\ . & . & . & -0.1802 & -0.3753 & -0.0747 & 0.9061 & . \end{bmatrix}, \quad (3.19)$$

and for forward C-transform, for $N = 8$, is given as

$$\mathbf{C}_8 = \begin{bmatrix} 1 & 0 & . & . & . & . & . & . \\ 0 & 1 & 0 & . & . & . & . & . \\ 0 & 0.9239 & -0.3827 & 0 & . & . & . & . \\ . & 0.3827 & 0.9239 & 0 & . & . & . & . \\ . & . & . & 0.9061 & 0.2126 & -0.3182 & -0.1802 & . \\ . & . & . & -0.0747 & 0.7682 & 0.5133 & -0.3753 & . \\ . & . & . & 0.3753 & -0.5133 & 0.7682 & -0.0747 & . \\ . & . & . & 0.1802 & 0.3753 & 0.2126 & 0.9061 & . \end{bmatrix}. \quad (3.20)$$

3.4 Transmission Analysis

The C-OFDM system block diagram for complex data format is shown in Fig. 3.3. It can be seen that when complex input data is used, ICT should be used twice in both the transmitter and the receiver: one for the real part and the other for the imaginary part of the information symbols. However, it is used only once when real modulation format such as the BPSK or the PAM is used. In this section, we will focus on complex constellation such as the QPSK and the 16-QAM. We consider block-by-block transmission where the information symbols are divided into blocks, each of length N . For generality, we express the OFDM transmitted sequence as \mathbf{s} , disregarding whether it comes from the WHT precoded DCT-OFDM system or the C-OFDM system as the BER derivation is valid for both of them. The output $N \times 1$ C-OFDM symbol after the ICT can be expressed as

$$\mathbf{s} = \mathbf{C}^T \mathbf{S}. \quad (3.21)$$

A zero padding guard of length N_g samples which must be larger than or equal to maximum access delay to prevent intersymbol interference (ISI) is then attached to the OFDM signal. The resulting $N_t \times 1$ vector, $N_t = N + N_g$ is then given as

$$\mathbf{u}^I = \Psi_{zp} \mathbf{s}^I, \quad (3.22a)$$

$$\mathbf{u}^Q = \Psi_{zp} \mathbf{s}^Q. \quad (3.22b)$$

The entries of the resulting redundant block are sequentially sent through the channel. Assume that the channel with $L + 1$ taps, its impulse response h_k can be written as

$$\tilde{h}_k = \sum_{l=0}^L h_l \delta_{k-\tau_l}, \quad (3.23)$$

where h_l and τ_l are the l^{th} path channel fading and delay respectively, and $L + 1$ is the number of paths of the channel. The received signal is the convolution of the transmitted redundant signal, \mathbf{u} , with the channel impulse response, \tilde{h} , and

corrupted by the AWGN which can be written as

$$\begin{aligned} y_k &= \left[u_k \circledast \tilde{h}_k \right] + v_k, \\ &= \sum_{d=0}^L u_{k-d} h_d + v_k. \end{aligned} \quad (3.24)$$

In (3.24), \circledast denotes the convolution operation and v is the AWGN with zero mean and variance $\sigma_v^2 = E[v_k^2]$. Equation (3.24) can be written in more expressive way, in matrix form, as

$$\mathbf{y} = \mathbf{H}_0 \mathbf{u} + \mathbf{v}, \quad (3.25)$$

where $\mathbf{u} = \mathbf{u}^I + j\mathbf{u}^Q$ and $\mathbf{y} = \mathbf{y}^I + j\mathbf{y}^Q$ and \mathbf{y} , \mathbf{u} and \mathbf{v} are an $N_t \times 1$ vectors. In (3.25), \mathbf{H}_0 is an $N_t \times N_t$ channel convolutional Toeplitz matrix defined in [41], whose elements l^{th} $0 \leq l \leq N_t - 1$ row and p^{th} , $0 \leq p \leq N_t - 1$ column are given as $H_0(l, p) = h(l - p)$ for $0 \leq (l - p) \leq L$ and $H_0(l, p) = 0$ otherwise. Thus its matrix and it is given in (2.12) as

$$\mathbf{H}_0 = \begin{bmatrix} h_0 & 0 & 0 & 0 & \dots & 0 & 0 \\ h_1 & h_0 & 0 & 0 & \dots & 0 & 0 \\ \dots & h_1 & h_0 & 0 & \dots & 0 & 0 \\ \dots & \dots & h_1 & \dots & \dots & 0 & 0 \\ h_L & \dots & \dots & \dots & \dots & \dots & \dots \\ 0 & h_L & \dots & \dots & \dots & \dots & \dots \\ 0 & 0 & \dots & \dots & \dots & \dots & \dots \\ 0 & 0 & 0 & h_L & \dots & h_1 & h_0 \end{bmatrix}. \quad (3.26)$$

The MMSE equalizer matrix, \mathbf{G}^{MMSE} , which is given as [90]

$$\begin{aligned} \mathbf{G}^{MMSE} &= E_s \left(E_s \mathbf{H}_0^H \mathbf{H}_0 + \sigma_v^2 \mathbf{I}_{N_t} \right)^{-1} \mathbf{H}_0^H, \\ &= \left(\mathbf{H}_0^H \mathbf{H}_0 + \frac{1}{\gamma_s} \mathbf{I}_{N_t} \right)^{-1} \mathbf{H}_0^H. \end{aligned} \quad (3.27)$$

In (3.27), $E_s = E[S_k^2]$ is the signal power per symbol, σ_v^2 is the AWGN noise power and $\gamma_s = \frac{E_s}{\sigma_v^2}$ is the SNR per symbol.

The equalized signal at the receiver side can be written as

$$\mathbf{y}_{eq}^{MMSE} = \mathbf{G}^{MMSE} \mathbf{y}. \quad (3.28)$$

Substitute \mathbf{y} in (3.25) into (3.28) yields

$$\mathbf{y}_{eq}^{MMSE} = \mathbf{G}^{MMSE} \mathbf{H}_0 \mathbf{u} + \mathbf{G}^{MMSE} \mathbf{v}. \quad (3.29)$$

By using singular value decomposition (SVD) algorithm, \mathbf{H}_0 can be factorized to $\mathbf{U}\mathbf{\Lambda}\mathbf{V}^{\mathbb{H}}$ [97], consequently, $\mathbf{H}_0^{\mathbb{H}}$ is equivalent to $\mathbf{V}\mathbf{\Lambda}^{\mathbb{H}}\mathbf{U}^{\mathbb{H}}$, where $\mathbf{\Lambda}$ is an $N_t \times N_t$ diagonal matrix, its diagonal elements are the square roots of the eigenvalues of $\mathbf{H}_0^{\mathbb{H}}\mathbf{H}_0$ arranged in a descending order, \mathbf{V} is a matrix with columns equal to eigenvectors of $\mathbf{H}_0^{\mathbb{H}}\mathbf{H}_0$ while the columns of \mathbf{U} are the eigenvectors of $\mathbf{H}_0\mathbf{H}_0^{\mathbb{H}}$. Therefore, by substituting for \mathbf{H}_0 into (3.27), \mathbf{G}^{MMSE} will be given as

$$\mathbf{G}^{MMSE} = \left(\mathbf{V}\mathbf{\Lambda}^{\mathbb{H}}\mathbf{\Lambda}\mathbf{V}^{\mathbb{H}} + \frac{1}{\gamma_s} \mathbf{I}_{N_t} \right)^{-1} \mathbf{V}\mathbf{\Lambda}^{\mathbb{H}}\mathbf{U}^{\mathbb{H}}. \quad (3.30)$$

Using $(\mathbf{A}\mathbf{B})^{-1} = \mathbf{B}^{-1}\mathbf{A}^{-1}$, (3.30) can be written as

$$\mathbf{G}^{MMSE} = \left[(\mathbf{V}\mathbf{\Lambda}^{\mathbb{H}})^{-1} \left(\mathbf{V}\mathbf{\Lambda}^{\mathbb{H}}\mathbf{\Lambda}\mathbf{V}^{\mathbb{H}} + \frac{1}{\gamma_s} \mathbf{I}_{N_t} \right) \right]^{-1} \mathbf{U}^{\mathbb{H}} \quad (3.31a)$$

$$= \left[\mathbf{\Lambda}\mathbf{V}^{\mathbb{H}} + (\mathbf{V}\mathbf{\Lambda}^{\mathbb{H}})^{-1} \frac{1}{\gamma_s} \mathbf{I}_{N_t} \right]^{-1} \mathbf{U}^{\mathbb{H}}. \quad (3.31b)$$

Using the fact that $\mathbf{V}^{\mathbb{H}} = \mathbf{V}^{-1}$, the first term of (3.31b) can be written in more expressive way as:

$$\mathbf{\Lambda}\mathbf{V}^{\mathbb{H}} = \mathbf{\Lambda} \left(\mathbf{\Lambda}^{\mathbb{H}}\mathbf{\Lambda}^{\mathbb{H}^{-1}} \right) \mathbf{V}^{-1} \quad (3.32a)$$

$$= \mathbf{\Lambda}\mathbf{\Lambda}^{\mathbb{H}} \left(\mathbf{\Lambda}^{\mathbb{H}^{-1}}\mathbf{V}^{-1} \right) \quad (3.32b)$$

$$= \mathbf{\Lambda}\mathbf{\Lambda}^{\mathbb{H}} \left(\mathbf{V}\mathbf{\Lambda}^{\mathbb{H}} \right)^{-1}. \quad (3.32c)$$

Substitute of (3.32c) into (3.31b), \mathbf{G}^{MMSE} can be simplified to

$$\mathbf{G}^{MMSE} = \left[\mathbf{\Lambda} \mathbf{\Lambda}^{\mathbb{H}} (\mathbf{V} \mathbf{\Lambda}^{\mathbb{H}})^{-1} + \frac{1}{\gamma_s} \mathbf{I}_{N_t} (\mathbf{V} \mathbf{\Lambda}^{\mathbb{H}})^{-1} \right]^{-1} \mathbf{U}^{\mathbb{H}}, \quad (3.33a)$$

$$= \left[\left(\mathbf{\Lambda} \mathbf{\Lambda}^{\mathbb{H}} + \frac{1}{\gamma_s} \mathbf{I}_{N_t} \right) (\mathbf{V} \mathbf{\Lambda}^{\mathbb{H}})^{-1} \right]^{-1} \mathbf{U}^{\mathbb{H}}, \quad (3.33b)$$

$$= \mathbf{V} \mathbf{\Lambda}^{\mathbb{H}} \left(\mathbf{\Lambda} \mathbf{\Lambda}^{\mathbb{H}} + \frac{1}{\gamma_s} \mathbf{I}_{N_t} \right)^{-1} \mathbf{U}^{\mathbb{H}}. \quad (3.33c)$$

At the receiver side, the received data \mathbf{y}_{eq}^{MMSE} is first processed by \mathbf{C} -transform as follows

$$\hat{\mathbf{S}}^{MMSE} = \mathbf{C} \mathbf{\Psi}_{zp}^T \mathbf{G}^{MMSE} \mathbf{H}_0 \mathbf{\Psi}_{zp} \mathbf{s} + \mathbf{C} \mathbf{\Psi}_{zp}^T \mathbf{G}^{MMSE} \mathbf{v}. \quad (3.34)$$

Substitute for \mathbf{s} in (3.14b) into (3.34) yield

$$\hat{\mathbf{S}}^{MMSE} = \mathbf{C} \mathbf{\Psi}_{zp}^T \mathbf{G}^{MMSE} \mathbf{H}_0 \mathbf{\Psi}_{zp} \mathbf{C}^T \mathbf{S} + \mathbf{C} \mathbf{\Psi}_{zp}^T \mathbf{G}^{MMSE} \mathbf{v}. \quad (3.35)$$

The noise signal $\mathbf{e}^{MMSE} = \hat{\mathbf{S}}^{MMSE} - \mathbf{S}$ is then given as

$$\begin{aligned} \mathbf{e}^{MMSE} &= (\mathbf{C} \mathbf{\Psi}_{zp}^T \mathbf{G}^{MMSE} \mathbf{H}_0 \mathbf{\Psi}_{zp} \mathbf{C}^T - \mathbf{I}_N) \mathbf{S} \\ &+ \mathbf{C} \mathbf{\Psi}_{zp}^T \mathbf{G}^{MMSE} \mathbf{v}. \end{aligned} \quad (3.36)$$

Substitute (3.33c) in (3.36) yield

$$\begin{aligned} \mathbf{e}^{MMSE} &= \left[\mathbf{C} \mathbf{\Psi}_{zp}^T \mathbf{V} \mathbf{\Lambda}^{\mathbb{H}} \left(\mathbf{\Lambda} \mathbf{\Lambda}^{\mathbb{H}} + \frac{1}{\gamma_s} \mathbf{I}_{N_t} \right)^{-1} \mathbf{U}^{\mathbb{H}} (\mathbf{U} \mathbf{\Lambda} \mathbf{V}^{\mathbb{H}}) \mathbf{\Psi}_{zp} \mathbf{C}^T - \mathbf{I}_N \right] \mathbf{S} \\ &+ \mathbf{C} \mathbf{\Psi}_{zp}^T \mathbf{V} \mathbf{\Lambda}^{\mathbb{H}} \left(\mathbf{\Lambda} \mathbf{\Lambda}^{\mathbb{H}} + \frac{1}{\gamma_s} \mathbf{I}_{N_t} \right)^{-1} \mathbf{U}^{\mathbb{H}} \mathbf{v}. \end{aligned} \quad (3.37)$$

Since the \mathbf{C} -transform is a real transform, then $\mathbf{C}^T = \mathbf{C}^{\mathbb{H}}$. Let $\mathbf{\Delta}_{N \times N_t}$ represents the combination $\mathbf{C} \mathbf{\Psi}_{zp}^T \mathbf{V}$ which will be written as $\mathbf{\Delta}$ only without the subscript for expression simplicity and $\overline{\mathbf{\Delta}}_{N_t \times N}$ represents the matrices combination $\mathbf{V}^{\mathbb{H}} \mathbf{\Psi}_{zp} \mathbf{C}^{\mathbb{H}}$. After some manipulation, (3.37) can be written as

$$\begin{aligned} \mathbf{e}^{MMSE} &= \left[\mathbf{\Delta} \mathbf{\Lambda}^{\mathbb{H}} \left(\mathbf{\Lambda} \mathbf{\Lambda}^{\mathbb{H}} + \frac{1}{\gamma_s} \mathbf{I}_{N_t} \right)^{-1} \mathbf{\Lambda} \overline{\mathbf{\Delta}} - \mathbf{I}_N \right] \mathbf{S} \\ &+ \mathbf{\Delta} \mathbf{\Lambda}^{\mathbb{H}} \left(\mathbf{\Lambda} \mathbf{\Lambda}^{\mathbb{H}} + \frac{1}{\gamma_s} \mathbf{I}_{N_t} \right)^{-1} \mathbf{U}^{\mathbb{H}} \mathbf{v}. \end{aligned} \quad (3.38)$$

In the first term of (3.38), \mathbf{I}_N can be written as $\Delta \mathbf{I}_{N_t} \bar{\Delta}$ and (3.38) can be written as

$$\begin{aligned} \mathbf{e}^{MMSE} &= \left[\Delta \mathbf{\Lambda}^H \left(\mathbf{\Lambda} \mathbf{\Lambda}^H + \frac{1}{\gamma_s} \mathbf{I}_{N_t} \right)^{-1} \mathbf{\Lambda} \bar{\Delta} - \Delta \mathbf{I}_{N_t} \bar{\Delta} \right] \mathbf{S} \\ &+ \Delta \mathbf{\Lambda}^H \left(\mathbf{\Lambda} \mathbf{\Lambda}^H + \frac{1}{\gamma_s} \mathbf{I}_{N_t} \right)^{-1} \mathbf{U}^H \mathbf{v}. \end{aligned} \quad (3.39)$$

For first term in (3.39), Δ and $\bar{\Delta}$ can be taken out of the brackets, hence, (3.39) can be written as

$$\begin{aligned} \mathbf{e}^{MMSE} &= \Delta \left[\mathbf{\Lambda}^H \left(\mathbf{\Lambda} \mathbf{\Lambda}^H + \frac{1}{\gamma_s} \mathbf{I}_{N_t} \right)^{-1} \mathbf{\Lambda} - \mathbf{I}_{N_t} \right] \bar{\Delta} \mathbf{S} \\ &+ \Delta \mathbf{\Lambda}^H \left(\mathbf{\Lambda} \mathbf{\Lambda}^H + \frac{1}{\gamma_s} \mathbf{I}_{N_t} \right)^{-1} \mathbf{U}^H \mathbf{v}. \end{aligned} \quad (3.40)$$

In (3.40), $\left[\mathbf{\Lambda}^H \left(\mathbf{\Lambda} \mathbf{\Lambda}^H + \frac{1}{\gamma_s} \mathbf{I}_{N_t} \right)^{-1} \mathbf{\Lambda} \right] = \mathbf{\Theta}_1$, $\left[\mathbf{\Lambda}^H \left(\mathbf{\Lambda} \mathbf{\Lambda}^H + \frac{1}{\gamma_s} \mathbf{I}_{N_t} \right)^{-1} \mathbf{\Lambda} - \mathbf{I}_{N_t} \right] = \mathbf{\Theta}_2$ and $\mathbf{\Lambda}^H \left(\mathbf{\Lambda} \mathbf{\Lambda}^H + \frac{1}{\gamma_s} \mathbf{I}_{N_t} \right)^{-1} = \mathbf{\Theta}_3$ where $\mathbf{\Theta}_1$, $\mathbf{\Theta}_2$ and $\mathbf{\Theta}_3$ are diagonal matrices with their i^{th} diagonal entries are respectively given as

$$\mathbf{\Theta}_{1i} = \frac{\gamma_s |\lambda_i|^2}{\gamma_s |\lambda_i|^2 + 1}, \quad (3.41a)$$

$$\mathbf{\Theta}_{2i} = \frac{-1}{\gamma_s |\lambda_i|^2 + 1}, \quad (3.41b)$$

$$\mathbf{\Theta}_{3i} = \frac{\gamma_s |\lambda_i|}{\gamma_s |\lambda_i|^2 + 1}. \quad (3.41c)$$

Where λ_i , ($i = 0, 1, 2, \dots, N_t - 1$) is the i^{th} element of the diagonal of $\mathbf{\Lambda}$ and $\gamma_s = \frac{E_s}{\sigma_v^2}$ is the signal power (per symbol)-to-noise ratio. Therefore, (3.40) can be rewritten as

$$\mathbf{e}^{MMSE} = \Delta \mathbf{\Theta}_2 \bar{\Delta} \mathbf{S} + \Delta \mathbf{\Theta}_3 \mathbf{U}^H \mathbf{v}. \quad (3.42)$$

Similarly, $\hat{\mathbf{S}}^{MMSE}$ in (3.35) can be rewritten as

$$\hat{\mathbf{S}}^{MMSE} = \Delta \mathbf{\Theta}_1 \bar{\Delta} \mathbf{S} + \Delta \mathbf{\Theta}_3 \mathbf{U}^H \mathbf{v} \quad (3.43)$$

The total noise power at the receiver side is $E[\mathbf{e}\mathbf{e}^H] = \text{tr}(\mathbf{e}\mathbf{e}^H)$ and is given as

$$\mathcal{P}_n^{MMSE} = \text{tr} [\Delta E_s \Theta_2^2 \overline{\Delta} + \Delta \sigma_v^2 \Theta_3^2 \overline{\Delta}] \quad (3.44a)$$

$$= \text{tr} [\Delta [E_s \Theta_2^2 + \sigma_v^2 \Theta_3^2] \overline{\Delta}]. \quad (3.44b)$$

In (3.44b), $[E_s \Theta_2^2 + \sigma_v^2 \Theta_3^2]$ is a diagonal matrix can be simplified as

$$\begin{aligned} [E_s \Theta_2^2 + \sigma_v^2 \Theta_3^2]_{i,i} &= \frac{E_s}{[\gamma_s |\lambda_i|^2 + 1]^2} + \frac{\sigma_v^2 \gamma_s^2 |\lambda_i|^2}{[\gamma_s |\lambda_i|^2 + 1]^2} \\ &= \frac{E_s}{[\gamma_s |\lambda_i|^2 + 1]^2} + \frac{E_s \gamma_s |\lambda_i|^2}{[\gamma_s |\lambda_i|^2 + 1]^2} \\ &= \frac{E_s}{\gamma_s |\lambda_i|^2 + 1}. \end{aligned} \quad (3.45)$$

Let $\Theta_{4i} = \text{diag}(\frac{1}{\gamma_s |\lambda_i|^2 + 1})$ and by substituting (3.45) into (3.44b) yields

$$\mathcal{P}_n^{MMSE} = \text{tr} [\Delta E_s \Theta_4 \overline{\Delta}]. \quad (3.46)$$

The total power of the received signal is $\mathcal{P}_s^{MMSE} = E[\hat{\mathbf{S}}\hat{\mathbf{S}}^H] = \text{tr}(\hat{\mathbf{S}}\hat{\mathbf{S}}^H)$ is given as

$$\mathcal{P}_s^{MMSE} = \text{tr} [\Delta E_s \Theta_1^2 \overline{\Delta} + \Delta \sigma_v^2 \Theta_3^2 \overline{\Delta}] \quad (3.47a)$$

$$= \text{tr} [\Delta [E_s \Theta_1^2 + \sigma_v^2 \Theta_3^2] \overline{\Delta}] \quad (3.47b)$$

$$= \text{tr} [\Delta E_s \Theta_1 \overline{\Delta}]. \quad (3.47c)$$

Therefore, the signal-to-noise ratio at the output of the m^{th} subchannel is given as

$$\beta_m^{MMSE} = \frac{[\Delta \Theta_1 \overline{\Delta}]_{m,m}}{[\Delta \Theta_4 \overline{\Delta}]_{m,m}}. \quad (3.48)$$

The overall BER can be given by averaging the BER for the individual subchannels and they are given for QPSK and 16-QAM respectively as:

$$P_e^{QPSK} = \frac{1}{N} \sum_{m=0}^{N-1} Q \left(\sqrt{\frac{[\Delta \Theta_1 \overline{\Delta}]_{m,m}}{[\Delta \Theta_4 \overline{\Delta}]_{m,m}}} \right), \quad (3.49)$$

and

$$P_e^{16-QAM} = \frac{3}{4N} \sum_{m=0}^{N-1} Q \left(\sqrt{\frac{[\Delta \Theta_1 \overline{\Delta}]_{m,m}}{5 [\Delta \Theta_4 \overline{\Delta}]_{m,m}}} \right). \quad (3.50)$$

Finally, the recovered transmitted bits are obtained by applying the demodulation process on the recovered complex modulated data symbols $\hat{\mathbf{S}}$. The advantages of employing the \mathbf{C} -transform in the OFDM systems can be attributed to the fact that the \mathbf{C} -transform is a compound transform gathering the effects of the WHT and the DCT transforms. Subsequently, the WHT further distributes the information symbols among the channel spectrum mitigating the effect of narrowband notches of the channel spectral as the data symbol on significantly attenuated subcarrier is not completely disappeared where it can be recovered from the other unaffected subcarriers.

It is noteworthy that the SNR approach in (3.48) is a general formula describing the BER performance of ZP-OFDM system with MMSE detection and can be applied to attain the BER performance for the DCT-OFDM or the DFT-OFDM systems simply by replacing the \mathbf{C} -transform by either the DCT or the DFT transform respectively.

3.5 Peak-to-average power ratio (PAPR)

The PAPR in the transmitted signal of the OFDM systems is considered as one of the main problems plaguing the OFDM systems, which arises from the addition of a large number of statistically independent symbols.

In chapter 2, we have explained that the superposition of the information symbols which are statistically independent is the reason of the high peak amplitude in the OFDM signal. It has been shown that in the case of the DCT-OFDM and the conventional OFDM schemes, this peak value can reach the order N when all the input information symbols are aligned in phase. However, this is not the case in the proposed C-OFDM system. This is because the \mathbf{C} -transform has a block diagonal structure, thus each N output samples from the ICT operation involves less than or equal to the sum of $\frac{N}{2}$ data symbols. Thus, the PAPR for the case of the C-OFDM system can be upper bounded as:

Suppose the input data symbols S_m ($m = 0, 1, \dots, N - 1$) are statistically independent and identically distributed (i.i.d), i.e. the real part S_m^I and the imaginary part S_m^Q are uncorrelated and orthogonal. Then, based on the central limit theorem, when N is considerably large, the distribution of both S_m^I and S_m^Q approaches

Gaussian distribution with zero mean [76] where

$$E_s = \frac{1}{2} E [|S_m^I|^2 + |S_m^Q|^2], \quad (3.51)$$

where $E[s]$ represents the expected value of the random variable s . The basic cause of the high PAPR in the OFDM signal is the Gaussian signal distribution that arises due to the (IFFT, IDCT or ICT) operation. The PAPR for a given OFDM block can be written as

$$PAPR \{s_k\} = \frac{\max_{0 \leq k \leq N-1} |s_k|^2}{E [|s_k|^2]}, \quad (3.52)$$

where $\max_{0 \leq k \leq N-1}$ denotes the maximum instantaneous power ratio and $E [|s_k|^2]$ denotes the average power of the signal. In the case of the conventional OFDM,

$$s_k = \frac{1}{\sqrt{N}} \sum_{m=0}^{N-1} S_m e^{j \frac{2\pi km}{N}}, \quad (3.53)$$

then $\max_{0 \leq k \leq N-1} |s_k|^2 \leq N |S_m|_{max}^2$ and $E [|s_k|^2] = E [|S_m|^2]$ and the PAPR can be computed and upper bounded as

$$PAPR \{s_k\} \leq N \frac{|S_m|_{max}^2}{E [|S_m|^2]}. \quad (3.54)$$

In (3.54), equality is attained at $k = 0$ where all the sub-symbols have the same phase. In particular, each of the N output samples from the IDCT or the IFFT transformation involves the sum of N data symbols. However, this is not the case in the proposed C-OFDM system. This is because the \mathbf{C} -transform has a block-diagonal-structure, thus each of N output samples from ICT operation involves less than or equal to the sum of $\frac{N}{2}$ data symbols. Thus, the PAPR for the case of the C-OFDM system can be upper bounded as

$$PAPR \{s_k\} \leq \frac{N}{2} \frac{|S_n|_{max}^2}{E [|S_n|^2]}. \quad (3.55)$$

The worst case of the PAPR is of order N for the conventional OFDM and the DCT-OFDM systems whilst it is of order $\frac{N}{2}$ for the proposed C-OFDM system. In general, the worst case of the PAPR has low probability of occurrence [98] and [99]. Our simulation results showed 1 dB improvement in the PAPR for the case of the proposed C-OFDM system in comparison with that for the DCT-OFDM and the

conventional OFDM system.

3.6 System Performance in the Presence of the CFO

The proposed C-OFDM system is slightly more sensitive to the CFO than both DCT-OFDM and the conventional OFDM systems when no synchronization algorithm is applied. This is because any shift in subcarrier frequency will spread over others by the WHT. However, all the DCT-OFDM, the conventional OFDM and the C-OFDM systems completely lost their orthogonality when CFO, normalized to the subcarrier spacing, is larger than or equal to 0.1 as it will be shown later in this chapter. Therefore, several CFO estimation techniques aimed to mitigate the effects of CFO within the OFDM systems have been proposed in the last few years [100], [94] and [95]. In spite of the proposed system sensitivity to the CFO, it restores its superiority over both the DCT-OFDM and the OFDM systems when a CFO estimation algorithm is used. The proposed system's block diagram in the presence of CFO and its estimation and compensation algorithm is shown in Fig. 3.4; where the Morelli and Mengali (M&M) algorithm [100] is used. The purpose of the IFFT transform is to generate a symbol consisting of L identical parts that are used in CFO estimation. They are generated by transmitting a pseudo-noise sequence on the frequencies multiple of L/T and set the rest to zero. If the switches Sw_1 and Sw_2 are set to position 1, then it would constitute a CFO estimation operation. Subsequently, they would be changed to position 0 to activate the proposed OFDM system transmission.

3.7 Computational Complexity Analysis

For any transform to stand as a good candidate for practical communication system, its complexity needs to be evaluated. Therefore, this section evaluates the arithmetic complexity of the C-transform and compare it with the WHT-DCT, the DCT and the FFT transforms. The complexity in this chapter is based on radix-2 single butterfly implementation for both algorithms. When it comes to real time implementation like in communication systems, the FFT and the DCT are usually

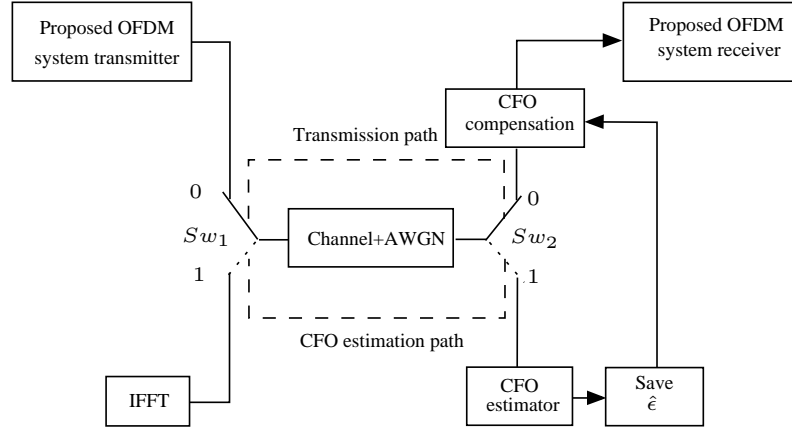


Figure 3.4: System block diagram in the presence of the CFO cancellation algorithm.

implemented in pipeline using single butterfly. In a single butterfly implementation, we only need to design one butterfly and repeat it leading to the best structure in terms of regularity, modularity, indexing and ease of implementation.

3.7.1 The C-Transform

As shown in (3.19) and (3.20), the **C**-transform has a Block Diagonal Structure (BDS) with more than $\frac{2}{3}$ of its matrix elements being zero; hence, its direct computation will involve $N^{\frac{2}{3}}$ real multiplications and $N(N-1)/3$ real additions only. Using fast algorithms, this can be reduced even further. The butterfly of transform with BDS is shown in Fig. 3.5. The total number of butterflies equal to $\frac{N}{2} \log_2 N$ and the number of trivial butterflies are given as

$$\begin{aligned} Butt_{Triv} &= \left[\frac{N}{2} + \frac{N}{4} + \frac{N}{8} + \frac{N}{16} + \dots + 1 \right] \\ &= N \left[\frac{1}{2} + \frac{1}{4} + \frac{1}{8} + \frac{1}{16} + \dots + \frac{1}{N} \right]. \end{aligned} \quad (3.56)$$

Using power series identity, (3.56) can be rewritten as

$$\begin{aligned} Butt_{Triv} &= N \left[\frac{N-1}{N} \right] \\ &= N-1. \end{aligned} \quad (3.57)$$

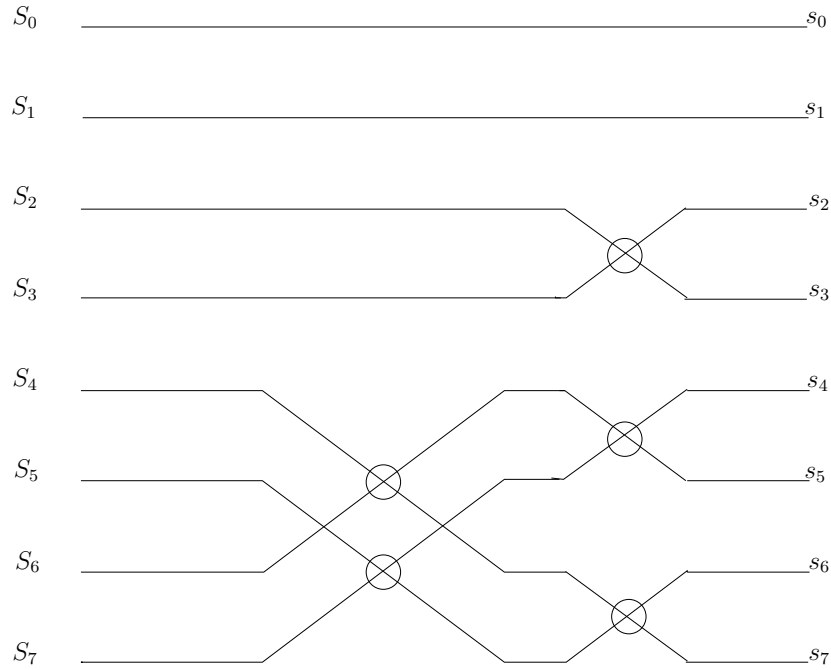
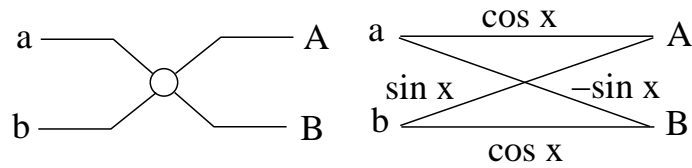
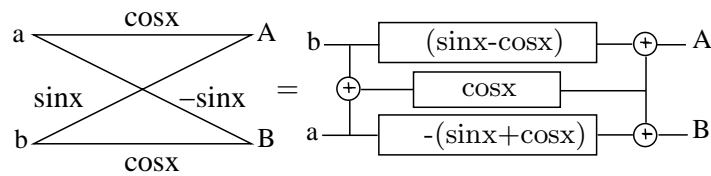


Figure 3.5: Butterfly structure of BDS transforms.



(a) C transform butterfly



(b) Modified butterfly

Figure 3.6: Butterflies of the **C**-transform:(a) C-transform butterfly, (b) Modified **C**-transform butterfly.

Thus, the total number of active butterflies of radix-2 fast algorithm for the **C**-transform is $\frac{N}{2} \log_2 N - (N - 1)$ which is given as

$$Butt_{flies} = \frac{N}{2} \log_2 N - N + 1, \tag{3.58}$$

where each butterfly can be analysed in more details as shown in Fig. 3.6

$$\begin{aligned}
 A &= a \cos x + b \sin x \\
 B &= -a \sin x + b \cos x.
 \end{aligned} \tag{3.59}$$

Each butterfly includes 4 real multiplications (R_M) and two real additions (R_A). Thus the complexity of the **C**-transform is then given as: $R_M = 2N \log_2 N - 4N + 4$ and $R_A = N \log_2 N - 2N + 2$.

The number of multiplications can be reduced as shown in Fig.3.6(b) as:

$$\begin{aligned}
 A &= (a + b) \cos x + b(\sin x - \cos x) \\
 &= a \cos x + b \cos x + b \sin x - b \cos x \\
 &= a \cos x + b \sin x
 \end{aligned} \tag{3.60}$$

$$\begin{aligned}
 B &= -a(\cos x + \sin x) + (a + b) \cos x \\
 &= -a \cos x - a \sin x + a \cos x + b \cos x \\
 &= -a \sin x + b \cos x
 \end{aligned} \tag{3.61}$$

One can easily notice that each butterfly involves 3 R_M and 3 R_A , the complexity of the **C** transform involves $R_M = \frac{3}{2}N \log_2 N - 3N + 3$ and $R_A = \frac{3}{2}N \log_2 N - 3N + 3$ and then the total number of real operations (R_O) is given as

$$R_O = 3N \log_2 N - 6N + 6 \tag{3.62}$$

It is worth mentioning that, when complex signalling is used, the arithmetic operations of **C**-transform would be twice of (3.62), one for real part and the other for imaginary part, and the overall complexity is given as

$$R_O = 6N \log_2 N - 12N + 12 \tag{3.63}$$

3.7.2 Discrete Cosine Transform (DCT)

The arithmetic complexity of fast implementation of the DCT based on single butterfly algorithm can be given as [101]: Number of real multiplications

$$R_M = \frac{N}{2} \log_2 N, \quad (3.64)$$

and number of real additions

$$R_A = N \log_2 N. \quad (3.65)$$

Thus the total number of real operation is given as

$$R_O = \frac{3N}{2} \log_2 N. \quad (3.66)$$

It is worth mentioning that when complex constellation is used such as in this work, the complexity above should be calculated twice (one for real part of the signal while the other for the imaginary part) and the arithmetic complexity will be equal to $R_O = 3N \log_2 N$

3.7.3 WHT-DCT

The arithmetic complexity of fast implementation of the WHT followed by the DCT can be given as: The WHT complexity involves only real additions, $R_A = N \log_2 N$, and no multiplications at all. The arithmetic operations of the radix-2 DCT using single butterfly algorithm is given in (3.64), (3.65) and (3.66). Then the total number of real multiplications and additions for the WHT-DCT is given by

$$R_O = \frac{5N}{2} \log_2 N \quad (3.67)$$

Same as for the case of **C**-transform, when complex constellation is used, (3.67) must be calculated twice and the arithmetic complexity will be given as

$$R_O(WHT - DCT) = 5N \log_2 N \quad (3.68)$$

Table 3.1: Comparison of Real Arithmetic Operations for the Proposed **C** Transform, DCT, WHT-DCT and FFT Transforms Under Complex Constellation Consideration.

N	CT		DCT		WHT-DCT		FFT	
	R_A	R_M	R_A	R_M	R_A	R_M	R_A	R_M
32	294	294	320	160	640	160	480	320
64	774	774	768	384	1536	384	1152	768
128	1926	1926	1792	896	3584	896	2688	1792
256	4614	4614	4096	2048	8192	2048	6144	4096
512	10758	10758	9216	4608	18432	4608	13824	9216
1024	24582	24582	20480	10240	40960	10240	30720	20480
2048	55302	55302	45056	22528	90112	22528	67584	45056
4096	122886	122886	98304	49152	196608	49152	147456	98304

3.7.4 Fast Fourier Transform (FFT)

It is worth mention that our true comparison is with DCT-OFDM system, however, comparison with FFT transform is added for further information. Considering the fact that each complex multiplication involves 4 real multiplications (R_M) and two real additions (R_A) or 3 real multiplications and 3 real additions, and each complex addition is equivalent to two real additions. The arithmetic complexity of the FFT, based on single butterfly and 4/2 implementation is given as:

$$R_M = 2N \log_2 N, \quad (3.69)$$

$$R_A = 3N \log_2 N. \quad (3.70)$$

Tables 3.1 and 3.2 show the computational complexity in terms of real additions and real multiplications and total number of operations respectively, for the **C**-transform, the DCT, the WHT-DCT and the FFT for different transform lengths N when complex constellation is considered (both the **C** transform and the WHT-DCT transform are used twice, one for the real part of the complex data while the other for the imaginary part). It is clear that the **C**-transform has lower total number of additions as well as it is better than the WHT-DCT in terms of multiplications.

Table 3.2: Total number of real operations.

N	CT R_O	DCT R_O	WHT-DCT R_O	FFT R_O
32	588	480	800	800
64	1548	1152	1920	1920
128	3852	2688	4480	4480
256	9228	6144	10240	10240
512	21516	13824	23040	23040
1024	49164	30720	51200	51200
2048	110604	67584	112640	112640
4096	245772	147456	245760	245760

3.8 Wire-line Applications of the Proposed Schemes

In this section we will examine the performance of the proposed C-OFDM in the discrete multi-tone (DMT) system as example of wire-line communication system and compare it with that of the DCT-DMT and DFT-DMT schemes. In the conventional DFT-DMT system as shown in Fig. 3.7, the input data of size N are first serial-to-parallel converted and modulated to data symbols. In order to ensure real data transmission, these modulated symbols at the input of the IFFT are forced to be Hermitian conjugate. This in turn requires a $2N \times 2N$ IFFT transform, thus $2N$ samples is the length of the transmitted signal. In other words, in order to transmit N modulated symbols, $2N$ samples are required for transmission. However, this can be completely avoided by using the proposed approach and real data modulation formats. Fig. 3.8 is a detailed block diagram for the proposed C-DMT system. Table 3.3 shows the complexity reduction of the C-DMT among the DFT-DMT as a result of avoiding the Hermitian constraint.

For the case of WHT-DCT-DMT, the ICT at the transmitter must be replaced by the WHT-IDCT and the CT at the receiver must be replaced by the IWHT-DCT. In comparison to the existed DCT-DMT system, both the proposed C-DMT and the DCT-DMT systems can avoid Hermitian constraint. However, the proposed C-DMT system appears more robust to multipath fading channels as it includes the WHT in its structure which further distributes the information symbols over the entire bandwidth.

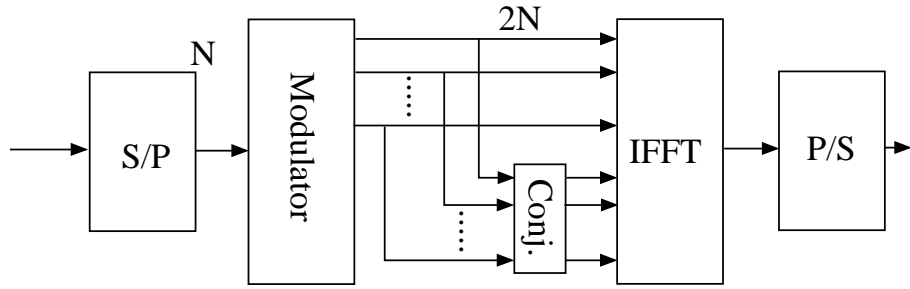


Figure 3.7: Transmitter block diagram of the DFT-DMT system.

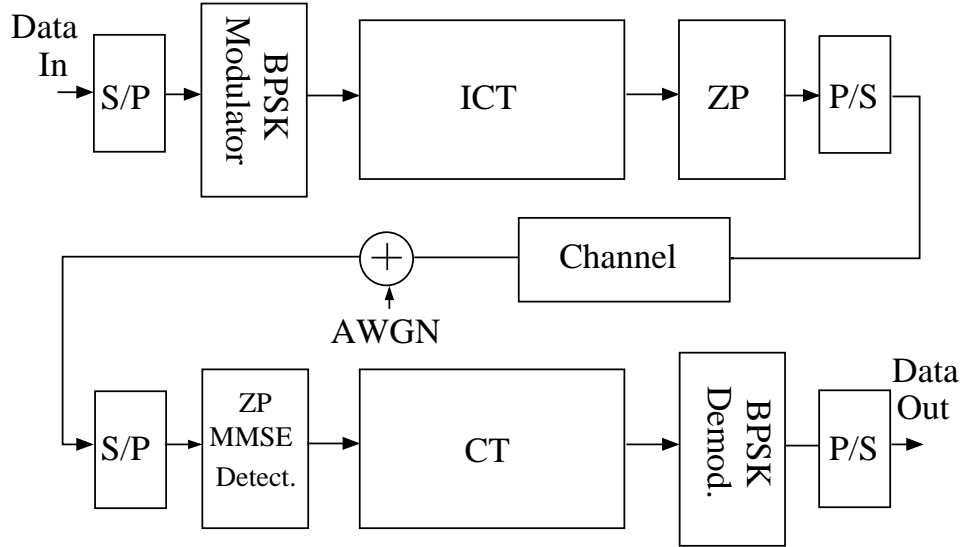


Figure 3.8: Transmitter block diagram of the C-DMT system.

Table 3.3: Comparison of real arithmetic operations of the proposed CT, the DCT and the FFT based-DMT systems.

N	DCT R_O	FFT R_O	CT R_O
256	3841	17936	5889

3.9 Simulation Results And Discussion

This section presents some results to demonstrate the performance of the proposed C-OFDM and compares them with that of the DCT-OFDM and the conventional OFDM systems. It should be noted that the true comparison should be with the DCT-OFDM system, however we added the comparison with the conventional OFDM system for more information.

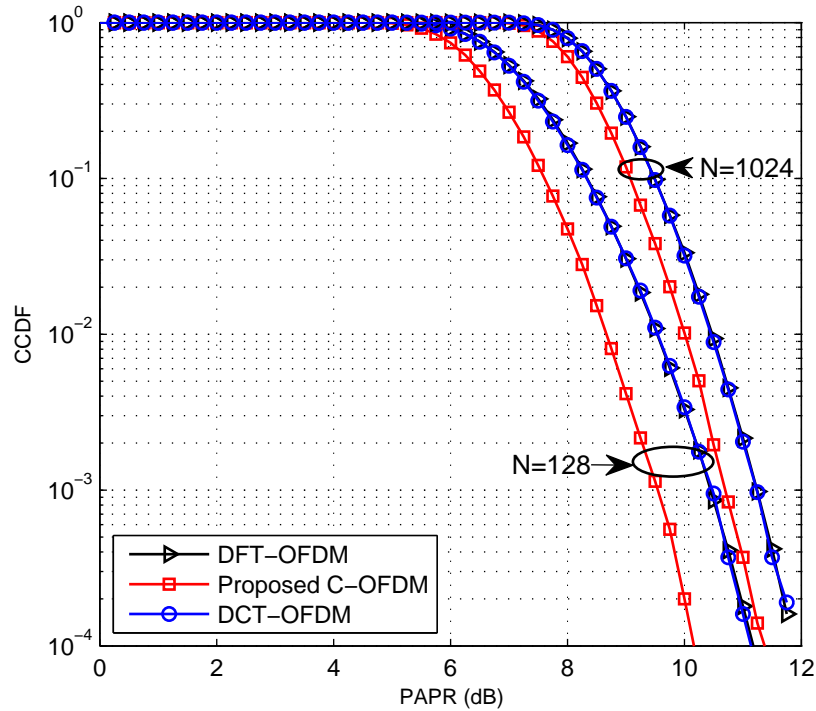


Figure 3.9: PAPR performance of the proposed C-OFDM, DCT-OFDM and the conventional DFT-OFDM systems using the 16-QAM modulation format, the DCT-OFDM and DFT-OFDM systems having the same graphs.

3.9.1 PAPR Reduction

A simulation was carried out for the C-OFDM, conventional OFDM and the DCT-OFDM systems, showing that the C-OFDM has the lowest PAPR for; different number of subcarriers ($N = 128$, and 1024) and 16-QAM modulation. In order to have an awareness and intuitive view of the PAPR statistics, complementary cumulative density function (CCDF) was plotted. Also to ensure the reliability of computer simulations, 100 000 OFDM symbols were generated to obtain each PAPR value. It is noted from Fig. 3.9 that the C-OFDM system has a better PAPR than the DCT-OFDM and DFT-OFDM for different numbers of subcarriers. It also shows that the DCT-OFDM system achieves the same PAPR as the conventional OFDM while the proposed C-OFDM achieved about 1 dB improvement at a CCDF of 10^{-4} . This is due to the fact that the \mathbf{C} -transform has a block-diagonal-structure that reduces the additions of the input data symbols which perform each OFDM sample.

Table 3.4: System parameters for simulations.

System Item	Parameter
Modulation	QPSK and 16-QAM
Synchronisation	Complete
Antenna type	Perfect
Channel type	AWGN, ITU pedestrian B and ITU vehicular A
Equalisation	Time domain MMSE equalizer
Number of Subcarriers (N)	1024
Guard type	ZP
Length of ZP	$\frac{N}{4}$
Bandwidth	10MHz

3.9.2 BER Performance

3.9.2.1 BER performance over AWGN Channel

The BER performance of the C-OFDM, DCT-OFDM and the conventional OFDM systems over the AWGN channel using the parameters that are given in Table 3.4 is shown in Fig 3.10. It reveals that all of these systems have the same performances over the AWGN channel. This is because the WHT does not have any effect on the AWGN noise power as it is already distributed equally among all the subchannels. Moreover, the WHT does not effect the signal power as it is unitary transform. However, the superiority of the C-OFDM system in terms of the BER performance is pronounced over multipath fading channels, which are more realistic in practical applications, providing high signal diversity and achieves significant performance gain over the conventional OFDM and DCT-OFDM systems as shown in the next section.

3.9.2.2 BER Performance over Wireless Multipath Channel

Besides the PAPR reduction, channel diversity exploitation is another advantage of adopting the C-transform in OFDM systems which is pronounced over multipath frequency selective channels. To illustrate this advantage, ITU pedestrian B and vehicular A channel models according to the WiMAX standard according to the parameters that are given in Table 3.4 above, and the ZP-MMSE detection were utilized in this work. Since the maximum channel delay is less than the guard interval, no ISI occurs in our simulations. In the case of the DCT-OFDM and DFT-

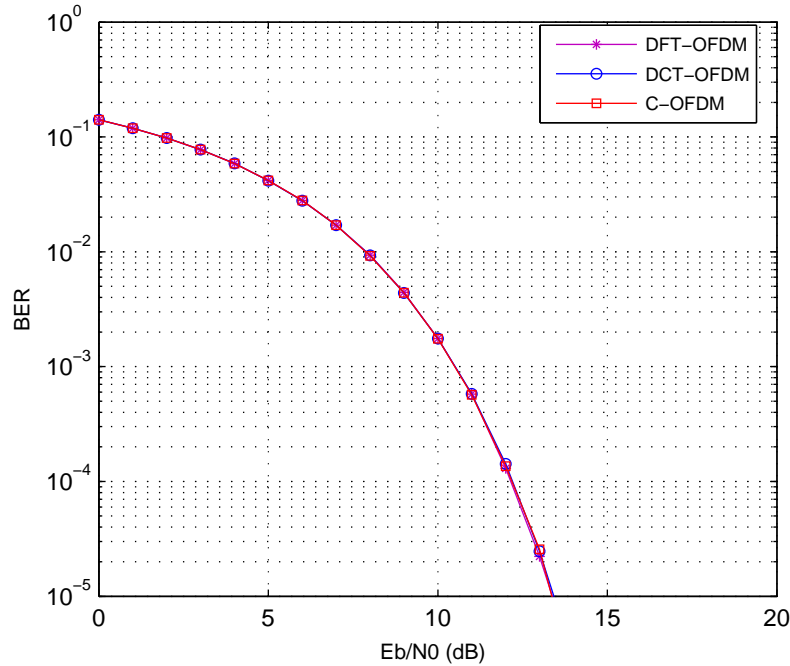


Figure 3.10: BER of the proposed C-OFDM, DCT-OFDM and DFT-OFDM systems over AWGN channel. All have the same graphs.

OFDM systems, the ICT/CT in Fig. 3.3 should be replaced by the unitary cosine transform matrix (IDCT/DCT) or unitary Fourier transform matrix (IDFT/DFT) respectively. Two signal constellations, QPSK and 16-QAM, were used in this work. The theoretical results are obtained by using the BER formulas that were given in (3.49) for the case of QPSK and (3.50) for the case of 16-QAM

It is observed from Figs. 3.11-3.14 that the theoretical BER performance results are in strong accord with the simulation results, providing that the proposed C-OFDM significantly outperforms both the DCT-OFDM and the OFDM systems under; pedestrian B and vehicular A channel models, and for QPSK and 16-QAM modulation formats.

The BER performance of the ZP-C-OFDM, ZP-DCT-OFDM and ZP-DFT-OFDM systems over the ITU class B pedestrian channel were compared, all for 16-QAM and QPSK modulation formats are shown in Figs. 3.11 and 3.12 respectively. It is evident that at 10^{-4} BER, the proposed C-OFDM system achieves about 10 dB E_b/N_0 gain over the ZP-DCT-OFDM and ZP-DFT-OFDM systems. This confirms our early hypothesis that the WHT, this in turns **C**-transform, combines the information symbols over many transmitted OFDM samples which leads to this high gain in E_b/N_0 . However, this gain is not achievable by the DCT-OFDM

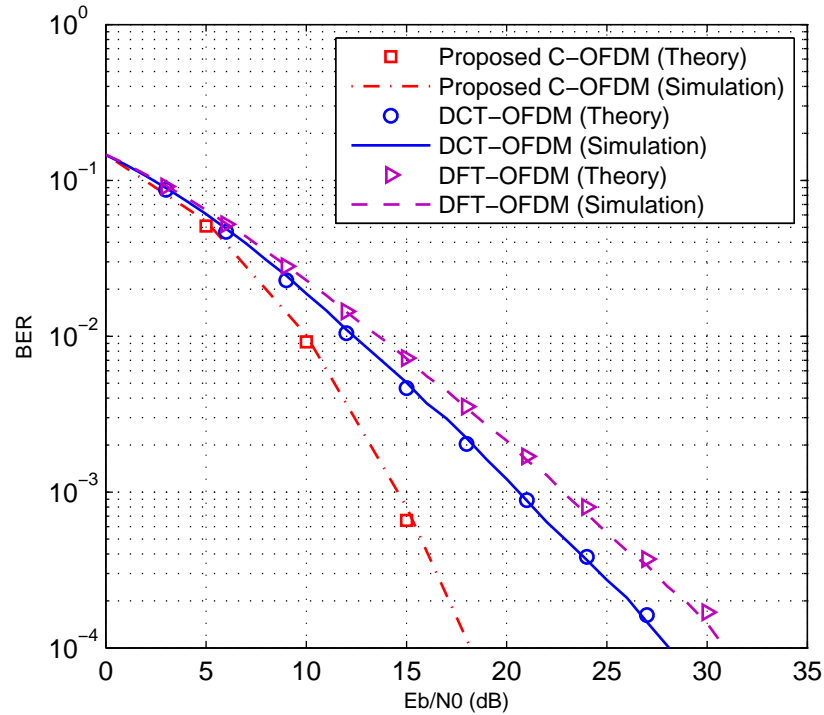


Figure 3.11: BER performance of the proposed C-OFDM, DCT-OFDM and DFT-OFDM systems over the ITU Pedestrian B channel and for the QPSK modulation, theory and simulation are in good agreement.

system as it lacks to the WHT in its structure.

Over the ITU vehicular A channel model, it is revealed from Figs. 3.13 and 3.14 that, for QPSK and 16-QAM modulation formats, the C-OFDM scheme still retains the valuable BER improvement in comparison with the DCT-OFDM and the DFT-OFDM schemes.

3.9.2.3 BER Performance In the Presence of the CFO

The BER performance in the presence of the proposed C-OFDM system, in the presence of the CFO, is compared with those of the DCT-OFDM and the DFT-OFDM systems with and without frequency synchronization algorithm is investigated in this subsection.

Fig. 3.15 shows the BER performance of the proposed OFDM, DCT-OFDM and DFT-OFDM systems when no CFO estimation algorithm is applied and for different values of the normalized CFO ϵ ($\epsilon = 0.03, 0.06$ and 0.1). It is evident that the proposed system is superior than others for small ϵ around 0.03 while it has a worse BER for ϵ around 0.06 . However, it is also evident that all of the

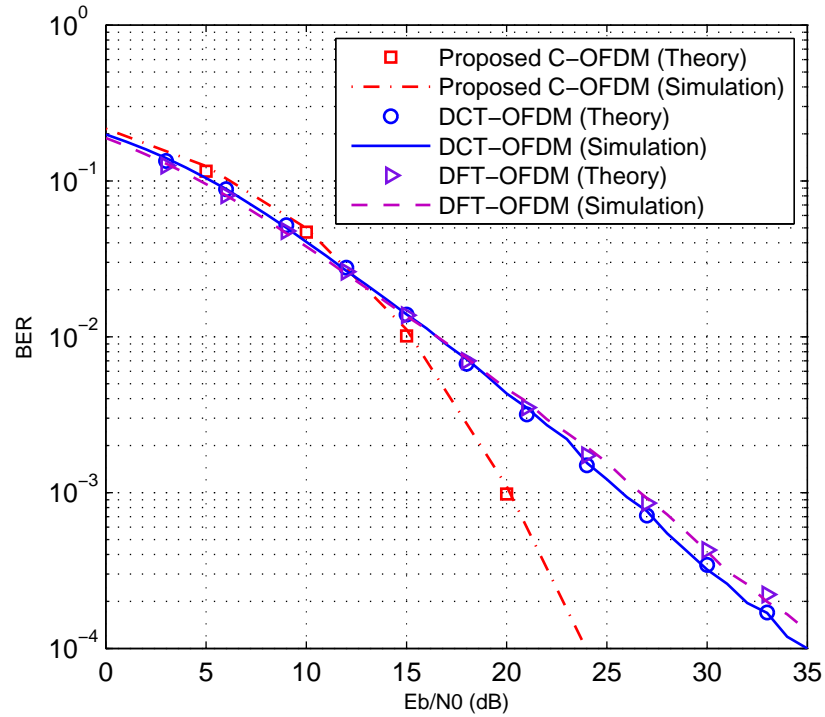


Figure 3.12: BER performance of the proposed C-OFDM, DCT-OFDM and DFT-OFDM systems over the ITU Pedestrian B channel and for the 16-QAM modulation, theory and simulation are in good agreement.

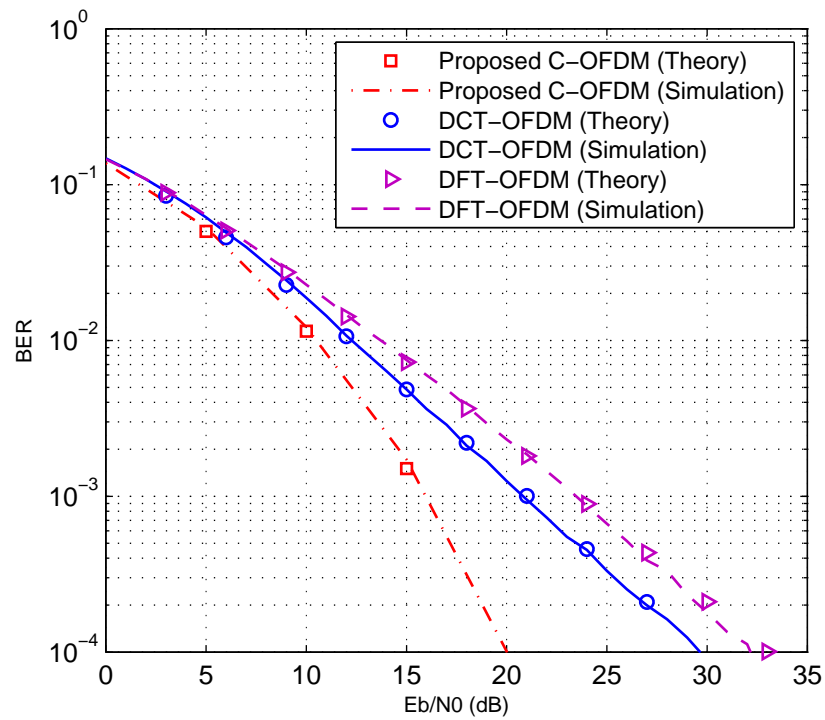


Figure 3.13: BER performance of the proposed C-OFDM, DCT-OFDM and DFT-OFDM systems over the ITU Vehicular A channel and for the QPSK modulation, theory and simulation are in good agreement.

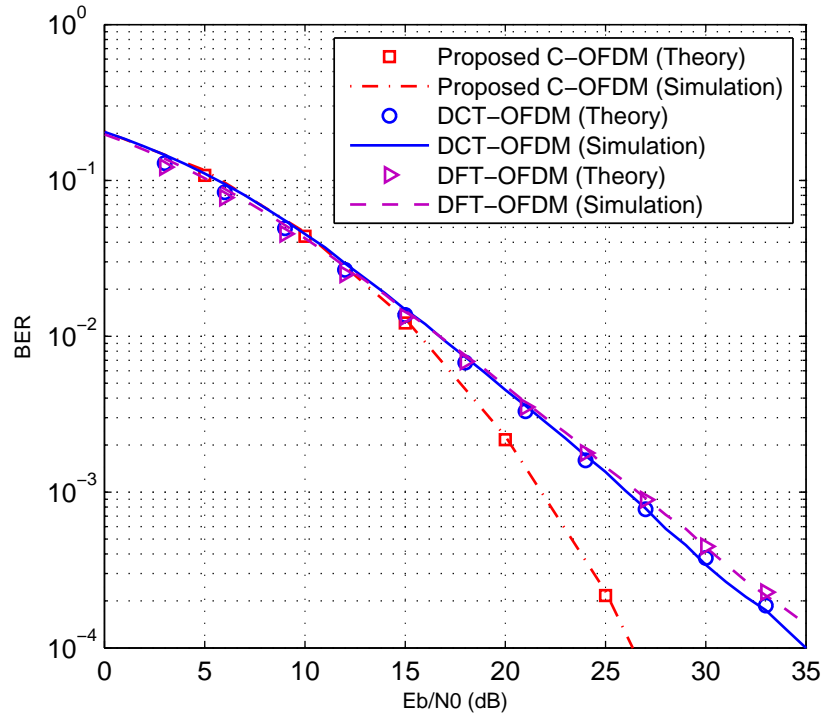


Figure 3.14: BER performance of the proposed C-OFDM, DCT-OFDM and DFT-OFDM systems over ITU Vehicular A channel and for the 16-QAM modulation, theory and simulation are in good agreement.

aforementioned systems will completely lose their orthogonality when ϵ is above 0.1. Fig. 3.16 shows the BER performance when the *M&M* [100] algorithm for CFO estimation is utilized in this simulation. Where the number of subcarriers are $N = 1024$, iterative data $L = 8$, $\epsilon = 2.628$ and (E_b/N_0) is set to be 25 dB in order to get a precise estimation. It is clearly shown that the proposed DCT-OFDM system outperforms both the DFT-OFDM and DFT-OFDM by approximately 10 dB (E_b/N_0) at 10^{-4} BER when either the 16-QAM or the QPSK constellation is used.

3.9.3 BER Performance over wire-line channel

In this subsection, we are considering perfect synchronization between the transmitted and received signals. The BER performances of the proposed scheme, DCT-DMT and DFT-DMT are shown in Fig. 3.17, both for BPSK modulation format. It is noticed from Fig. 3.17 that the simulation and theory results are in marvellous agreement; providing that the proposed scheme achieves significant E_b/N_0 gain over the other systems. It also shows that the BER performance of the DCT-DMT is

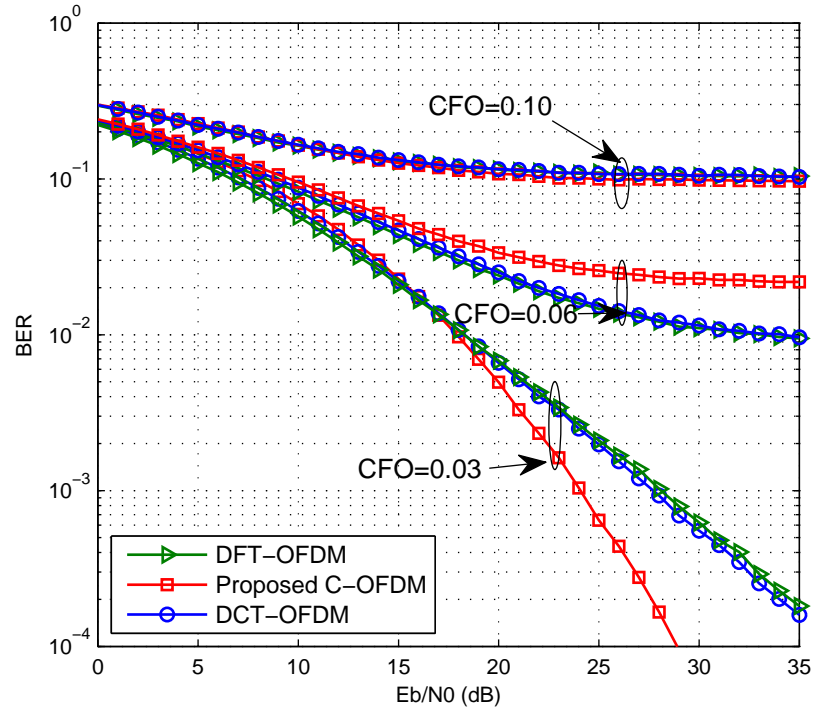


Figure 3.15: BER performance for the proposed C-OFDM, DCT-OFDM and the DFT-OFDM systems over the ITU vehicular class A channel and CFO=0.03, 0.06 and 0.1 and 16-QAM modulation format.

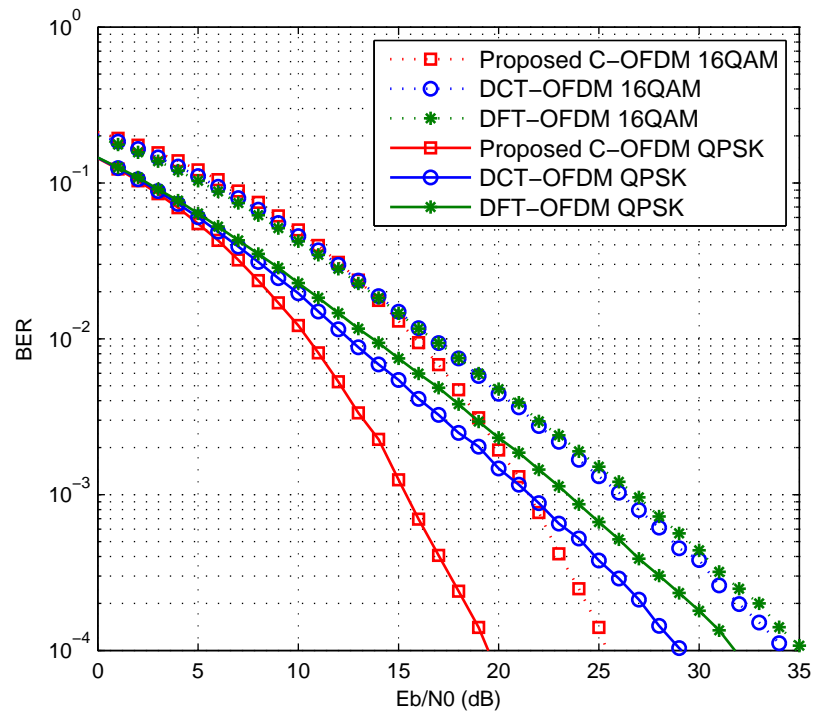


Figure 3.16: BER performance for the proposed C-OFDM, DCT-OFDM and the DFT-OFDM systems over the ITU vehicular class A channel and CFO=2.628 when the QPSK and the 16-QAM modulation formats are used.

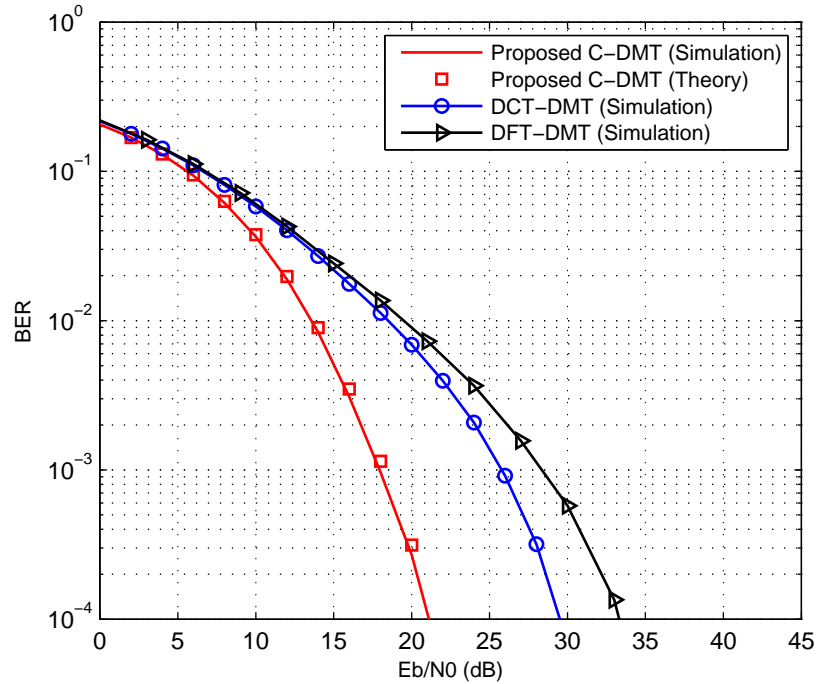


Figure 3.17: BER performance for the proposed C-DMT, DCT-DMT and DFT-DMT systems for the BPSK modulation formats; simulation and theory results are in marvellous agreement.

slightly better than the DFT-DMT system. The proposed WHT-DCT-DMT scheme achieved about 8 dB gain in E_b/N_0 over the DCT-DMT system and around 9 dB over the conventional DFT-DMT systems at 10^{-6} BER.

3.10 Conclusion

In this chapter, a new multicarrier system have been introduced using the WHT-IDCT/DCT/WHT or IC/C transform. The important conclusion is that the adoption of **C**-transform in OFDM systems rather than the DCT or the DFT could achieve better BER performance and PAPR reduction. It has been proved that the C-OFDM system achieves about 10 dB E_b/N_0 at 10^{-4} BER over both DCT-OFDM and DFT-OFDM systems when ITU pedestrian and vehicular channel models are used. This is because the use of the **C**-transform which internally employs WHT, is averaging the SNR over all the subcarriers, which increases the diversity of the transmitted signal. Theoretical BER analysis of the proposed C-OFDM system is also presented and compared with simulation results. It is also found that the proposed scheme is still keep its advantages in BER performance in the presence of

CFO when compensation algorithm is used.

Another advantage of the proposed C-OFDM which was explored in this chapter is the PAPR reduction. Simulation results confirmed that the PAPR of the transmitted signal in the case of the C-OFDM system is lower than both the DCT-OFDM and the DFT-OFDM systems by about 1 dB. This fact is due to the block diagonal structure of the \mathbf{C} -transform, where the maximum signal superposition and number of additions required to perform each transmitted samples is $N/2$ rather than N in the case of the DCT-OFDM and the OFDM systems.

Chapter 4

Efficient OFDM System Based on New \mathbf{X} -Transform for PAPR Reduction and Diversity Enhancement

4.1 Introduction

Signal diversity in OFDM systems is a very effective technique to increase the immunity of the OFDM signal against the deleterious effects of multipath channels. In Chapter Three, a developed OFDM system based on real-valued trigonometric transforms with the ZP guard interval was presented. The proposed system was found to offer advantages in terms of BER improvement, reducing the modulation scheme complexity, avoiding Hermitian constraint when real data format is used over baseband transmission and achieving some reduction in the PAPR. However, a single one-tap equalizer is inapplicable in the case of the C-OFDM where the scheme is lacking to the convolution-multiplication property. The PAPR and complexity reduction were good, however, they are not significant and further reduction are still on demand.

Motivated by the aforementioned requirements, this chapter presents a new fast orthogonal \mathbf{X} -transform. The proposed \mathbf{X} -transform has a sparse matrix structure with all its elements being zeros except along the diagonals. This makes this transform extremely fast, easy and cheap to implement with high speed and low power

consumption. The proposed \mathbf{X} -transform is then used in implementation of a new OFDM named X-OFDM to reduce the complexity, the PAPR and the BER significantly [84] and [85]. Unlike the C-OFDM, the proposed X-OFDM can be implemented with either ZP or CP. For the case of CP, the proposed \mathbf{X} -transform is applied only in the transmitter and the single one-tap equalizer is applicable in the receiver.

The proposed X-OFDM exploits the channel diversity and achieves close BER performance to that of the single carrier frequency domain equalizer (SC-FDE) and significant SNR gain over the conventional OFDM system. Moreover, the proposed scheme hugely reduces the PAPR of the OFDM signal that affects the conventional OFDM system. The proposed X-OFDM scheme is close in complexity to the SC-FDE whereas achieves improved BER performance than the SC-FDE in the presence of the carrier frequency offset (CFO) that arises from frequency mismatch of the transceivers local oscillators, which is a kind of Doppler shift [31]. We also utilized the Morelli and Mengali (M&M) [100] synchronization algorithm to X-OFDM scheme. The BER performance of the proposed scheme is evaluated theoretically and by computer simulation in this chapter over the ITU channel for both the QPSK and the 16-QAM constellations.

The proposed system, for the case of the MMSE detection, is found to be more resilient to the multipath channels than the conventional OFDM system. This is attributed to the fact that the DHT further distributes the information symbols among the whole spectrum. Hence, the data on highly attenuated subcarriers will not be completely missed as it can be recovered from the other subcarriers using the DHT as will be shown mathematically and by simulation later in this chapter. However, this phenomenon does not occur in the OFDM systems counterpart.

Furthermore, the PAPR of the proposed system is also evaluated in this chapter and compared with the PAPR of the OFDM, WHT precoded OFDM and SC-FDE systems. The proposed X-OFDM system is found to reduce the PAPR value by approximately 6 dB over the OFDM owing to the reduction in the superposition of the input symbols that perform each OFDM output sample from N to two. The SC-FDE achieves 3 dB in the PAPR reduction over the proposed X-OFDM independently of the number of subcarriers.

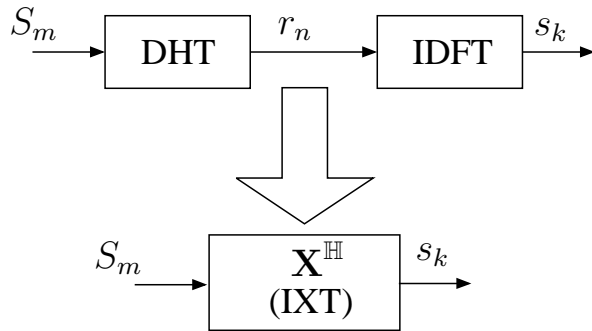


Figure 4.1: Schematic diagram of the proposed \mathbf{X} -transform.

4.2 X-Transform and X-OFDM System

The method producing the inverse proposed \mathbf{X} -transform (IXT) starts with the calculation of the DHT; the DHT is then multiplied by the IDFT as shown in Fig. 4.1. The IXT can mathematically be expressed as

$$\mathbf{X}^{\mathbb{H}} = \mathbf{F}^{\mathbb{H}} \mathbf{A}, \quad (4.1)$$

where $(\cdot)^{\mathbb{H}}$ represents the Hermitian (complex conjugate) operation, \mathbf{F} is the normalized $N \times N$ Fourier matrix and \mathbf{A} is the normalized $N \times N$ Hartley matrix. The elements of the proposed \mathbf{X} matrix can be calculated by using the basic definitions of the discrete Fourier and Hartley transforms as follows: Consider the case when the data symbols are complex and uniformly drawn from a specific constellation such as M-QAM or QPSK are divided into blocks of size N . Each sequence $\mathbf{S}^T = [S_0, S_1, \dots, S_{N-1}]$ modulates N orthogonal subcarriers by using the DHT. It is well known that the DHT is an orthogonal real-valued transform with identical forward and inverse matrices. The output modulated sequence $\mathbf{r}^T = [r_0, r_1, \dots, r_{N-1}]$ is then given as

$$r_n = \sum_{m=0}^{N-1} a_{n,m} S_m, \quad (n = 0, 1, 2, \dots, N-1), \quad (4.2)$$

where $a_{n,m}$ represents the n^{th} row m^{th} column elements of the Hartley matrix \mathbf{A} . (4.2) can be rewritten based on the basic definition of \mathbf{A} as

$$r_n = \frac{1}{\sqrt{N}} \sum_{m=0}^{N-1} S_m \left[\text{cas} \left(\frac{2\pi nm}{N} \right) \right]. \quad (4.3)$$

In (4.3), $\text{cas}\left(\frac{2\pi nm}{N}\right) = \cos\left(\frac{2\pi nm}{N}\right) + \sin\left(\frac{2\pi nm}{N}\right)$. It follows that the output samples r_n ($0 \leq n \leq N-1$) are processed by the IFFT in order to increase the diversity. The resulted signal, $\mathbf{s}^T = [s_0, s_1, \dots, s_{N-1}]$, is a compound signal and can be expressed as

$$s_k = \frac{1}{\sqrt{N}} \sum_{n=0}^{N-1} r_n e^{j\frac{2\pi nk}{N}} \quad (k = 0, 1, 2, \dots, N-1). \quad (4.4)$$

Substituting (4.3) into (4.4) yields

$$s_k = \frac{1}{N} \sum_{n=0}^{N-1} \sum_{m=0}^{N-1} S_m \text{cas}\left(\frac{2\pi nm}{N}\right) e^{j\frac{2\pi nk}{N}}. \quad (4.5)$$

By using trigonometric identities, (4.5) can be written as

$$\begin{aligned} s_k &= \frac{1}{N} \sum_{m=0}^{N-1} S_m \sum_{n=0}^{N-1} \frac{1}{2} \left[\cos \frac{2\pi n}{N} (m-k) + \cos \frac{2\pi n}{N} (m+k) \right] \\ &\quad + j \frac{1}{2} \left[\cos \frac{2\pi n}{N} (m-k) - \cos \frac{2\pi n}{N} (m+k) \right]. \end{aligned} \quad (4.6)$$

In more expressive form, (4.6) can be rewritten as

$$s_k = \sum_{m=0}^{N-1} S_m X_{km}, \quad (k = 0, 1, 2, \dots, N-1), \quad (4.7)$$

where X_{km} is the k^{th} , ($0 \leq k \leq N-1$), row and the m^{th} , ($0 \leq m \leq N-1$) column element of the \mathbf{X}^{H} (inverse \mathbf{X} transform (IXT)). In matrix form, (4.7) can be written as

$$\mathbf{s} = \mathbf{X}^{\text{H}} \mathbf{S}, \quad (4.8)$$

where \mathbf{S} is $N \times 1$ vector. From (4.6) one can notice the following; $X_{k,m} = 1$ when $k = m = 1$ or $k = m = \frac{N}{2}$, $X_{k,m} = \frac{1}{2} + j\frac{1}{2}$ when $k = m$ and $X_{k,m} = \frac{1}{2} - j\frac{1}{2}$ when

$k = N - m$ and $X_{km} = 0$ elsewhere. The inverse \mathbf{X} transform can be expressed as

$$\mathbf{X}^{\mathbb{H}} = \frac{1}{2} \begin{bmatrix} 2 & 0 & 0 & 0 & \dots & 0 & 0 & 0 \\ 0 & 1+j1 & 0 & 0 & \dots & 0 & 0 & 1-j1 \\ 0 & 0 & 1+j1 & 0 & \dots & 0 & 1-j1 & 0 \\ 0 & 0 & 0 & \dots & \cdot & \dots & 0 & 0 \\ \cdot & \cdot & \cdot & 0 & 2 & 0 & \cdot & \cdot \\ \cdot & \cdot & \cdot & \dots & \cdot & \dots & \cdot & \cdot \\ \vdots & 0 & 0 & 1-j1 & 0\dots 0 & 1+j1 & 0 & \vdots \\ 0 & 0 & 1-j1 & 0 & \dots & 0 & 1+j1 & 0 \\ 0 & 1-j1 & 0 & 0 & \dots & 0 & 0 & 1+j1 \end{bmatrix}, \quad (4.9)$$

while the forward \mathbf{X} transform is given as

$$\mathbf{X} = \frac{1}{2} \begin{bmatrix} 2 & 0 & 0 & 0 & \dots & 0 & 0 & 0 \\ 0 & 1-j1 & 0 & 0 & \dots & 0 & 0 & 1+j1 \\ 0 & 0 & 1-j1 & 0 & \dots & 0 & 1+j1 & 0 \\ 0 & 0 & 0 & \dots & \cdot & \dots & 0 & 0 \\ \cdot & \cdot & \cdot & 0 & 2 & 0 & \cdot & \cdot \\ \cdot & \cdot & \cdot & \dots & \cdot & \dots & \cdot & \cdot \\ \vdots & 0 & 0 & 1+j1 & 0\dots 0 & 1-j1 & 0 & \vdots \\ 0 & 0 & 1+j1 & 0 & \dots & 0 & 1-j1 & 0 \\ 0 & 1+j1 & 0 & 0 & \dots & 0 & 0 & 1-j1 \end{bmatrix}. \quad (4.10)$$

It should be noted that this new transform is named the \mathbf{X} -transform because the non zero elements in its transform matrix has an X shape. For more illustration,

both $\mathbf{X}^{\mathbb{H}}$ and \mathbf{X} are given for $N = 8$ respectively as:

$$\mathbf{X}_8^{\mathbb{H}} = \frac{1}{2} \begin{bmatrix} 2 & 0 & 0 & 0 & 0 & 0 & 0 & 0 \\ 0 & 1+j1 & 0 & 0 & 0 & 0 & 0 & 1-j1 \\ 0 & 0 & 1+j1 & 0 & 0 & 0 & 1-j1 & 0 \\ 0 & 0 & 0 & 1+j1 & 0 & 1-j1 & 0 & 0 \\ 0 & 0 & 0 & 0 & 2 & 0 & 0 & 0 \\ 0 & 0 & 0 & 1-j1 & 0 & 1+j1 & 0 & 0 \\ 0 & 0 & 1-j1 & 0 & 0 & 0 & 1+j1 & 0 \\ 0 & 1-j1 & 0 & 0 & 0 & 0 & 0 & 1+j1 \end{bmatrix}, \quad (4.11)$$

$$\mathbf{X}_8 = \frac{1}{2} \begin{bmatrix} 2 & 0 & 0 & 0 & 0 & 0 & 0 & 0 \\ 0 & 1-j1 & 0 & 0 & 0 & 0 & 0 & 1+j1 \\ 0 & 0 & 1-j1 & 0 & 0 & 0 & 1+j1 & 0 \\ 0 & 0 & 0 & 1-j1 & 0 & 1+j1 & 0 & 0 \\ 0 & 0 & 0 & 0 & 2 & 0 & 0 & 0 \\ 0 & 0 & 0 & 1+j1 & 0 & 1-j1 & 0 & 0 \\ 0 & 0 & 1+j1 & 0 & 0 & 0 & 1-j1 & 0 \\ 0 & 1+j1 & 0 & 0 & 0 & 0 & 0 & 1-j1 \end{bmatrix}. \quad (4.12)$$

4.3 Theoretical Analysis of the BER Performance Over Multipath Channels

The system block diagram is shown in Fig. 4.2. Consider block-by-block transmission where the information symbols are divided into blocks, each of length N . These symbols modulate N subcarriers by the mean of inverse \mathbf{X} -transform as it has been given in (4.8). Then a CP of length N_g samples, must be no less than the maximum excess delay of the multipath channel, is then appended to the OFDM signal to prevent the inter-symbol interference (ISI). It follows that the received signal after being passed through a multipath frequency-selective fading channel of $L + 1$ taps ($h_l \neq 0, \forall 0 < l < L$) and corrupted by additive white Gaussian noise (AWGN) v , is given as [91]

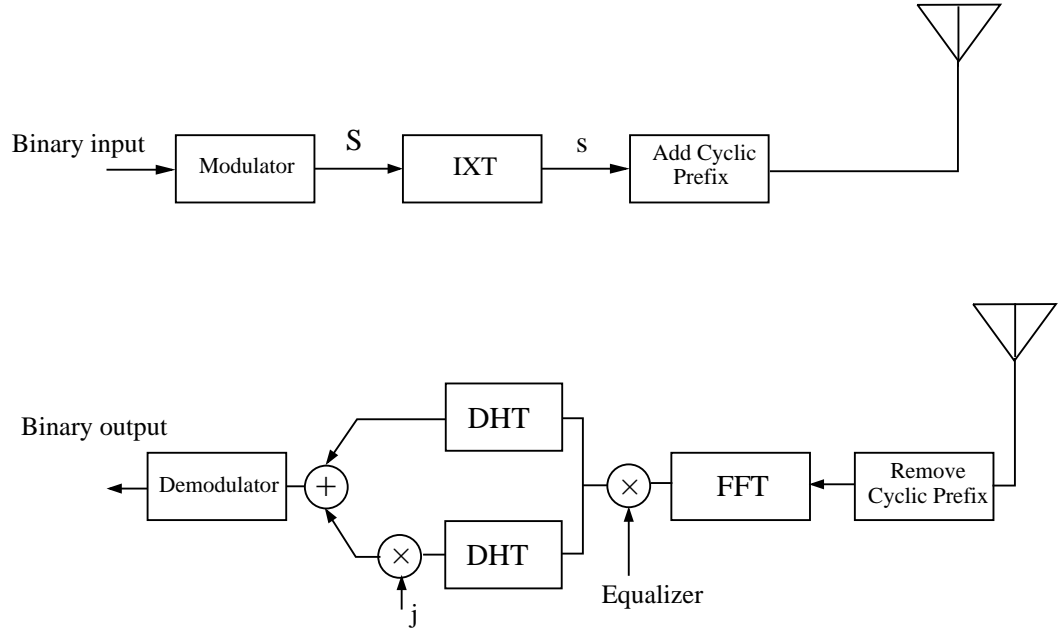


Figure 4.2: Proposed X-OFDM system block diagram.

$$y_k = \sum_{l=0}^L h_l s_{k-l} + v_k. \quad (4.13)$$

The received signal y_k is then processed by the FFT transform and the produced signal can be written as

$$Y_n = \frac{1}{\sqrt{N}} \sum_{k=0}^{N-1} y_k e^{-j \frac{2\pi nk}{N}} + \Omega_n. \quad (4.14)$$

In (4.14), Ω_n is the frequency domain representation of the AWGN (v_k). Substitute (4.4) into (4.13) and then substitute the latter into (4.14) yields

$$Y_n = \frac{1}{N^{3/2}} \sum_{k=0}^{N-1} \left[\sum_{l=0}^L h_l \left\{ \sum_{n=0}^{N-1} r_n e^{j \frac{2\pi n(k-l)}{N}} \right\} \right] e^{-j \frac{2\pi nk}{N}} + \Omega_n. \quad (4.15)$$

After some algebra, (4.15) can be rewritten as

$$\begin{aligned} Y_n &= r_n \sum_{l=0}^L h_l e^{-j \frac{2\pi nl}{N}} + \Omega_n, \\ &= r_n H_n + \Omega_n \quad (n = 0, 1, 2, \dots, N-1). \end{aligned} \quad (4.16)$$

In (4.16), $H_n = \sum_{l=0}^L h_l e^{-j \frac{2\pi nl}{N}}$, ($0 \leq n \leq N-1$) is the channel transfer function corresponding to the n^{th} subchannel. The channel equalization is performed in the

frequency domain after the FFT and before the DHT by applying either MMSE or ZF equalizer as shown in Fig. 4.2. Unlike the conventional OFDM system where the channel equalization and data detection are performed in the same domain (frequency domain), in our proposed X-OFDM system, the channel equalization and data detection are implemented in different domains. This difference in domains of the data detection leads to the interesting properties of the proposed scheme as it will be shown later in the current chapter.

This chapter emphasise on the BER derivation of the proposed X-OFDM system for the 16-QAM and the QPSK modulation formats and for the ZF and the MMSE equalizers. However, the derivation is still valid for other modulation formats. The BER for the QPSK and the 16-QAM constellations are given respectively as (2.23) and (2.24). Hence, to evaluate the BER performance, the signal-to-noise ratio (β_s) at the receiver side after the equalization must be evaluated. Inspired by the approach in [37], the BER performance of our proposed X-OFDM system is evaluated in the next subsections for a multipath fading channels and for both the QPSK and the 16-QAM constellations.

The channel effects on the received signal in (4.16) must be removed, this can be achieved using either the ZF or the MMSE equalizer as follows

4.3.1 Zero-Forcing Equalizer

The ZF equalizer can be achieved simply by dividing each individual symbol of the received vector Y_n in the frequency domain by the corresponding value of the channel transfer function H_n as

$$\hat{r}_n = \frac{Y_n}{H_n}. \quad (4.17)$$

Substitute Y_n in (4.16) into (4.17), \hat{r}_n can then be written as

$$\hat{r}_n = r_n + \xi_n, \quad (4.18)$$

where $\xi_n = \frac{\Omega_n}{H_n}$ represents the amplified noise part. Substituting (4.2) into (4.18) yields

$$\hat{r}_n = \sum_{m=0}^{N-1} a_{n,m} S_m + \xi_n. \quad (4.19)$$

It follows that the equalized signal \hat{r}_n is then transformed by the DHT, \mathbf{A} matrix, as follows

$$q_i^{ZF} = \sum_{n=0}^{N-1} a_{i,n} \hat{r}_n, \quad (i = 0, 1, 2, \dots, N-1). \quad (4.20)$$

This in turn leads to the following

$$q_i^{ZF} = \sum_{n=0}^{N-1} a_{i,n} \left(\sum_{m=0}^{N-1} a_{n,m} S_m \right) + \sum_{n=0}^{N-1} a_{i,n} \xi_n, \quad (i = 0, 1, 2, \dots, N-1). \quad (4.21)$$

Owing to the orthogonality property of the DHT, $\sum_{n=0}^{N-1} a_{i,n} \times a_{n,m}$ is equal to 1 when $m = i$ and zero elsewhere, the first term of (4.21) is equal to S_i , hence (4.21) can be written as

$$q_i^{ZF} = S_i + \hat{\xi}_i, \quad (4.22)$$

where $\hat{\xi}_i = \sum_{n=0}^{N-1} a_{i,n} \xi_n$. The total error signal which is the difference between the transmitted and the detected symbols, $e_i^{ZF} = q_i^{ZF} - S_i$, will be written as

$$\begin{aligned} e_i^{ZF} &= \hat{\xi}_i \\ &= \sum_{n=0}^{N-1} a_{i,n} \xi_n \\ &= \sum_{n=0}^{N-1} a_{i,n} \left(\frac{\Omega_n}{H_n} \right) \end{aligned} \quad (4.23)$$

Thus, the signal to noise ratio will be given as

$$\begin{aligned} \beta_i^{ZF} &= \frac{E[|S_i|^2]}{E[|e_i|^2]} \\ &= \frac{E[S_i S_i^*]}{E[e_i^{ZF} e_i^{ZF*}]} \\ &= \frac{E_s}{\mathcal{P}_{n_i}^{ZF}} \end{aligned} \quad (4.24)$$

where E_s is the symbol energy, is equal to $4E_b$ for the case of the 16-QAM whereas equal to $2E_b$ for the case of the QPSK and $\mathcal{P}_{n_i}^{ZF}$ is the noise power which is given as

$$\mathcal{P}_{n_i}^{ZF} = \sigma_v^2 \sum_{n=0}^{N-1} |a_{i,n}|^2 \frac{1}{|H_n|^2}. \quad (4.25)$$

Substituting (4.25) into (4.24) yields

$$\beta_i^{ZF} = \frac{\gamma_s}{\sum_{n=0}^{N-1} |a_{i,n}|^2 \frac{1}{|H_n|^2}}, \quad (4.26)$$

where $\gamma_s = \frac{E_s}{\sigma_v^2}$ is the signal energy (in terms of symbol) to noise ratio. By substituting (4.26) into (2.23) and (2.24), the BER performance of the QPSK and the 16-QAM modulations are given as:

$$P_e^{QPSK} = \frac{1}{N} \sum_{i=1}^N Q \left(\sqrt{\frac{\gamma_s}{\sum_{n=0}^{N-1} |a_{i,n}|^2 \frac{1}{|H_n|^2}}} \right), \quad (4.27)$$

$$P_e^{16-QAM} = \frac{3}{4N} \sum_{i=1}^N Q \left(\sqrt{\frac{\gamma_s}{5 \sum_{n=0}^{N-1} |a_{i,n}|^2 \frac{1}{|H_n|^2}}} \right). \quad (4.28)$$

It can be seen from (4.26) that for the proposed X-OFDM system, the SNR of each individual subcarrier, β_i^{ZF} , depends on the sum of all H_n , ($n = 0, 1, \dots, N - 1$). In other words, the effects of the subchannel with a deep notch will be distributed over the other subchannels, which is the same case for the SC-FDE scheme. In case of the conventional OFDM system, only the symbols that correspond to deep notches subchannels will be affected independently from the other subchannels. This could be considered as an advantage for the OFDM system over the proposed X-OFDM and the SC-FDE schemes when the ZF equalizer is used where greatly attenuated subchannel ($H_n \simeq 0$) will affect the whole system performance in the case of the X-OFDM system. However, the performance of our proposed system is far superior than that of the OFDM system in the case of the MMSE detection as will be explained in the next section.

4.3.2 Minimum Mean-Square-Error Equalizer

The MMSE equalizer, χ_n , is defined as

$$\begin{aligned} \chi_n &= \frac{E_s H_n^*}{E_s |H_n|^2 + \sigma_v^2} \\ &= \frac{\gamma_s H_n^*}{1 + \gamma_s |H_n|^2} \end{aligned} \quad (4.29)$$

It follows that the equalized signal is then given as

$$\hat{r}_n = r_n H_n \chi_n + \Omega_n \chi_n \quad (4.30)$$

substituting (4.2) into (4.30) yields

$$\hat{r}_n = \sum_{m=0}^{N-1} a_{n,m} S_m H_n \chi_n + \Omega_n \chi_n \quad (4.31)$$

This equalized signal is then transformed by the DHT to detect the data symbols which are given as

$$\begin{aligned} q_i^{MMSE} &= \sum_{n=0}^{N-1} a_{i,n} \left(\sum_{m=0}^{N-1} a_{n,m} S_m H_n \chi_n \right) \\ &+ \sum_{n=0}^{N-1} a_{i,n} \Omega_n \chi_n \quad (k = 0, 1, 2, \dots, N-1) \end{aligned} \quad (4.32)$$

Similar to the case of the ZF equalizer, due to the orthogonality property of the DHT, the first term of (4.32) can be simplified to $\sum_{n=0}^{N-1} S_i H_n \chi_n$, hence, (4.32) will be written as

$$q_i^{MMSE} = \sum_{n=0}^{N-1} S_i \frac{\gamma_s |H_n|^2}{1 + \gamma_s |H_n|^2} + \sum_{n=0}^{N-1} a_{i,n} \Omega_n \chi_n \quad (4.33)$$

The error signal is then calculated as the difference between the transmitted and the received data symbols, $e_i^{MMSE} = q_i^{MMSE} - S_i$, and can be written as

$$\begin{aligned} e_i^{MMSE} &= \sum_{n=0}^{N-1} S_i H_n \chi_n - S_i + \sum_{n=0}^{N-1} a_{i,n} \Omega_n \chi_n \\ &= \sum_{n=0}^{N-1} [H_n \chi_n - 1] S_i + \sum_{n=0}^{N-1} a_{i,n} \Omega_n \chi_n \end{aligned} \quad (4.34)$$

In (4.34), $H_n \chi_n - 1 = \frac{-1}{1 + \gamma_s |H_n|^2}$. Thus, (4.34) can be written as

$$e_i^{MMSE} = S_i \sum_{n=0}^{N-1} \frac{-1}{1 + \gamma_s |H_n|^2} + \sum_{n=0}^{N-1} a_{i,n} \Omega_n \frac{\gamma_s H_n^*}{1 + \gamma_s |H_n|^2} \quad (4.35)$$

Since the DHT is a unitary transform, it does not affect the calculation of the power ($\sum_{n=0}^{N-1} |a_{i,n}|^2 = 1$). In other words, all \mathbf{S} , \mathbf{r} and \mathbf{s} have the same average power E_s and as the data symbols and the AWGN are statistically independent, the noise

power of the i^{th} subchannel is then expressed as

$$\begin{aligned}
 \mathcal{P}_{n_i}^{MMSE} &= E [|e_i^{MMSE}|^2] \\
 &= \sum_{n=0}^{N-1} |a_{i,n}|^2 \frac{E_s}{[1 + \gamma_s |H_n|^2]^2} + \sum_{n=0}^{N-1} |a_{i,n}|^2 \frac{\sigma_v^2 \gamma_s^2 |H_n|^2}{[1 + \gamma_s |H_n|^2]^2} \\
 &= \sum_{n=0}^{N-1} |a_{i,n}|^2 \frac{E_s}{[1 + \gamma_s |H_n|^2]^2} + \sum_{n=0}^{N-1} |a_{i,n}|^2 \frac{E_s \gamma_s |H_n|^2}{[1 + \gamma_s |H_n|^2]^2}, \\
 &= \sum_{n=0}^{N-1} |a_{i,n}|^2 \frac{E_s}{1 + \gamma_s |H_n|^2}.
 \end{aligned} \tag{4.36}$$

The signal power $\mathcal{P}_{s_i}^{MMSE} = E [|q_i^{MMSE}|^2]$ and it is given as

$$\begin{aligned}
 \mathcal{P}_{s_i}^{MMSE} &= \sum_{n=0}^{N-1} |a_{i,n}|^2 \frac{E_s \gamma_s^2 |H_n|^4}{[1 + \gamma_s |H_n|^2]^2} + \sum_{n=0}^{N-1} |a_{i,n}|^2 \frac{E_s \gamma_s |H_n|^2}{[1 + \gamma_s |H_n|^2]^2}, \\
 &= \sum_{n=0}^{N-1} |a_{i,n}|^2 \frac{E_s \gamma_s |H_n|^2}{1 + \gamma_s |H_n|^2}.
 \end{aligned} \tag{4.37}$$

Then, the SNR of the i^{th} subchannel $\beta_i^{MMSE} = \frac{\mathcal{P}_{s_i}^{MMSE}}{\mathcal{P}_{n_i}^{MMSE}}$ is given as

$$\beta_i^{MMSE} = \frac{\sum_{n=0}^{N-1} |a_{i,n}|^2 \frac{\gamma_s |H_n|^2}{1 + \gamma_s |H_n|^2}}{\sum_{n=0}^{N-1} |a_{i,n}|^2 \frac{1}{1 + \gamma_s |H_n|^2}}. \tag{4.38}$$

It can be seen from (4.38) that β_i^{MMSE} for the i^{th} subcarrier is averaged by the mean of the DHT. This significantly improves the BER performance of the proposed scheme, especially when the channel has narrowband deep notches in its spectral.

The BER performance of the X-OFDM system for the QPSK and the 16-QAM modulations is then given as:

$$P_e^{QPSK} = \frac{1}{N} \sum_{i=0}^{N-1} Q \left(\sqrt{\frac{\sum_{n=0}^{N-1} |a_{i,n}|^2 \frac{\gamma_s |H_n|^2}{1 + \gamma_s |H_n|^2}}{\sum_{n=0}^{N-1} |a_{i,n}|^2 \frac{1}{1 + \gamma_s |H_n|^2}}} \right), \tag{4.39}$$

$$P_e^{16-QAM} = \frac{3}{4N} \sum_{i=0}^{N-1} Q \left(\sqrt{\frac{\sum_{n=0}^{N-1} |a_{i,n}|^2 \frac{\gamma_s |H_n|^2}{1 + \gamma_s |H_n|^2}}{5 \sum_{n=0}^{N-1} |a_{i,n}|^2 \frac{1}{1 + \gamma_s |H_n|^2}}} \right). \tag{4.40}$$

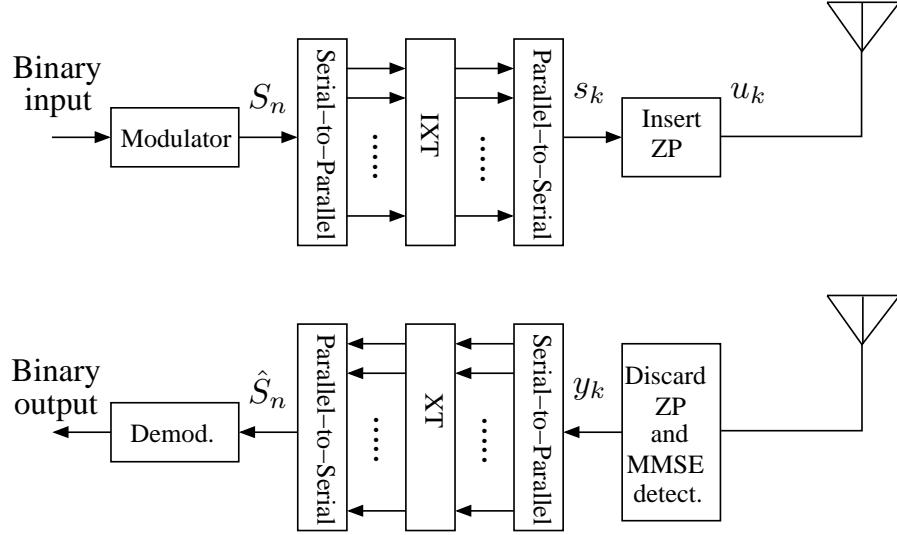


Figure 4.3: Block diagram of the X-OFDM scheme with ZP

4.4 X-OFDM with Zero-Padding (ZP)

The proposed X-OFDM system can also be implemented with ZP [85] as in the case of the C-OFDM in the previous chapter. In this case, the inverse \mathbf{X} -transform is used at the transmitter and the forward \mathbf{X} -transform is used at the receiver to implement the modulation/demodulation scheme as shown in Fig. 4.3. Following the same procedure in chapter three for the C-OFDM, the transmission process of the ZP-X-OFDM can be investigated as

$$\mathbf{r} = \mathbf{A}\mathbf{s}. \quad (4.41)$$

The transmitted signal, after being processed by IXT, is padded with zeros of length N_g , must be greater than or equal to the maximum excess delay of the multipath propagation channel. Mathematically, this can be expressed as: The resulting redundant signal is of length $N_t = N + N_g$ and can be expressed as

$$\mathbf{u} = \mathbf{\Psi}_{zp}\mathbf{s}, \quad (4.42)$$

where $\mathbf{\Psi}_{zp}$ is a $N_t \times N$ matrix is given in (2.18) The transmitted signal is then convolved with the channel and corrupted by the AWGN; it can be written as

$$\begin{aligned} \mathbf{y} &= \mathbf{H}_0\mathbf{u} + \mathbf{v}, \\ &= \mathbf{H}_0\mathbf{\Psi}_{zp}\mathbf{s} + \mathbf{v}. \end{aligned} \quad (4.43)$$

In (4.43), \mathbf{H}_0 is as given in (3.26) in chapter three. The equalization is performed at the receiver side using MMSE detection. The equalized signal at the receiver side was given in (3.29) as

$$\mathbf{y}_{eq} = \mathbf{\Psi}_{zp}^T \mathbf{G} \mathbf{H}_0 \mathbf{u} + \mathbf{\Psi}_{zp}^T \mathbf{G} \mathbf{v} \quad (4.44)$$

At the receiver side, the \mathbf{X} -transform is used to demodulate the received data, \mathbf{y}_{eq} as follows

$$\hat{\mathbf{S}} = \mathbf{X} \mathbf{\Psi}_{zp}^T \mathbf{G} \mathbf{H}_0 \mathbf{\Psi}_{zp} \mathbf{s} + \mathbf{X} \mathbf{\Psi}_{zp}^T \mathbf{G} \mathbf{v}, \quad (4.45a)$$

$$= \mathbf{X} \mathbf{\Psi}_{zp}^T \mathbf{G} \mathbf{H}_0 \mathbf{\Psi}_{zp} \mathbf{X}^H \mathbf{S} + \mathbf{X} \mathbf{\Psi}_{zp}^T \mathbf{G} \mathbf{v}. \quad (4.45b)$$

For mathematical convenient, the equalizer matrix \mathbf{G} can be factorized in (3.27)-(3.33c) in chapter three and it is given as

$$\mathbf{G} = \left[\mathbf{\Lambda} \mathbf{\Lambda}^H (\mathbf{V} \mathbf{\Lambda}^H)^{-1} + \frac{1}{\gamma_s} \mathbf{I}_{N_t} (\mathbf{V} \mathbf{\Lambda}^H)^{-1} \right]^{-1} \mathbf{U}^H, \quad (4.46a)$$

$$= \mathbf{V} \mathbf{\Lambda}^H \left(\mathbf{\Lambda} \mathbf{\Lambda}^H + \frac{1}{\gamma_s} \mathbf{I}_{N_t} \right)^{-1} \mathbf{U}^H. \quad (4.46b)$$

The noise signal $\mathbf{e}^{MMSE} = \hat{\mathbf{S}} - \mathbf{S}$ is then given as

$$\mathbf{e}^{MMSE} = (\mathbf{X} \mathbf{\Psi}_{zp}^T \mathbf{G} \mathbf{H}_0 \mathbf{\Psi}_{zp} \mathbf{X}^H - \mathbf{I}_N) \mathbf{S} + \mathbf{X} \mathbf{\Psi}_{zp}^T \mathbf{G} \mathbf{v}. \quad (4.47)$$

Substituting (4.46b) into (4.47) yield

$$\begin{aligned} \mathbf{e}^{MMSE} &= \left[\mathbf{X} \mathbf{\Psi}_{zp}^T \mathbf{V} \mathbf{\Lambda}^H \left(\mathbf{\Lambda} \mathbf{\Lambda}^H + \frac{1}{\gamma_s} \mathbf{I}_{N_t} \right)^{-1} \mathbf{U}^H (\mathbf{U} \mathbf{\Lambda} \mathbf{V}^H) \mathbf{\Psi}_{zp} \mathbf{X}^H - \mathbf{I}_N \right] \mathbf{S} \\ &\quad + \mathbf{X} \mathbf{\Psi}_{zp}^T \mathbf{V} \mathbf{\Lambda}^H \left(\mathbf{\Lambda} \mathbf{\Lambda}^H + \frac{1}{\gamma_s} \mathbf{I}_{N_t} \right)^{-1} \mathbf{U}^H \mathbf{v}. \end{aligned} \quad (4.48)$$

Let $\mathbf{\Delta}_{N \times N_t}$ represents matrices combination, $\mathbf{X} \mathbf{\Psi}_{zp}^T \mathbf{V}$, and $\overline{\mathbf{\Delta}}_{N_t \times N}$ represents the matrices combination $\mathbf{V}^H \mathbf{\Psi}_{zp} \mathbf{X}^H$ where $\mathbf{\Delta}_{N \times N_t} \overline{\mathbf{\Delta}}_{N_t \times N} = \mathbf{I}_N$. Therefore, after some algebra, (4.48) can be written as

$$\begin{aligned} \mathbf{e}^{MMSE} &= \left[\mathbf{\Delta} \mathbf{\Lambda}^H \left(\mathbf{\Lambda} \mathbf{\Lambda}^H + \frac{1}{\gamma_s} \mathbf{I}_{N_t} \right)^{-1} \mathbf{\Lambda} \overline{\mathbf{\Delta}} - \mathbf{I}_N \right] \mathbf{S} \\ &\quad + \mathbf{\Delta} \mathbf{\Lambda}^H \left(\mathbf{\Lambda} \mathbf{\Lambda}^H + \frac{1}{\gamma_s} \mathbf{I}_{N_t} \right)^{-1} \mathbf{U}^H \mathbf{v}. \end{aligned} \quad (4.49)$$

This can be simplified to

$$\begin{aligned} \mathbf{e}^{MMSE} &= \mathbf{\Delta} \left[\mathbf{\Lambda}^{\mathbb{H}} \left(\mathbf{\Lambda} \mathbf{\Lambda}^{\mathbb{H}} + \frac{1}{\gamma_s} \mathbf{I}_{N_t} \right)^{-1} \mathbf{\Lambda} - \mathbf{I}_{N_t} \right] \overline{\mathbf{\Delta}} \mathbf{S} \\ &\quad + \mathbf{\Delta} \mathbf{\Lambda}^{\mathbb{H}} \left(\mathbf{\Lambda} \mathbf{\Lambda}^{\mathbb{H}} + \frac{1}{\gamma_s} \mathbf{I}_{N_t} \right)^{-1} \mathbf{U}^{\mathbb{H}} \mathbf{v}. \end{aligned} \quad (4.50)$$

In (4.50), $\left[\mathbf{\Lambda}^{\mathbb{H}} \left(\mathbf{\Lambda} \mathbf{\Lambda}^{\mathbb{H}} + \frac{1}{\gamma_s} \mathbf{I}_{N_t} \right)^{-1} \mathbf{\Lambda} \right] = \mathbf{\Theta}_1$ is a diagonal matrix, its i^{th} diagonal elements are given as $\frac{\gamma_s |\lambda_i|^2}{\gamma_s |\lambda_i|^2 + 1}$, $\left[\mathbf{\Lambda}^{\mathbb{H}} \left(\mathbf{\Lambda} \mathbf{\Lambda}^{\mathbb{H}} + \frac{1}{\gamma_s} \mathbf{I}_{N_t} \right)^{-1} \mathbf{\Lambda} - \mathbf{I}_{N_t} \right] = \mathbf{\Theta}_2$ with i^{th} diagonal element given as $\frac{-1}{\gamma_s |\lambda_i|^2 + 1}$ and $\mathbf{\Lambda}^{\mathbb{H}} \left(\mathbf{\Lambda} \mathbf{\Lambda}^{\mathbb{H}} + \frac{1}{\gamma_s} \mathbf{I}_{N_t} \right)^{-1} = \mathbf{\Theta}_3$ where its i^{th} diagonal element given as $\frac{\gamma_s |\lambda_i|}{\gamma_s |\lambda_i|^2 + 1}$ where $\lambda_i, (i = 0, 1, 2, \dots, N_t - 1)$ is the i^{th} diagonal element of $\mathbf{\Lambda}$. Therefore, (4.50) can be written as

$$\mathbf{e}^{MMSE} = \mathbf{\Delta} \mathbf{\Theta}_2 \overline{\mathbf{\Delta}} \mathbf{S} + \mathbf{\Delta} \mathbf{\Theta}_3 \mathbf{U}^{\mathbb{H}} \mathbf{v}. \quad (4.51)$$

Similarly, $\hat{\mathbf{S}}$ in (4.45b) can be written as

$$\hat{\mathbf{S}} = \mathbf{\Delta} \mathbf{\Theta}_1 \overline{\mathbf{\Delta}} \mathbf{S} + \mathbf{\Delta} \mathbf{\Theta}_3 \mathbf{U}^{\mathbb{H}} \mathbf{v}. \quad (4.52)$$

The noise power of all subcarriers at the receiver side is $E \left[\mathbf{e}^{MMSE} \mathbf{e}^{MMSE \mathbb{H}} \right] = \text{tr}(\mathbf{e}^{MMSE} \mathbf{e}^{MMSE \mathbb{H}})$ and is given as

$$\mathcal{P}_n^{MMSE} = \text{tr} \left[\mathbf{\Delta} E_s \mathbf{\Theta}_2^2 \overline{\mathbf{\Delta}} + \mathbf{\Delta} \mathbf{\Lambda}^2 \mathbf{\Theta}_3^2 \overline{\mathbf{\Delta}} \right] \quad (4.53a)$$

$$= \text{tr} \left[\mathbf{\Delta} \left[E_s \mathbf{\Theta}_2^2 + \sigma^2 \mathbf{\Theta}_3^2 \right] \overline{\mathbf{\Delta}} \right]. \quad (4.53b)$$

In (4.53b), $E_s \left[\mathbf{\Theta}_2^2 + \frac{1}{\gamma_s} \mathbf{\Theta}_3^2 \right]$ is a diagonal matrix can be simplified as

$$\begin{aligned} \left[\mathbf{\Theta}_2^2 + \frac{1}{\gamma_s} \mathbf{\Theta}_3^2 \right]_{i,i} &= \frac{1}{[\gamma_s |\lambda_i|^2 + 1]^2} + \frac{\gamma_s |\lambda_i|^2}{[\gamma_s |\lambda_i|^2 + 1]^2} \\ &= \frac{1}{\gamma_s |\lambda_i|^2 + 1}. \end{aligned} \quad (4.54)$$

Let $\mathbf{\Theta}_4 = \text{diag}(\frac{1}{\gamma_s |\lambda_i|^2 + 1})$ and by substituting (4.54) into (4.53b) yields

$$\mathcal{P}_n^{MMSE} = \text{tr} \left[\mathbf{\Delta} E_s \mathbf{\Theta}_4 \overline{\mathbf{\Delta}} \right] \quad (4.55)$$

The received signal power which is carried on all subcarriers is $\mathcal{P}_s^{MMSE} = E[\hat{\mathbf{S}}\hat{\mathbf{S}}^H] = \text{tr}(\hat{\mathbf{S}}\hat{\mathbf{S}}^H)$ is given as

$$\mathcal{P}_s^{MMSE} = \text{tr} [\Delta E_s \Theta_1^2 \bar{\Delta} + \Delta \sigma_v^2 \Theta_3^2 \bar{\Delta}], \quad (4.56a)$$

$$= \text{tr} [\Delta [E_s \Theta_1^2 + \sigma_v^2 \Theta_3^2] \bar{\Delta}] \quad (4.56b)$$

$$= \text{tr} [\Delta E_s \Theta_1 \bar{\Delta}]. \quad (4.56c)$$

Therefore, the signal-to-noise ratio at the output of the m^{th} subchannel is given as

$$\beta_m = \frac{[\Delta \Theta_1 \bar{\Delta}]_{m,m}}{[\Delta \Theta_4 \bar{\Delta}]_{m,m}}. \quad (4.57)$$

BER of m^{th} subchannel is given for the QPSK and the 16-QAM modulations, respectively as

$$P_e^{QPSK} = \frac{1}{N} \sum_{m=0}^{N-1} Q \left(\sqrt{\frac{[\Delta \Theta_1 \bar{\Delta}]_{m,m}}{[\Delta \Theta_4 \bar{\Delta}]_{m,m}}} \right). \quad (4.58)$$

$$P_e^{16-QAM} = \frac{3}{4N} \sum_{m=0}^{N-1} Q \left(\sqrt{\frac{[\Delta \Theta_1 \bar{\Delta}]_{m,m}}{5 [\Delta \Theta_4 \bar{\Delta}]_{m,m}}} \right). \quad (4.59)$$

4.5 Complexity Analysis and Comparison

This section evaluates the number of arithmetic operations of the proposed \mathbf{X} -transform and compares them with those of the FFT and the FHT-FFT transforms based on fast algorithms.

4.5.1 The \mathbf{X} Transform

The \mathbf{X} -transform includes $\frac{N-2}{2}$ units, each unit is shown in Fig. 4.4. Each single multiplication of complex data $x+jy$ by $1+j1$ equals to $(x-y)+j(x+y)$, that means it involves 2 real additions (R_A). Thus, the complexity of the direct implementation of the \mathbf{X} -transform can be given as:

$$s_k = 0.5S_m(1+j1) + 0.5S_{N-m}(1-j1), \quad (4.60)$$

$$s_{N-k} = 0.5S_m(1-j1) + 0.5S_{N-m}(1+j1). \quad (4.61)$$

By ignoring the scaling factor, it is obvious from Fig. 4.4 that each unit includes 4 complex additions (C_A) which equivalent to $8 R_A$ per unit. Then the overall complexity is given as

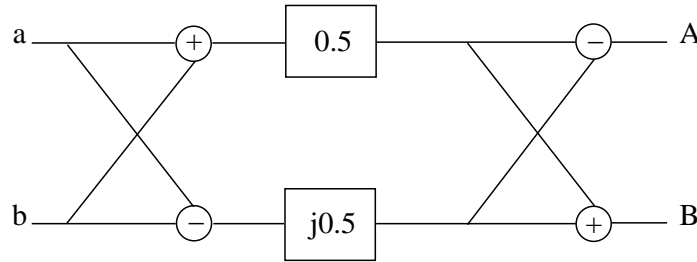


Figure 4.4: Basic unit of \mathbf{X} transform.

$$R_A = 4(N - 2). \quad (4.62)$$

4.5.2 Fast Fourier Transform (FFT)

Considering the fact that each complex multiplication involves 4 real multiplications (R_M) and 2 real additions (R_A) or 3 real multiplications and 3 real additions, and each complex addition is equivalent to $2 R_A$. The arithmetic complexity of FFT, based on single butterfly and 4/2 implementation is given as:

$$R_M = 2N \log_2 N, \quad (4.63)$$

$$R_A = 3N \log_2 N. \quad (4.64)$$

Therefore, the total number of real operations of radix-2 FFT based on single butterfly implementation is given as

$$R_T = 5N \log_2 N. \quad (4.65)$$

4.5.3 Fast Hartley-Fourier Transform (FHT-FFT)

The arithmetic complexity of the radix-2 fast Hartley transform (FHT) based on single butterfly implementation is given as:

$$R_M = N \log_2 N, \quad (4.66)$$

Table 4.1: Comparison based on real arithmetic operations of transmitter of the proposed X-OFDM and the conventional OFDM based on single butterfly implementation.

N	XT			FFT		
	R_A	R_M	R_O	R_A	R_M	R_O
32	120	0	120	480	320	800
64	248	0	248	1152	768	1920
128	504	0	504	2688	1792	4480
256	1016	0	1016	6144	4096	10240
512	2040	0	2040	13824	9216	23040
1024	4088	0	4088	30720	20480	51200
2048	8184	0	8184	67584	45056	112640
4096	16376	0	16376	147456	98304	245760

$$R_A = \frac{3}{2}N \log_2 N. \quad (4.67)$$

For data that are drawn from complex constellation, the FHT is calculated twice, one for the real part and the other for the imaginary part of a complex information. Consequently, the arithmetic operations of the FHT-FFT will be 2 times of (4.66) and (4.67) in addition to the arithmetic operations of FFT given in (4.63) and (4.64), so the overall arithmetic operations are given as:

$$R_M = 4N \log_2 N, \quad (4.68)$$

and

$$R_A = 6N \log_2 N. \quad (4.69)$$

4.5.4 Transmitter Complexities

Table 4.1 shows the computational complexity of the transmitter of the X-OFDM and the OFDM for different transform sizes N and when the information data are complex symbols. It is clear from Table I that the implementation of the \mathbf{X} transform involves no multiplications at all and much less additions than the FFT. Hence the \mathbf{X} transform is faster than the FFT and considerably reduce the transmitter complexity.

4.5.5 Receiver Complexities

The complexity at the receiver depends on the equalization. If the equalization is carried out in the time domain, ignoring the complexity of the equalizer itself which is the same for all systems, the complexity of the X-OFDM and the conventional OFDM receivers will be the same as the complexity of the transmitter which is shown in Table 4.1.

However, if the equalisation is carried out in the frequency domain, then the receiver complexities are as given in Table 4.2.

Table 4.2: Comparison based on real arithmetic operations of the receiver of the proposed X-OFDM and the conventional OFDM systems based on single butterfly implementation.

N	FHT-FFT			FFT		
	R_A	R_M	R_O	R_A	R_M	R_O
32	960	640	1600	480	320	800
64	2304	1536	3840	1152	768	1920
128	5376	3584	8960	2688	1792	4480
256	12288	8192	20480	6144	4096	10240
512	27648	18432	46080	13824	9216	23040
1024	61440	40960	102400	30720	20480	51200
2048	135168	90112	225280	67584	45056	112640
4096	294912	196608	491520	147456	98304	245760

For the X-OFDM, the complexity at the receiver is more than that one at transmitter as the \mathbf{X} transform is not implemented directly at the receiver because the channel gain is compensated in the frequency domain between the FFT and DHT. Therefore, the receiver complexity of the X-OFDM system requires two DHTs in addition to a single FFT which is ultimately the same complexity as DHT precoded OFDM receiver.

4.5.6 Complexity of X-OFDM versus C-OFDM

For fair comparison, we consider both system with ZP guard interval. Ignoring the complexity of the equalizer itself which is the same for all systems, for complex information symbols, the transmitter and receiver complexity of X-OFDM is twice of (4.62) while, for the case of \mathbf{C} -transform, it is four-times of the complexity that given in (3.62), two at the transmitter and the other two at the receiver, one for real part while the another for the imaginary part of the complex information symbols.

For the case of real information symbols, it is required only two of (4.62), one at the transmitter and the other at the receiver.

4.5.7 Complexity of X-OFDM Versus SC-FDE

The proposed system complexity in comparison with SC-OFDM when the equalization is carried out in the frequency domain can be explained as follows: The complexity of the \mathbf{X} transform that is given in (4.62) for the transmitter, in addition to the receiver complexity of FHT-FFT that is given in (4.68) and (4.69). Thus the over all complexity is given as $R_M = 4N \log_2 N$ and $R_A = N(6 \log_2 N + 4) - 8$. However, for the case of SC-FDE, there is no transformation complexity in the transmitter whilst single extra IFFT with complexity given in (4.63) and (4.64) at the receiver with over all $R_M = 4N \log_2 N$ and over all $R_A = 6N \log_2 N$. Therefore, the SC-FDE has the same number of multiplications as the proposed X-OFDM system, but $4(N - 2)$ fewer additions than X-OFDM. This can be considered to be negligible if we consider the overall complexity.

4.6 CFO Effects on BER Performance Over Multipath Channels

Carrier frequency offset (CFO) that is caused by frequency mismatch of local oscillators has significant effects on the BER performance of OFDM systems as it produces inter-carrier interference (ICI) that destroys the orthogonality of the subcarriers. As a result, it is so important to investigate the validity of the proposed system in the presence of the CFO. The received signal at the receiver side in the presence of the CFO could be expressed by matrix form as

$$\begin{aligned} \mathbf{y} &= \mathbf{\Upsilon} \mathbf{H}_0 \mathbf{s} + \mathbf{v}, \\ &= \mathbf{\Upsilon} \mathbf{H}_0 \mathbf{X}^{\mathbb{H}} \mathbf{S} + \mathbf{v}. \end{aligned} \quad (4.70)$$

In (4.70), $\mathbf{\Upsilon}$ is a diagonal matrix, the elements of the diagonal are given as $e^{j \frac{2\pi\epsilon(0:N-1)}{N}}$, ϵ is the CFO normalized to the subcarrier spacing. Because of the CP, the channel matrix \mathbf{H}_0 becomes a circulant matrix and it is diagonalized by pre and post multiplications by $\mathbf{F}^{\mathbb{H}}$ and \mathbf{F} . Only for clarity, the transform $\mathbf{X}^{\mathbb{H}}$ in (4.70) is expressed

by its origins, it follows that the received signal can be written as

$$\begin{aligned}
 \mathbf{Y} &= \mathbf{A}\mathbf{F}\mathbf{T}\mathbf{H}\mathbf{F}^{\mathbb{H}}\mathbf{A}\mathbf{S} + \mathbf{A}\mathbf{F}\mathbf{v}, \\
 &= \mathbf{A}\underbrace{\mathbf{F}\mathbf{T}\mathbf{F}^{\mathbb{H}}}_{\mathbf{\Pi}}\underbrace{\mathbf{F}\mathbf{H}\mathbf{F}^{\mathbb{H}}}_{\mathbf{\bar{H}}}\underbrace{\mathbf{A}\mathbf{S}}_{\mathbf{r}} + \mathbf{A}\mathbf{\Omega}, \\
 &= \mathbf{A}\mathbf{\Pi}\mathbf{\bar{H}}\mathbf{r} + \mathbf{A}\mathbf{\Omega},
 \end{aligned} \tag{4.71}$$

where $\mathbf{\bar{H}}$ is a diagonal matrix, its diagonal elements are the frequency domain representation of the channel impulse response, $H_n = \sum_{l=0}^{L-1} h_l e^{-j\frac{2\pi nl}{N}}$ and $\mathbf{\Pi} = \mathbf{F}\mathbf{T}\mathbf{F}^{\mathbb{H}}$ denotes ICI matrix. Without CFO, $\mathbf{\Pi}$ in (4.71) will be reduced to the identity matrix and single-tap equalizer is applicable as shown in the BER derivation, section IV. However, the presence of the CFO produces ICI which leads to significant degradation in system performance. For the case of the OFDM, (4.71) can be written as

$$\mathbf{Y} = \mathbf{\Pi}\mathbf{\bar{H}}\mathbf{S} + \mathbf{\Omega}. \tag{4.72}$$

From (4.71) and (4.72), the proposed scheme acting better than the SC-FDE in the presence of CFO which cause fast fading (rapid change) in channel impulse response. This is because the SC-FDE signal, represented by data symbols, convolved directly with this channel impulse response as there is no transform to multiplex the data symbols at the transmitter. However, for the case of our proposed system, the data symbols are first multiplexed by the \mathbf{X} -transform before it passes through the channel leading to improved BER performance in comparison to the SC-FDE in the presence of the CFO or over fast fading channels. In other words, the sensitivity of SC-FDE system to CFO is more than our proposed X-OFDM system because in our proposed scheme, the ICI affects the multiplexed signal, \mathbf{r} , rather than the information symbols directly which is the case for SC-FDE as the information symbols pass through the channel without being multiplexed by any transform.

It can also be observed from (4.72) that, for the case of the conventional OFDM system, the CFO introduces ICI on the information symbols which are not the signal that convolved with the channel impulse response. In other words, in the case of conventional OFDM, the data symbols are first transformed to a time domain signal before it convolved with the channel impulse response, hence it is less sensitive to

the CFO or the fast fading channels than both the X-OFDM and the SC-FDE. This is also confirmed by computer simulations. However, the X-OFDM as well as SC-OFDM systems restore their superiority over the DFT-OFDM system when CFO estimation algorithms are used.

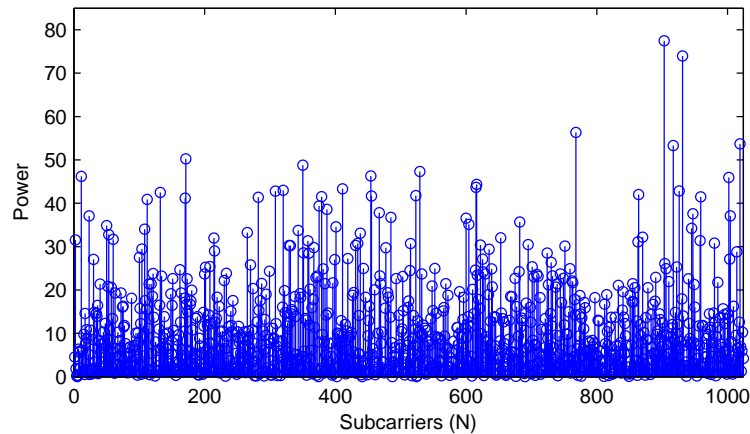
In this work, Morelli and Mengali (M&M) algorithm [100] is used with some modification to be applicable for our proposed system. Unlike the conventional OFDM system where the IFFT is used to generate a symbol consisting of L identical parts that are used for the CFO estimation. They are generated by transmitting a pseudo-noise sequence on the frequencies multiple of L/T and setting zeros on the rest. In our proposed system, L identical sequences, each N/L in length have to be passed through the DHT transform to produce the required pseudo-noise sequence in the frequencies multiple of L/T and setting zeros on the rest which in turn pass through the IFFT. In other words, these L identical sequences pass through the \mathbf{X} -transform in order to be used for the CFO estimation.

4.7 Simulation results and discussions

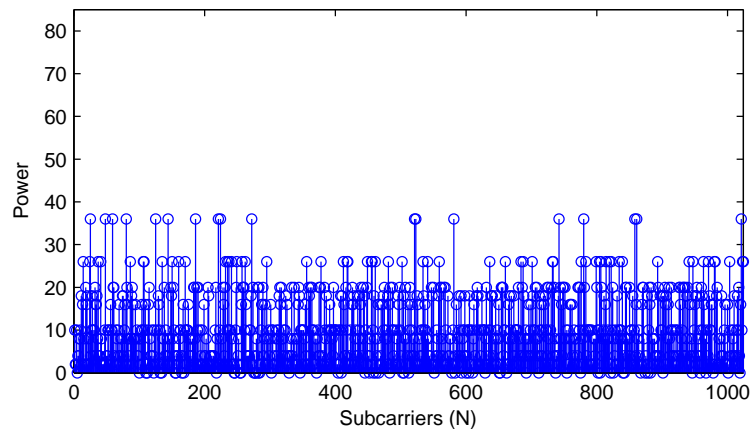
4.7.1 PAPR of the Proposed Scheme

The \mathbf{X} -transform reserves the average power of the signal that is transformed by the \mathbf{X} -transform exactly as the DFT. However, it can enormously reduce the peak power of the time domain OFDM signal as it hugely reduces the number of additions of data symbols that performs each OFDM sample from N in the case of conventional OFDM to only two in the case of the proposed X-OFDM scheme. In general, the maximum PAPR is $10 \log_{10} N$ in the case of the conventional OFDM while it is only $10 \log_{10} 2$ in the case of the proposed X-OFDM. This is clearly shown in Fig. 4.5, where it can be observed that for the case of the system that based on the conventional DFT, the instantaneous peak power can approach more than twice that of the proposed X-OFDM scheme, as shown in Figs 4.5(a) and 4.5(b).

Simulation was carried out for the X-OFDM, OFDM WHT precoded OFDM and SC-FDE systems for a number of subcarriers $N = 1024$ and 16-QAM modulation formats. In order to have an awareness and intuitive view of the PAPR statistics, complementary cumulative density function (CCDF) was plotted. Also to ensure the reliability of computer simulations, 100 000 OFDM frames were generated to



(a) Power in OFDM signal.



(b) Power in X-OFDM signal.

Figure 4.5: Power in OFDM signal (a) the conventional system and (b) the proposed system.

obtain each PAPR value. It is observed from Fig. 4.6 that the X-OFDM system has a lower PAPR than the OFDM and WHT precoded OFDM systems, where it has achieved about 6 dB improvement in the PAPR reduction at a CCDF value of 10^{-4} over the DFT-OFDM system and 5 dB over WHT precoded OFDM system. This is due to the fact that the \mathbf{X} transform reduces the superposition of the input encoded information symbols which form each OFDM sample. It can be seen from Fig. 4.6 that the SC-FDE system is 3 dB better than the proposed scheme as the former is single carrier system not a multiplexing scheme. This is independent from the number of subcarriers used.

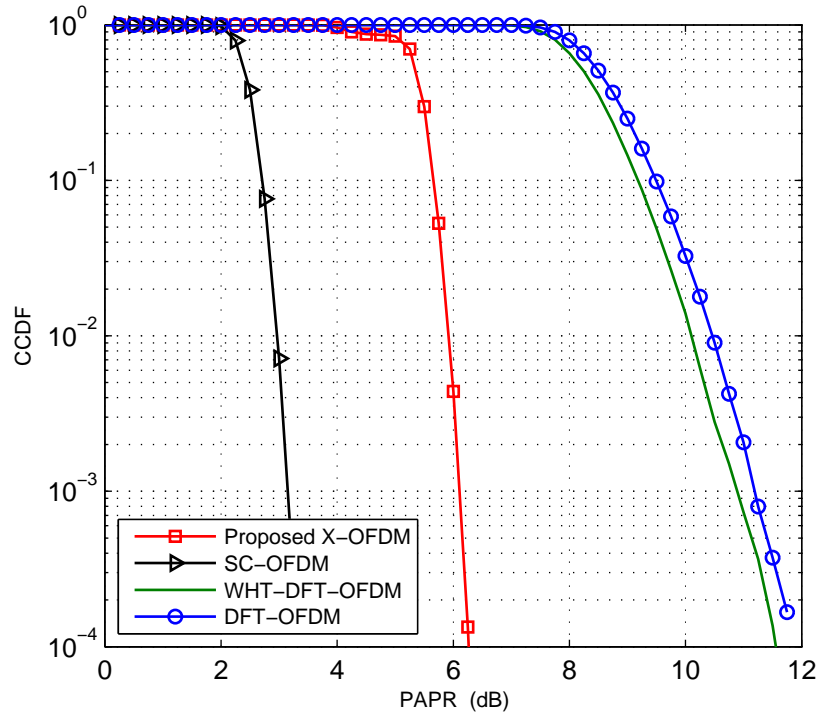


Figure 4.6: PAPR performance of the proposed X-OFDM, SC-FDE, WHT-OFDM and the conventional OFDM systems, using 16-QAM modulation and $N = 1024$.

Table 4.3: System parameters for simulations.

System Item	Parameter
Antenna type	Perfect
Modulation	QPSK and 16-QAM
Synchronisation	Complete
Channel type	ITU pedestrian B and ITU vehicular A
Equalisation	One-tap FDE
Number of Subcarriers (N)	1024
Duration of CP	$N/4$
Bandwidth	10MHz

4.7.2 BER Performance

4.7.2.1 Over Multipath Channels

The BER performance of the proposed X-OFDM system is evaluated in this section, over ITU channel pedestrian class B and vehicular class A, mathematically and by simulation and compared with that of the OFDM system and the SC-FDE system, for the 16-QAM and the QPSK modulations. The simulation is carried out according to the WiMAX standard with parameters are given in Table 4.3.

Figs 4.7 and 4.8 show the BER performance of the proposed X-OFDM, SC-FDE and the OFDM systems over pedestrian and vehicular channel models respectively for both the 16-QAM and the QPSK modulations. The theoretical results in Figs 4.7 and 4.8 are obtained by using the BER formulas that are given in (4.27) and (4.28) for the case of ZF and (4.39) and (4.40) for the case of MMSE equalizer. It is noticeable that the simulated BER results agree with the theoretical BER results. It is evident from Figs. 4.7 and 4.8 that the proposed X-OFDM system achieves the same BER performance as SC-FDE and it is superior to the OFDM by about 15 dB E_b/N_0 . This in turn, supports our early explanation that the DHT distributes the effect of the channel dips over all other subcarriers which leads to the BER improvement. This is, however, not attainable in the conventional OFDM system counterpart as the information symbols on significantly attenuated subcarriers can not be recovered from the unaffected spectrum. It is also noteworthy that for the case of the OFDM system, the BER performance for the QPSK constellation is better than 16-QAM by about 3 dB E_b/N_0 , whilst it is about 6 dB E_b/N_0 better than that of the 16-QAM modulation for the case of our proposed X-OFDM system. This indicates that the proposed scheme can achieve further improvement as the constellation order is reduced.

It is also noted from Figs. 4.9-4.10 that, for the case of the ZF equalizer, the conventional OFDM outperforms both the SC-FDE and proposed X-OFDM systems by about 3 dB in terms of the BER performance for each QPSK and 16-QAM constellation.

To the end of this discussion, theoretical results corroborated by computer simulation in Figs. 4.7-4.10 show that for the case of the ZF detection, the OFDM system outperforms SC-FDE and our proposed system in term of BER performance. How-

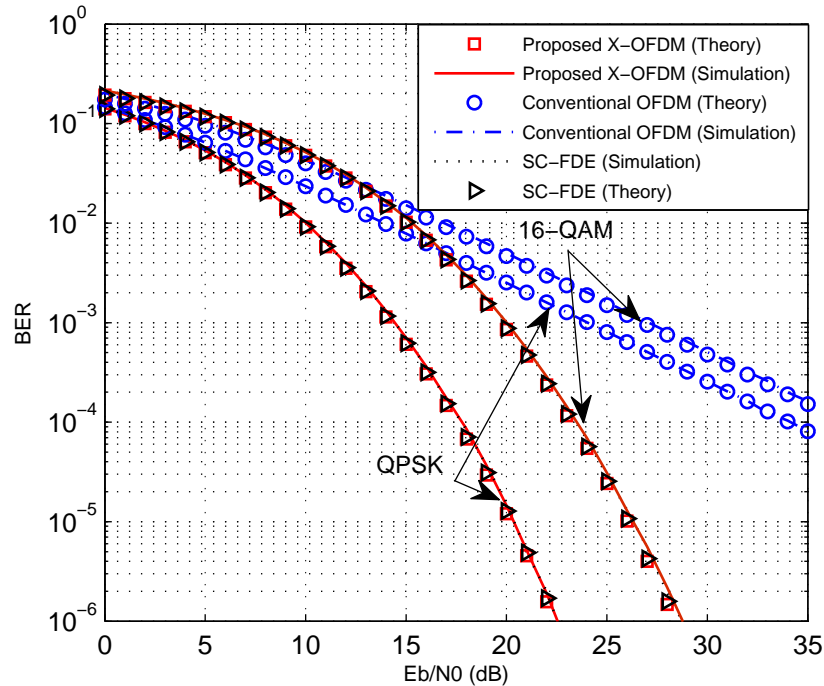


Figure 4.7: BER performance of the proposed X-OFDM, OFDM and SC-FDE systems for QPSK and 16-QAM modulations over ITU pedestrian B channel and MMSE detection.

ever, for the MMSE detection and at 10^{-4} BER, the proposed X-OFDM scheme can achieve around 15 dB E_b/N_0 gain over the OFDM system for different channel models and modulation formats, that is, as good performance as SC-FDE systems.

4.7.2.2 In the Presence of CFO

In this section we will examine the performance of the proposed X-OFDM system over frequency selective fast fading channels. The simulation is carried out according to the WiMAX standard where the rapid change in the international telecommunication union (ITU) pedestrian B channel is modelled by the frequency offset as a kind of Doppler shift. The results of 16-QAM and 64-QAM modulation is then mainly compared with the performance of the SC-FDE and the conventional OFDM. The transmission bandwidth is 10 MHz, the carrier frequency is 4 GHz and the number of subcarriers $N = 1024$ and CP of length $\frac{N}{4}$.

Fig. 4.11 shows the BER performance of the examined systems when the modulation is 16-QAM and for normalized CFO ($\epsilon = 0.025, 0.035$ and 0.05).

Over all the CFO scenarios, the proposed X-OFDM is less sensitive the CFO or fast variation of the channel than the SC-FDE. This is because the data symbols

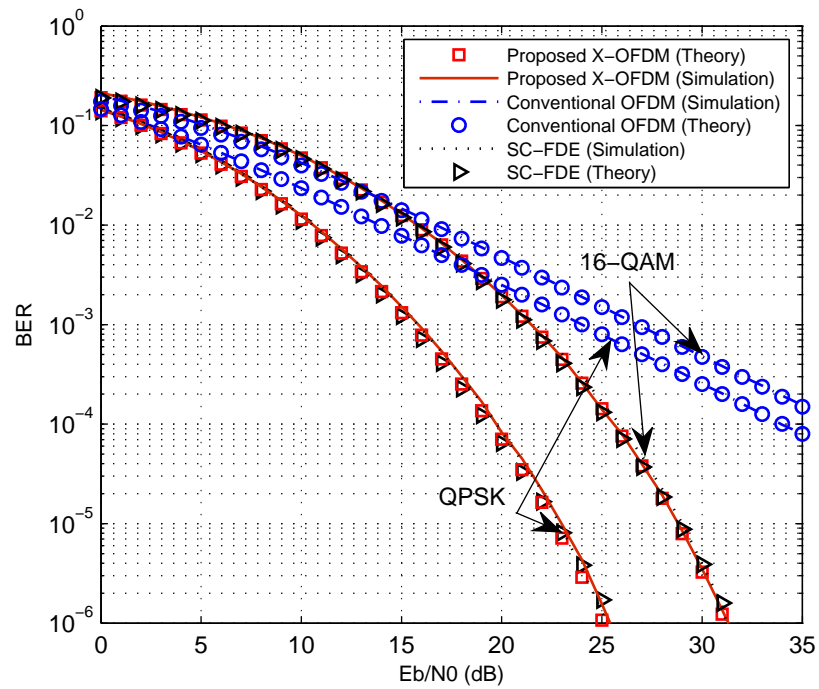


Figure 4.8: BER performance of the proposed X-OFDM, OFDM and SC-FDE systems for QPSK and 16-QAM modulations over ITU vehicular A channel and MMSE detection.

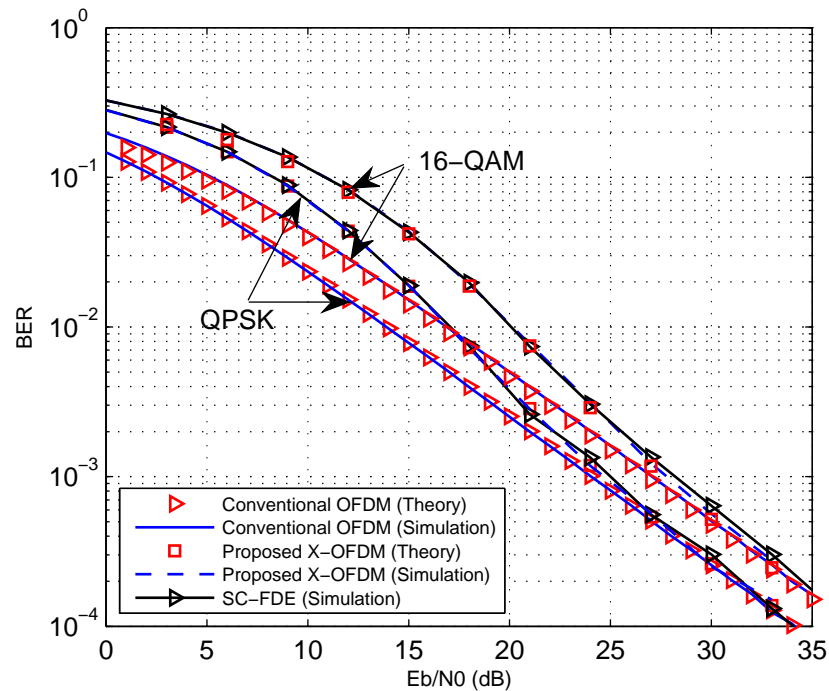


Figure 4.9: BER performance of the proposed X-OFDM, SC-FDE and the OFDM systems for QPSK and 16-QAM modulations over ITU pedestrian B channel and ZF detection.

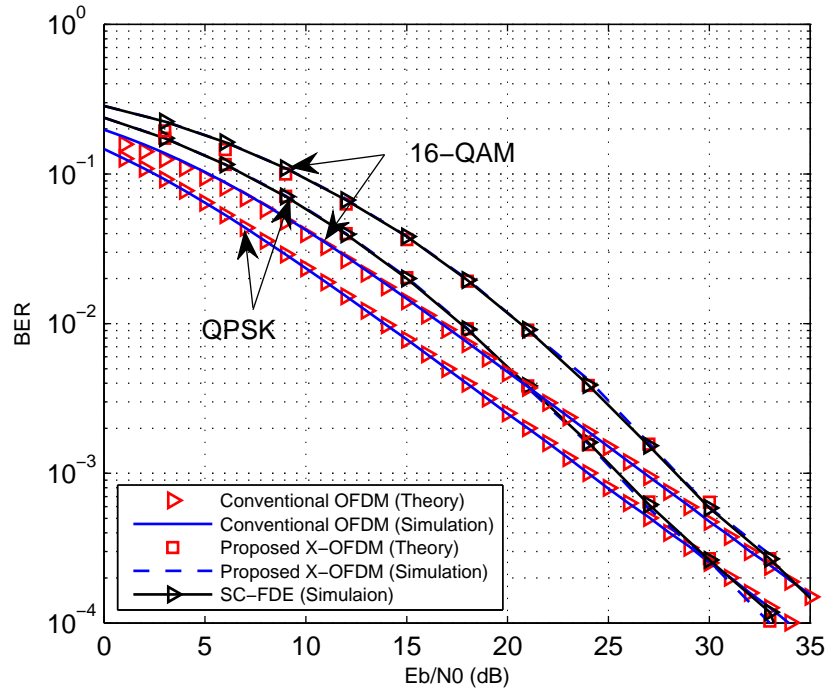


Figure 4.10: BER performance of the proposed X-OFDM, SC-FDE and the OFDM systems for QPSK and 16-QAM modulations over ITU vehicular A channel and ZF detection.

in the case of the SC-FDE convolved with the channel impulse response directly as there is no transform at the transmitter to multiplex the data symbols, which is not the case in our proposed scheme where the data symbols are multiplexed by the \mathbf{X} -transform before they convolved with the channel. In other words, when a CFO synchronization algorithm is used, the requirement of repeating the synchronization algorithm after certain number of frames is less in the case of our proposed system than the case of the SC-FDE which is an advantage to the proposed X-OFDM over the SC-FDE.

In comparison with the conventional OFDM, the proposed X-OFDM system is more sensitive to the CFO. However, it is still achieve better BER performance when the CFO= 0.025 and 0.035 as shown in Fig. 4.11.

This advantages of the proposed X-OFDM over the SC-FDE are also revealed for higher-level modulation (64-QAM) as shown in Fig. 4.12.

Fig. 4.13 shows the BER performance when the $M\&M$ [100] algorithm for CFO estimation is employed in this simulation where the number of subcarriers are $N = 1024$, iterative data $L_i = 8$, $\epsilon = 3.42$ and (E_b/N_0) is set to be 25 dB in order to get a precise estimation. It is clearly shown that the proposed X-OFDM and SC-FDE

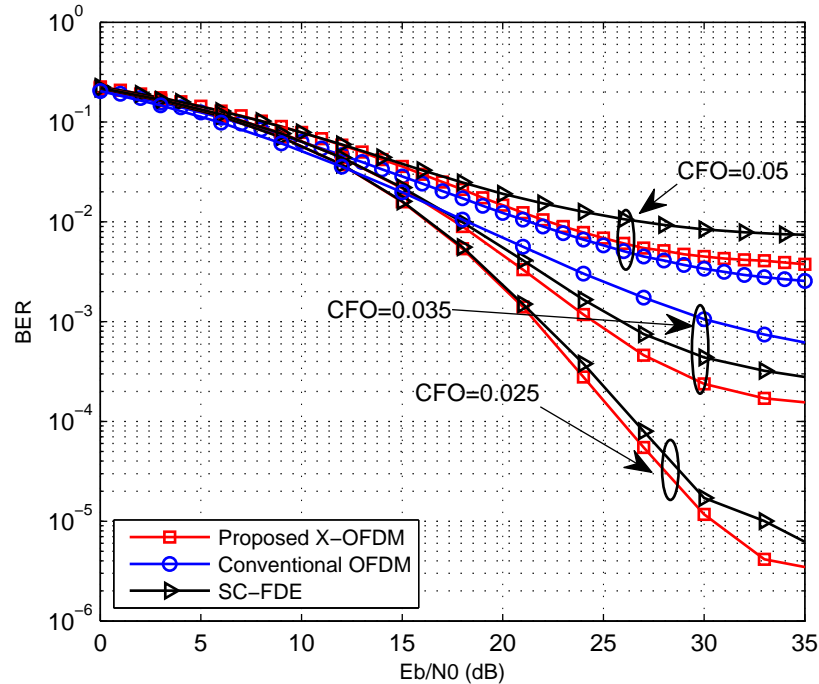


Figure 4.11: BER performance for the proposed X-OFDM and the OFDM systems over ITU pedestrian class B channel and CFO=0.02, 0.035 and 0.05 and 16-QAM modulation.

systems outperform the conventional OFDM system.

4.7.2.3 Coded and Coded-Interleaved Systems

For further investigation for the proposed scheme, forward error coding (FEC) is embedded with the proposed scheme and compared with coded OFDM. convolutional coding/Viterbi decoding is used with code rate equal to 0.5. Figs. 4.14 and 4.15 show the BER performances of coded X-OFDM and coded DFT-OFDM systems for the QPSK and the 16-QAM modulations and over vehicular A channel models respectively. It is clear that our proposed scheme is still superior to the conventional OFDM systems by about 12 dB E_b/N_0 gain at 10^{-4} BER.

4.8 Conclusion

In this chapter, a new fast orthogonal transform was introduced. This transform is named the **X**-transform because the non-zero elements of its matrix form the letter X. The new transform and its complexity are analysed and compared with the FFT, showing that the proposed **X**-transform has much lower arithmetic operations and

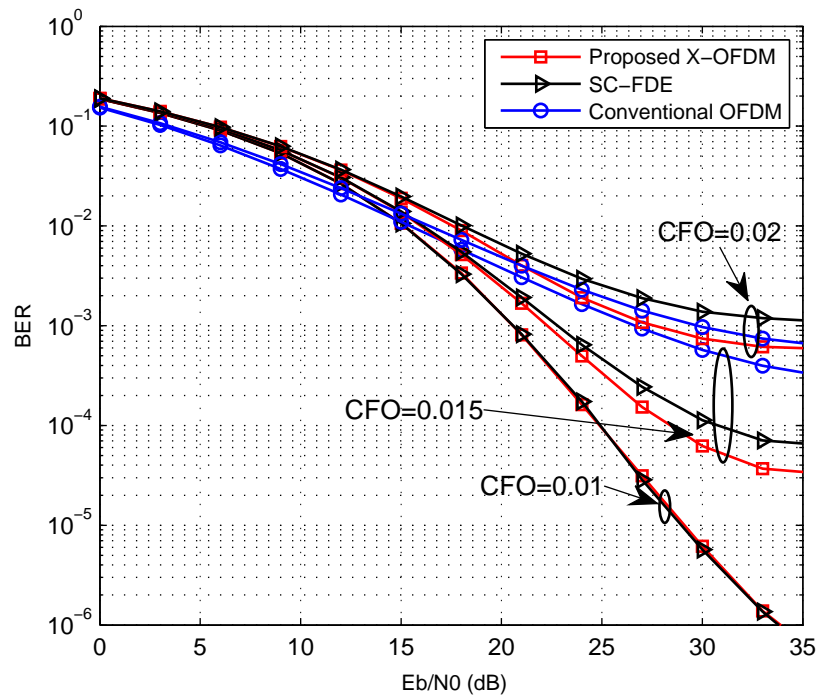


Figure 4.12: BER performance for the proposed X-OFDM and the OFDM systems over ITU pedestrian class B channel and CFO=0.01, 0.015 and 0.02 and 64-QAM modulation.

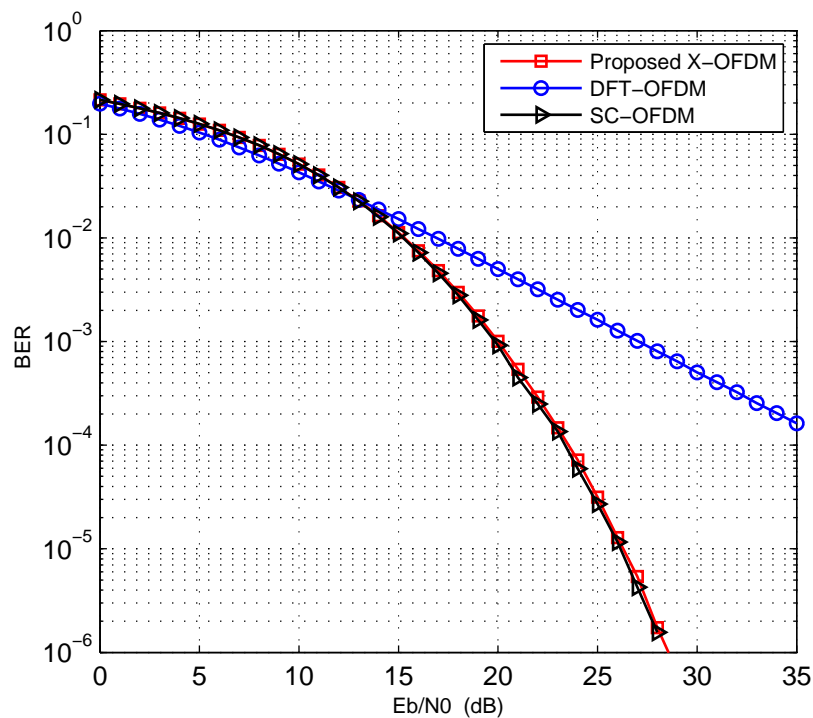


Figure 4.13: BER performance for the proposed X-OFDM, DFT-OFDM and SC-OFDM systems over ITU pedestrian class B channel and CFO=3.42 when 16-QAM modulation format and $M\&M$ synchronization algorithm are employed.

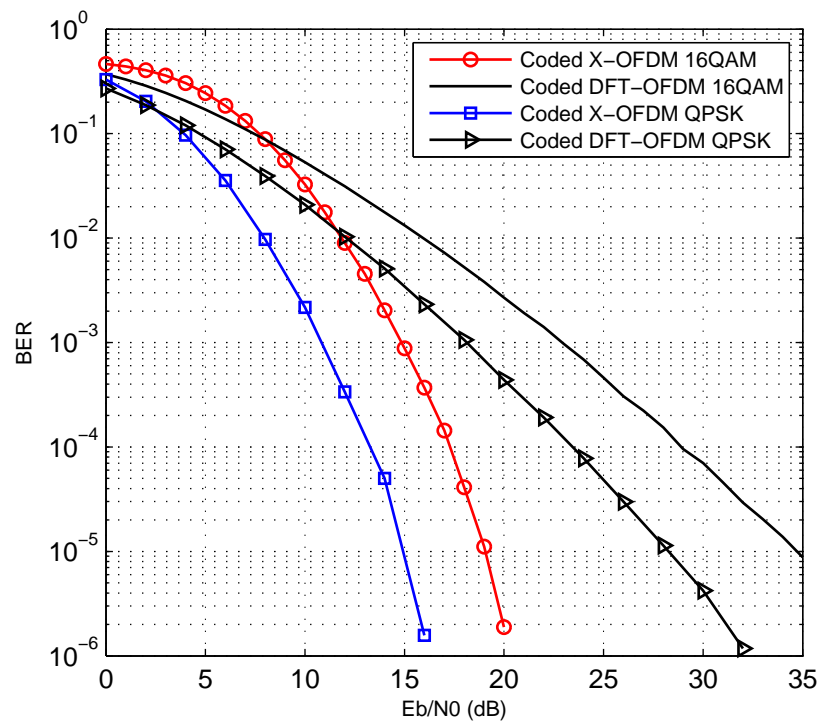


Figure 4.14: BER performance of coded proposed X-OFDM and coded OFDM systems for QPSK and 16-QAM modulations over ITU pedestrian B channel.

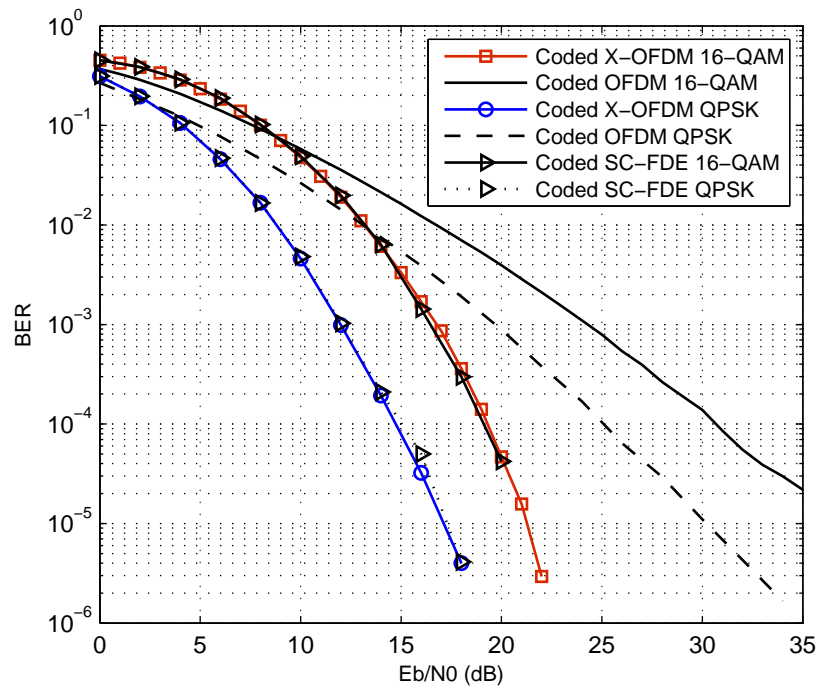


Figure 4.15: BER performance of coded proposed X-OFDM and coded OFDM systems for QPSK and 16-QAM modulations over ITU vehicular A channel.

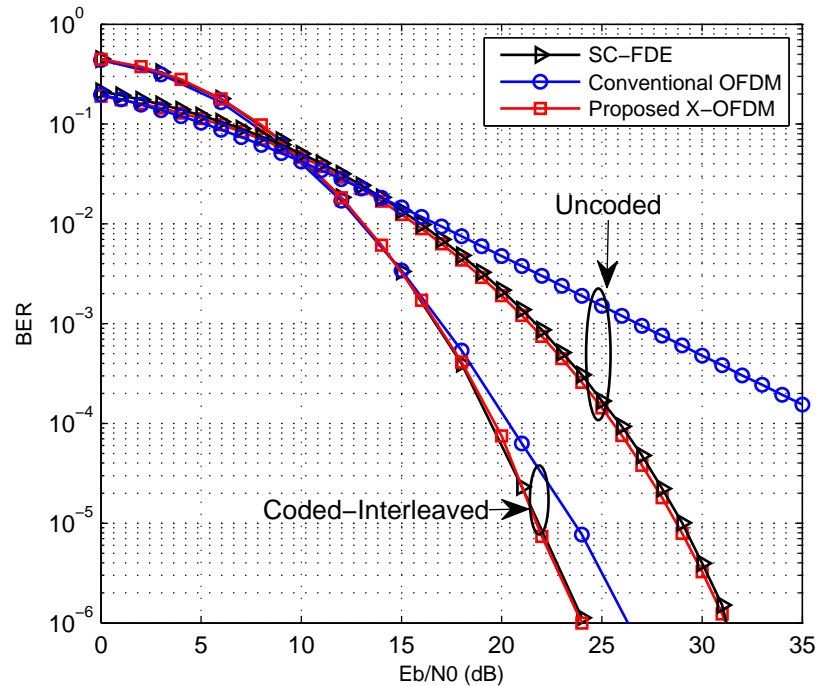


Figure 4.16: BER performance of coded-interleaved X-OFDM, coded-interleaved SC-FDE and coded-interleaved OFDM systems versus uncoded systems for 16-QAM modulation over ITU vehicular A channel.

complexity than the FFT. The \mathbf{X} -transform was then used as OFDM to produce the new X-OFDM. Mathematical analysis and simulation results have shown that the proposed X-OFDM system outperforms the conventional OFDM system in both PAPR and BER. The BER performances over ITU pedestrian and vehicular channel models were evaluated theoretically and by simulation for the QPSK and the 16-QAM modulations. The results showed that the proposed X-OFDM is better than the conventional OFDM by about 15 dB E_b/N_0 at 10^{-4} BER and achieves the same BER performance as SC-FDE system. The sensitivity of the proposed X-OFDM system to the CFO was investigated, revealing that the proposed scheme is better than the SC-FDE in its sensitive to the CFO, and it is more sensitive to the CFO in comparison to the conventional OFDM. The proposed scheme was also found to achieve a huge reduction of PAPR for all subcarriers in comparison with the conventional OFDM system. The applications of the proposed scheme can be extended to multiple input-multiple output (MIMO).

Chapter 5

Low Complexity \mathbf{X} -OFDM System for STBC Diversity Enhancement Over Frequency-Selective Fading Channels

5.1 Introduction

With increased reliance on the signal diversity for the OFDM, new schemes are constantly being developed to meet the demand of high speed broadband communications. In this chapter, the \mathbf{X} -transform is utilized in space-time block coding (STBC) OFDM (ST-OFDM) transmitter implementation where the \mathbf{X} -transform is used instead of the DFT. The \mathbf{X} -transform is used in transmitter implementation of the proposed ST- \mathbf{X} -OFDM which reduces the complexity enormously. The proposed ST- \mathbf{X} -OFDM system has the same single tap equalizer complexity as the approach in [75] with significant reduction in transmitter complexity. Unlike the approach in [75], the proposed system requires only two low complexity \mathbf{X} -transforms at the transmitter even though the data are drawn from complex constellation. The proposed ST- \mathbf{X} -OFDM system exploits the channel diversity and achieves significant SNR gain over the ST-OFDM systems. Moreover, the proposed scheme significantly mitigates the PAPR problem that affects the ST-OFDM system. The BER performance of the proposed scheme is evaluated theoretically and by computer simulation in this chapter over the ITU channel for both the QPSK and 16-QAM signal map-

ping. A precise BER derivation which tightly matches the simulated results is also presented in this chapter; over a diverse range of antenna diversity scenarios and mapping schemes. It is evident that the proposed ST-X-OFDM scheme achieves important SNR gain over the conventional ST-OFDM systems.

5.2 Proposed System

The proposed Alamouti ST-X-OFDM system with two transmit antennas at the transmitter and one antenna at the receiver is shown in Fig.5.1. The mapper is used to convert the binary data into a specific constellation. In this chapter, two kinds of constellation are used; quadrature phase-shift-keying (QPSK) and 16-array quadrature-amplitude-modulation (16-QAM). The information symbols, $\mathbf{S}^{(b)}$, $b = 1, 2$, are divided into two blocks, each of $N \times 1$ dimension. These information vectors are assumed to be zero-mean and carry the same power; its covariance matrix is given as:

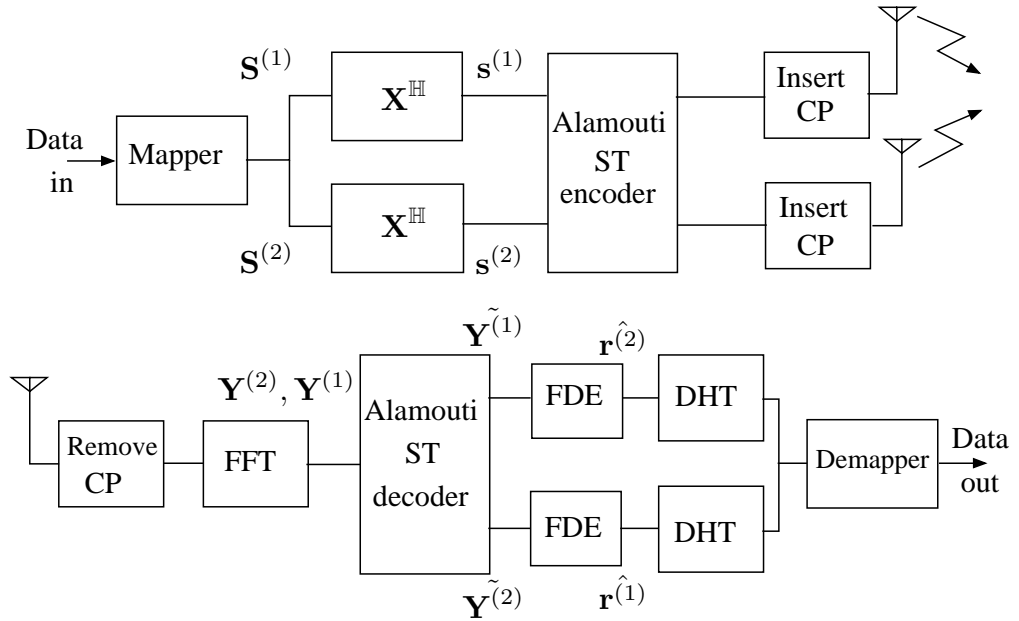


Figure 5.1: Proposed Alamouti ST-X-OFDM system block diagram.

$$\begin{aligned}
 \mathbf{R}_S &= E \left[\mathbf{S}^{(b)} \mathbf{S}^{(b)*} \right], \quad (b = 1, 2), \\
 &= E_s \mathbf{I}_N,
 \end{aligned} \tag{5.1}$$

where E_s is the signal energy per symbol. Each information vector is then aligned to a specific branch at the transmitter for modulation. Each information vector is processed by the DHT as:

$$r_n^{(b)} = \mathbf{A}_n \mathbf{S}^{(b)}, \quad (5.2a)$$

$$= \sum_{m=0}^{N-1} a_{n,m} S_m^{(b)}, \quad (b = 1, 2), \quad (5.2b)$$

where \mathbf{A}_n is the n^{th} row of the DHT matrix, \mathbf{A} , and $a_{n,m}$ denotes the n^{th} row, m^{th} column of the matrix \mathbf{A} . In matrix form, the Hartley modulated symbols in (5.2) can be written as

$$\mathbf{r}^{(b)} = \mathbf{A} \mathbf{S}^{(b)} \quad (b = 1, 2). \quad (5.3)$$

Alamouti STBC is then applied to the resulted vectors, $\mathbf{r}^{(1)}$ and $\mathbf{r}^{(2)}$, to produce two signals that aligned to the antennas at the transmitter. These signals are given as:

$$\begin{bmatrix} -\mathbf{r}^{(2)*} & \mathbf{r}^{(1)} \\ \mathbf{r}^{(1)*} & \mathbf{r}^{(2)} \end{bmatrix}. \quad (5.4)$$

The first column of (5.4) represents the signals from the first and second antenna at the transmitter to be simultaneously transmitted at time t . The second column of (5.4) denotes the signals to be simultaneously transmitted from the first and second transmitter antennas during the next transmission at time $t + T_s$, and $(\cdot)^*$ is the complex conjugate. The IFFT is then used for processing the resulting vectors as

$$s_k^{(b)} = \frac{1}{\sqrt{N}} \sum_{n=0}^{N-1} r_n^{(b)} e^{j \frac{2\pi nk}{N}}, \quad (k = 0, 1, \dots, N-1), \quad (5.5a)$$

$$s_k^{(b)\dagger} = \frac{1}{\sqrt{N}} \sum_{n=0}^{N-1} r_n^{(b)*} e^{j \frac{2\pi nk}{N}}, \quad (k = 0, 1, \dots, N-1), \quad (5.5b)$$

where $j = \sqrt{-1}$. In matrix form, (5.5) can be written as:

$$\mathbf{s}^{(b)} = \mathbf{F}^{\text{H}} \mathbf{r}^{(b)}, \quad (5.6a)$$

$$\mathbf{s}^{(b)\dagger} = \mathbf{F}^{\text{H}} \mathbf{r}^{(b)*}, \quad (5.6b)$$

where $\mathbf{s}^{(b)\dagger} = [s_1^{(b)*}, s_2^{(b)*}, \dots, s_{N-1}^{(b)*}, s_0^{(b)*}]^T$, \mathbf{F} is the normalized FFT matrix and $(\cdot)^{\mathbb{H}}$ is the Hermitian operation. Therefore, and for the aim of reducing the complexity by combining the DHT and IFFT transforms into single low complexity unitary transform, Alamouti code is performed after the IFFT as:

$$\mathbf{s}^{(b)} = \mathbf{F}^{\mathbb{H}} \mathbf{A} \mathbf{S}^{(b)}, \quad (5.7)$$

and then a modified Alamouti code is performed on $\mathbf{s}^{(b)}$, $b = 1, 2$, vectors as:

$$\begin{bmatrix} -\mathbf{s}^{(2)\dagger} & \mathbf{s}^{(1)} \\ \mathbf{s}^{(1)\dagger} & \mathbf{s}^{(2)} \end{bmatrix}. \quad (5.8)$$

5.3 Reducing Transmitter Complexity

From the above analysis, it can be seen that to convert the information symbols, \mathbf{S} , into OFDM symbols, \mathbf{s} , the information symbols must be processed by the DHT followed by the IFFT. When \mathbf{S} is complex, the DHT operation must be performed twice at each branch, one for the real part of \mathbf{S} whereas the another for the imaginary part. This means that for the case of Alamouti STBC system with two transmit antennas, four-times of the DHT as well as two-times of the FFT complexity is required.

The complexity of the DHT together with that of the IFFT is very high. To merge the DHT and the IFFT into the low complexity \mathbf{X} -transform and cancel the unnecessary arithmetic operations, following the same steps in chapter four. (5.7) is written in the fundamental kernel form as

$$s_k^{(b)} = \frac{1}{N} \sum_{n=0}^{N-1} \sum_{m=0}^{N-1} S_m^{(b)} \text{cas} \left(\frac{2\pi nm}{N} \right) e^{j \frac{2\pi nk}{N}}, \quad (5.9)$$

where $\text{cas}(\frac{2\pi nm}{N}) = \cos(\frac{2\pi nm}{N}) + \sin(\frac{2\pi nm}{N})$. By using trigonometric identities, (5.9) can be written as

$$\begin{aligned} s_k^{(b)} &= \frac{1}{N} \sum_{m=0}^{N-1} S_m^{(b)} \sum_{n=0}^{N-1} \frac{1}{2} \left[\cos \frac{2\pi n}{N} (m-k) + \cos \frac{2\pi n}{N} (m+k) \right] \\ &\quad + j \frac{1}{2} \left[\cos \frac{2\pi n}{N} (m-k) - \cos \frac{2\pi n}{N} (m+k) \right]. \end{aligned} \quad (5.10)$$

Equation (5.10) can be rewritten in more expressive form as

$$s_k^{(b)} = \sum_{m=0}^{N-1} S_m^{(b)} X_{km}, \quad (k = 0, 1, 2, \dots, N-1), \quad (5.11)$$

where X_{km} is the k^{th} , ($0 \leq k \leq N-1$), row and the m^{th} , ($0 \leq m \leq N-1$) column element of the \mathbf{X}^{H} (inverse \mathbf{X} transform (IXT)). From (5.10) one can notice the following; $X_{k,m} = 1$ when $k = m = 1$ or $k = m = \frac{N}{2}$, $X_{k,m} = \frac{1}{2} + j\frac{1}{2}$ when $k = m$ and $X_{k,m} = \frac{1}{2} - j\frac{1}{2}$ when $k = N - m$ and $X_{km} = 0$ elsewhere. Thus equation (5.7) can be rewritten as

$$\mathbf{s}^{(b)} = \mathbf{X}^{\text{H}} \mathbf{S}^{(b)}. \quad (5.12)$$

The inverse \mathbf{X} -transform can be expressed an in (4.11) as

$$\mathbf{X}_8^{\text{H}} = \frac{1}{2} \begin{bmatrix} 2 & 0 & 0 & 0 & 0 & 0 & 0 & 0 \\ 0 & 1+j1 & 0 & 0 & 0 & 0 & 0 & 1-j1 \\ 0 & 0 & 1+j1 & 0 & 0 & 0 & 1-j1 & 0 \\ 0 & 0 & 0 & 1+j1 & 0 & 1-j1 & 0 & 0 \\ 0 & 0 & 0 & 0 & 2 & 0 & 0 & 0 \\ 0 & 0 & 0 & 1-j1 & 0 & 1+j1 & 0 & 0 \\ 0 & 0 & 1-j1 & 0 & 0 & 0 & 1+j1 & 0 \\ 0 & 1-j1 & 0 & 0 & 0 & 0 & 0 & 1+j1 \end{bmatrix}. \quad (5.13)$$

To avoid the intersymbol interference (ISI) between consecutive transmitted symbols, a cyclic prefix (CP), the last N_g samples of the symbol in (5.12) must be no less than the maximum access delay, is appended to the beginning of the same symbol to alleviate the ISI.

5.4 Two Transmit Antennas and One Receive Antenna (2×1)

Consider two transmission phases; at the first phase, the two OFDM signals $\mathbf{s}^{(1)}$ and $\mathbf{s}^{(2)}$ are simultaneously transmitted at a specific time t from antenna 1 and antenna 2 respectively. It follows that, at the second phase, $-\mathbf{s}^{(2)\dagger}$ and $\mathbf{s}^{(1)\dagger}$ are simultaneously transmitted at time $t+T_s$ from antenna 1 and antenna 2 respectively.

5.4 Two Transmit Antennas and One Receive Antenna (2×1)

The transmitted signal from the b^{th} transmitter antenna to the receive antenna passes through a multipath frequency-selective fading channels ($h_l^{(b)} \neq 0, \forall 0 < l < L$) of $L+1$ taps and corrupted by an additive white Gaussian noise (AWGN) v . The channels $h_l^{(1)}$ and $h_l^{(2)}$ are assumed but not necessary to have the same number of taps. Assuming that the channels are statistically independent and invariant during two OFDM consecutive symbols. Therefore the consecutive received signals at time t , $y_k^{(1)}$, and $t + T_s$, $y_k^{(2)}$, can be respectively written as:

$$y_k^{(1)} = \sum_{l=0}^L h_l^{(1)} s_{k-l}^{(1)} + \sum_{l=0}^L h_l^{(2)} s_{k-l}^{(2)} + v_k^{(1)}, \quad (5.14)$$

and

$$y_k^{(2)} = - \sum_{l=0}^L h_l^{(1)} s_{k-l}^{(2)\dagger} + \sum_{l=0}^L h_l^{(2)} s_{k-l}^{(1)\dagger} + v_k^{(2)}. \quad (5.15)$$

The guard interval, represented by the CP, is then discarded from the received signal $y_k^{(b)}$. The resulted signal is then processed by the FFT producing signal in frequency domain which can be written as:

$$Y_n^{(b)} = \frac{1}{\sqrt{N}} \sum_{k=0}^{N-1} y_k^{(b)} e^{-j\frac{2\pi nk}{N}} \quad (n = 0, 1, \dots, N-1). \quad (5.16)$$

For $b = 1$ and by substituting (5.14) into (5.16) yield:

$$\begin{aligned} Y_n^{(1)} &= \frac{1}{\sqrt{N}} \left[\sum_{k=0}^{N-1} \left(\sum_{l=0}^L h_l^{(1)} s_{k-l}^{(1)} \right) e^{-j\frac{2\pi nk}{N}} + \sum_{k=0}^{N-1} \left(\sum_{l=0}^L h_l^{(2)} s_{k-l}^{(2)} \right) e^{-j\frac{2\pi nk}{N}} \right. \\ &\quad \left. + \sum_{k=0}^{N-1} v_k^{(1)} e^{-j\frac{2\pi nk}{N}} \right]. \end{aligned} \quad (5.17)$$

Substituting (5.5) into (5.17) yield

$$\begin{aligned} Y_n^{(1)} &= \frac{1}{N} \sum_{k=0}^{N-1} \left[\sum_{l=0}^L h_l^{(1)} \left(\sum_{n=0}^{N-1} r_n^{(1)} e^{j\frac{2\pi n(k-l)}{N}} \right) \right] e^{-j\frac{2\pi nk}{N}} \\ &\quad + \sum_{k=0}^{N-1} \left[\sum_{l=0}^L h_l^{(2)} \left(\sum_{n=0}^{N-1} r_n^{(2)} e^{j\frac{2\pi n(k-l)}{N}} \right) \right] e^{-j\frac{2\pi nk}{N}} \\ &\quad + \sum_{k=0}^{N-1} v_k^{(1)} e^{-j\frac{2\pi nk}{N}}. \end{aligned} \quad (5.18)$$

Because of the orthogonality property of the FFT, (5.18) can be simplified to

$$\begin{aligned} Y_n^{(1)} &= r_n^{(1)} \sum_{l=0}^L h_l^{(1)} e^{-j\frac{2\pi nl}{N}} + r_n^{(2)} \sum_{l=0}^L h_l^{(2)} e^{-j\frac{2\pi nl}{N}} + \Omega_n^{(1)}, \\ &= r_n^{(1)} H_n^{(1)} + r_n^{(2)} H_n^{(2)} + \Omega_n^{(1)}. \end{aligned} \quad (5.19)$$

Similarly, $Y_n^{(2)*}$ can be written as

$$Y_n^{(2)*} = r_n^{(1)} H_n^{(2)*} - r_n^{(2)} H_n^{(1)*} + \Omega_n^{(2)*}. \quad (5.20)$$

In (5.19) and (5.20), Ω_n is the frequency domain representation of the AWGN (v_k) and $H_n = \sum_{l=0}^L h_l e^{-i\frac{2\pi nl}{N}}$, ($0 \leq n \leq N-1$) is the channel transfer function. In more expressive form, (5.19) and (5.20) can be written as:

$$Y_n^{(1,2)} = H_n^{(1,2)} r_n^{(1,2)} + \Omega_n^{(1,2)}, \quad (5.21)$$

where $Y_n^{(1,2)} = [Y_n^{(1)} \quad Y_n^{(2)*}]^T$, $H_n^{(1,2)} = \begin{bmatrix} H_n^{(1)} & H_n^{(2)} \\ H_n^{(2)*} & -H_n^{(1)*} \end{bmatrix}$, $r_n^{(1,2)} = [r_n^{(1)} \quad r_n^{(2)}]^T$ and $\Omega_n^{(1,2)} = [\Omega_n^{(1)} \quad \Omega_n^{(2)*}]^T$. To generalise (5.21) to all $n = 0, 1, \dots, N-1$, we use the following notations: $\mathbf{h}^{(1)} = \text{diag}(H_n^{(1)})_{n=0}^{N-1}$, $\mathbf{h}^{(2)} = \text{diag}(H_n^{(2)})_{n=0}^{N-1}$, $\mathbf{Y}^{(1)} = (Y_n^{(1)})_{n=0}^{N-1}$, $\mathbf{Y}^{(2)} = (Y_n^{(2)})_{n=0}^{N-1}$, $\mathbf{\Omega}^{(1)} = (\Omega_n^{(1)})_{n=0}^{N-1}$. Therefore, (5.21) can be written as

$$\mathbf{Y}^{(1,2)} = \mathbf{H}^{(1,2)} \mathbf{r}^{(1,2)} + \mathbf{\Omega}^{(1,2)}, \quad (5.22)$$

where $\mathbf{Y}^{(1,2)} = \begin{bmatrix} \mathbf{Y}^{(1)} \\ \mathbf{Y}^{(2)*} \end{bmatrix}$, $\mathbf{H}^{(1,2)} = \begin{bmatrix} \mathbf{h}^{(1)} & \mathbf{h}^{(2)} \\ \mathbf{h}^{(2)*} & -\mathbf{h}^{(1)*} \end{bmatrix}$, $\mathbf{r}^{(1,2)} = \begin{bmatrix} \mathbf{r}^{(1)} \\ \mathbf{r}^{(2)} \end{bmatrix}$ and $\mathbf{\Omega}^{(1,2)} = \begin{bmatrix} \mathbf{\Omega}^{(1)} \\ \mathbf{\Omega}^{(2)*} \end{bmatrix}$.

In matrix form, (5.22) can be written as

$$\begin{bmatrix} \mathbf{Y}^{(1)} \\ \mathbf{Y}^{(2)*} \end{bmatrix} = \begin{bmatrix} \mathbf{h}^{(1)} & \mathbf{h}^{(2)} \\ \mathbf{h}^{(2)*} & -\mathbf{h}^{(1)*} \end{bmatrix} \begin{bmatrix} \mathbf{r}^{(1)} \\ \mathbf{r}^{(2)} \end{bmatrix} + \begin{bmatrix} \mathbf{\Omega}^{(1)} \\ \mathbf{\Omega}^{(2)*} \end{bmatrix}. \quad (5.23)$$

At the receiver side, the Alamouti decoder is then performed to produce two vectors, $\tilde{\mathbf{Y}}^{(1)}$ and $\tilde{\mathbf{Y}}^{(2)*}$ as:

$$\tilde{\mathbf{Y}}^{(1,2)} = \left[\mathbf{H}^{(1,2)} \right]^{\mathbb{H}} \mathbf{Y}^{(1,2)}, \quad (5.24)$$

where $\tilde{\mathbf{Y}}^{(1,2)} = \left[\tilde{\mathbf{Y}}^{(1)} \quad \tilde{\mathbf{Y}}^{(2)*} \right]^T$. Therefore, these two vectors are given as

$$\tilde{\mathbf{Y}}^{(1)} = (\mathbf{h}^{(1)*} \mathbf{h}^{(1)} + \mathbf{h}^{(2)} \mathbf{h}^{(2)*}) \mathbf{r}^{(1)} + \mathbf{h}^{(1)*} \boldsymbol{\Omega}^{(1)} + \mathbf{h}^{(2)} \boldsymbol{\Omega}^{(2)*}, \quad (5.25a)$$

$$\tilde{\mathbf{Y}}^{(2)*} = (\mathbf{h}^{(2)*} \mathbf{h}^{(2)} + \mathbf{h}^{(1)} \mathbf{h}^{(1)*}) \mathbf{r}^{(2)} + \mathbf{h}^{(2)*} \boldsymbol{\Omega}^{(1)} - \mathbf{h}^{(1)} \boldsymbol{\Omega}^{(2)*}. \quad (5.25b)$$

In (5.25), $\mathbf{h}^{(1)*} \mathbf{h}^{(1)} + \mathbf{h}^{(2)} \mathbf{h}^{(2)*}$ is a diagonal matrix its diagonal elements are given as $(|H_n^{(1)}|^2 + |H_n^{(2)}|^2)_{n=0}^{N-1}$. More expressively, in elements form, (5.25) can be written as

$$\tilde{Y}_n^{(1)} = r_n^{(1)} (|H_n^{(1)}|^2 + |H_n^{(2)}|^2) + \Omega_n^{(1)} H_n^{(1)*} + \Omega_n^{(2)*} H_n^{(2)}, \quad (5.26)$$

and

$$\tilde{Y}_n^{(2)*} = r_n^{(2)} (|H_n^{(1)}|^2 + |H_n^{(2)}|^2) + \Omega_n^{(1)} H_n^{(2)*} - \Omega_n^{(2)*} H_n^{(1)}. \quad (5.27)$$

The channel equalization is then performed in frequency domain, after the FFT, for instance, ZF and MMSE equalizers are taken into consideration in this work as:

5.4.1 Zero-Forcing (ZF) Equalizer

The compensation for the channel effects on the received signal can be achieved by ZF equalizer by simply dividing each individual sample of the received vector, $\tilde{Y}_n^{(1)}$ in (5.26), and $\tilde{Y}_n^{(2)*}$ in (5.27), by the corresponding value of the channel transfer function $(|H_n^{(1)}|^2 + |H_n^{(2)}|^2)$ as:

$$\hat{r}_n^{(1)} = \frac{\tilde{Y}_n^{(1)}}{|H_n^{(1)}|^2 + |H_n^{(2)}|^2}. \quad (5.28)$$

For the sake of brevity, the notation $\Sigma_n = |H_n^{(1)}|^2 + |H_n^{(2)}|^2$ is used. Thus, (5.28) is written as

$$\begin{aligned} \hat{r}_n^{(1)} &= \frac{\tilde{Y}_n^{(1)}}{\Sigma_n}, \\ &= r_n + \xi_n^{(1)} + \xi_n^{(2)}, \end{aligned} \quad (5.29)$$

where $\xi_n^{(1)} = \frac{\Omega_n^{(1)} H_n^{(1)*}}{\Sigma_n}$ and $\xi_n^{(2)} = \frac{\Omega_n^{(2)*} H_n^{(2)}}{\Sigma_n}$ represent the amplified AWGN noise part from the two consecutive received signals. Substituting (5.2) into (5.29) yields

$$\hat{r}_n = \sum_{m=0}^{N-1} a_{n,m} S_m + \xi_n^{(1)} + \xi_n^{(2)}. \quad (5.30)$$

After removing the channel gain, the equalized signal, \hat{r}_n , is then transformed by the matrix \mathbf{A} as follows

$$q_i^{ZF} = \sum_{n=0}^{N-1} a_{i,n} \hat{r}_n \quad (i = 0, 1, 2, \dots, N-1). \quad (5.31)$$

Substituting (5.30) into (5.31) yields

$$\begin{aligned} q_i^{ZF} &= \sum_{n=0}^{N-1} a_{i,n} \left(\sum_{m=0}^{N-1} a_{n,m} S_m \right) + \sum_{n=0}^{N-1} a_{i,n} \xi_n^{(1)} \\ &\quad + \sum_{n=0}^{N-1} a_{i,n} \xi_n^{(2)} \quad (i = 0, 1, 2, \dots, N-1). \end{aligned} \quad (5.32)$$

Since the DHT is an orthogonal transform, $\sum_{n=0}^{N-1} a_{i,n} \times a_{n,m}$ equal to 1 only when $m = i$ and zero elsewhere, the first term of (5.32) equals to S_i , hence, (5.32) can be written as

$$q_i^{ZF} = S_i + \hat{\xi}_i^{(1)} + \hat{\xi}_i^{(2)}, \quad (5.33)$$

where $\hat{\xi}_i^{(1)} = \sum_{n=0}^{N-1} a_{i,n} \xi_n^{(1)}$ and $\hat{\xi}_i^{(2)} = \sum_{n=0}^{N-1} a_{i,n} \xi_n^{(2)}$.

The difference between the transmitted and received signals, $e_i^{ZF} = q_i^{ZF} - S_i$, is the error signal, it can be written as

$$\begin{aligned} e_i^{ZF} &= \hat{\xi}_i^{(1)} + \hat{\xi}_i^{(2)}, \\ &= \sum_{n=0}^{N-1} a_{i,n} \xi_n^{(1)} + \sum_{n=0}^{N-1} a_{i,n} \xi_n^{(2)}. \end{aligned} \quad (5.34)$$

5.4 Two Transmit Antennas and One Receive Antenna (2×1)

By substituting the equivalents of $\xi_n^{(1)}$ and $\xi_n^{(2)}$ into (5.34), the latter can be written as

$$\begin{aligned}
 e_i^{ZF} &= \hat{\xi}_i^{(1)} + \hat{\xi}_i^{(2)} \\
 &= \sum_{n=0}^{N-1} a_{i,n} \xi_n^{(1)} + \sum_{n=0}^{N-1} a_{i,n} \xi_n^{(2)} \\
 &= \sum_{n=0}^{N-1} a_{i,n} \left(\frac{\Omega_n^{(1)} H_n^{(1)*}}{\Sigma_n} \right) + \sum_{n=0}^{N-1} a_{i,n} \left(\frac{\Omega_n^{(2)*} H_n^{(2)}}{\Sigma_n} \right). \tag{5.35}
 \end{aligned}$$

The noise power, $\mathcal{P}_{n_i^{ZF}} = E[|e_i^{ZF}|^2]$, is given as:

$$\mathcal{P}_{n_i^{ZF}} = \sigma_v^2 \sum_{n=0}^{N-1} |a_{i,n}|^2 \frac{|H_n^{(1)}|^2}{\Sigma_n^2} + \sigma_v^2 \sum_{n=0}^{N-1} |a_{i,n}|^2 \frac{|H_n^{(2)}|^2}{\Sigma_n^2} \tag{5.36a}$$

$$= \sigma_v^2 \sum_{n=0}^{N-1} |a_{i,n}|^2 \frac{|H_n^{(1)}|^2 + |H_n^{(2)}|^2}{\Sigma_n^2} \tag{5.36b}$$

$$= \sigma_v^2 \sum_{n=0}^{N-1} |a_{i,n}|^2 \frac{1}{\Sigma_n}. \tag{5.36c}$$

Thus, the signal to noise ratio will be given as:

$$\beta_i^{ZF} = \frac{E[|S_i|^2]}{E[|e_i^{ZF}|^2]} \tag{5.37a}$$

$$= \frac{E[S_i S_i^*]}{E[e_i^{ZF} e_i^{ZF*}]} \tag{5.37b}$$

$$= \frac{E_s}{\mathcal{P}_{n_i^{ZF}}}, \tag{5.37c}$$

where E_s is the symbol power, it is equal to $4E_b$ for the case of the 16-QAM whilst equal to $2E_b$ for the case of the QPSK. Substituting (5.36c) into (5.37c) yields

$$\beta_i^{ZF} = \frac{\gamma_s}{\sum_{n=0}^{N-1} |a_{i,n}|^2 \frac{1}{\Sigma_n}}, \tag{5.38}$$

where $\gamma_s = \frac{E_s}{\sigma_v^2}$ is the signal power (in terms of symbol) to noise ratio. The BER of the individual subchannels are respectively given as in [92] as follows:

$$P_e^{M-PSK} = \frac{\mu}{m_b} \frac{1}{N} \sum_{m=0}^{N-1} Q \left(\sqrt{2\beta_m} \sin\left(\frac{\pi}{M}\right) \right), \tag{5.39}$$

and

$$P_e^{M-QAM} = \frac{4 - 2^{(2-m_b/2)}}{m_b} \frac{1}{N} \sum_{m=0}^{N-1} Q \left(\sqrt{\frac{3\beta_m}{M-1}} \right). \quad (5.40)$$

In (5.39) and (5.40), μ denotes the number of nearest neighbours signal points ($\mu_{QPSK} = 2$ and $\mu_{16-QAM} = 3$), M is the level on constellation and $m_b = \log_2 M$ represents the number of bits in each digitally encoded symbol, $Q(x)$ denotes the Q-function of x and β_m is the signal power, per symbol, to noise power ratio. In other words, by substituting the specific parameters that assigned to the QPSK and the 16-QAM modulations and substituting (5.38) into (5.39) and (5.40), the BER is respectively given as:

$$P_e^{QPSK} = \frac{1}{N} \sum_{i=1}^N Q \left(\sqrt{\frac{\gamma_s}{\sum_{n=0}^{N-1} |a_{i,n}|^2 \frac{1}{\Sigma_n}}} \right), \quad (5.41)$$

and

$$P_e^{16-QAM} = \frac{3}{4N} \sum_{i=1}^N Q \left(\sqrt{\frac{\gamma_s}{5 \sum_{n=0}^{N-1} |a_{i,n}|^2 \frac{1}{\Sigma_n}}} \right). \quad (5.42)$$

5.4.2 Minimum Mean-Square-Error (MMSE) Equalizer

The MMSE equalizer, χ_n , is defined as:

$$\begin{aligned} \chi_n &= \frac{E_s}{E_s \Sigma_n + \sigma_v^2}, \\ &= \frac{\gamma_s}{1 + \gamma_s \Sigma_n}. \end{aligned} \quad (5.43)$$

The MMSE equalization is achieved by multiplying the signal $\hat{r}_n^{(b)}$ by χ_n as:

$$\hat{r}_n^{(1)} = r_n \Sigma_n \chi_n + \Omega_n^{(1)} H_n^{(1)*} \chi_n + \Omega_n^{(2)*} H_n^{(2)} \chi_n. \quad (5.44)$$

Substituting (5.2) into (5.44) yields

$$\hat{r}_n^{(1)} = \sum_{m=0}^{N-1} a_{n,m} S_m \Sigma_n \chi_n + \Omega_n^{(1)} H_n^{(1)*} \chi_n + \Omega_n^{(2)*} H_n^{(2)} \chi_n. \quad (5.45)$$

The resulted signal is then transformed by the DHT to recover the transmitted symbols as

$$\begin{aligned}
 q_i^{MMSE} &= \sum_{n=0}^{N-1} a_{i,n} \left(\sum_{m=0}^{N-1} a_{n,m} S_m \Sigma_n \chi_n \right) + \sum_{n=0}^{N-1} a_{i,n} \Omega_n^{(1)} H_n^{(1)*} \chi_n \\
 &+ \sum_{n=0}^{N-1} a_{i,n} \Omega_n^{(2)*} H_n^{(2)} \chi_n.
 \end{aligned} \tag{5.46}$$

Same as the case of the ZF equalizer, because of the orthogonality property of the DHT, the first term of (5.46) can be simplified to $\sum_{n=0}^{N-1} S_i H_n \chi_n$, thus (5.46) can be written as

$$q_i^{MMSE} = \sum_{n=0}^{N-1} a_{i,n} S_i \frac{\gamma_s \Sigma_n}{1 + \gamma_s \Sigma_n} + \sum_{n=0}^{N-1} a_{i,n} \Omega_n^{(1)} \frac{\gamma_s H_n^{(1)*}}{1 + \gamma_s \Sigma_n} + \sum_{n=0}^{N-1} a_{i,n} \Omega_n^{(2)*} \frac{\gamma_s H_n^{(2)}}{1 + \gamma_s \Sigma_n}. \tag{5.47}$$

The signal power, $\sigma_{s_i}^2 = E[|q_i^{MMSE}|^2]$, is given as

$$\begin{aligned}
 \mathcal{P}_{s_i}^{MMSE} &= \sum_{n=0}^{N-1} |a_{i,n}|^2 \frac{E_s \gamma_s^2 |\Sigma_n|^2}{[1 + \gamma_s \Sigma_n]^2} + \sum_{n=0}^{N-1} |a_{i,n}|^2 \frac{\sigma_v^2 \gamma_s^2 |H_n^{(1)}|^2}{[1 + \gamma_s \Sigma_n]^2} \\
 &+ \sum_{n=0}^{N-1} |a_{i,n}|^2 \frac{\sigma_v^2 \gamma_s^2 |H_n^{(2)}|^2}{[1 + \gamma_s \Sigma_n]^2}.
 \end{aligned} \tag{5.48}$$

In second and third terms of (5.48), $\sigma_v^2 \gamma_s^2 = E_s \gamma_s$. Thus, (5.48) can be written as

$$\begin{aligned}
 \mathcal{P}_{s_i}^{MMSE} &= \sum_{n=0}^{N-1} |a_{i,n}|^2 \frac{E_s \gamma_s^2 |\Sigma_n|^2}{[1 + \gamma_s \Sigma_n]^2} + \sum_{n=0}^{N-1} |a_{i,n}|^2 \frac{E_s \gamma_s |H_n^{(1)}|^2}{[1 + \gamma_s \Sigma_n]^2} \\
 &+ \sum_{n=0}^{N-1} |a_{i,n}|^2 \frac{E_s \gamma_s |H_n^{(2)}|^2}{[1 + \gamma_s \Sigma_n]^2}.
 \end{aligned} \tag{5.49}$$

After some manipulation, (5.49) can be written as

$$\begin{aligned}
 \mathcal{P}_{s_i}^{MMSE} &= \sum_{n=0}^{N-1} |a_{i,n}|^2 \frac{E_s \gamma_s^2 |\Sigma_n|^2}{[1 + \gamma_s \Sigma_n]^2} + \sum_{n=0}^{N-1} |a_{i,n}|^2 \frac{E_s \gamma_s}{[1 + \gamma_s \Sigma_n]^2} (|H_n^{(1)}|^2 + |H_n^{(2)}|^2) \\
 &= \sum_{n=0}^{N-1} |a_{i,n}|^2 \frac{E_s \gamma_s \Sigma_n}{1 + \gamma_s \Sigma_n}.
 \end{aligned} \tag{5.50}$$

The error signal is then calculated as the difference between the transmitted and the received data symbols, $e_i^{MMSE} = q_i^{MMSE} - S_i$, can be written as

$$\begin{aligned}
 e_i^{MMSE} &= \sum_{n=0}^{N-1} a_{i,n} S_i \frac{\gamma_s \Sigma_n}{1 + \gamma_s \Sigma_n} - S_i + \sum_{n=0}^{N-1} a_{i,n} \Omega_n^{(1)} \frac{\gamma_s H_n^{(1)*}}{1 + \gamma_s \Sigma_n} + \sum_{n=0}^{N-1} a_{i,n} \Omega_n^{(2)*} \frac{\gamma_s H_n^{(2)}}{1 + \gamma_s \Sigma_n} \\
 &= \sum_{n=0}^{N-1} a_{i,n} \left[\frac{\gamma_s \Sigma_n}{1 + \gamma_s \Sigma_n} - 1 \right] S_i + \sum_{n=0}^{N-1} a_{i,n} \Omega_n^{(1)} \frac{\gamma_s H_n^{(1)*}}{1 + \gamma_s \Sigma_n} \\
 &\quad + \sum_{n=0}^{N-1} a_{i,n} \Omega_n^{(2)*} \frac{\gamma_s H_n^{(2)}}{1 + \gamma_s \Sigma_n}. \tag{5.51}
 \end{aligned}$$

In (5.51), $\frac{\gamma_s \Sigma_n}{1 + \gamma_s \Sigma_n} - 1 = \frac{-1}{1 + \gamma_s \Sigma_n}$. Thus (5.51) can be rewritten as

$$\begin{aligned}
 e_i^{MMSE} &= S_i \sum_{n=0}^{N-1} a_{i,n} \frac{-1}{1 + \gamma_s \Sigma_n} + \sum_{n=0}^{N-1} a_{i,n} \Omega_n^{(1)} \frac{\gamma_s H_n^{(1)*}}{1 + \gamma_s \Sigma_n} \\
 &\quad + \sum_{n=0}^{N-1} a_{i,n} \Omega_n^{(2)*} \frac{\gamma_s H_n^{(2)}}{1 + \gamma_s \Sigma_n}. \tag{5.52}
 \end{aligned}$$

Since the DHT is a unitary transform, it does not affect the calculation of the power ($\sum_{n=0}^{N-1} |a_{i,n}|^2 = 1$). In other words, all \mathbf{S} , \mathbf{r} and \mathbf{s} have the same average power E_s and as the data symbols and the AWGN are statistically independent, the noise power of the i^{th} subchannel, $\mathcal{P}_{n_i^{MMSE}} = E[|e_i^{MMSE}|^2]$, is then expressed as

$$\begin{aligned}
 \mathcal{P}_{n_i^{MMSE}} &= \sum_{n=0}^{N-1} |a_{i,n}|^2 \frac{E_s}{[1 + \gamma_s \Sigma_n]^2} + \sum_{n=0}^{N-1} |a_{i,n}|^2 \frac{E_s \gamma_s |H_n^{(1)}|^2}{[1 + \gamma_s \Sigma_n]^2} \\
 &\quad + \sum_{n=0}^{N-1} |a_{i,n}|^2 \frac{E_s \gamma_s |H_n^{(2)}|^2}{[1 + \gamma_s \Sigma_n]^2}. \tag{5.53}
 \end{aligned}$$

After some manipulation, (5.53) can be simplified to

$$\begin{aligned}
 \mathcal{P}_{n_i^{MMSE}} &= \sum_{n=0}^{N-1} |a_{i,n}|^2 \frac{E_s}{[1 + \gamma_s \Sigma_n]^2} + \sum_{n=0}^{N-1} |a_{i,n}|^2 \frac{E_s \gamma_s}{[1 + \gamma_s \Sigma_n]^2} (|H_n^{(1)}|^2 + |H_n^{(2)}|^2) \\
 &= \sum_{n=0}^{N-1} |a_{i,n}|^2 \frac{E_s}{1 + \gamma_s \Sigma_n}. \tag{5.54}
 \end{aligned}$$

The SNR of the i^{th} subchannel $\beta_i^{MMSE} = \frac{\mathcal{P}_{s_i^{MMSE}}}{\mathcal{P}_{n_i^{MMSE}}}$ is then given as

$$\beta_i^{MMSE} = \frac{\sum_{n=0}^{N-1} |a_{i,n}|^2 \frac{\gamma_s \Sigma_n}{1+\gamma_s \Sigma_n}}{\sum_{n=0}^{N-1} |a_{i,n}|^2 \frac{1}{1+\gamma_s \Sigma_n}}. \quad (5.55)$$

The overall BER, for QPSK and 16-QAM modulation formats, can be respectively given as:

$$P_e^{QPSK} = \frac{1}{N} \sum_{i=0}^{N-1} Q \left(\sqrt{\frac{\sum_{n=0}^{N-1} |a_{i,n}|^2 \frac{\gamma_s \Sigma_n}{1+\gamma_s \Sigma_n}}{\sum_{n=0}^{N-1} |a_{i,n}|^2 \frac{1}{1+\gamma_s \Sigma_n}}} \right), \quad (5.56)$$

and

$$P_e^{16-QAM} = \frac{3}{4N} \sum_{i=0}^{N-1} Q \left(\sqrt{\frac{\sum_{n=0}^{N-1} |a_{i,n}|^2 \frac{\gamma_s \Sigma_n}{1+\gamma_s \Sigma_n}}{5 \sum_{n=0}^{N-1} |a_{i,n}|^2 \frac{1}{1+\gamma_s \Sigma_n}}} \right). \quad (5.57)$$

5.5 Two Transmit and Two Receive Antennas (2×2)

Further diversity, hence, further performance improvement in the proposed ST-X-OFDM systems' transmission can be achieved at the cost of adding another antenna at the receiver. Thus, the system is with two antennas at the transmitter and two antennas at the receiver (2×2) as shown in Fig. 5.2. At the receive antenna (1), the received signals during the time symbols t and $t + T_s$ are given, respectively, as in (5.14) and (5.15)

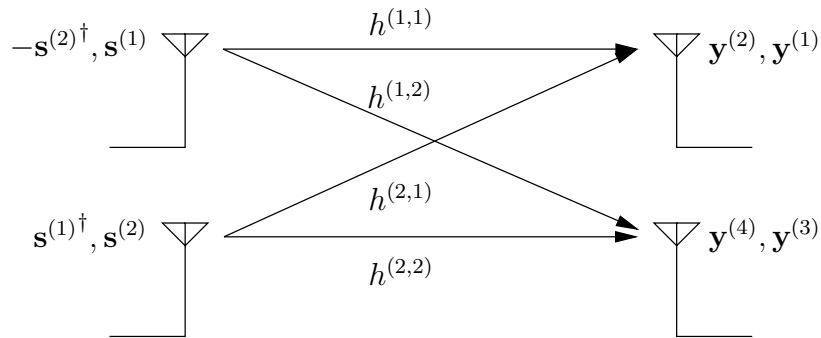


Figure 5.2: Two transmit antennas and two receive antennas.

$$y_k^{(1)} = \sum_{l=0}^L h_l^{(1,1)} s_{k-l}^{(1)} + \sum_{l=0}^L h_l^{(2,1)} s_{k-l}^{(2)} + v_k^{(1)}, \quad (5.58)$$

and

$$y_k^{(2)} = - \sum_{l=0}^L h_l^{(1,1)} s_{k-l}^{(2)\dagger} + \sum_{l=0}^L h_l^{(2,1)} s_{k-l}^{(1)\dagger} + v_k^{(2)}. \quad (5.59)$$

At the other receive antenna (2), the received signals during the time symbols t and $t + T_s$ are given as:

$$y_k^{(3)} = \sum_{l=0}^L h_l^{(1,2)} s_{k-l}^{(1)} + \sum_{l=0}^L h_l^{(2,2)} s_{k-l}^{(2)} + v_k^{(1)}, \quad (5.60)$$

and

$$y_k^{(4)} = - \sum_{l=0}^L h_l^{(1,2)} s_{k-l}^{(2)\dagger} + \sum_{l=0}^L h_l^{(2,2)} s_{k-l}^{(1)\dagger} + v_k^{(2)}. \quad (5.61)$$

After discarding the CP from each received signal, followed by the FFT process, the resulted signals can be written as:

$$\mathbf{Y}^{(1)} = \mathbf{h}^{(1,1)} \mathbf{r}^{(1)} + \mathbf{h}^{(2,1)} \mathbf{r}^{(2)} + \boldsymbol{\Omega}^{(1)}, \quad (5.62a)$$

$$\mathbf{Y}^{(2)*} = \mathbf{h}^{(2,1)*} \mathbf{r}^{(1)} - \mathbf{h}^{(1,1)*} \mathbf{r}^{(2)} + \boldsymbol{\Omega}^{(2)*}, \quad (5.62b)$$

$$\mathbf{Y}^{(3)} = \mathbf{h}^{(1,2)} \mathbf{r}^{(1)} + \mathbf{h}^{(2,2)} \mathbf{r}^{(2)} + \boldsymbol{\Omega}^{(3)}, \quad (5.62c)$$

$$\mathbf{Y}^{(4)*} = \mathbf{h}^{(2,2)*} \mathbf{r}^{(1)} - \mathbf{h}^{(1,2)*} \mathbf{r}^{(2)} + \boldsymbol{\Omega}^{(4)*}. \quad (5.62d)$$

In matrix form, the above equations can be written as

$$\mathbf{Y}' = \mathbf{H}' \mathbf{r}' + \boldsymbol{\Omega}' \quad (5.63)$$

where;

$$\mathbf{Y}' = \begin{bmatrix} \mathbf{Y}^{(1)} \\ \mathbf{Y}^{(2)*} \\ \mathbf{Y}^{(3)} \\ \mathbf{Y}^{(4)*} \end{bmatrix}, \quad \mathbf{H}' = \begin{bmatrix} \mathbf{h}^{(1,1)} & \mathbf{h}^{(2,1)} \\ \mathbf{h}^{(2,1)*} & -\mathbf{h}^{(1,1)*} \\ \mathbf{h}^{(1,2)} & \mathbf{h}^{(2,2)} \\ \mathbf{h}^{(2,2)*} & -\mathbf{h}^{(1,2)*} \end{bmatrix}, \quad \mathbf{r}' = \begin{bmatrix} \mathbf{r}^{(1)} \\ \mathbf{r}^{(2)} \end{bmatrix} \quad \text{and} \quad \boldsymbol{\Omega}' = \begin{bmatrix} \boldsymbol{\Omega}^{(1)} \\ \boldsymbol{\Omega}^{(2)*} \\ \boldsymbol{\Omega}^{(3)} \\ \boldsymbol{\Omega}^{(4)*} \end{bmatrix}. \quad \text{Alamouti}$$

STBC encoder is then applied to the received signals as follows:

$$\tilde{\mathbf{Y}}' = \mathbf{H}'^{\text{H}} \mathbf{Y}'. \quad (5.64)$$

Thus the two vectors, $\mathbf{Y}^{\tilde{(1)'}}$ and $\mathbf{Y}^{\tilde{(2)'}}$ are respectively given as:

$$\begin{aligned} \mathbf{Y}^{\tilde{(1)'}} &= \left(\mathbf{h}^{(1,1)*} \mathbf{h}^{(1,1)} + \mathbf{h}^{(2,1)} \mathbf{h}^{(2,1)*} + \mathbf{h}^{(1,2)*} \mathbf{h}^{(1,2)} + \mathbf{h}^{(2,2)} \mathbf{h}^{(2,2)*} \right) \mathbf{r}^{(1)} + \\ &\quad \mathbf{h}^{(1,1)*} \boldsymbol{\Omega}^{(1)} + \mathbf{h}^{(2,1)} \boldsymbol{\Omega}^{(2)*} + \mathbf{h}^{(1,2)*} \boldsymbol{\Omega}^{(3)} + \mathbf{h}^{(2,2)} \boldsymbol{\Omega}^{(4)*}, \end{aligned} \quad (5.65)$$

and

$$\begin{aligned} \mathbf{Y}^{\tilde{(2)'}} &= \left(\mathbf{h}^{(2,1)*} \mathbf{h}^{(2,1)} + \mathbf{h}^{(1,1)} \mathbf{h}^{(1,1)*} + \mathbf{h}^{(2,2)*} \mathbf{h}^{(2,2)} + \mathbf{h}^{(1,2)} \mathbf{h}^{(1,2)*} \right) \mathbf{r}^{(2)} + \\ &\quad \mathbf{h}^{(2,1)*} \boldsymbol{\Omega}^{(1)} - \mathbf{h}^{(1,1)} \boldsymbol{\Omega}^{(2)*} + \mathbf{h}^{(2,2)*} \boldsymbol{\Omega}^{(3)} - \mathbf{h}^{(1,2)} \boldsymbol{\Omega}^{(4)*}. \end{aligned} \quad (5.66)$$

In element form, each sample of the above detected information vectors can be written in terms of channel frequency response values respectively as:

$$\begin{aligned} Y_n^{\tilde{(1)'}} &= \left(|H_n^{(1,1)}|^2 + |H_n^{(2,1)}|^2 + |H_n^{(1,2)}|^2 + |H_n^{(2,2)}|^2 \right) r_n^{(1)} + \\ &\quad H_n^{(1,1)*} \Omega_n^{(1)} + H_n^{(2,1)} \Omega_n^{(2)*} + H_n^{(1,2)*} \Omega_n^{(3)} + H_n^{(2,2)} \Omega_n^{(4)*} \\ &= \Sigma'_n r_n^{(1)} + H_n^{(1,1)*} \Omega_n^{(1)} + H_n^{(2,1)} \Omega_n^{(2)*} + H_n^{(1,2)*} \Omega_n^{(3)} + H_n^{(2,2)} \Omega_n^{(4)*}, \end{aligned} \quad (5.67)$$

and

$$\begin{aligned} Y_n^{\tilde{(2)'}} &= \left(|H_n^{(1,1)}|^2 + |H_n^{(2,1)}|^2 + |H_n^{(1,2)}|^2 + |H_n^{(2,2)}|^2 \right) r_n^{(2)} + \\ &\quad H_n^{(2,1)*} \Omega_n^{(1)} - H_n^{(1,1)} \Omega_n^{(2)*} + H_n^{(2,2)*} \Omega_n^{(3)} - H_n^{(1,2)} \Omega_n^{(4)*} \\ &= \Sigma'_n r_n^{(2)} + H_n^{(2,1)*} \Omega_n^{(1)} - H_n^{(1,1)} \Omega_n^{(2)*} + H_n^{(2,2)*} \Omega_n^{(3)} - H_n^{(1,2)} \Omega_n^{(4)*}, \end{aligned} \quad (5.68)$$

where $\Sigma'_n = |H_n^{(1,1)}|^2 + |H_n^{(2,1)}|^2 + |H_n^{(1,2)}|^2 + |H_n^{(2,2)}|^2$. Following the same derivation procedure of two transmit and one receive antennas yields the BER formulas that are given in (5.41) and (5.42) for the ZF equalizer, however, with replacing Σ_n by Σ'_n as

$$P_e^{QPSK} = \frac{1}{N} \sum_{i=1}^N Q \left(\sqrt{\frac{\gamma_s}{\sum_{n=0}^{N-1} |a_{i,n}|^2 \frac{1}{\Sigma'_n}}} \right), \quad (5.69)$$

and

$$P_e^{16-QAM} = \frac{3}{4N} \sum_{i=1}^N Q \left(\sqrt{\frac{\gamma_s}{5 \sum_{n=0}^{N-1} |a_{i,n}|^2 \frac{1}{\Sigma'_n}}} \right), \quad (5.70)$$

and (5.56) and (5.57) for MMSE equalizer are the same but with replacing Σ_n by Σ'_n as

$$P_e^{QPSK} = \frac{1}{N} \sum_{i=0}^{N-1} Q \left(\sqrt{\frac{\sum_{n=0}^{N-1} |a_{i,n}|^2 \frac{\gamma_s \Sigma'_n}{1+\gamma_s \Sigma'_n}}{\sum_{n=0}^{N-1} |a_{i,n}|^2 \frac{1}{1+\gamma_s \Sigma'_n}}} \right), \quad (5.71)$$

and

$$P_e^{16-QAM} = \frac{3}{4N} \sum_{i=0}^{N-1} Q \left(\sqrt{\frac{\sum_{n=0}^{N-1} |a_{i,n}|^2 \frac{\gamma_s \Sigma'_n}{1+\gamma_s \Sigma'_n}}{5 \sum_{n=0}^{N-1} |a_{i,n}|^2 \frac{1}{1+\gamma_s \Sigma'_n}}} \right). \quad (5.72)$$

5.6 Complexity analysis

In this section we will calculate the arithmetic operations of the proposed ST-X-OFDM system and compare it with the conventional ST-OFDM system and UP-ST-OFDM system [75] for a diverse of unitary precoders such as WHT and DHT, all based on single butterfly algorithms. It is noteworthy mention that the DHT is not mentioned in specific as one of the precoders in UP-ST-OFDM system. However we added it here for more information.

The receiver complexity of our proposed system is roughly the same as the receiver complexity of the UP-ST-OFDM system. However, the proposed ST-X-OFDM system involves significant transmitter complexity reduction compared to the UP-ST-OFDM system. Therefore, in this section we are considering the complexity analysis of the proposed ST-X-OFDM system only at the transmitter when the information symbols are considered to be drawn from complex constellation.

5.6.1 X Transform

The \mathbf{X} -transform includes $\frac{N-2}{2}$ units. Each single multiplication of complex data $x + jy$ by $1 + j1$ equals to $(x - y) + j(x + y)$, that means it involves 2 real additions (R_A). Thus, the complexity of the direct implementation of the \mathbf{X} -transform involves $4(N - 2)$ real additions (R_A s) and no multiplications at all. As shown in Fig. 5.1, twice the complexity of \mathbf{X} transform is required at the transmitter of the proposed ST-X-OFDM system and the overall complexity is then given as $R_A = 8(N - 2)$.

5.6.2 ST-OFDM

Considering the fact that each complex multiplication involves 4 real multiplications (R_M) and two real additions (R_A) or 3 real multiplications and 3 real additions, and each complex addition is equivalent to two real additions. The arithmetic complexity of the FFT, based on single butterfly and 4/2 implementation is given as: $R_M = 2N \log_2 N$ and $R_A = 3N \log_2 N$. For ST-OFDM system, twice the above complexity is required at the transmitter, hence, the overall transmitter complexity is given as: $R_M = 4N \log_2 N$ and $R_A = 6N \log_2 N$. However, the complexity at the receiver of the conventional ST-OFDM is fewer than the complexity at the receiver of the proposed system but the price is the significant BER performance improvement when used the proposed scheme.

5.6.3 UP-ST-OFDM

Consider multicarrier system with three different precoders, WHT and DHT.

5.6.3.1 WHT precoder

The WHT complexity includes just $R_A = N \log_2 N$ real additions, hence the overall transmitter complexity is four-times the complexity of the WHT in addition to twice the arithmetic operations of FFT which is given as: $R_M = 4N \log_2 N$ and $R_A = 10N \log_2 N$.

5.6.3.2 DHT precoder

The arithmetic complexity of the radix-2 fast Hartley transform (FHT) based on single butterfly implementation is given as: $R_M = N \log_2 N$, and $R_A = \frac{3}{2}N \log_2 N$. For data that are drawn from complex constellation, FHT should be calculated twice for each signal $\mathbf{S}^{(1)}$ and $\mathbf{S}^{(2)}$, one for the real part and the other for the imaginary part of a complex information in addition to twice the complexity of FFT. Consequently, the arithmetic operations of FHT-FFT will be four-times that of the FHT in addition to twice of the arithmetic operations of the FFT, so the overall arithmetic operations are given as: $R_M = 8N \log_2 N$, and $R_A = 12N \log_2 N$.

Table 5.1: Comparison based on real arithmetic operations of the X-transform and other transforms that used in the ST-OFDM.

N	ST-X-OFDM			ST-OFDM			DHT-UP-ST-OFDM		
	R_A	R_M	R_O	R_A	R_M	R_O	R_A	R_M	R_O
32	120	0	120	960	640	1600	1920	1280	3200
64	248	0	248	2304	1536	3840	4608	3072	7680
128	504	0	504	5376	3584	8960	10752	7168	17920
256	1016	0	1016	12288	8192	20480	24576	16384	40960
512	2040	0	2040	27648	18432	46080	55296	36864	92160
1024	4088	0	4088	61440	40960	102400	122880	91920	204800
2048	8184	0	8184	135168	90112	225280	270336	180224	450560
4096	16376	0	16376	294912	196608	491520	589824	393216	983040

Table 5.2: System parameters for simulations.

System Item	Parameter
Antenna type	Perfect
Antenna diversity	2×1 and 2×2
Modulation	QPSK and 16-QAM
Synchronisation	Complete
Channel type	ITU pedestrian B and ITU vehicular A
Equalisation	One-tap FDE
Number of Subcarriers (N)	1024
Duration of CP	$N/4$
Bandwidth	10MHz

5.7 Simulation results and discussions

In this section, we verify the performance of the proposed ST-X-OFDM system and compare it with the existing ST-OFDM system. Further verification is achieved in this section by comparing the simulation results with the theory one. The mapping scheme that used in our simulation are the QPSK and the 16-QAM, total number of modulated symbols are 2048, hence, 1024 symbols are assigned to each antenna. ITU pedestrian B and vehicular class A channel models according to the WiMAX standard and parameters used in Table 5.2 are used. A CP of duration $25.6\mu s$ is attached to each transmitted OFDM symbol. The CP in both cases is greater than the maximum channels' echo delays, providing that the simulation is ISI free over both the channel models. Simulation is carried out over MMSE and ZF detection for a diverse of three schemes: one transmit-one receive antenna (SISO), two transmit and one receive antennas (2×1) and two transmit and two receive antennas (2×2).

5.7.1 BER Performance Over Multipath Channels

Figs. 5.3-5.10 show the BER performance of the proposed ST-X-OFDM and the conventional ST-OFDM systems for MMSE and ZF detection, QPSK and 16-QAM modulation formats and different antenna diversity over ITU pedestrian B and vehicular A channel models. The theoretical results in Figs. 5.3-5.10 are obtained by using the BER formulas that are given in (5.41) and (5.42) for the case of ZF detection and QPSK and 16-QAM respectively and (5.56) and (5.57) for the case of MMSE detection and QPSK and 16-QAM respectively. It is noticeable that theoretical results are precisely agree with the simulation results.

It is obvious from Figs. 5.3-5.6 that for MMSE detection, at 10^{-4} BER, the proposed ST-X-OFDM can achieve about 15 dB E_b/N_0 gain for over ST-OFDM systems when 16-QAM modulation format is used and even further up to 17 dB for QPSK in the case of SISO. For the case of 2×1 , this E_b/N_0 gain is reduced to 6 dB for the case of 16-QAM and to about 7 dB for the case of QPSK. For the case of 2×2 , the proposed ST-X-OFDM outperforms the ST-OFDM systems by about 3 dB for the case when the 16-QAM and QPSK are used.

As the advantage of ST-X-OFDM over ST-OFDM is on frequency diversity enhancement, the severity of the channel is a key important to explore the advantages of the proposed ST-X-OFDM. Hence, in the case of 2×1 , the channel effect on the BER performance become less than SISO as time diversity is introduced by the transmitter antennas and this is the reason why the E_b/N_0 achievement is reduced as the antennas diversity increase where the channel effects on the transmitted signal reduced.

It is also noted from Figs. 5.7-5.10 that, for the case of the ZF equalizer, the conventional DFT-OFDM outperforms our proposed X-OFDM system by about 3 dB in terms of the BER performance for each QPSK and 16-QAM constellation.

In the case of 2×1 system and for the case of ZF equalizer, unlike SISO where the BER performance of X-OFDM system is worse than BER performance of DFT-OFDM system whereas X-OFDM system is much better than DFT-OFDM system for the case of MMSE equalizer, the BER performance of ST-X-OFDM system is better than the BER performance of ST-DFT-OFDM systems for both ZF and MMSE equalizers. This can be attributed to the reason that the equivalent channel for specific subcarrier is $H_n^{(1)} + H_n^{(2)}$ in the case of 2×1 rather than H_n in the

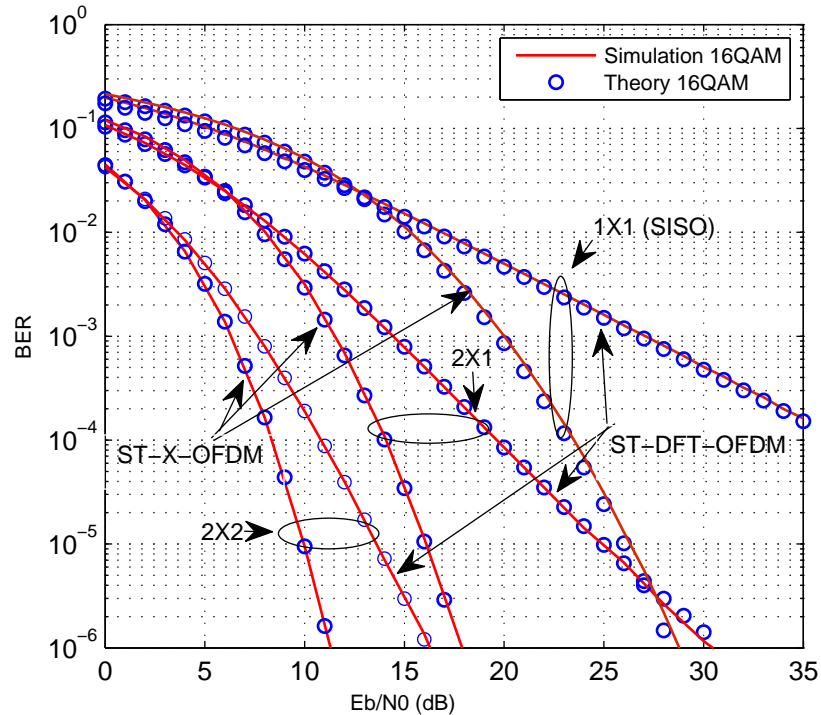


Figure 5.3: BER performance of the proposed ST-X-OFDM and the conventional ST-OFDM systems over pedestrian B channel model, MMSE detection and 16-QAM modulation format.

SISO where the latter is much more likely to highly attenuated and dominate the noise in ZF equalizer, when $H_n \simeq 0$ than $H_n^{(1)} + H_n^{(2)}$ which is much less likely to be greatly attenuated at same frequency instant n . However the performance of ZF-ST-X-OFDM is still about 1 dB worse than MMSE-ST-X-OFDM as the latter can mitigate the problem of null zero subchannels.

In the case of 2×2 system, the MMSE and ZF performances at ST-X-OFDM systems are in marvellous agreement.

5.8 Conclusion

A new MIMO STBC-OFDM system has been presented in this chapter. The transmitter of the proposed scheme is based on a unitary very low complexity \mathbf{X} -transform instead of the traditional IFFT. This has hugely reduced the transmitter complexity and led to significant transmission improvement in comparison with the conventional ST-OFDM. Exact mathematical expression that calculates the BER performance over multipath channels has been derived in this work. It has been shown mathematically and by computer simulation over ITU multipath frequency-selective fading

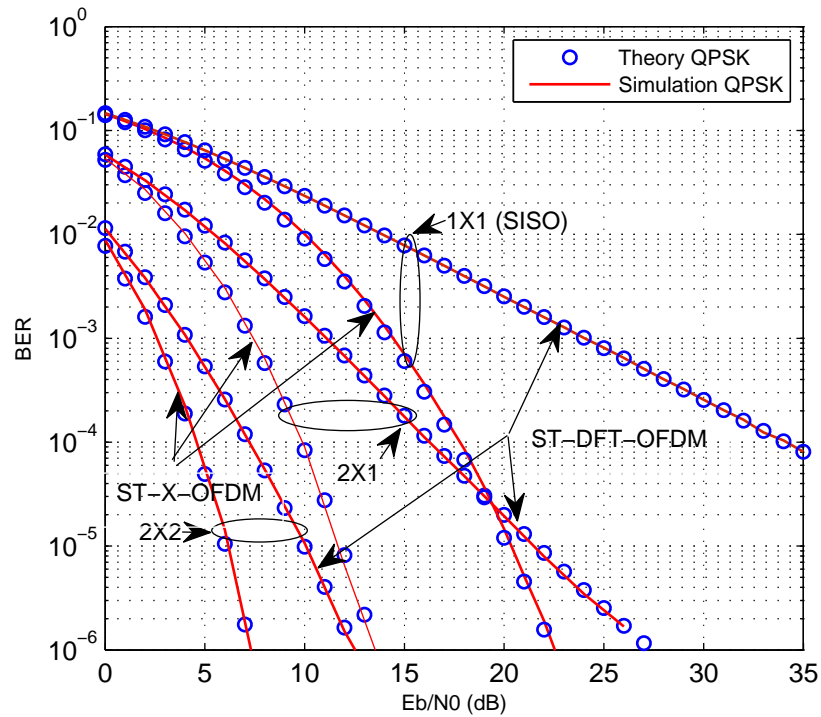


Figure 5.4: BER performance of the proposed ST-X-OFDM and the conventional ST-OFDM over pedestrian B channel model, MMSE detection and QPSK modulation format.

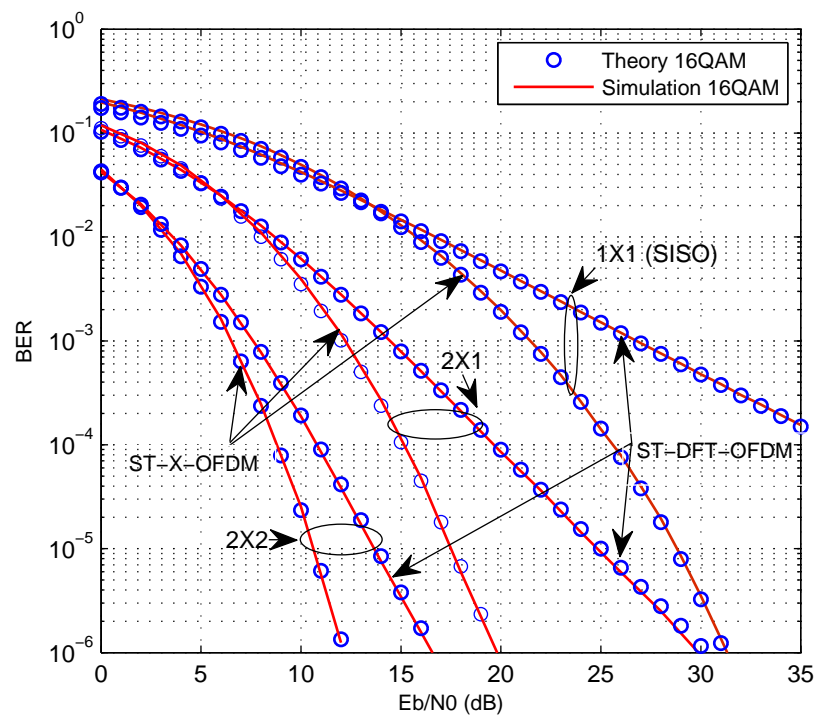


Figure 5.5: BER performance of the proposed ST-X-OFDM and the conventional ST-OFDM systems over vehicular A channel model, MMSE detection and the 16-QAM modulation.

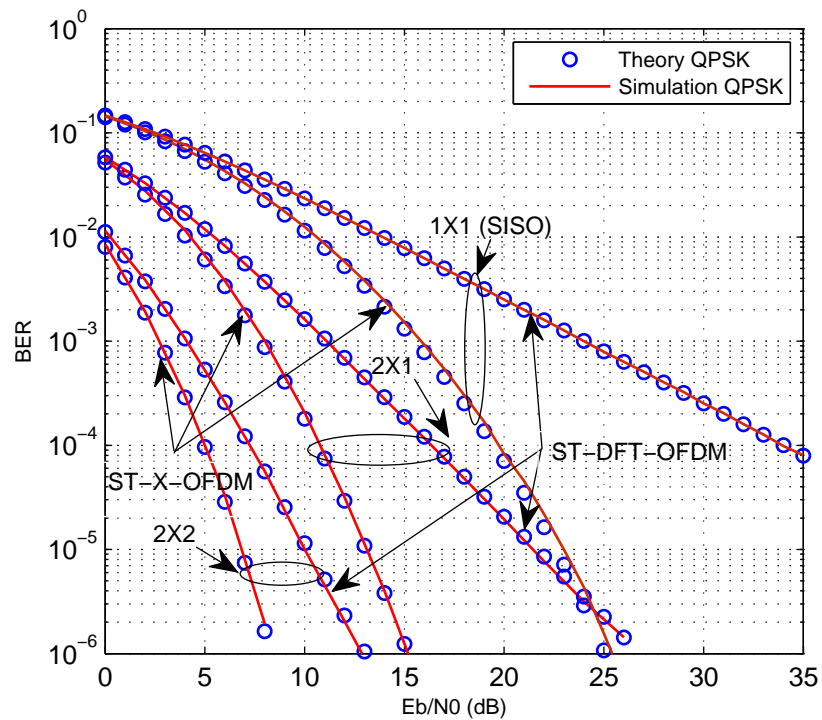


Figure 5.6: BER performance of the proposed ST-X-OFDM and the conventional ST-OFDM systems over vehicular A channel model, MMSE detection and the QPSK modulation.

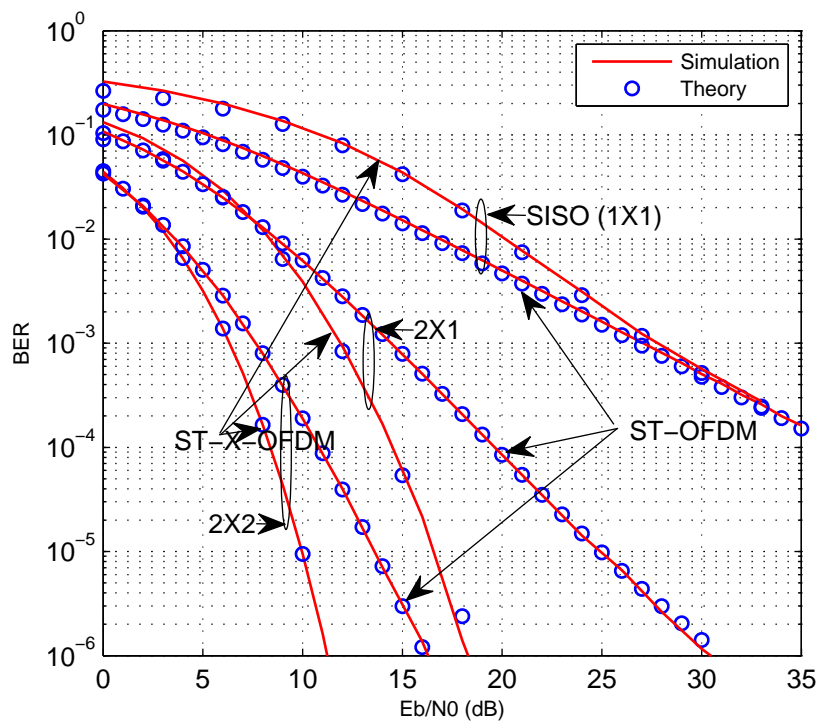


Figure 5.7: BER performance of the proposed ST-X-OFDM and the conventional ST-OFDM systems over pedestrian B channel model, ZF detection and the 16-QAM modulation.

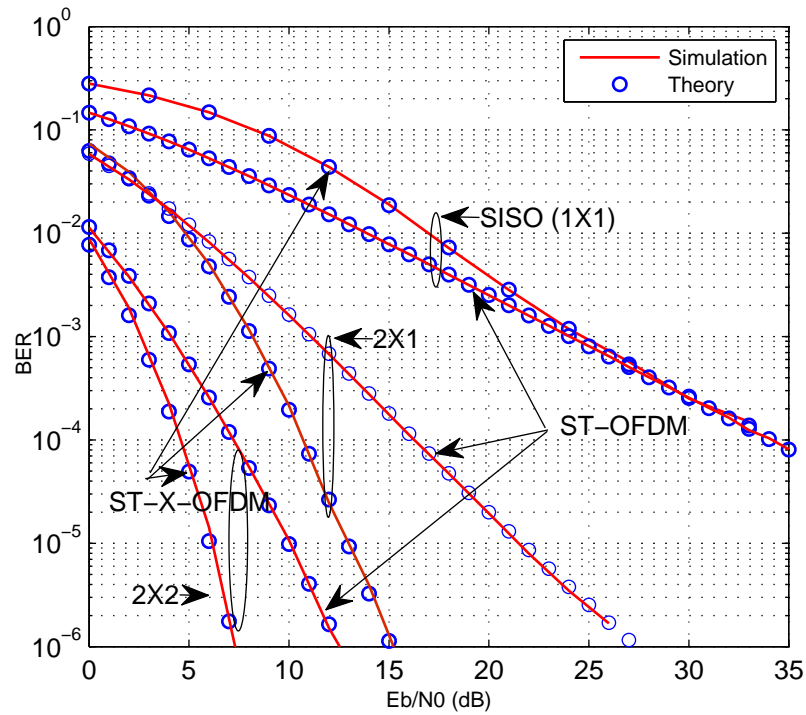


Figure 5.8: BER performance of the proposed ST-X-OFDM and the conventional ST-OFDM systems over pedestrian B channel model, ZF detection and the QPSK modulation.

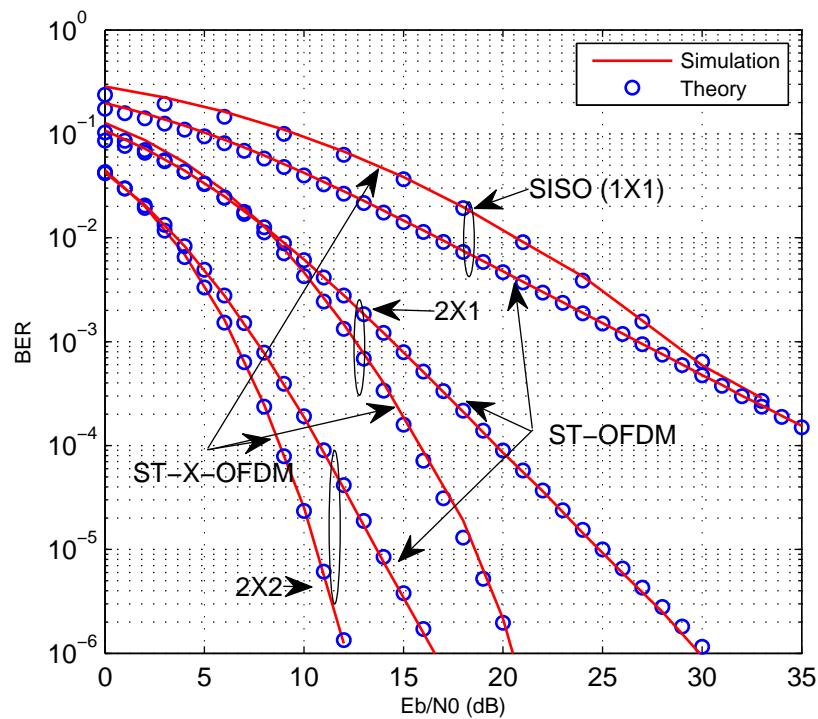


Figure 5.9: BER performance of the proposed ST-X-OFDM and the conventional ST-OFDM systems over vehicular A channel model, ZF detection and the 16-QAM modulation.

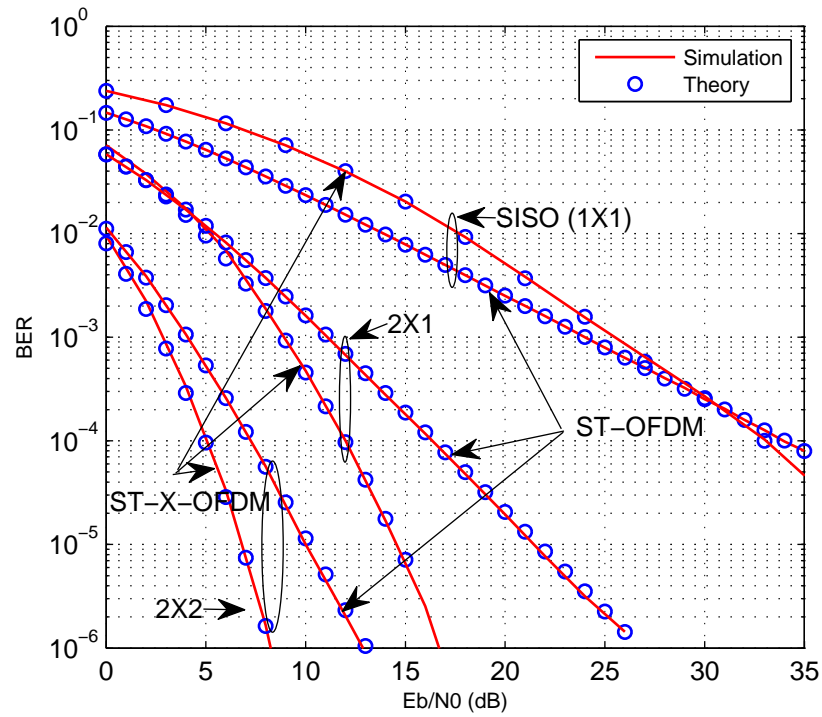


Figure 5.10: BER performance of the proposed ST-X-OFDM and the conventional ST-OFDM systems over vehicular A channel model, ZF detection and the QPSK modulation.

channel that the proposed ST-X-OFDM achieves valuable SNR gain in comparison to conventional ST-OFDM.

Chapter 6

BER Performance of Unitary Precoded OFDM Systems in the Presence of SSPA

6.1 Introduction

To this point it has been shown that both the proposed C-OFDM and X-OFDM schemes can reduce the PAPR of the transmitted signal to a different level in comparison with the conventional OFDM. However, reducing the PAPR does not usually improve the BER performance in the presence of solid-state power amplifiers (SSPAs) as the reduction technique might produce another kind of distortion that affects the transmission of the OFDM signal. Therefore this chapter is set to investigate the PAPR reduction and the BER performance of unitary precoded OFDM (UP-OFDM) systems, which is the principle of the proposed schemes, with different unitary transforms and in the presence of the SSPA.

The main contributions of this chapter are summarized as:

- An investigation (mathematically and by computer simulation) of the BER performance of the C-OFDM system in the presence of the SSPA with different input back offs (IBOs) over AWGN and multipath channels.
- An investigation (mathematically and by computer simulation) of the BER performance of the WHT, DCT, DHT (X-OFDM) and the DFT (SC-FDE) precoded DFT-OFDM system in the presence of the SSPA with different input

back offs (IBOs) and 16-QAM modulation over multipath channels.

- Introducing a fair comparison of all the above unitary transforms utilization as a channel independent precoder in the OFDM; this comparison includes the PAPR reduction and BER performance in the presence of the SSPA.
- A presentation of SSPA effects mitigation technique using a conventional coding/Viterbi decoding technique for the UP-OFDM systems.

Analytical analysis and simulation results show that the C-OFDM reduces the PAPR to some value and achieves BER improvement when the modulation is the QPSK, or 16-QAM and the SSPA is with high input back-off (IBO) (higher than 5 dB. It also shows that the C-OFDM leads to BER performance degradation of the 16-QAM when the IBO is below 5 dB [86].

Analytical and simulation results also show that the \mathbf{X} -transform, which is a DHT precoded DFT, achieves significant BER improvement in the OFDM system, even in the presence of the SSPA distortion. The simulation results also show that the DCT and the WHT precoded DFT-OFDM can lead to BER impairment in the presence of the SSPA. Furthermore, a coding technique is proposed in this chapter to mitigate the sensitivity of the UP-OFDM systems to the SSPA nonlinearity. Simulation results also show that the coded UP-OFDM approximately matched the performance of all the unitary precoders.

6.2 PAPR of the C-OFDM System

The PAPR of the OFDM transmitted signal is considered as one of the main problems plaguing the OFDM systems, which arises from the addition of a large number of statistically independent symbols. It has been shown in Fig. 3.9 in Chapter Three that the \mathbf{C} -transform can reduce the PAPR of the OFDM system by about 1 dB in comparison to the DCT-OFDM and the conventional OFDM systems. This was attributed to the fact that in the case of the C-OFDM, the maximum number of possible superposition of data symbols to perform each OFDM sample is $N/2$ rather than N in the case of the DCT-OFDM and the DFT-OFDM. In other words, The worst case of the PAPR is of order N for the DFT-OFDM and the DCT-OFDM systems whilst it is of order $N/2$ for the C-OFDM system. In general, the worst

case of the PAPR has low probability of occurrence [98]-[99]. Our simulation results showed 1 dB improvement in PAPR for the case of the proposed C-OFDM system in comparison with that for the DCT-OFDM or the DFT-OFDM system.

The question is to what extent and under which conditions this PAPR reduction can improve the BER performance in the presence of nonlinear distortion that induced by the SSPAs?. The answer of this question will be detailed and clarified in sections 6.5 and 6.6 in the current chapter.

6.3 PAPR of Unitary precoded OFDM Systems

Using different unitary precoders in the conventional OFDM that based on the DFT can lead to different levels in the PAPR reduction. The WHT changes the phases of input symbols, hence, reduces the probability that the input symbols are aligned in phase and ultimately reduces the peak value of the WHT precoded OFDM signal.

The DCT is a state-of-the-art transform in data compression. It compresses the input symbols in the first few samples and leaves the rest either zeros or with negligible values [102]. Therefore, when these compressed data are processed by the IFFT at the transmitter, they have a lower PAPR as the number of additions of the input symbols is reduced.

The DHT precoded DFT leads to low complexity \mathbf{X} -transform which leads to an enormous reduction in the number of additions, leading to few additions in the input symbols and ultimately a reduction in the PAPR.

Fig. 6.1 shows the complementary cumulative density function (CCDF) of the unitary precoded OFDM system for a diverse of precoders (WHT, DCT, DHT and DFT) are used, number of subcarriers, $N = 1024$ and the 16-QAM constellation.

It can be observed from Fig. 6.1 that the DFT precoded OFDM (SC-FDE) has the lowest PAPR compared to the WHT, DCT precoded OFDM systems and the X-OFDM system. This result is acceptable as the SC-FDE is a single carrier, not multiplexing scheme, where the signal passes to the channel without being accumulated. The X-OFDM can reduce the PAPR by approximately 6 dB at a CCDF value of 10^{-4} over the conventional OFDM system, 5 dB over the WHT precoded OFDM and around 2.8 dB over the DCT precoded OFDM system.

When the PAPR reduction is not sufficient to drive the high-power amplifier

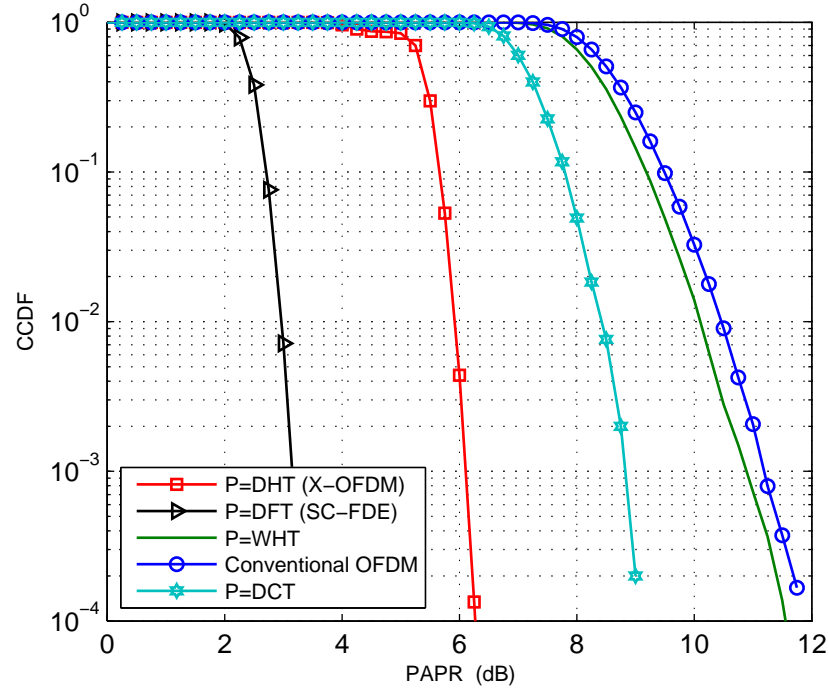


Figure 6.1: PAPR performance of the conventional OFDM and UP-OFDM systems with precoder matrix WHT, DCT, DHT (X-OFDM) and the DFT (SC-FDE), using the 16-QAM modulation and $N = 1024$.

(HPA) in the linear region, amplitude clipping in the OFDM signals which may lead to a nonlinear attenuation is occurred. Furthermore, as the receiver includes a precoder in its structure, this attenuation will be further distributed across the entire spectrum, leading to a degradation in the BER performance as it will be shown in next sections in this chapter.

6.4 SSPA Model

In multicarrier (MC) communications, in particular the OFDM, the HPA is the major source that causes nonlinear distortion. The nonlinear distortion arises when the dynamic range of the input signal is larger than the saturation level of the HPA as shown in Fig. 6.2. We consider the case that the transmitter is the one that encompasses the SSPA in its structure. Define input-back-off (IBO) of the HPA, the operating point of the HPA, as the ratio between the maximum input power to the average power,

$$\text{IBO} = 10 \log_{10} \frac{P_{max}}{P_{av}}, \quad (6.1)$$

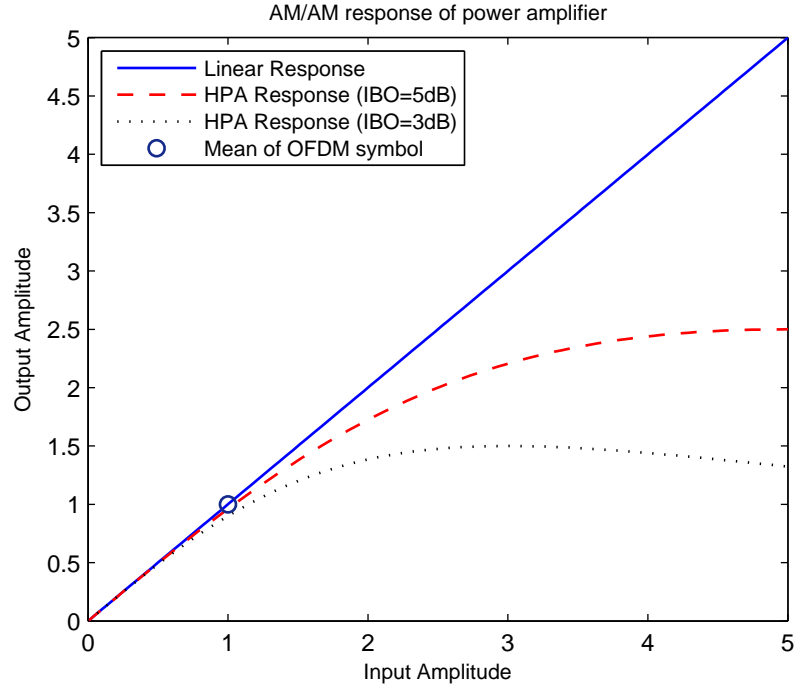


Figure 6.2: Nonlinear characteristics of the SSPA

where P_{max} and P_{av} denote, respectively, the maximum (saturation) power and the average power of the amplifier. The amplified signal is given as

$$\bar{u}_k = u_k G_a[|u_k|], \quad (6.2)$$

where $G_a[|u_k|]$ is the amplifier gain and it is given as [77]

$$G_a[|u_k|] = \frac{A_m[|u_k|] e^{j\phi[|u_k|]}}{|u_k|}, \quad (6.3)$$

where $\phi[|u_k|]$ represents the amplitude modulation/phase modulation (AM/PM) conversion of non-linear power amplifier and $A_m[|u_k|]$ represents the amplitude modulation/amplitude modulation (AM/AM) conversion of non-linear power amplifier which is given as

$$A_m[|u_k|] = \frac{|u_k|}{\left[1 + \left(\frac{|u_k|}{A_s}\right)^{2\varphi}\right]^{\frac{1}{2\varphi}}}. \quad (6.4)$$

In (6.4), A_s is the amplifier input saturation voltage and φ is a parameter that controls the transition smoothness from linear region to saturation region. For an HPA with small IBO, the saturation level, A_s , is small. This in turn leads to

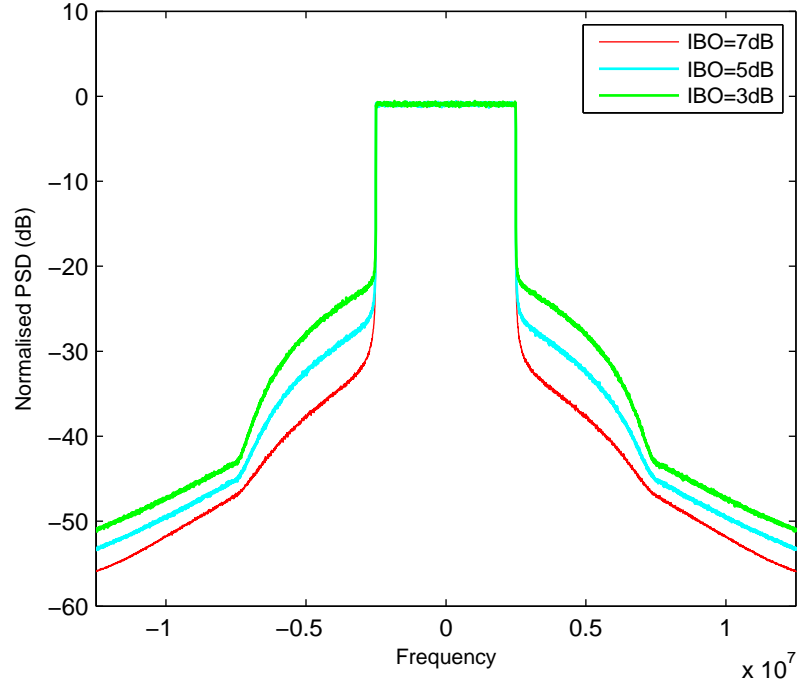


Figure 6.3: Effect of the IBO on the spectrum of the OFDM signal using the SSPA with $N=1024$.

amplitude clippings and ultimately BER performance impairment. According to the above, IBO is a key-factor that defines the dynamic range of the HPA. This is clearly shown in Fig. 6.3 where it shows that the lower the IBO is, the higher out-of-band radiation is.

6.5 Transmission performance of the C-OFDM in the presence of the SSPA

As the SSPA has a dynamic range shorter than that of the OFDM signal, signal clipping which leads to nonlinear distortion is occurred. The output signal, after the amplifier, is the sum of a useful amplified replica of the input signal and uncorrelated nonlinear distortion noise which can be written as [103]

$$\begin{aligned} \bar{\mathbf{u}} &= \hat{\mathbf{u}} + \bar{\mathbf{v}}, \\ &= \eta \mathbf{u} + \bar{\mathbf{v}}, \end{aligned} \tag{6.5}$$

where η is the amplifier attenuation on the useful part and $\bar{\mathbf{v}}$ is the distortion part of the output signal. The output signal of the amplifier then passes through the

channel. The channel is a multipath frequency-selective fading channel with L taps, its impulse response \tilde{h}_k can be written as

$$\tilde{h}_k = \sum_{i=0}^{L-1} h_i \delta_{k-\tau_i}, \quad (6.6)$$

where h_i and τ_i are the i^{th} path channel fading and delay respectively, and L is the number of paths of the channel. The received signal is a convolution between the transmitted signal and the multipath channel and corrupted by the AWGN. Therefore, the received signal is written as

$$y_k = \bar{u}_k \circledast \tilde{h}_k + v_k, \quad (6.7)$$

where \circledast denotes the convolution operation and v_k is the AWGN. It follows that the received signal can be written as

$$y_k = \sum_{n=0}^{L-1} \bar{u}_{k-n} h_n + v_k. \quad (6.8)$$

(6.8) can be rewritten in a more expressive way in matrix form as

$$\mathbf{y} = \mathbf{H}_0 \bar{\mathbf{u}} + \mathbf{v}, \quad (6.9)$$

where \mathbf{y} and $\bar{\mathbf{u}}$ are $N_t \times 1$ vectors given as $\bar{\mathbf{u}} = \bar{\mathbf{u}}^I + j\bar{\mathbf{u}}^Q$ and $\mathbf{y} = \mathbf{y}^I + j\mathbf{y}^Q$. In (6.9), \mathbf{H}_0 is a $N_t \times N_t$ channel convolutional Toeplitz matrix defined in [41] and given in (3.26). Substituting (6.5) into (6.9) yields

$$\begin{aligned} \mathbf{y} &= \mathbf{H}_0(\eta\mathbf{u} + \bar{\mathbf{v}}) + \mathbf{v}, \\ &= \eta\mathbf{H}_0\mathbf{u} + \mathbf{H}_0\bar{\mathbf{v}} + \mathbf{v}, \\ &= \eta\mathbf{H}\mathbf{s} + \mathbf{H}_0\bar{\mathbf{v}} + \mathbf{v}. \end{aligned} \quad (6.10)$$

In (6.10), $\mathbf{H} = \mathbf{H}_0\Psi_{zp}^T$ is an $N_t \times N$ matrix. The equalized signal after the MMSE equalizer at the receiver side can be written as

$$\mathbf{y}_{eq} = \mathbf{G}^{MMSE} \mathbf{y}, \quad (6.11a)$$

$$= \mathbf{G}^{MMSE} \eta\mathbf{H}\mathbf{s} + \mathbf{G}^{MMSE} \mathbf{H}_0\bar{\mathbf{v}} + \mathbf{G}^{MMSE} \mathbf{v}, \quad (6.11b)$$

where \mathbf{G}^{MMSE} is given as

$$\mathbf{G}^{MMSE} = E_s(E_s\mathbf{H}^H\mathbf{H} + \sigma_v^2\mathbf{I}_N)^{-1}\mathbf{H}^H. \quad (6.12)$$

At the receiver side, the received data (\mathbf{y}_{eq}) is first processed by \mathbf{C} -transform as follows

$$\hat{\mathbf{S}} = \mathbf{C}\mathbf{y}_{eq}. \quad (6.13)$$

Substituting (6.11b) into (6.13) yields

$$\hat{\mathbf{S}} = \mathbf{C}\mathbf{G}^{MMSE}\eta\mathbf{H}\mathbf{s} + \mathbf{C}\mathbf{G}^{MMSE}\mathbf{H}_0\bar{\mathbf{v}} + \mathbf{C}\mathbf{G}^{MMSE}\mathbf{v}, \quad (6.14a)$$

$$= \mathbf{C}\mathbf{G}^{MMSE}\eta\mathbf{H}\mathbf{C}^T\mathbf{S} + \mathbf{C}\mathbf{G}^{MMSE}\mathbf{H}_0\bar{\mathbf{v}} + \mathbf{C}\mathbf{G}^{MMSE}\mathbf{v}. \quad (6.14b)$$

Finally, the recovered transmitted bits are obtained by applying the de-mapping process on the recovered complex modulated data symbols $\hat{\mathbf{S}}$.

The noise signal $\mathbf{e} = \hat{\mathbf{S}} - \mathbf{S}$ is then given as

$$\mathbf{e} = (\mathbf{C}\mathbf{G}^{MMSE}\eta\mathbf{H}\mathbf{C}^T - \mathbf{I}_N)\mathbf{S} + \mathbf{C}\mathbf{G}^{MMSE}\mathbf{H}_0\bar{\mathbf{v}} + \mathbf{C}\mathbf{G}^{MMSE}\mathbf{v}. \quad (6.15)$$

It is obvious that in the absence of the SSPA ($\eta = 1$ and $\bar{\mathbf{v}} = 0$) and for perfect channel equalization, the first two terms of (6.15) is equal to zero, $(\mathbf{C}\mathbf{G}^{MMSE}\eta\mathbf{H}\mathbf{C}^T - \mathbf{I}_N)\mathbf{S} + \mathbf{C}\mathbf{G}^{MMSE}\mathbf{H}_0\bar{\mathbf{v}} = 0$. However, the SSPA produces these kinds of distortion even in the case of perfect channel equalization, hence, it causes significant BER performance degradation unless an external algorithm is used.

6.6 Results and Discussions of the C-OFDM System

Here we will use the same simulation parameters that used in Chapter Three, however, with the SSPA as a nonlinear source of distortion. To make clear picture about whether the BER gain comes from the PAPR reduction or from the enhanced diversity of the C-OFDM signal, simulation is run at two stages. Firstly, the simulation is run over the AWGN channel. As the C-OFDM has no diversity advantages over the DCT-OFDM and the conventional OFDM when the channel is the AWGN, the

SNR gain is then only comes from the PAPR reduction. Secondly, the simulation is run over the ITU multipath channel where the advantages of signal enhanced diversity revealed in this case.

6.6.1 Over AWGN Channel

The BER performance of the C-OFDM, DCT-OFDM and the conventional OFDM systems for the QPSK and the 16-QAM modulations over the AWGN channel is shown in Figs. 6.4, 6.5 and 6.6 for IBO= 7 dB, 5 dB and 3 dB respectively. It is obvious that for the case of the QPSK, the SSPA has no noticeable effects on the performance of the C-OFDM system. However, for the case of the 16-QAM, it can be seen from Figs. 6.4, 6.5 and 6.6 that although the C-OFDM has lower PAPR than the DCT-OFDM and the conventional OFDM, the performance of the others OFDM systems, in the presence of the SSPA, is better than that of the C-OFDM when the modulation is the 16-QAM. This is because the reduction in the PAPR is not sufficient to keep the C-OFDM signal within the dynamic range of the amplifier. However, this is not a problem when the QPSK modulation format is used, or the 16-QAM constellation together with coding technique as it will be shown later in section 6.7.

6.6.2 Over Multipath Channels

The BER performance of the C-OFDM, DCT-OFDM and the conventional OFDM over the ITU pedestrian and vehicular channel models for the 16-QAM and the QPSK modulation is shown in Figs 6.7, 6.8 and 6.9 for IBO=7, 5, and 3 dB respectively. It can be noted that the BER performance of the C-OFDM for the case of the QPSK modulation is not affected by the nonlinearity distortion of the SSPA. This is because the costellation points of the QPSK modulation are far enough to prevent the interference. However, for the case of the 16-QAM modulation, it is obvious from Figs 6.7, 6.8 and 6.9 that the C-OFDM approximately achieves the same significant gain as the case when without SSPA when the IBO=7dB. However, the lower IBO (IBO=5 dB and IBO=3 dB), the sensitivity to the SSPA distortion is arose.

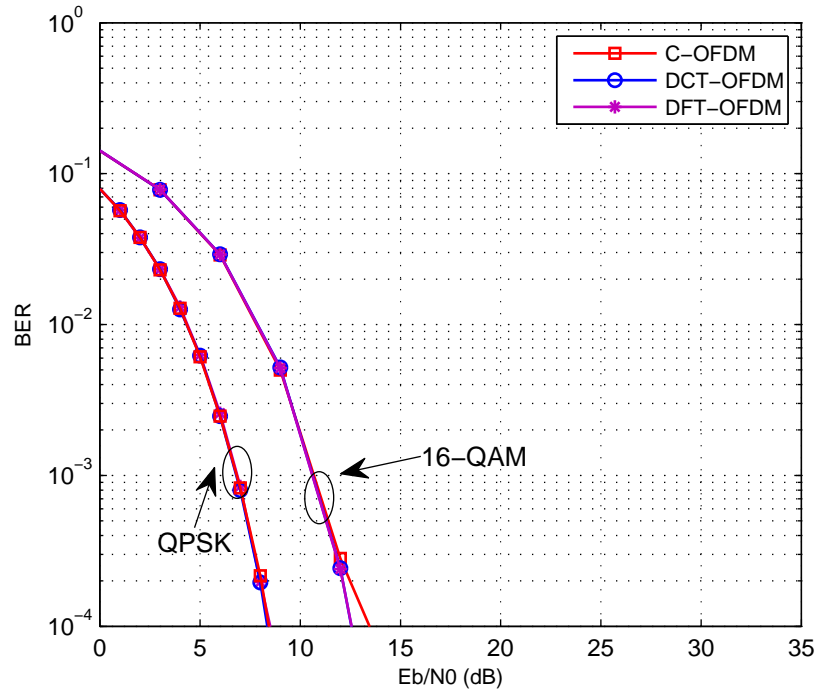


Figure 6.4: BER performance of the C-OFDM, DCT-OFDM and the conventional OFDM systems of the QPSK and 16-QAM modulations with the SSPA of (IBO=7dB) over the AWGN channel.

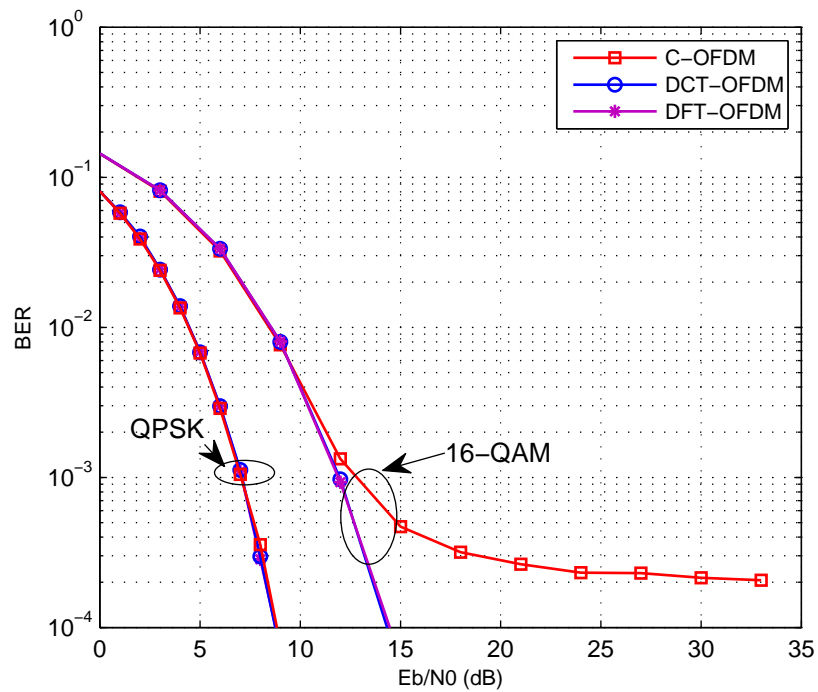


Figure 6.5: BER performance of the C-OFDM, DCT-OFDM and the conventional OFDM systems of the QPSK and 16-QAM modulations with the SSPA of (IBO=5dB) over the AWGN channel.

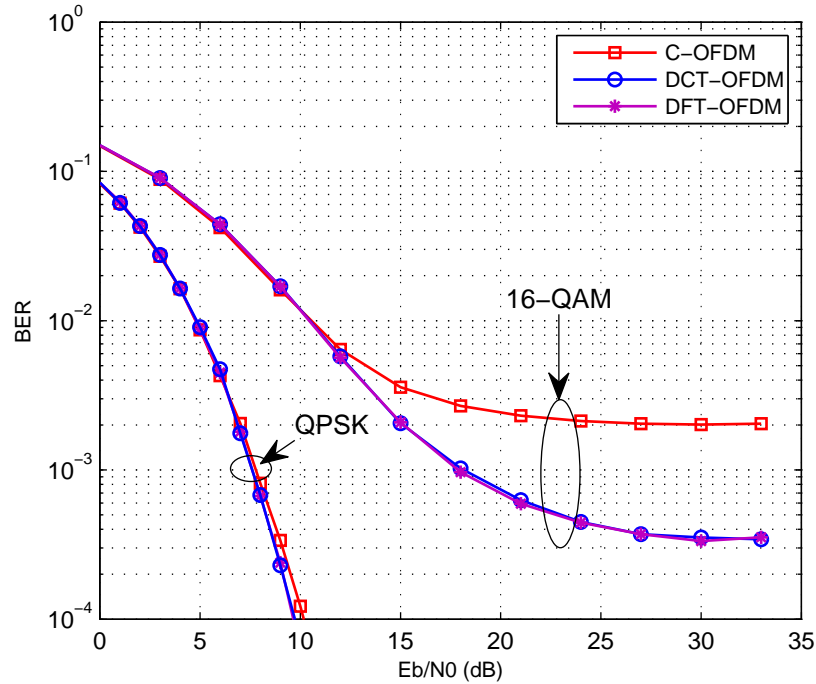
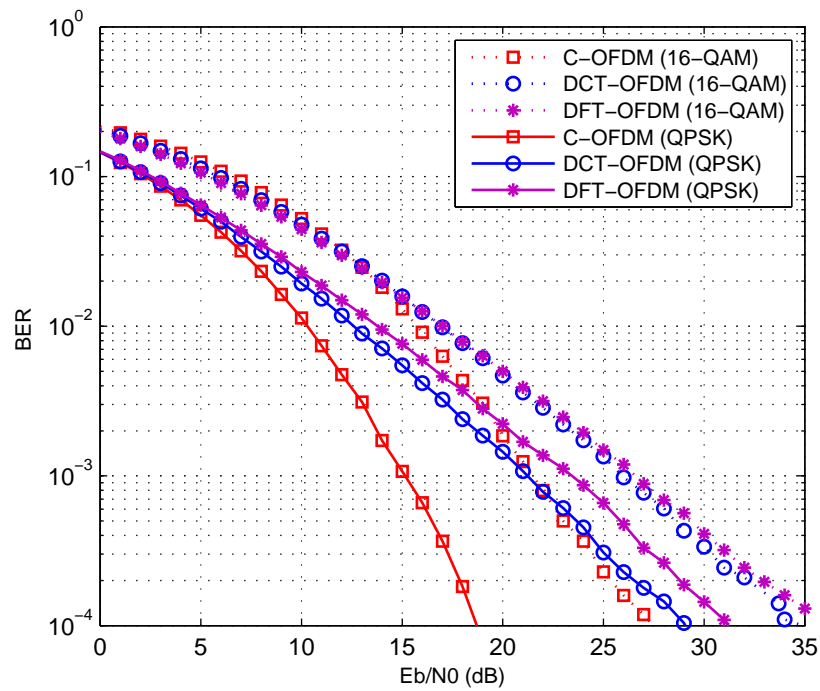


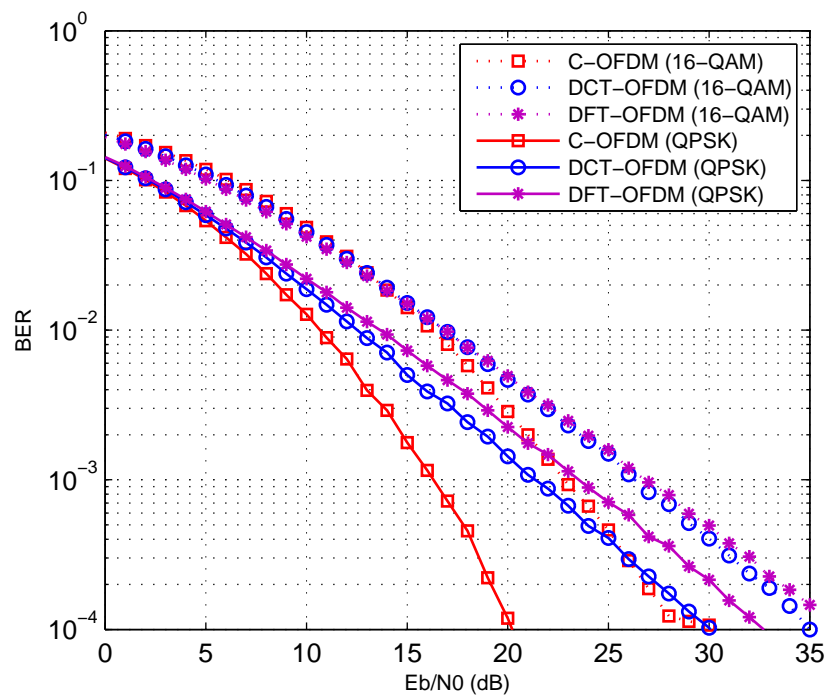
Figure 6.6: BER performance of the C-OFDM, DCT-OFDM and the conventional OFDM systems of the QPSK and 16-QAM modulations with the SSPA of (IBO=3dB) over the AWGN channel.

6.7 Coded C-OFDM System in the Presence of the SSPA

In this section we use coding technique to mitigate the sensitivity of the C-OFDM system to the SSPA nonlinearity when the mapper is the 16-QAM. Convolutional coding/Viterbi encoding algorithm with a code rate equal to 1/2 is utilized with the C-OFDM, the DCT-OFDM and the conventional OFDM systems. It is worth mentioning that there are more efficient coding techniques; however we used the convolutional coding in this chapter only to demonstrate the effects of coding on the SSPA distortion on the C-OFDM system. Figs. 6.10(a) and 6.10(b) show the BER performance of the aforementioned OFDM systems when the IBO of the SSPA is 5 dB and 3 dB respectively. It can be observed from Figs. 6.10(a) and 6.10(b) that for coded systems, the proposed scheme gains around 10 dB E_b/N_0 at 10^{-4} BER even when the IBO of the SSPA reduced to 3 dB.

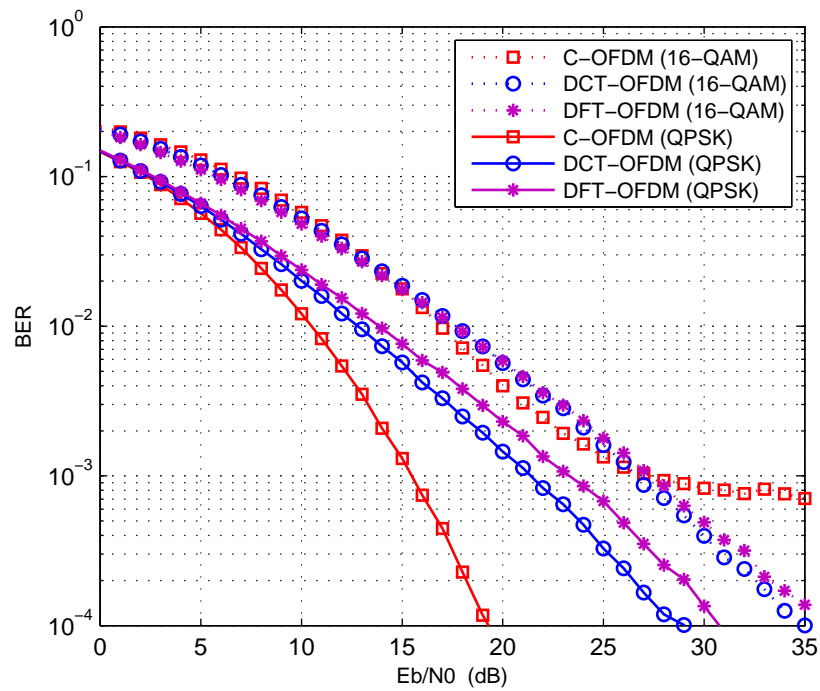


(a) Pedestrian IBO=7 dB.

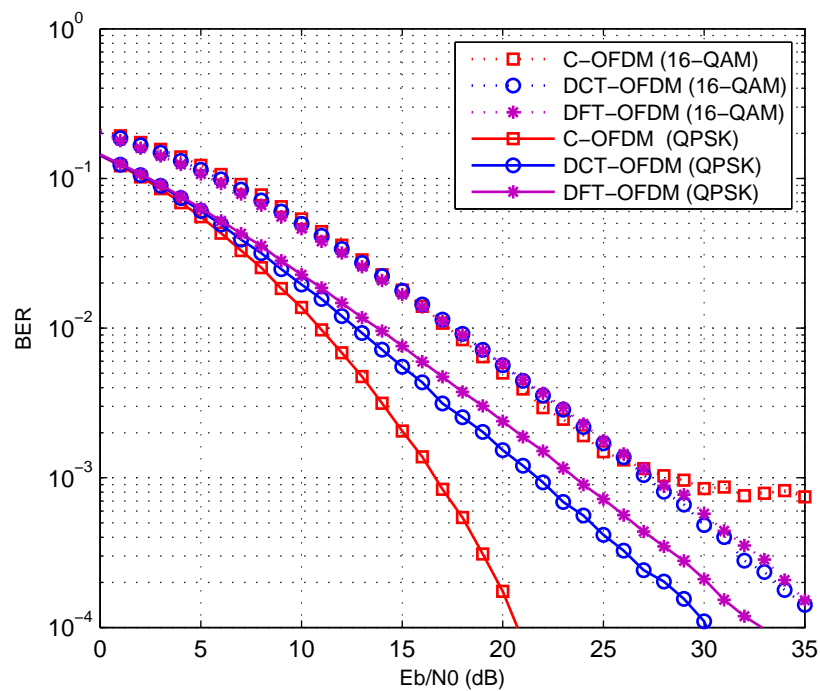


(b) Vehicular IBO=7 dB.

Figure 6.7: BER performance of the C-OFDM, DCT-OFDM, and DFT-OFDM of the 16-QAM and the QPSK modulations with SSPA of IBO=7 dB over the ITU channel (a: pedestrian B and b: vehicular A).

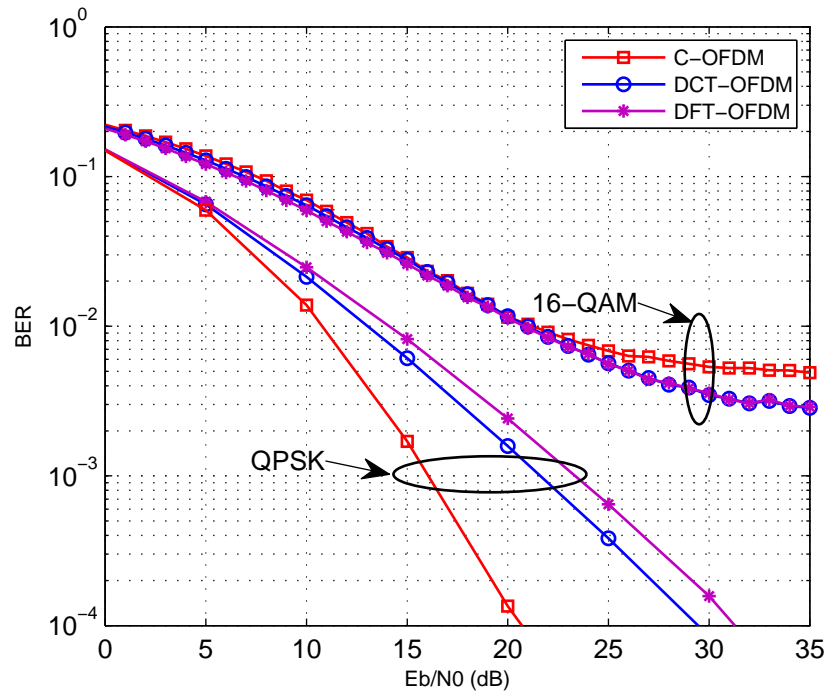


(a) Pedestrian IBO=5 dB.

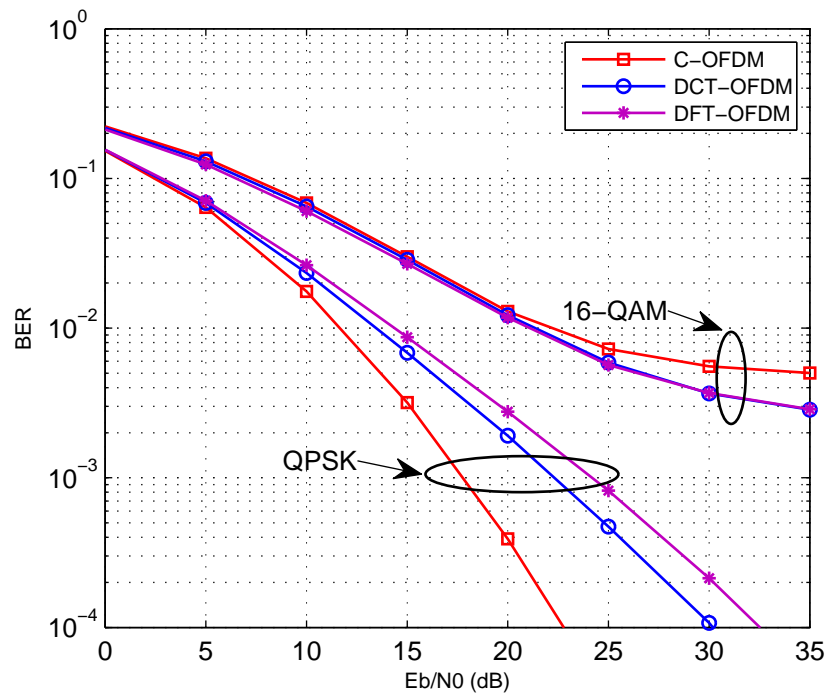


(b) Vehicular IBO=5 dB.

Figure 6.8: BER performance of the C-OFDM, DCT-OFDM, and DFT-OFDM of the 16-QAM and the QPSK modulations with SSPA of IBO=5 dB over the ITU channel (a: pedestrian B and b: vehicular A).

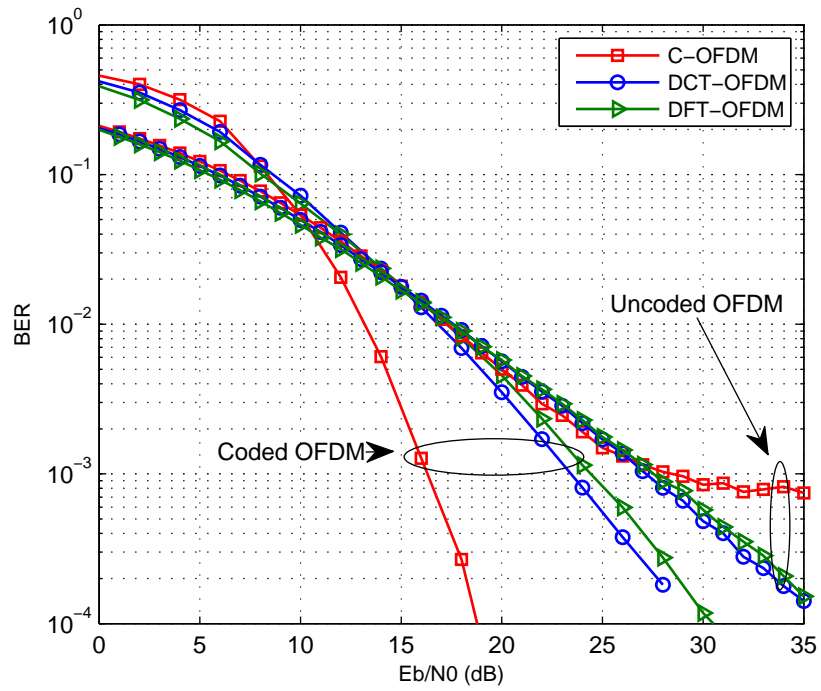


(a) Pedestrian IBO=3 dB.

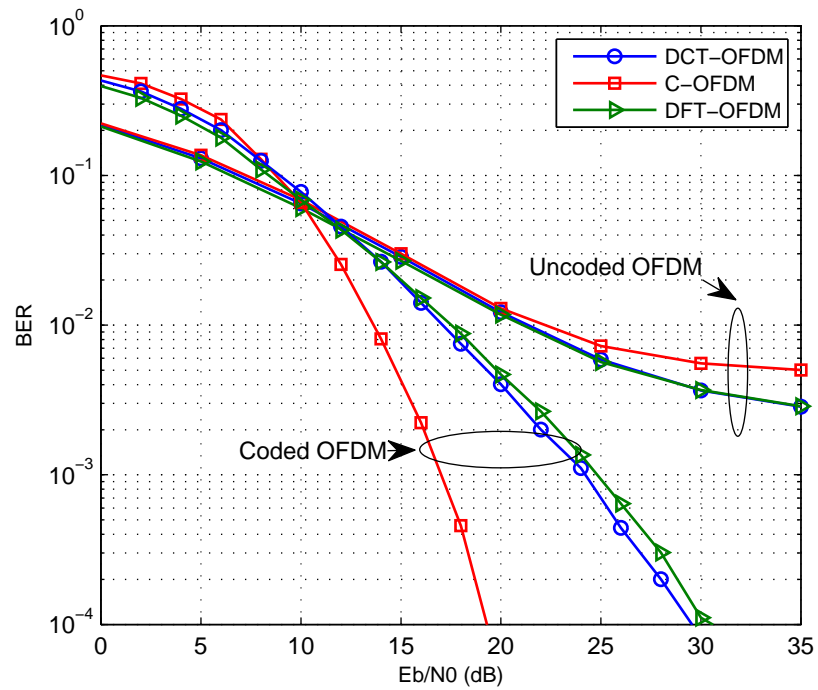


(b) Vehicular IBO=3 dB.

Figure 6.9: BER performance of the C-OFDM, DCT-OFDM, and DFT-OFDM of the 16-QAM and the QPSK modulations with SSPA of IBO=3 dB over the ITU channel (a: pedestrian B and b: vehicular A).



(a) Vehicular IBO=5 dB.



(b) Vehicular IBO=3 dB.

Figure 6.10: BER performances of uncoded/coded proposed C-OFDM, DCT-OFDM and DFT-OFDM systems in the presence of SSPA over ITU class A vehicular channel for 16-QAM modulation formats (a: IBO=5 dB and b: IBO=3 dB).

6.8 Performance Analysis of the UP-OFDM in the Presence of the SSPA

In precoded OFDM systems, the information symbols are first processed by the unitary precoder $\mathbf{P}_{N \times N}$ as

$$\mathbf{r} = \mathbf{P}\mathbf{S}, \quad (6.16)$$

where $\mathbf{S} = [S_0, S_1, \dots, S_{N-1}]^T$, is the information symbols that are drawn from the modulator and $(\cdot)^T$ is the transpose operation. The produced symbol is then processed by the inverse FFT (IFFT) as

$$s_k = \frac{1}{\sqrt{N}} \sum_{n=0}^{N-1} r_n e^{j \frac{2\pi kn}{N}}, \quad (k = 0, 1, 2, \dots, N-1). \quad (6.17)$$

A guard interval represented by a cyclic prefix (CP), which is a copy of last N_g samples of \mathbf{s} is appended to the beginning to mitigate the intersymbol interference (ISI). From (6.17), s_k can be written as

$$s_k = \frac{1}{\sqrt{N}} \sum_{\substack{z=0 \\ z \neq n}}^{N-1} r_z e^{j \frac{2\pi kz}{N}} + \frac{1}{\sqrt{N}} r_n e^{j \frac{2\pi kn}{N}}. \quad (6.18)$$

Let $g_k = \frac{1}{\sqrt{N}} \sum_{\substack{z=0 \\ z \neq n}}^{N-1} r_z e^{j \frac{2\pi kz}{N}}$ and substitute (6.18) into (6.2) yields

$$\begin{aligned} u_k &= \left(g_k + \frac{1}{\sqrt{N}} r_n e^{j \frac{2\pi kn}{N}} \right) G_a \left[\left| g_k + \frac{1}{\sqrt{N}} r_n e^{j \frac{2\pi kn}{N}} \right| \right] \\ &= g_k G_a \left[\left| g_k + \frac{1}{\sqrt{N}} r_n e^{j \frac{2\pi kn}{N}} \right| \right] \\ &+ \frac{1}{\sqrt{N}} r_n e^{j \frac{2\pi kn}{N}} G_a \left[\left| g_k + \frac{1}{\sqrt{N}} r_n e^{j \frac{2\pi kn}{N}} \right| \right]. \end{aligned} \quad (6.19)$$

It is clear that u_k in (6.19) consists of two terms, the first term is an amplified version of $N-1$ statistically independent symbols that have been accumulated by the IFFT at the transmitter, while the second term is the symbol to be detected after the FFT at the receiver. In the case of the OFDM, the first term of (6.19) is much higher than the second term which leads to significant distortion. Regarding the SC-FDE, the first term, g_k , of (6.19) is equal to zero due to the information symbol at the transmitter is not multiplexed with other symbols. The received signal at the

6.8 Performance Analysis of the UP-OFDM in the Presence of the SSPA

receiver side is then given as

$$y_k = u_k \circledast \tilde{h}_k + v_k, \quad (6.20)$$

where \mathbf{v} is the AWGN with zero mean and variance $\sigma_v^2 = E\{|v_k|^2\}$, $E\{\cdot\}$ denotes the expectation operation and \circledast represents a convolution process. At the receiver side, the CP extension is discarded from the received signal, hence, the resulting signal after the FFT can be written as

$$\begin{aligned} \hat{Y}_n &= \frac{1}{\sqrt{N}} \sum_{n=0}^{N-1} y_k e^{j\frac{2\pi kn}{N}} \\ &= H_n U_n + \Omega_n, \end{aligned} \quad (6.21)$$

where $H_n = \sum_{i=0}^L h_i e^{-j\frac{2\pi ni}{N}}$, ($0 \leq n \leq N-1$) is the channel transfer function corresponding to the n^{th} subchannel, Ω_n is the frequency domain representation of the AWGN, \mathbf{v} , and U_n can be written from (6.19) as

$$U_n = \frac{1}{\sqrt{N}} \sum_{k=0}^{N-1} u_k e^{-j\frac{2\pi nk}{N}}, \quad (n = 0, 1, 2, \dots, N-1). \quad (6.22)$$

Substitute (6.19) into (6.22) yields

$$\begin{aligned} U_n &= \frac{1}{\sqrt{N}} \sum_{k=0}^{N-1} \left(g_k + \frac{1}{\sqrt{N}} r_n e^{j\frac{2\pi nk}{N}} \right) \\ &G_a \left[\left| g_k + \frac{1}{\sqrt{N}} r_n e^{j\frac{2\pi nk}{N}} \right| \right] e^{-j\frac{2\pi nk}{N}} \end{aligned} \quad (6.23)$$

Using the following equality

$$\left| g_k + \frac{1}{\sqrt{N}} r_n e^{j\frac{2\pi nk}{N}} \right| = \left| g_k e^{-j\frac{2\pi kn}{N}} + \frac{1}{\sqrt{N}} r_n \right|, \quad (6.24)$$

(6.23) will be written as

$$\begin{aligned} U_n &= \frac{1}{\sqrt{N}} \sum_{k=0}^{N-1} g_k G_a \left[\left| g_k e^{-j\frac{2\pi kn}{N}} + \frac{1}{\sqrt{N}} r_n \right| \right] e^{-j\frac{2\pi nk}{N}} \\ &+ \frac{1}{N} \sum_{k=0}^{N-1} r_n G_a \left[\left| g_k e^{-j\frac{2\pi kn}{N}} + \frac{1}{\sqrt{N}} r_n \right| \right] \end{aligned} \quad (6.25)$$

6.8 Performance Analysis of the UP-OFDM in the Presence of the SSPA

where $e^{j\frac{2\pi nk}{N}}e^{-j\frac{2\pi nk}{N}} = 1$. After some manipulations, (6.25) can be rewritten in compact form as

$$U_n = \frac{r_n}{N} \sum_{k=0}^{N-1} G_a \left[\left| \frac{1}{\sqrt{N}} r_n + g_k e^{-j\frac{2\pi nk}{N}} \right| \right] + \frac{1}{\sqrt{N}} \sum_{k=0}^{N-1} g_k G_a \left[\left| \frac{1}{\sqrt{N}} r_n + g_k e^{-j\frac{2\pi nk}{N}} \right| \right] e^{-j\frac{2\pi nk}{N}}. \quad (6.26)$$

Let

$$\mathcal{G} = \sum_{k=0}^{N-1} \frac{G_a}{N} \left[\left| \frac{1}{\sqrt{N}} r_n + g_k e^{-j\frac{2\pi nk}{N}} \right| \right], \quad (6.27)$$

is the amplifier amplitude distortion, and

$$\mathcal{L}_n = \frac{1}{\sqrt{N}} \sum_{k=0}^{N-1} g_k G_a \left[\left| \frac{1}{\sqrt{N}} r_n + g_k e^{-j\frac{2\pi nk}{N}} \right| \right] e^{-j\frac{2\pi nk}{N}}, \quad (6.28)$$

is the SSPA nonlinear distortion noise. Therefore, (6.26) can be rewritten as

$$U_n = \mathcal{G}r_n + \mathcal{L}_n. \quad (6.29)$$

Substituting (6.29) into \hat{Y}_n in (6.21) and considering the minimum mean-squared error (MMSE) equalization, the equalized signal, \hat{r}_n , is then given as

$$\hat{r}_n = U_n \frac{E_s |H_n|^2}{E_s |H_n|^2 + \sigma_v^2} + \Omega_n \frac{E_s H_n^*}{E_s |H_n|^2 + \sigma_v^2}, \quad (6.30)$$

where $(\cdot)^*$ is the conjugate operation. The received signal after the inverse of the precoder can be written as

$$\begin{aligned} \hat{q}_i &= S_i \sum_{n=0}^{N-1} \mathcal{G} \frac{p_{i,n} \gamma_s |H_n|^2}{\gamma_s |H_n|^2 + 1} + \sum_{n=0}^{N-1} \mathcal{L}_n \frac{p_{i,n} \gamma_s |H_n|^2}{\gamma_s |H_n|^2 + 1} \\ &+ \sum_{n=0}^{N-1} \frac{p_{i,n} \Omega_n \gamma_s H_n^*}{\gamma_s |H_n|^2 + 1}, \end{aligned} \quad (6.31)$$

where $p_{i,n}$ is the i^{th} row, n^{th} column element of the precoder matrix and γ_s is the signal-to-noise ratio (SNR) per symbol. It follows that, after some algebra, the error

$e_i = \hat{q}_i - S_i$ is given as

$$\begin{aligned}
 e_i &= S_i \sum_{n=0}^{N-1} \frac{p_{i,n} \gamma_s |H_n|^2 (\mathcal{G} - 1)}{\gamma_s |H_n|^2 + 1} - \sum_{n=0}^{N-1} \frac{S_i p_{i,n}}{\gamma_s |H_n|^2 + 1} \\
 &+ \sum_{n=0}^{N-1} \mathfrak{L}_n \frac{p_{i,n} \gamma_s |H_n|^2}{\gamma_s |H_n|^2 + 1} + \sum_{n=0}^{N-1} \frac{p_{i,n} \Omega_n \gamma_s H_n^*}{\gamma_s |H_n|^2 + 1}
 \end{aligned} \tag{6.32}$$

One can notice that the first and third terms on the right-hand-side (RHS) of (6.32) are SSPA noise made. For the case of conventional OFDM, \mathfrak{L}_n^{OFDM} is very high as $N - 1$ OFDM samples are involved in constructing g_k . For the case of SC-FDE, $\mathfrak{L}_n^{SC-FDE} = 0$ as $g_k = 0$ and for the case of $\mathbf{P} = \text{DHT}$, $\mathfrak{L}_n^{UP-OFDM} \ll \mathfrak{L}_n^{OFDM}$ as it involves much lower PAPR. Therefore, BER performance of the SC-FDE scheme is the best in the presence of the SSPA as it is single carrier technique. On other hand, the BER performance of the DHT precoded OFDM is better than the conventional OFDM system.

6.9 Results and Discussions

In our simulation, number of subcarriers $N = 1024$, length of the cyclic prefix $CP = \frac{N}{4}$ and 16-QAM modulation format is used. SSPA high power amplifier is utilized at the transmitter side after adding the cyclic prefix as a nonlinear source of distortion. To separate the diversity gain from the gain that comes from PAPR reduction, simulation is performed in two stages. Firstly, BER performance over AWGN channel where the gain only comes from PAPR reduction as there is no diversity benefit from using precoders over AWGN channel and secondly, the BER performance over ITU vehicular A channel.

6.9.1 Over AWGN Channel

Figs. 6.11, 6.12 and 6.13 show the BER performance of the UP-OFDM with WHT, DCT, DHT and FFT precoders for the 16-QAM modulation and IBO=7 dB, 5 dB and 3 dB respectively. It can be seen that the UP-OFDM achieved the best BER performance when the precoder $\mathbf{P} = \text{DFT}$ (SC-FDE). This is expected result as the SC-FDE is single carried system and the PAPR problem is only occurred in multicarrier (MC) systems. Among the MC systems, when $\mathbf{P} = \text{DHT}$ leads to the

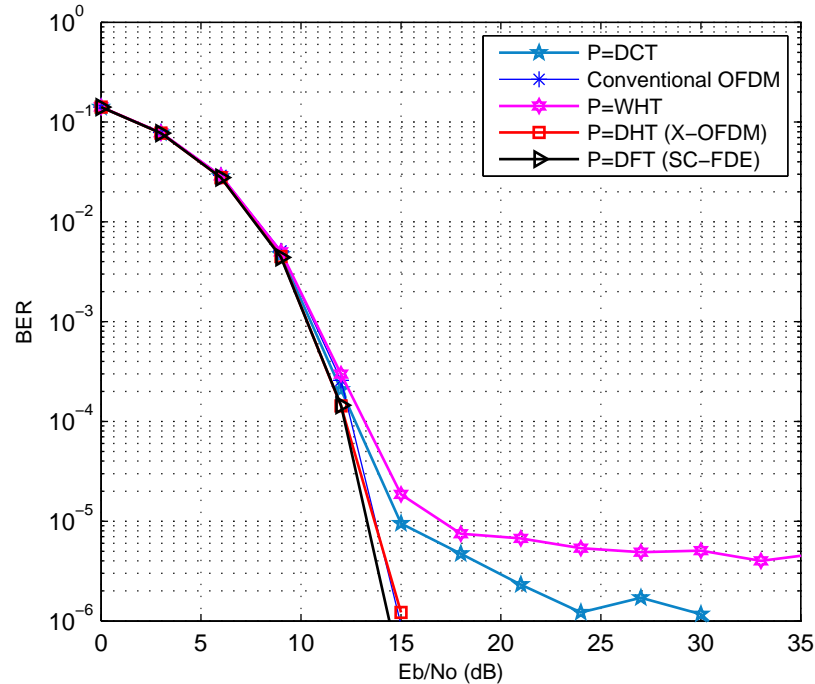


Figure 6.11: BER performance of the DFT (SC-FDE), DHT (X-OFDM), DCT, WHT precoded OFDM and the conventional OFDM for the 16-QAM modulation with the SSPA (IBO=7 dB) over the AWGN channel.

best performance as it has the lowest PAPR that nearly keep dynamic range of the OFDM signal within the linear region of the power amplifier. When P=WHT or DCT, the BER performance has worse BER performance than the conventional OFDM despite they reduce the PAPR for a certain levels. In Fig. 6.12 when the IBO=5 dB, the conventional OFDM can achieve reasonable performance. However, this performance become completely unreliable when the IBO reduced to 3 dB as shown in Fig. 6.13.

6.9.2 Over Multipath Channels

We have explained in section 6.6.2 for the C-OFDM that the unitary precoded system is not sensible or with negligible sensitivity to the nonlinear distortion when the constellation is the QPSK. However, the high level modulation schemes such as the 16-QAM is used, the sensitivity to the SSPA distortion arose which is the same case for the UP-OFDM.

For the case of the 16-QAM modulation, the BER performance of the UP-OFDM system with different precoders and channel models are shown in Figs. 6.14, 6.15 and 6.16 for IBO= 7dB, 5dB and 3dB respectively. It is obvious from all these figures

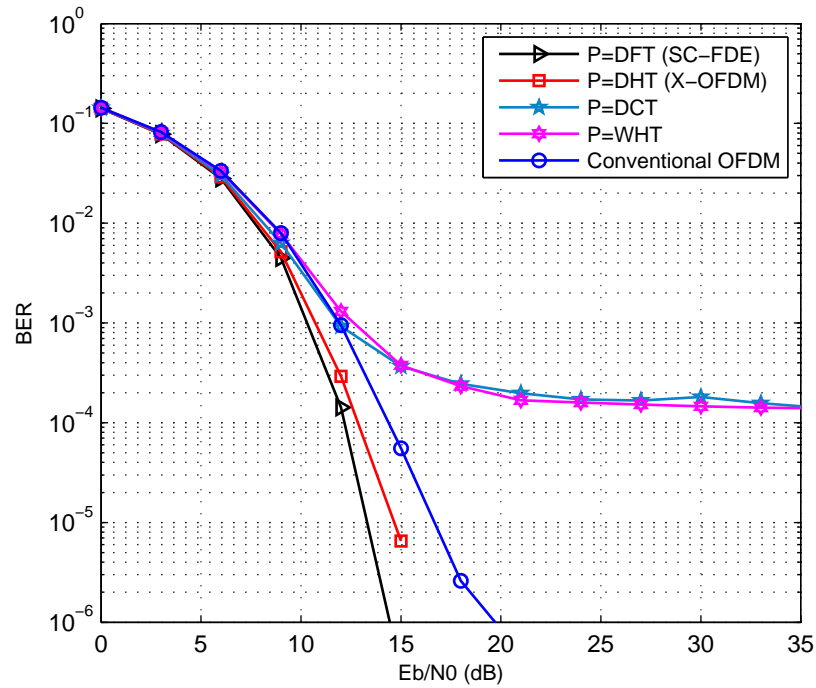


Figure 6.12: BER performance of the DFT (SC-FDE), DHT (X-OFDM), DCT, WHT precoded OFDM and the conventional OFDM for the 16-QAM modulation with the SSPA (IBO=5 dB) over the AWGN channel.

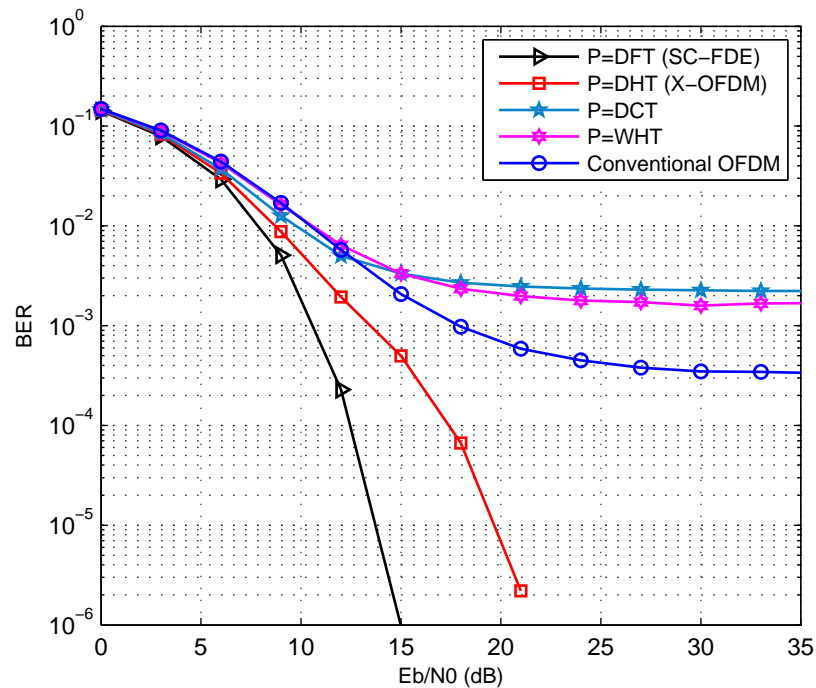


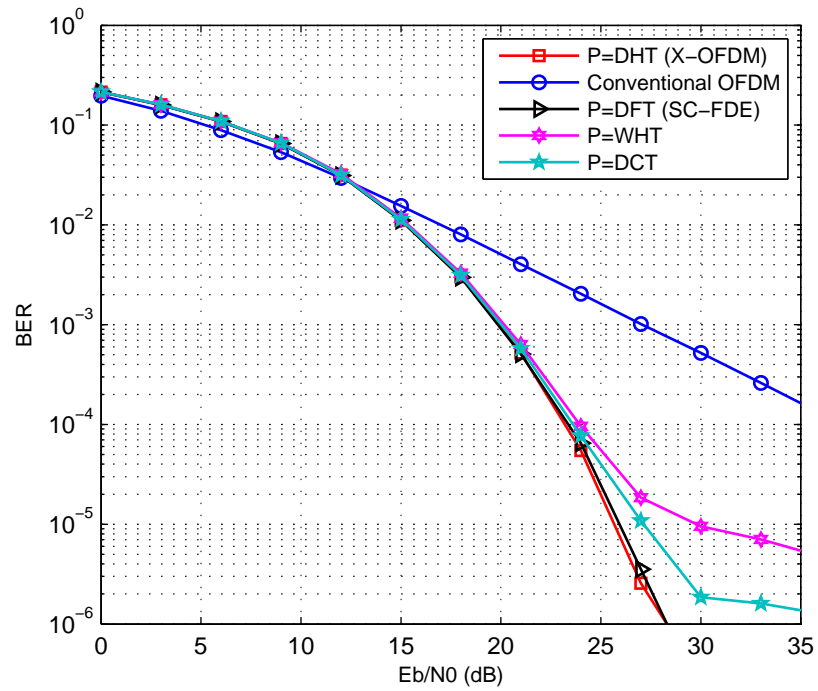
Figure 6.13: BER performance of the DFT (SC-FDE), DHT (X-OFDM), DCT, WHT precoded OFDM and the conventional OFDM for the 16-QAM modulation with the SSPA (IBO=3 dB) over the AWGN channel.

that the sensitivity of the UP-OFDM to the SSPA nonlinear distortion depends on the type of the unitary transform (precoder) in used. Although the WHT and DCT precoded OFDM have lower PAPR than the conventional OFDM, their performances are more sensitive to the clippings than the conventional OFDM and can have a worse BER performance especially when the SSPA has lower IBO. On the other hand, as the DHT achieves relatively more PAPR reduction that keep the signal within the linear region of the SSPA, it can achieve the same performance as the SC-FDE and still satisfy the valuable improvement in BER performance over the conventional OFDM.

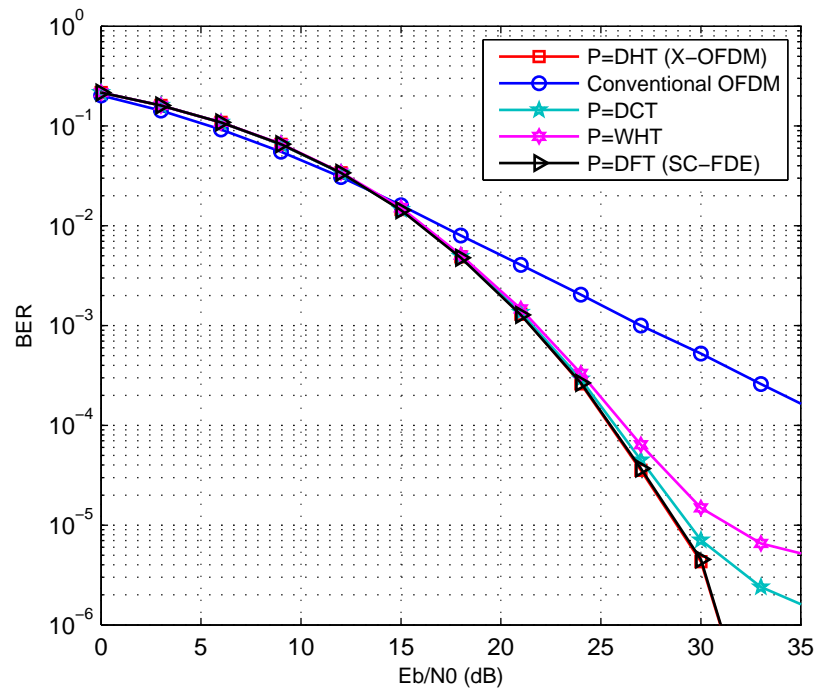
It can also notice from Fig 6.14 that for the case when the IBO is 7 dB, the UP-OFDM systems can still achieve significant SNR gain (around 14 dB) over the conventional OFDM at 10^{-4} BER. However, the performances of different precoders become more distinguishable at and below 10^{-5} BER. When the the IBO of the SSPA is reduced to 5 dB, the WHT and DCT precoded OFDM move a part from the X-OFDM and SC-FDE at 10^{-3} and become flooring at 10^{-4} BER as shown in Fig. 6.15. When the IBO further reduced to 3 dB as in Fig. 6.15, the BER performance of the X-OFDM and SC-FDE still achieve important SNR gain in comparison to the conventional OFDM whereas the BER performance of WHT and DCT precoded OFDM become even worse than the conventional OFDM.

6.9.3 Coded UP-OFDM over the Multipath Channel

In this section, a convolutional coding/Viterbi encoding algorithm with a 1/2 code rate is used to mitigate the effects of the SSPA on the BER performance of the UP-OFDM. Fig. 6.17 (6.17(a) for IBO=5 dB and 6.17(b) for IBO=3 dB) depicts that, for coded UP-OFDM systems, all P=DFT, DHT, DCT and WHT have identical BER performance, achieving approximately 13 dB signal-to-noise ratio (SNR) gain over the conventional coded OFDM at 10^{-4} BER. The coding technique is so efficient that it mitigates the effects of clipping distortion on the DCT and the WHT precoded OFDM and maintains their advantages even in the presence of the SSPA with IBO=3 dB.

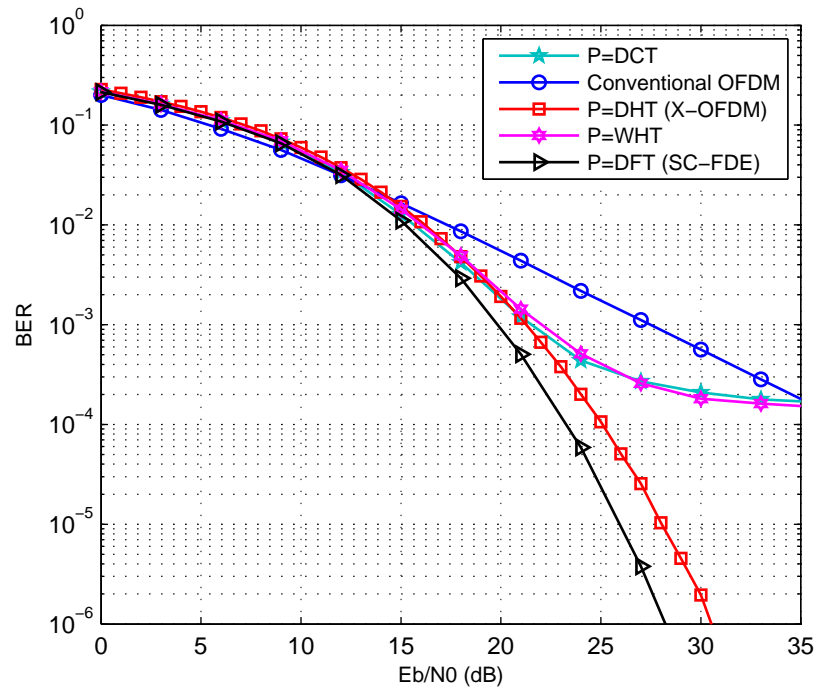


(a) Pedestrian IBO=7 dB.

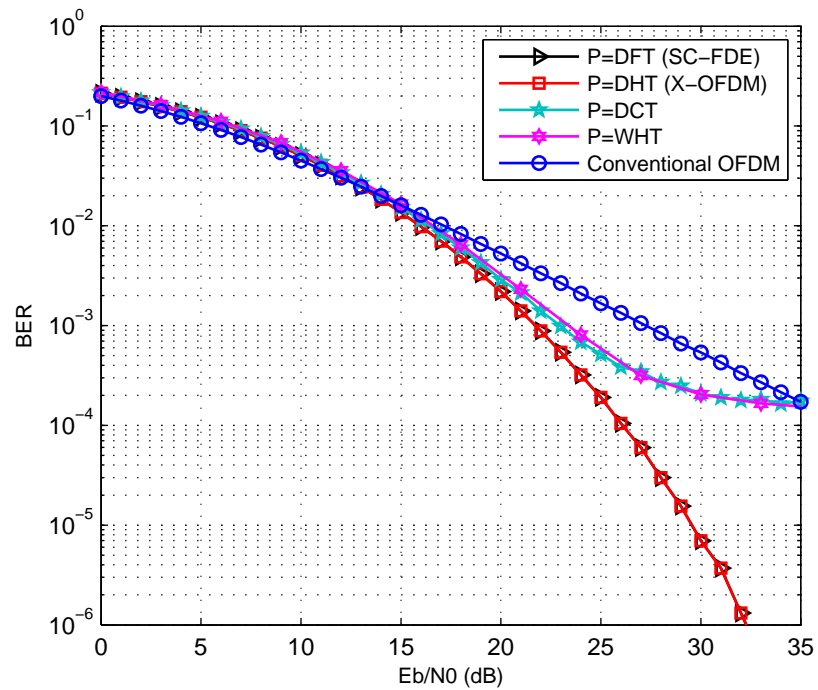


(b) Vehicular IBO=7 dB.

Figure 6.14: BER performance of the DFT (SC-FDE), DHT (X-OFDM), DCT, WHT precoded OFDM and the conventional OFDM for the 16-QAM modulation with the SSPA of IBO=7 dB over the ITU channel (a: Pedestrian B and b: Vehicular A).

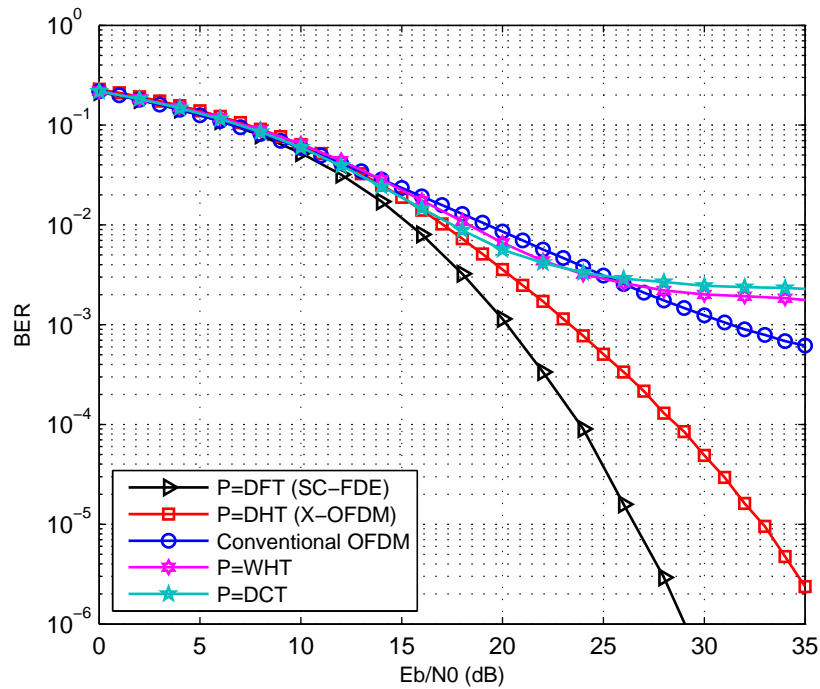


(a) Pedestrian IBO=5 dB.

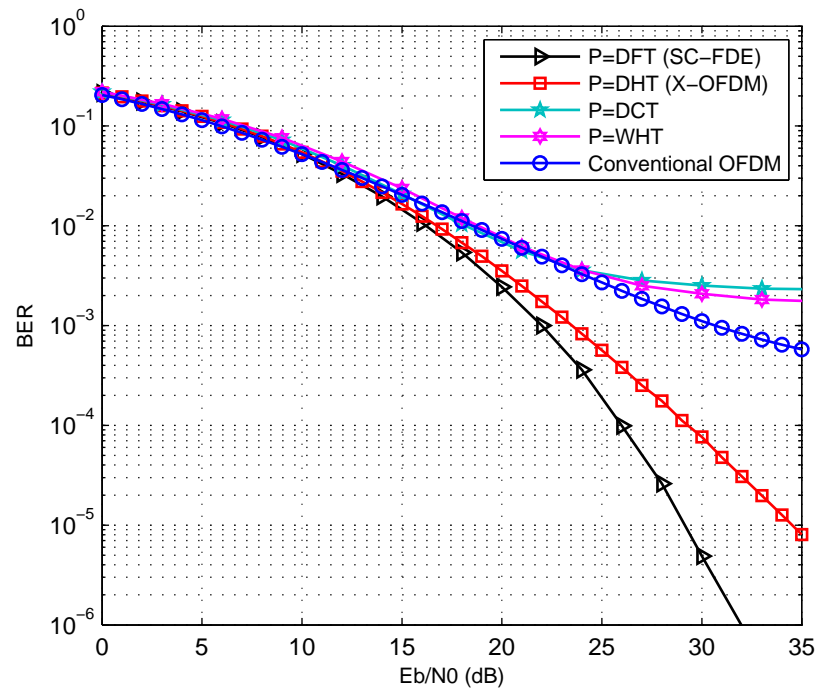


(b) Vehicular IBO=5 dB.

Figure 6.15: BER performance of the DFT (SC-FDE), DHT (X-OFDM), DCT, WHT precoded OFDM and the conventional OFDM for the 16-QAM modulation with the SSPA of IBO=5 dB over the ITU channel (a: Pedestrian B and b: Vehicular A).

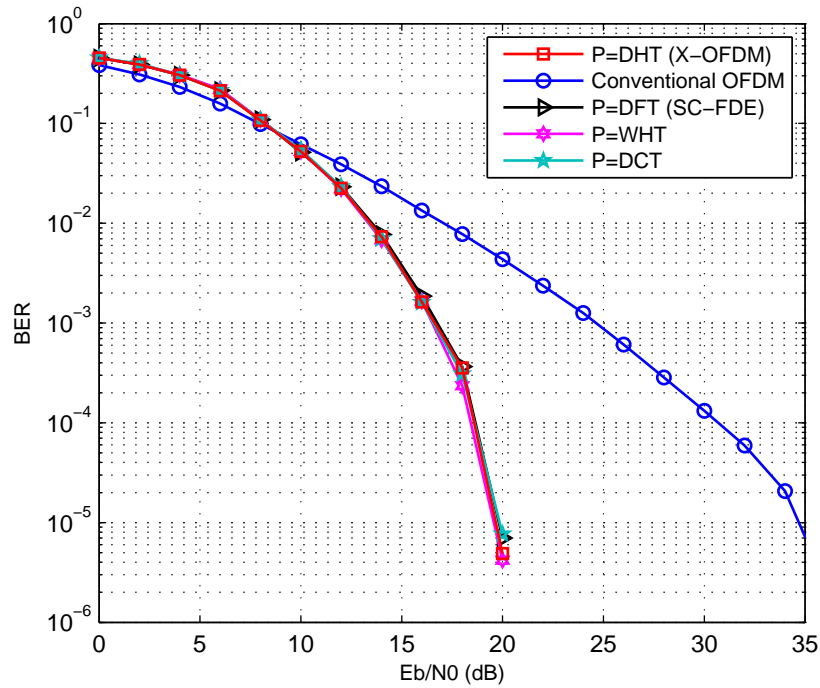


(a) Pedestrian IBO=3 dB.

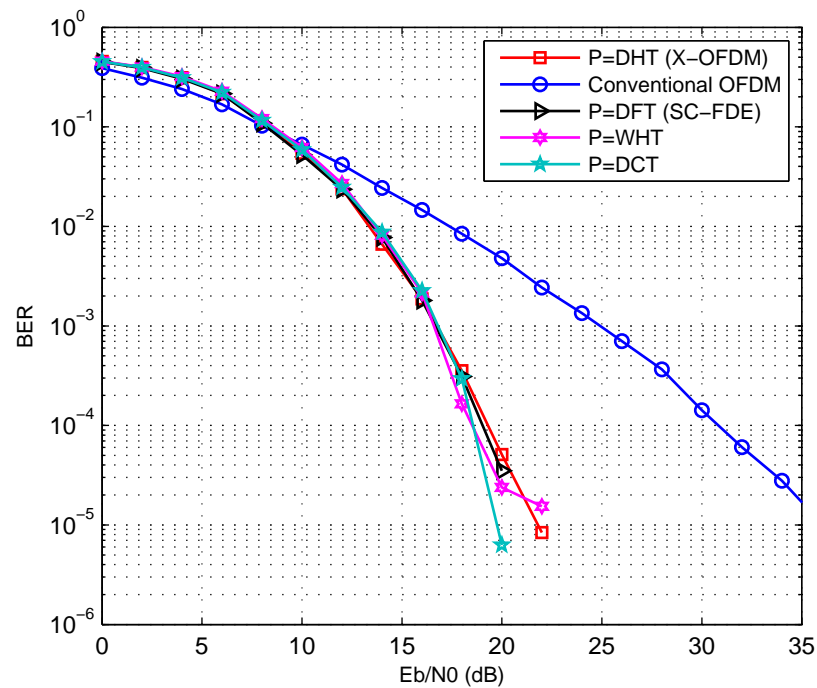


(b) Vehicular IBO=3 dB.

Figure 6.16: BER performance of the DFT (SC-FDE), DHT (X-OFDM), DCT, WHT precoded OFDM and the conventional OFDM for the 16-QAM modulation with the SSPA of IBO=3 dB over the ITU channel (a: Pedestrian B and b: Vehicular A).



(a) Vehicular IBO=5 dB.



(b) Vehicular IBO=3 dB.

Figure 6.17: BER performances of the coded DFT (SC-FDE), DHT (X-OFDM), DCT, WHT precoded OFDM and the conventional OFDM for the 16-QAM modulation with the SSPA over the ITU class A vehicular channel for the 16-QAM modulation (a: IBO=5 dB and b: IBO=3 dB).

6.10 Conclusion

In this chapter, the effects of the SSPA nonlinearities on the BER performance of the C-OFDM and a unitary precoded UP-OFDM system have been demonstrated and treated. A comparison of different unitary precoders such as WHT, DCT, DHT and DFT has been conducted in the presence of the SSPA with different IBOs. The main conclusion that can be drawn from this chapter is that using unitary channel independent precoders can enhance the diversity and reduce the PAPR but might lead to high sensitivity to nonlinear distortion. When the 16-QAM modulation is used, some unitary precoders such as the WHT and the DCT caused problems in the presence of the SSPA, while the DHT (X-OFDM) proved to have a robustness against the nonlinear distortion. A forward error coding scheme was found to be efficient in mitigating the precoding systems' sensitivity to the SSPA distortion where the coded UP-OFDM has the same performance for all P=the DHT (X-OFDM), DFT (SC-FDE), DCT and the WHT.

Chapter 7

Conclusion and Future Work

7.1 Conclusion

Equipping a transceiver of the OFDM system with a properly designed precoder has attracted much research attention in the last decade. In particular, the unitary channel independent precoders, where no CSI is required at the transmitter, is found to be efficient in improving the OFDM systems. The advantage of such a combination is its robustness against multipath channels, where it was shown that the system BER performance can be improved when such precoders are added to the transceiver of the OFDM system. These precoders were also found to reduce the PAPR of the OFDM signal to certain levels depending on the precoder type. However, the problem is that they are complex and require more hardware, because the precoder and the modulation transform are presented separately. Moreover, in the past, the emphasis was only on the BER and PAPR reduction with no investigation into the extent to which this PAPR reduction can affect positively or negatively the system performance in the presence of high power amplifiers (HPAs).

The motivation behind this research was to produce new OFDM systems based on low complexity orthogonal transforms to reduce the complexity of the modulation scheme. Two different schemes were produced: OFDM based on real trigonometric transform, and OFDM based on very low complexity \mathbf{X} -transform. It also investigates the performance of both systems in the presence of SSPAs.

In this thesis, two new OFDM schemes based on two different unitary transforms was introduced. These two schemes are named C-OFDM and X-OFDM schemes. both of these proposed schemes utilize the same principle, channel independent

precoder, to combine the data symbols in frequency domain to increase the diversity.

Each one of the proposed scheme was found to have some different characteristics than the other. As the C-OFDM system is based on a real transform, thus it can avoid the I/Q imbalance when the data symbols are real. It can also avoid the Hermitian constraint on the input data when it is applied on baseband transmission such as the DMT. Furthermore, the proposed C-OFDM achieved about 10 dB SNR gain at 10^{-4} BER in comparison to the DFT-OFDM and the DCT-OFDM systems. It also reduced the PAPR by about 1 dB. Despite the superiority of the C-OFDM in the aforementioned scenarios, the single tap equaliser, same as that for DFT-OFDM, may not be applicable in the case of the C-OFDM.

The second scheme was based on low complexity unitary \mathbf{X} -transform which involves complex elements in its matrix structure. The X-OFDM scheme enables single tap equalizer exactly the same as the one used for the DFT-OFDM. It achieved about 15 dB SNR gain at 10^{-4} BER in comparison to the DFT-OFDM. Furthermore, it reduced the average PAPR by about 6 dB.

The \mathbf{X} -transform was utilized in implementation of the transmitter of the ST-OFDM system instead of the traditional FFT. To significantly reduce the transmitter complexity, the ST encoder has performed after the IFFT, and both the DHT and the IFFT were merged into a single unitary low complexity \mathbf{X} -transform. It has been shown mathematically and by computer simulation over an ITU multipath frequency-selective fading channel that the proposed ST-X-OFDM achieved valuable SNR gain in comparison to conventional ST-OFDM.

The effects of the SSPA non-linearities on the BER performance of a unitary precoded OFDM (UP-OFDM) system have been demonstrated and treated. A comparison of different unitary precoders such as WHT, DCT, DHT and the DFT has been conducted in the presence of the SSPA with different IBOs. Using unitary channel independent precoders can enhance the diversity and reduce the PAPR, however, this might lead to high sensitivity to nonlinear distortion. When the 16-QAM modulation is used, some unitary precoders such as the WHT and the DCT caused problems in the presence of the SSPA, while others such as the DFT and the DHT proved to have a robustness against the nonlinear distortion. A forward error coding scheme was found to be efficient in mitigating the precoding systems' sensitivity to the SSPA distortion where the coded UP-OFDM has the same performance

for all precoders (DFT, DHT, DCT and the WHT).

7.2 Future Work

- The C-OFDM system may be implemented with a single-tap equalizer by finding a way to implement the convolution in the DCT domain.
- Examine the C-OFDM scheme to manage the optical communications. Investigating the C-OFDM application in optical communication is worthwhile as the \mathbf{C} -transform is real transform, hence, requiring no Hermitian constraint condition on the data symbols. Moreover, utilizing the \mathbf{C} -transform in optical communications is expected to improve the BER performance due to the signal diversity enhancement.
- Examine the applications of the X-OFDM scheme to manage different kinds of widespread communications. These include investigating the implementation of the X-OFDM system in cooperative technology with different protocols to highlight the validity of the X-OFDM system in this widespread scheme. The proposed X-OFDM systems might also be implemented in optical communications system which is expected to achieve good performance. This research project concentrated primarily on point-to-point (single user) communication, therefore it is quite helpful if the application of the proposed schemes in multiuser uplink and downlink schemes are also investigated. Finally, investigating the validity of the proposed schemes with different kinds of power amplifiers such as the travelling wave tube amplifiers (TWTA) which is mainly used in satellite communications to give a validity of the proposed schemes in satellite communications.
- Impulse noise is a serious source of distortion that occurs in power line communications. Therefore, it will be worth examining the proposed C-OFDM and X-OFDM systems when such kinds of noise occur to extend the application of the proposed schemes in this thesis.
- The equalization of the X-OFDM system may be implemented in Hartley domain that enables the \mathbf{X} -transform to be utilized in the receiver side which

could reduce the receiver complexity enormously without the necessity to time-domain equalizer.

- Among all this thesis work the channel state information (CSI) is assumed to be perfectly known channel, therefore, the case when the CSI is not known at the receiver needs to be studied.
- The proposed schemes might also be implemented in hardware by using the field-programmable gate array (FPGA).

Appendix A

Submitted Paper to IEEE

Transactions on Communications

[84]

Under review for possible publication in



Efficient OFDM System Based on New Transform for PAPR Reduction and Diversity Enhancement

Journal:	<i>IEEE Transactions on Communications</i>
Manuscript ID:	TCOM-TPS-11-0770
Manuscript Type:	Transactions Paper Submissions
Date Submitted by the Author:	15-Nov-2011
Complete List of Authors:	Al-Sodani, Hussein Abdullah; Newcastle University, SchSchool of Electrical, Electronic and Computer Engineering Boussakta, Said; Newcastle University, School of Electrical, Electronic and Computer Engineering
Keyword:	Discrete Fourier transforms, Discrete Hartley transforms, Communication systems, Transforms

SCHOLARONE™
Manuscripts

Review

IEEE Transactions on Communications

Efficient OFDM System Based on New Transform for PAPR Reduction and Diversity Enhancement

Hussein Abdullah Al-Sodani, *Student Member, IEEE* and Said Boussakta, *Senior Member, IEEE*.

School of Electrical, Electronic and Computer Engineering,
Newcastle University, NE1 7RU,
Newcastle upon Tyne, UK

Abstract

A new orthogonal frequency division multiplexing (OFDM) based on a new low complexity \mathbf{X} transform, which combines the effect of the discrete Hartley transform (DHT) and discrete Fourier transform (DFT), is presented in this paper. The computational complexity of the proposed \mathbf{X} transform is evaluated and compared with that of the FFT and FHT-FFT. The bit-error rate (BER) performance of the proposed system is evaluated by mathematics and simulation over multipath channel model when QPSK and 16QAM modulation formats are utilized. Simulation results are corroborated with the theoretical results proving that, for minimum mean-square-error (MMSE) detection, the proposed system is more resilient to multipath transmission than the conventional OFDM system. Furthermore, it is evidenced by simulation that the proposed scheme is better than the DFT-OFDM system even when it encompasses high power amplifiers (HPAs) in its structure. Additionally, the proposed scheme shows significant reduction in peak-to-average power ratio (PAPR) compared to the conventional DFT-OFDM system while it retains the same average power. This is owing to the significant reduction in the superposition of the input data symbols to perform each output OFDM sample which in turn leads to significant reduction in PAPR.

Index Terms

Discrete Hartley transform (DHT), discrete Fourier transform (DFT), orthogonal frequency division multiplexing (OFDM), peak-to-average power ratio (PAPR) and carrier frequency offset (CFO).

I. INTRODUCTION

MULTICARRIER modulation (MCM) based on orthogonal frequency division multiplexing (OFDM) has received remarkable attention in the last two decades [1]-[3] because of its peculiar characteristics with bandwidth efficiency and immunity against multipath fading channels. Therefore, this modulation is widely adopted for wireless broadband communications systems as well as wire-line communications such as an asymmetric digital subcarrier loop (ADSL) and a power line communications (PLC) [4]-[5]. In spite of the success of the conventional OFDM system which is based on discrete Fourier transform (DFT) as a modulation technique in many fields of applications and standards, the diversity provided by uncoded OFDM system is still not adequate to mitigate the dispersive effects of severe hostile channels. This can be attributed to the whole bit-error-rate (BER) performance dominated by the subcarrier with the smallest signal energy per bit to noise ratio E_b/N_0 [6]-[7] leading to a poor performance over

IEEE Transactions on Communications

1 channels with narrowband deep notches spectral. Therefore, uncoded DFT-OFDM systems can not prevails.
2
3 Furthermore, its high peak-to-average power ration (PAPR) is considered as one of the major obstacles
4
5 to the design of a reliable OFDM system. As a result, several techniques have been proposed to reduce
6
7 the high PAPR within the OFDM systems including amplitude clipping, partial transmit sequence (PTS)
8
9 and selective-mapping (SLM) [8]-[9]. Their complexity, however, is relatively high as only one of several
10
11 generated sequences is used for transmission. On the other hand, some research have been conducted with
12
13 the aim to improve the transmission of OFDM systems by using discrete Hartley transform (DHT) [10]-
14
15 [14], discrete cosine transform (DCT) [15]-[18] or a precoder. The technique of using different unitary
16
17 transforms as a channel independent precoder to improve the BER performance of OFDM systems was
18
19 demonstrated in [19] claiming that the Walsh-Hadamard transform (WHT) is one of the transforms that can
20
21 achieve optimum BER performance. Further investigation regarding the WHT precoded OFDM shows that
22
23 it does not only improve the BER performance [20] but also reduce the PAPR [21]. The PAPR reduction,
24
25 however, is poor and has relatively high complexity.
26
27
28
29
30
31
32 In this paper, a new very low complexity X transform which combines the effects of the DHT and the DFT
33
34 transforms is proposed to produce a new X-OFDM system. The proposed system has the same complexity
35
36 of single one-tap equalizer and meets the desired features of the DFT-OFDM system without its main
37
38 drawbacks. The proposed X-OFDM system exploits the channel diversity and achieves significant E_b/N_0
39
40 gain over the conventional MC-OFDM systems. Moreover, the proposed scheme significantly mitigates
41
42 the PAPR problem that affects the DFT-OFDM system.
43
44
45
46 The BER performance of the proposed scheme is evaluated theoretically and by computer simulation in this
47
48 paper over international telecommunication union (ITU) channel for both quadrature phase-shift keying
49
50 (QPSK) and 16 quadrature amplitude modulation (16QAM) formats. Additionally, the BER performance
51
52 of the proposed scheme in the presence of solid state power amplifier (SSPA) with different input-
53
54 backoff (IBO) is investigated in this work and compared with the conventional DFT-OFDM system.
55
56
57 The effect of carrier frequency offset (CFO) that arises from frequency mismatch of the transceivers local
58
59 oscillators on the proposed system is also evaluated and compared with the DFT-OFDM system, when
60

1 both no synchronization algorithm is applied and when utilizing the Morelli and Mengali (M&M) [22]
 2
 3 synchronization algorithm. Furthermore, the PAPR of the proposed system is also evaluated in this paper
 4
 5 and compared with the PAPR of the DFT-OFDM. The proposed system, for the case of the minimum
 6
 7 mean-square error (MMSE) detection, is found to be far more resilient to the multipath environment and to
 8
 9 achieve about $15dB$ in E_b/N_0 at 10^{-4} BER in comparison with the conventional DFT-OFDM system. This
 10
 11 is attributed to the fact that the individual bit power is distributed over the whole frequency spectrum using
 12
 13 the DHT while this phenomenon does not occur in the DFT-OFDM systems counterpart. Furthermore, the
 14
 15 proposed transform reduces the PAPR value by approximately $6dB$ over the DFT-OFDM system owing
 16
 17 to the reduction in the superposition of the input symbols which perform each OFDM output sample from
 18
 19 N to two. The superiority of the proposed system in BER performance is evident even in the presence of
 20
 21 the CFO that comes from local oscillators mismatch at the transmitter and the receiver when a frequency
 22
 23 synchronization algorithm is performed.
 24
 25

26
 27 The rest of this paper is organized as follows: Section II lays out the arithmetic dimensions of the proposed
 28
 29 \mathbf{X} transform. The computational complexity of the \mathbf{X} transform is introduced in section III. Theoretical
 30
 31 analysis of the BER performance of the proposed X-OFDM system over a multipath fading channels for
 32
 33 the ZF and MMSE detection is introduced in section IV. Section V demonstrates the system performance
 34
 35 in the presence of the HPA, whilst system performance in the presence of the CFO is presented in section
 36
 37 VI. Section VII is devoted to the PAPR. Simulation results and discussions are presented in section VIII.
 38
 39 Finally, the conclusions are drawn out in section IX.
 40
 41
 42
 43
 44

45 A. Notations and Preliminaries

46
 47 1) : The term X-OFDM and DFT-OFDM are referred to our proposed OFDM system and the
 48
 49 conventional OFDM system respectively.
 50
 51

52
 53 2) : The Notation \mathbf{A} is used to represent the $N \times N$ Hartley matrix while the notation \mathbf{F} represents
 54
 55 an $N \times N$ Fourier matrix and their elements are respectively given as:
 56
 57

$$58 a_{n,m} = \frac{1}{\sqrt{N}} \cos\left(\frac{2\pi nm}{N}\right) + \sin\left(\frac{2\pi nm}{N}\right) \quad (1)$$

59
 60 IEEE Transactions on Communications

$$f_{n,m} = \frac{1}{\sqrt{N}} e^{-j2\pi nm/N} \quad (2)$$

3) : $(\cdot)^T$ and $(\cdot)^H$ denote the transpose and Hermitian operations respectively.

4) : The notation \mathbf{I}_N represents the $N \times N$ identity matrix.

5) : The function $E[x]$ denotes the expected value of random variable x .

II. TRANSFORM ANALYSIS

Let us consider the complex data symbols that are uniformly drawn from a specific constellation such as M-array quadrature amplitude modulation (M-QAM) or quadrature phase-shift keying (QPSK) are divided into blocks of size N . Each sequence $\mathbf{S}^T = [S_0, S_1, \dots, S_{N-1}]$ modulates N orthogonal subcarriers by using the DHT. It is well known that the DHT is an orthogonal real valued transform with identical forward and inverse matrices. The output modulated sequence $\mathbf{r}^T = [r_0, r_1, \dots, r_{N-1}]$ is then given as

$$r_n = \sum_{m=0}^{N-1} a_{n,m} S_m \quad (n = 0, 1, 2, \dots, N-1) \quad (3)$$

where $a_{n,m}$ represents the n_{th} row m_{th} column elements of the Hartley matrix \mathbf{A} . Equation (3) can be rewritten based on the basic definition of \mathbf{A} as

$$r_n = \frac{1}{\sqrt{N}} \sum_{m=0}^{N-1} S_m \left[\text{cas}\left(\frac{2\pi nm}{N}\right) \right] \quad (n = 0, 1, 2, \dots, N-1) \quad (4)$$

In (4), $\text{cas}\left(\frac{2\pi nm}{N}\right) = \cos\left(\frac{2\pi nm}{N}\right) + \sin\left(\frac{2\pi nm}{N}\right)$. It follows that the output samples r_n ($0 \leq n \leq N-1$) are processed by the IFFT in order to increase the diversity. The resulting signal $\mathbf{s}^T = [s_0, s_1, \dots, s_{N-1}]$ is a compound signal and can be expressed as

$$s_k = \frac{1}{\sqrt{N}} \sum_{n=0}^{N-1} r_n e^{j\frac{2\pi nk}{N}} \quad (k = 0, 1, 2, \dots, N-1) \quad (5)$$

Substituting Eq. (4) into (5) yields

$$s_k = \frac{1}{N} \sum_{n=0}^{N-1} \sum_{m=0}^{N-1} S_m \text{cas}\left(\frac{2\pi nm}{N}\right) e^{j\frac{2\pi nk}{N}} \quad (6)$$

by using trigonometric identities, (6) can be rewritten as

$$s_k = \frac{1}{N} \sum_{m=0}^{N-1} S_m \sum_{n=0}^{N-1} \frac{1}{2} \left[\cos\left(\frac{2\pi n}{N}(m-k)\right) + \cos\left(\frac{2\pi n}{N}(m+k)\right) \right] + j \frac{1}{2} \left[\cos\left(\frac{2\pi n}{N}(m-k)\right) - \cos\left(\frac{2\pi n}{N}(m+k)\right) \right] \quad (7)$$

1
2
3
4
5
6
7
8
9
10
11
12
13
14
15
16
17
18
19
20
21
22
23
24
25
26
27
28
29
30
31
32
33
34
35
36
37
38
39
40
41
42
43
44
45
46
47
48
49
50
51
52
53
54
55
56
57
58
59
60

Equation (7) can be rewritten in more expressive form as

$$s_k = \sum_{m=0}^{N-1} S_m X_{km} \quad (k = 0, 1, 2, \dots, N-1) \quad (8)$$

where X_{km} is the k_{th} , ($0 \leq k \leq N-1$), row and the m_{th} , ($0 \leq m \leq N-1$) column element of the \mathbf{X}^H (inverse \mathbf{X} transform (IXT)). In matrix form, (8) can be rewritten as

$$\mathbf{s} = \mathbf{X}^H \mathbf{S} \quad (9)$$

where \mathbf{S} is $N \times 1$ vector. From (7) one can notice the following; $X_{k,m} = 1$ when $k = m = 1$ or $k = m = \frac{N}{2}$, $X_{k,m} = \frac{1}{2} + j\frac{1}{2}$ when $k = m$ and $X_{k,m} = \frac{1}{2} - j\frac{1}{2}$ when $k = N - m$ and $X_{km} = 0$ elsewhere.

The inverse \mathbf{X} transform can be expressed as

$$\mathbf{X}^H = \frac{1}{2} \begin{bmatrix} 2 & 0 & 0 & 0 & \dots & 0 & 0 & 0 \\ 0 & 1+j1 & 0 & 0 & \dots & 0 & 0 & 1-j1 \\ 0 & 0 & 1+j1 & 0 & \dots & 0 & 1-j1 & 0 \\ 0 & 0 & 0 & \dots & \cdot & \dots & 0 & 0 \\ \cdot & \cdot & \cdot & 0 & 2 & 0 & \cdot & \cdot \\ \cdot & \cdot & \cdot & \dots & \cdot & \dots & \cdot & \cdot \\ \vdots & 0 & 0 & 1-j1 & 0 \dots 0 & 1+j1 & 0 & \vdots \\ 0 & 0 & 1-j1 & 0 & \dots & 0 & 1+j1 & 0 \\ 0 & 1-j1 & 0 & 0 & \dots & 0 & 0 & 1+j1 \end{bmatrix} \quad (10)$$

while the forward \mathbf{X} transform is given as

$$\mathbf{X} = \frac{1}{2} \begin{bmatrix} 2 & 0 & 0 & 0 & \dots & 0 & 0 & 0 \\ 0 & 1-j1 & 0 & 0 & \dots & 0 & 0 & 1+j1 \\ 0 & 0 & 1-j1 & 0 & \dots & 0 & 1+j1 & 0 \\ 0 & 0 & 0 & \dots & \cdot & \dots & 0 & 0 \\ \cdot & \cdot & \cdot & 0 & 2 & 0 & \cdot & \cdot \\ \cdot & \cdot & \cdot & \dots & \cdot & \dots & \cdot & \cdot \\ \vdots & 0 & 0 & 1+j1 & 0 \dots 0 & 1-j1 & 0 & \vdots \\ 0 & 0 & 1+j1 & 0 & \dots & 0 & 1-j1 & 0 \\ 0 & 1+j1 & 0 & 0 & \dots & 0 & 0 & 1-j1 \end{bmatrix} \quad (11)$$

and for more illustration, both \mathbf{X}^H and \mathbf{X} are given for $N = 8$ in (12) and (13) respectively as

$$\mathbf{X}_8^H = \frac{1}{2} \begin{bmatrix} 2 & 0 & 0 & 0 & 0 & 0 & 0 & 0 \\ 0 & 1+j1 & 0 & 0 & 0 & 0 & 0 & 1-j1 \\ 0 & 0 & 1+j1 & 0 & 0 & 0 & 1-j1 & 0 \\ 0 & 0 & 0 & 1+j1 & 0 & 1-j1 & 0 & 0 \\ 0 & 0 & 0 & 0 & 2 & 0 & 0 & 0 \\ 0 & 0 & 0 & 1-j1 & 0 & 1+j1 & 0 & 0 \\ 0 & 0 & 1-j1 & 0 & 0 & 0 & 1+j1 & 0 \\ 0 & 1-j1 & 0 & 0 & 0 & 0 & 0 & 1+j1 \end{bmatrix} \quad (12)$$

$$\mathbf{X}_8 = \frac{1}{2} \begin{bmatrix} 2 & 0 & 0 & 0 & 0 & 0 & 0 & 0 \\ 0 & 1-j1 & 0 & 0 & 0 & 0 & 0 & 1+j1 \\ 0 & 0 & 1-j1 & 0 & 0 & 0 & 1+j1 & 0 \\ 0 & 0 & 0 & 1-j1 & 0 & 1+j1 & 0 & 0 \\ 0 & 0 & 0 & 0 & 2 & 0 & 0 & 0 \\ 0 & 0 & 0 & 1+j1 & 0 & 1-j1 & 0 & 0 \\ 0 & 0 & 1+j1 & 0 & 0 & 0 & 1-j1 & 0 \\ 0 & 1+j1 & 0 & 0 & 0 & 0 & 0 & 1-j1 \end{bmatrix} \quad (13)$$

III. COMPLEXITY ANALYSIS AND COMPARISON

This section evaluates the number of arithmetic operations of the proposed \mathbf{X} transform and compare them with those of FFT and FHT-FFT transforms based on fast algorithms.

A. \mathbf{X} Transform

The \mathbf{X} transform includes $\frac{N-2}{2}$ units. Each single multiplication of complex data $x + jy$ by $1 + j1$ equals to $(x - y) + j(x + y)$, that means it involves 2 real additions (R_A). Thus, the complexity of the direct implementation of the \mathbf{X} transform can be given as

$$\begin{aligned} A &= a(0.5)(1 + j1) + b(0.5)(1 - j1) \\ &= 0.5(a + b) - j0.5(b - a) \end{aligned} \quad (14)$$

$$\begin{aligned} B &= a(0.5)(1 - j1) + b(0.5)(1 + j1) \\ &= 0.5(a + b) + j0.5(b - a) \end{aligned} \quad (15)$$

By ignoring the multiplication by 0.5, each unit includes 4 complex additions (C_A) that gives 8 R_A per unit. Then the overall complexity is given as

$$R_A = 4(N - 2) \quad (16)$$

B. FFT

Considering the fact that each complex multiplication involves 4 real multiplications (R_M) and two real additions (R_A) or 3 real multiplications and 3 real additions, and each complex addition is equivalent to two real additions. The arithmetic complexity of the FFT, based on single butterfly and 4/2 implementation is given as:

$$R_M = 2N \log_2 N \quad (17)$$

TABLE I
COMPARISON BASED ON REAL ARITHMETIC OPERATIONS OF THE PROPOSED X TRANSFORM AND OTHER TRANSFORMS THAT USED IN OFDM SYSTEMS UNDER COMPLEX CONSTELLATION CONSIDERATION

N	XT			FFT			FHT-FFT		
	R_A	R_M	R_O	R_A	R_M	R_O	R_A	R_M	R_O
32	120	0	120	480	320	800	960	640	1600
64	248	0	248	1152	768	1920	2304	1536	3840
128	504	0	504	2688	1792	4480	5376	3584	8960
256	1016	0	1016	6144	4096	10240	12288	8192	20480
512	2040	0	2040	13824	9216	23040	27648	18432	46080
1024	4088	0	4088	30720	20480	51200	61440	40960	102400
2048	8184	0	8184	67584	45056	112640	135168	90112	225280
4096	16376	0	16376	147456	98304	245760	294912	196608	491520

$$R_A = 3N \log_2 N \quad (18)$$

C. FHT-FFT

The arithmetic complexity of the radix-2 fast Hartley transform (FHT) based on single butterfly implementation is given as

$$R_M = N \log_2 N \quad (19)$$

$$R_A = \frac{3}{2} N \log_2 N \quad (20)$$

and for data that are drawn from complex constellation, FHT should be calculated twice, one for the real part and the other for the imaginary part of a complex information. Consequently, the arithmetic operations of FHT-FFT will be 2 times of (19) and (20) in addition to the arithmetic operations of FFT given in (17) and (18), so the overall arithmetic operations are given as:

$$R_M = 4N \log_2 N \quad (21)$$

$$R_A = 6N \log_2 N \quad (22)$$

Table I shows the computational complexity for the X, FFT and FHT-FFT transforms for different transform sizes N , and when the information data are considered to be drawn from a complex constellation.

It is clear that the direct implementation of the X transform involves no multiplications at all and much less additions than both the FFT and FHT-FFT. Hence the X transform is faster than the FFT and FHT-FFT.

1
2
3
4
5
6
7
8
9
10
11
12
13
14
15
16
17
18
19
20
21
22
23
24
25
26
27
28
29
30
31
32
33
34
35
36
37
38
39
40
41
42
43
44
45
46
47
48
49
50
51
52
53
54
55
56
57
58
59
60

IV. THEORETICAL ANALYSIS OF BER PERFORMANCE OVER MULTIPATH CHANNEL

The system blocks diagram is shown in Fig. 1. Consider block by block transmission where the information symbols are divided into blocks, each of length N . These symbols modulate N subcarriers by the mean of inverse \mathbf{X} transform as it has been given in (9). Then a cyclic prefix (CP) of length G samples, must be no less than the maximum excess delay of the multipath channel, is then appended to the OFDM signal to prevent the inter-symbol interference (ISI). It follows that the received signal after being passed through a multipath frequency-selective fading channel of $L+1$ taps ($h_k = 0, \forall L < k < 0$) and corrupted by additive white Gaussian noise (AWGN) w is given as [23]

$$y_k = \sum_{l=0}^L h_l s_{k-l} + w_k \quad (23)$$

the received signal y_k is then processed by the FFT transform and the produced signal can be written as

$$\begin{aligned} Y_n &= \frac{1}{\sqrt{N}} \sum_{k=0}^{N-1} y_k e^{-j\frac{2\pi nk}{N}} + \Omega_n \\ &= \frac{1}{N^{3/2}} \sum_{k=0}^{N-1} \left[\sum_{l=0}^L h_l \left\{ \sum_{n=0}^{N-1} r_n e^{j\frac{2\pi n(k-l)}{N}} \right\} \right] e^{-j\frac{2\pi nk}{N}} + \Omega_n \\ &= r_n \sum_{l=0}^L h_l e^{-j\frac{2\pi nl}{N}} + \Omega_n \\ &= r_n H_n + \Omega_n \quad (n = 0, 1, 2, \dots, N-1) \end{aligned} \quad (24)$$

In (24), Ω_n is the frequency domain representation of AWGN (w_n) and $H_n = \sum_{l=0}^L h_l e^{-j\frac{2\pi nl}{N}}$, ($0 \leq n \leq N-1$) is the channel transfer function corresponding to the n_{th} subchannel. The channel equalization is performed in the frequency domain after the FFT and before the DHT transform by applying either minimum mean-square error (MMSE) or zero-forcing (ZF) equalizer as shown in Fig. 1. Unlike the conventional DFT-OFDM system where the channel equalization and data detection are performed in the same domain (frequency domain), in our proposed X-OFDM system, the channel equalization and data detection are implemented in different domains. This difference in domains of the data detection leads to an interesting properties of the proposed scheme as it will be shown later in this work. In this work we will emphasise the BER derivation of the proposed X-OFDM system for 16QAM and QPSK modulation formats and for the ZF and MMSE equalizers. However, our derivation is still valid for other modulation

1
2 formats.

3
4 The BER for QPSK and 16QAM modulation formats are given in [24] respectively as:

$$5 \quad P_e^{QPSK} = Q(\sqrt{\beta_s}) \quad (25)$$

$$6 \quad P_e^{16QAM} = \frac{3}{4}Q\left(\sqrt{\frac{\beta_s}{5}}\right) \quad (26)$$

7
8 Hence, to evaluate the BER performance, the signal energy-to-noise power ratio (β_s) at the receiver side
9 after the equalization should be evaluated. Inspired by the approach in [19], the BER performance of our
10 proposed X-OFDM system is evaluated in the next subsections for a multipath fading channels and for
11 both the QPSK and 16QAM constellations.
12

13 The channel effects on the received signal in (24) has to be removed, this can be achieved using either
14 ZF or MMSE equalizer as follows
15

16 A. Zero-Forcing Equalizer

17 The ZF equalizer can be achieved by simply dividing each individual sample of the received vector Y_n
18 in the frequency domain by the corresponding value of the channel transfer function H_n as
19

$$20 \quad \hat{r}_n = \frac{Y_n}{H_n} \quad (27)$$

$$21 \quad = r_n + \xi_n$$

22 where $\xi_n = \frac{\Omega_n}{H_n}$ represents the amplified noise part. Substituting (3) into (27) yields

$$23 \quad \hat{r}_n = \sum_{m=0}^{N-1} a_{n,m} S_m + \xi_n \quad (28)$$

24 It follows that the equalized signal \hat{r}_n is then processed by mean of the discrete Hartley transform \mathbf{A} as
25 follows
26

$$27 \quad q_i^{ZF} = \sum_{n=0}^{N-1} a_{i,n} \hat{r}_n \quad (i = 0, 1, 2, \dots, N-1) \quad (29)$$

28 This in turn leads to the following

$$29 \quad q_i^{ZF} = \sum_{n=0}^{N-1} a_{i,n} \left(\sum_{m=0}^{N-1} a_{n,m} S_m \right) + \sum_{n=0}^{N-1} a_{i,n} \xi_n \quad (i = 0, 1, 2, \dots, N-1) \quad (30)$$

Owing to the orthogonality property of the DHT, $a_{i,n} \times a_{n,m}$ equal to 1 when $m = i$ and zero elsewhere, the first term of (30) equals to S_i and (30) can be rewritten as

$$q_i^{ZF} = S_i + \hat{\xi}_i \quad (31)$$

where $\hat{\xi}_i = \sum_{n=0}^{N-1} a_{i,n} \xi_n$.

The total error signal which is the difference between the encoded symbols and the detected symbols

$e_i = q_i - S_i$ can be written as

$$\begin{aligned} e_i^{ZF} &= \hat{\xi}_i \\ &= \sum_{n=0}^{N-1} a_{i,n} \xi_n \\ &= \sum_{n=0}^{N-1} a_{i,n} \left(\frac{\Omega_n}{H_n} \right) \end{aligned} \quad (32)$$

Thus, the signal to noise ratio will be given as

$$\beta_i^{ZF} = \frac{E[|S_i|^2]}{E[|e_i|^2]} \quad (33a)$$

$$= \frac{E[S_i S_i^*]}{E[e_i^{ZF} e_i^{ZF*}]} \quad (33b)$$

$$= \frac{E_s}{\sigma_{n_i}^2} \quad (33c)$$

where E_s is the symbol power, equals to $4E_b$ for the case of 16QAM whilst it is equal to $2E_b$ for the case of QPSK and $\sigma_{n_i}^2$ is the noise power and it is given as

$$\sigma_{n_i}^2 = N_0 \sum_{n=0}^{N-1} |a_{i,n}|^2 \frac{1}{|H_n|^2} \quad (34)$$

Substituting (34) into (33c) yields

$$\beta_i^{ZF} = \frac{\gamma_s}{\sum_{n=0}^{N-1} |a_{i,n}|^2 \frac{1}{|H_n|^2}} \quad (35)$$

where $\gamma_s = \frac{E_s}{N_0}$ is the signal power (in terms of symbol) to noise ratio. By substituting (35) into (25)

and (26), the BER performances for QPSK and 16QAM modulation formats are given as:

$$P_e^{QPSK} = \frac{1}{N} \sum_{i=1}^N Q\left(\sqrt{\frac{\gamma_s}{\sum_{n=0}^{N-1} |a_{i,n}|^2 \frac{1}{|H_n|^2}}}\right) \quad (36)$$

$$P_e^{16QAM} = \frac{3}{4N} \sum_{i=1}^N Q\left(\sqrt{\frac{\gamma_s}{5 \sum_{n=0}^{N-1} |a_{i,n}|^2 \frac{1}{|H_n|^2}}}\right) \quad (37)$$

It can be seen from (35) that for the proposed X-OFDM system, the SNR of each individual subcarrier, β_i^{ZF} , depends on the average of the channel transfer function. In other words, the effects of the subchannel with a deep notch will be distributed over the other subchannels. In case of the conventional OFDM system, only the symbols that correspond to deep notches subchannels will be affected independently from the other subchannels. This could be considered as an advantage for the DFT-OFDM system over the proposed X-OFDM system when the ZF equalizer is used where greatly attenuated subchannel ($H_n \simeq 0$) will affect the whole system performance. However, the performance of our proposed system is far superior than that of the DFT-OFDM system in the case of the MMSE detection as will be explained in the next section.

B. Minimum Mean-Square-Error Equalizer

The MMSE equalizer, Δ_n , is defined as

$$\begin{aligned} \Delta_n &= \frac{E_s H_n^*}{E_s |H_n|^2 + N_0} \\ &= \frac{\gamma_s H_n^*}{1 + \gamma_s |H_n|^2} \end{aligned} \quad (38)$$

It follows that the equalized signal is given as

$$\hat{r}_n = r_n H_n \Delta_n + \Omega_n \Delta_n \quad (39)$$

substituting (3) into (39) yields

$$\hat{r}_n = \sum_{m=0}^{N-1} a_{n,m} S_m H_n \Delta_n + \Omega_n \Delta_n \quad (40)$$

This equalized signal is then processed by the DHT transform to detect the encoded symbols which are given as

$$q_i^{MMSE} = \sum_{n=0}^{N-1} a_{i,n} \left(\sum_{m=0}^{N-1} a_{n,m} S_m H_n \Delta_n \right) + \sum_{n=0}^{N-1} a_{i,n} \Omega_n \Delta_n \quad (41)$$

Similar to the case of the ZF equalizer, due to the orthogonality property of the DHT transform, the first term of (41) can be simplified to $\sum_{n=0}^{N-1} S_i H_n \Delta_n$ and Eq. (41) can be rewritten as

$$q_i^{MMSE} = \sum_{n=0}^{N-1} S_i \frac{\gamma_s |H_n|^2}{1 + \gamma_s |H_n|^2} + \sum_{n=0}^{N-1} a_{i,n} \Omega_n \Delta_n \quad (42)$$

The error signal is then calculated as the difference between the transmitted and the received data symbols,

$e_i^{MMSE} = q_i^{MMSE} - S_i$, and can be written as

$$\begin{aligned} e_i^{MMSE} &= \sum_{n=0}^{N-1} S_i H_n \Delta_n - S_i + \sum_{n=0}^{N-1} a_{i,n} \Omega_n \Delta_n \\ &= \sum_{n=0}^{N-1} [H_n \Delta_n - 1] S_i + \sum_{n=0}^{N-1} a_{i,n} \Omega_n \Delta_n \end{aligned} \quad (43)$$

In (43), $H_n \Delta_n - 1 = \frac{-1}{1 + \gamma_s |H_n|^2}$. Thus Eq. (43) can be rewritten as

$$e_i^{MMSE} = S_i \sum_{n=0}^{N-1} \frac{-1}{1 + \gamma_s |H_n|^2} + \sum_{n=0}^{N-1} a_{i,n} \Omega_n \frac{\gamma_s H_n^*}{1 + \gamma_s |H_n|^2} \quad (44)$$

Since the DHT is a unitary transform, it does not affect the calculation of the power ($\sum_{n=0}^{N-1} |a_{i,n}|^2 = 1$).

In other words, all \mathbf{S} , \mathbf{r} and \mathbf{s} have the same average power E_s and as the data symbols and the AWGN are statistically independent, the noise power of the i_{th} subchannel is then expressed as

$$\begin{aligned} \sigma_{n_i}^2{}^{MMSE} &= E[|e_i^{MMSE}|^2] \\ &= \sum_{n=0}^{N-1} |a_{i,n}|^2 \frac{E_s}{[1 + \gamma_s |H_n|^2]^2} + \sum_{n=0}^{N-1} |a_{i,n}|^2 \frac{N_0 \gamma_s^2 |H_n|^2}{[1 + \gamma_s |H_n|^2]^2} \\ &= \sum_{n=0}^{N-1} |a_{i,n}|^2 \frac{E_s}{[1 + \gamma_s |H_n|^2]^2} + \sum_{n=0}^{N-1} |a_{i,n}|^2 \frac{E_s \gamma_s |H_n|^2}{[1 + \gamma_s |H_n|^2]^2} \\ &= \sum_{n=0}^{N-1} |a_{i,n}|^2 \frac{E_s}{1 + \gamma_s |H_n|^2} \end{aligned} \quad (45)$$

The signal power $\sigma_{s_i}^2{}^{MMSE} = E[|q_i^{MMSE}|^2]$ and it is given as

$$\begin{aligned} \sigma_{s_i}^2{}^{MMSE} &= \sum_{n=0}^{N-1} |a_{i,n}|^2 \frac{E_s \gamma_s^2 |H_n|^4}{[1 + \gamma_s |H_n|^2]^2} + \sum_{n=0}^{N-1} |a_{i,n}|^2 \frac{E_s \gamma_s |H_n|^2}{[1 + \gamma_s |H_n|^2]^2} \\ &= \sum_{n=0}^{N-1} |a_{i,n}|^2 \frac{E_s \gamma_s |H_n|^2}{1 + \gamma_s |H_n|^2} \end{aligned} \quad (46)$$

Then the SNR of the i_{th} subchannel $\beta_i^{MMSE} = \frac{\sigma_{s_i}^2{}^{MMSE}}{\sigma_{n_i}^2{}^{MMSE}}$ is then given as

$$\beta_i^{MMSE} = \frac{\sum_{n=0}^{N-1} |a_{i,n}|^2 \frac{\gamma_s |H_n|^2}{1 + \gamma_s |H_n|^2}}{\sum_{n=0}^{N-1} |a_{i,n}|^2 \frac{1}{1 + \gamma_s |H_n|^2}} \quad (47)$$

It is obvious from (47) that β_i^{MMSE} for the i_{th} subcarrier is averaged by the mean of the DHT transform.

This significantly improves the BER performance of the proposed scheme, especially when the channel

1
2
3
4
5
6
7
8
9
10
11
12
13
14
15
16
17
18
19
20
21
22
23
24
25
26
27
28
29
30
31
32
33
34
35
36
37
38
39
40
41
42
43
44
45
46
47
48
49
50
51
52
53
54
55
56
57
58
59
60

has narrowband deep notches in its spectral.

The BER performance of the X-OFDM system for QPSK and 16QAM is then given as:

$$P_e^{QPSK} = \frac{1}{N} \sum_{i=0}^{N-1} Q\left(\sqrt{\frac{\sum_{n=0}^{N-1} |a_{i,n}|^2 \frac{\gamma_s |H_n|^2}{1+\gamma_s |H_k|^2}}{\sum_{n=0}^{N-1} |a_{i,n}|^2 \frac{1}{1+\gamma_s |H_n|^2}}}\right) \quad (48)$$

$$P_e^{16QAM} = \frac{3}{4N} \sum_{i=0}^{N-1} Q\left(\sqrt{\frac{\sum_{n=0}^{N-1} |a_{i,n}|^2 \frac{\gamma_s |H_n|^2}{1+\gamma_s |H_k|^2}}{5 \sum_{n=0}^{N-1} |a_{i,n}|^2 \frac{1}{1+\gamma_s |H_n|^2}}}\right) \quad (49)$$

V. SYSTEM PERFORMANCE IN THE PRESENCE OF HPA

In MC communication systems, the HPA is the major source of nonlinear distortion that arises when the dynamic range of the input signal is larger than the saturation level of the HPA. Therefore, for any communication system to stand as a good candidate for practical applications, its performance in the presence of the HPA needs to be evaluated. Consequently, in this section, we consider the case that the transmitter is the one that encompasses solid state power amplifier (SSPA) in its structure and investigate the BER performance of the proposed X-OFDM system and compare it with the BER performance of the conventional DFT-OFDM system. The complex envelope of the amplifier input signal $s(t) = \rho(t)e^{j\theta(t)}$, where $\rho(t)$ and $\theta(t)$ represent the amplitude and the phase of the signal respectively and the output signal is given as

$$u_k = s_k G_a[|s_k|] \quad (50)$$

where $G_a[|s_k|]$ is the amplifier gain and it is given as [25]

$$G_a[|s_k|] = \frac{A_m[|s_k|] e^{j\phi[|s_k|]}}{|s_k|} \quad (51)$$

where $\phi[|s_k|]$ represents the amplitude modulation/phase modulation AM/PM conversion of the non-linear power amplifier and $A_m[|s_k|]$ represents the amplitude modulation/amplitude modulation AM/AM conversion of the non-linear power amplifier is given as

$$A_m[|s_k|] = \frac{|s_k|}{\left[1 + \left(\frac{|s_k|}{A_s}\right)^{2p}\right]^{\frac{1}{2p}}} \quad (52)$$

In (52), p is a parameter which controls the transition smoothness from the linear region to the saturation region. Input back-off (IBO) is the operating point of the HPA and it can be defined as

$$IBO = 10 \log_{10} \frac{P_{in,max}}{P_{in,av}} \quad (53)$$

where $P_{in,max}$ and $P_{in,av}$ denote the maximum (saturation) and the average powers of the signal at the input of the amplifier respectively and $A_s = \sqrt{P_{av} IBO}$ is the amplifier input saturation voltage.

According to the above, IBO is the key factor that defines the dynamic range of HPA. Amplitude clippings are produced within the OFDM system when the OFDM signal with a peak larger than the maximum input of the HPA, this, in turn, leads to intermodulation interference (IMI) and BER performance degradation. However, this is not the case in our proposed scheme due to the use of Hartley transform together with the IFFT to produce the \mathbf{X} transform that significantly reduces the peak power of the X-OFDM signal.

From (5), s_k can be rewritten as [26]

$$s_k = \frac{1}{\sqrt{N}} \sum_{\substack{n=0 \\ n \neq z}}^{N-1} r_n e^{j \frac{2\pi nk}{N}} + \frac{1}{\sqrt{N}} r_z e^{j \frac{2\pi kz}{N}} \quad (54)$$

Substituting (54) into (50) yields

$$\begin{aligned} u_k &= \left(g_k + \frac{1}{\sqrt{N}} r_z e^{j \frac{2\pi kz}{N}} \right) G_a \left[\left| g_k + \frac{1}{\sqrt{N}} r_z e^{j \frac{2\pi kz}{N}} \right| \right] \\ &= g_k G_a \left[\left| g_k + \frac{1}{\sqrt{N}} r_z e^{j \frac{2\pi kz}{N}} \right| \right] + \frac{1}{\sqrt{N}} r_z e^{j \frac{2\pi kz}{N}} G_a \left[\left| g_k + \frac{1}{\sqrt{N}} r_z e^{j \frac{2\pi kz}{N}} \right| \right] \end{aligned} \quad (55)$$

where $g_k = \frac{1}{\sqrt{N}} \sum_{\substack{n=0 \\ n \neq z}}^{N-1} r_n e^{j \frac{2\pi kn}{N}}$. It is clear that u_k in (55) consists of two terms, the first term is an amplified version of the $N - 1$ statistically independent symbols that have been added by the IFFT at the transmitter while the second term is the signal to be detected after FFT at the receiver. In the case of DFT-OFDM, the first term is much bigger than the second term which leads to significant distortion while is much lower in the case of X-OFDM as it is single symbol rather than $N - 1$ in DFT-OFDM counterpart.

VI. CFO EFFECTS ON BER PERFORMANCE OVER MULTIPATH CHANNEL

Carrier frequency offset CFO that is caused by frequency mismatch of local oscillators has significant effects on the BER performance of OFDM systems as it produces inter-carrier interference (ICI) that

1
2 destroys the orthogonality of the subcarriers. As a result, it is so important to investigate the validity of
3
4 the proposed system in the presence of CFO. The received signal at the receiver side in the presence of
5
6 the CFO could be expressed by matrix form as

$$7 \quad \mathbf{y} = \Psi \mathbf{H} \mathbf{s} + \mathbf{w}$$

$$8 \quad = \Psi \mathbf{H} \mathbf{X}^H \mathbf{S} + \mathbf{w} \quad (56)$$

9
10 In (56), Ψ is a diagonal matrix, the elements of the diagonal are given as $e^{j2\pi\epsilon(0:N-1)/N}$, ϵ is the CFO
11
12 normalized to the subcarrier spacing, and \mathbf{H} is the channel matrix given as

$$13 \quad \mathbf{H} = \begin{bmatrix} 14 \quad h_0 & 0 & 0 & 0 & \dots & 0 & 0 \\ 15 \quad h_1 & h_0 & 0 & 0 & \dots & 0 & 0 \\ 16 \quad \cdot & h_1 & h_0 & 0 & \dots & 0 & 0 \\ 17 \quad \cdot & \cdot & h_1 & \cdot & \dots & \cdot & 0 \\ 18 \quad h_L & \cdot & \cdot & \cdot & \dots & \cdot & \cdot \\ 19 \quad 0 & h_L & \cdot & \cdot & \dots & \cdot & \cdot \\ 20 \quad 0 & 0 & \cdot & \cdot & \dots & \cdot & \cdot \\ 21 \quad 0 & 0 & 0 & h_L & \dots & h_1 & h_0 \end{bmatrix} \quad (57)$$

22
23 Because of the CP, the channel matrix \mathbf{H} becomes a circulant matrix and it is diagonalized by pre and
24
25 post multiplications by \mathbf{F}^H and \mathbf{F} . Only for clarity, the transform \mathbf{X}^H in (56) is expressed by its origins,
26
27 it follows that the received signal after DFT transform can be written as

$$28 \quad \mathbf{Y} = \mathbf{F} \Psi \mathbf{H} \mathbf{F}^H \mathbf{A} \mathbf{S} + \mathbf{F} \mathbf{w}$$

$$29 \quad = \mathbf{F} \Psi \mathbf{F}^H \mathbf{F} \mathbf{H} \mathbf{F}^H \mathbf{A} \mathbf{S} + \Omega$$

$$30 \quad = \mathbf{F} \Psi \mathbf{F}^H \Theta \mathbf{A} \mathbf{S} + \Omega \quad (58)$$

31
32 where Θ is a diagonal matrix, its diagonal elements are the frequency domain representation of the channel
33
34 impulse response, $H_n = \sum_{l=0}^{L-1} h_l e^{-j\frac{2\pi nl}{N}}$ and $n = 0, 1, 2, \dots, N-1$. It is obvious that, without CFO, the
35
36 single-tap equalizer is applicable as it has been shown earlier in this work. However, the presence of
37
38 CFO produces ICI which leads to significant degradation in system performance. Moreover, the ICI is
39
40 worse after being processed by the DHT transform, as the latter distributes this noise among the other
41
42 subcarriers. Therefore, when no synchronization algorithm is used, our proposed X-OFDM system shows
43
44 more sensitivity to the CFO than the DFT-OFDM system as any shift in the frequency of any subcarrier
45
46
47
48
49
50
51
52
53
54
55
56
57
58
59
60

1
2 will be spread over the others because of the DHT transform. However, the X-OFDM system restores its
3
4 superiority over the DFT-OFDM system when CFO estimation algorithms are used. In this work, Morelli
5
6 and Mengali (M&M) algorithm [22] is used. However, unlike the DFT-OFDM system where the IFFT
7
8 is used to generate a symbol consisting of L identical parts that are used for the CFO estimation. They
9
10 are generated by transmitting a pseudo-noise sequence on the frequencies multiple of L/T and setting
11
12 zero on the rest. In our proposed system, L identical sequences, each N/L in length have to be passed
13
14 through the DHT transform to produce the required pseudo-noise sequence in the frequencies multiple of
15
16 L/T and setting zero on the rest which in turn pass through the IFFT. In other words, these L identical
17
18 sequences pass through the \mathbf{X} transform in order to be used for the CFO estimation.
19
20
21
22

23 VII. PAPR REDUCTION

24
25 Non-linear devices within the OFDM systems such as the high-power amplifier (HPA) and the digital-to-
26
27 analog (D/A) converter are sensitive to the PAPR of the transmitted signal. Thus, the PAPR is considered to
28
29 be one of the major OFDM drawbacks and it has undergone intense attention in the last decades. Suppose
30
31 that the input data streams $S_m(0 \leq m \leq N - 1)$ are statistically independent and identically distributed
32
33 (i.i.d), i.e. the real part S_m^I and the imaginary part S_m^Q are uncorrelated and orthogonal. Therefore, based
34
35 on the central limit theorem, when N is considerably large, the distribution of both S_m^I and S_m^Q approach
36
37 Gaussian distribution with zero mean [27]. The basic cause of high PAPR in the OFDM signal is the
38
39 Gaussian signal distribution which arises due to the IFFT operation.
40
41
42
43

44 In particular, every single DFT-OFDM sample involves the sum of N different statistically independent
45
46 encoded data symbols that drawn from specific constellation (QPSK or 16 QAM in this work). Therefore,
47
48 the maximum PAPR occurs when all the symbols have the same phase and maximum PAPR will equal to
49
50 N in this case. Compared to the conventional OFDM, the utilization of the \mathbf{X} transform reduces the PAPR
51
52 by more than 6 dB. Furthermore, the PAPR of our proposed X-OFDM system is still the same and does
53
54 not depend on N while, for the case of conventional DFT-OFDM system, the PAPR of the transmitted
55
56 signal increases as the number of subcarrier N is increased. This is because the number of additions of
57
58 input information symbols that perform each output X-OFDM sample are reduced from N to 2.
59
60

1
2
3
4
5
6
7
8
9
10
11
12
13
14
15
16
17
18
19
20
21
22
23
24
25
26
27
28
29
30
31
32
33
34
35
36
37
38
39
40
41
42
43
44
45
46
47
48
49
50
51
52
53
54
55
56
57
58
59
60

VIII. SIMULATION RESULTS AND DISCUSSIONS

A. PAPR of the Proposed System

Simulation was carried out for the X-OFDM and DFT-OFDM systems for a number of subcarriers $N = 128$ and 16 QAM modulation formats. In order to have an awareness and intuitive view of the PAPR statistics, complementary cumulative density function (CCDF) was plotted. Also to ensure the reliability of computer simulations, 100 000 OFDM frames were generated to obtain each PAPR value. It is observed from Fig. 2 that the X-OFDM system has a lower PAPR than the DFT-OFDM system, where it has achieved about 6 dB improvement in the PAPR reduction at a CCDF value of 10^{-4} over the DFT-OFDM system. This is due to the fact that the \mathbf{X} transform reduces the superposition of the input encoded information symbols which form each OFDM sample.

B. BER Performance

1) *Over a Multipath environment:* The BER performance of the proposed X-OFDM system is evaluated in this section mathematically and by simulation and compared with that of the DFT-OFDM system. The simulation is carried out according to the WiMAX standard where we used the following parameters. The transmission bandwidth is 10MHz , the carrier frequency is 4GHz and the number of subcarriers $N = 1024$: The transmitted OFDM symbol duration is $128\mu\text{s}$ including a CP of duration $25.6\mu\text{s}$ to prevent ISI. ITU channel pedestrian class B with a maximum spread delay equal to $3.7\mu\text{s}$ and vehicular class A with a maximum spread delay $2.51\mu\text{s}$ are used. Figs 3 and 4 show the BER performance of the proposed X-OFDM and conventional DFT-OFDM systems over pedestrian and vehicular channel models respectively for both 16 QAM and QPSK modulation formats. It is noticeable that the simulated BER results agree with the theoretical BER results. It is evident that the proposed X-OFDM system is superior to the conventional DFT-OFDM by about 15 dB E_b/N_0 . This, in turn, verifies our early argument that the DHT transform distributes the effect of the channel dips over all other subcarriers which leads to the BER improvement. This is, however, not attainable in the conventional DFT-OFDM system counterpart as the information symbols on significantly attenuated subcarriers can not be recovered from the unaffected spectrum. It is also noteworthy that for the case of conventional DFT-OFDM system, the BER performance

1
2 for the QPSK constellation is better than 16QAM by about 3dB E_b/N_0 , whilst it is about 6 dB E_b/N_0
3
4 better than that of 16 QAM modulation for the case of our proposed X-OFDM system. This indicates
5
6 that the proposed scheme can achieve further improvement as the constellation order is reduced.
7

8
9 It is also noted from Figs. 5-6 that, for the case of the ZF equalizer, the conventional DFT-OFDM
10
11 outperforms our proposed X-OFDM system by about 3dB in terms of the BER performance for each
12
13 QPSK and 16QAM constellation.
14

15
16 To the end of this discussion, theoretical results corroborated by computer simulation in Figs. 3-6 show that
17
18 for the case of the ZF detection, the conventional DFT-OFDM system outperforms our proposed system
19
20 in term of the BER performance. However, for the MMSE detection and at 10^{-4} BER, the proposed
21
22 X-OFDM scheme can achieve around 15 dB E_b/N_0 gain over the conventional DFT-OFDM system for
23
24 different channel models and modulation formats.
25

26
27 2) *In the Presence of HPA:* In our simulation, SSPA high power amplifier is utilized at the transmitter
28
29 side after adding the cyclic prefix. Figs. 7 and 10 show the BER performance of the proposed X-OFDM
30
31 and the conventional MC DFT-OFDM systems under a diverse of ITU channel models (pedestrian A and
32
33 vehicular B), IBO (5dB and 3 dB) and modulation formats (QPSK and 16 QAM). As the advantages
34
35 of the X-OFDM system over the DFT-OFDM systems are the relatively huge reductions in PAPR and
36
37 diversity exploitation, as shown in Figs. 7 and 8, for the case of IBO= 5dB and the conditions of both
38
39 channel models and modulation formats, show the proposed system is much less sensitive to the non-
40
41 linear distortion of the HPA which is affecting the conventional DFT-OFDM system. Owing to our early
42
43 assertion that the IBO is the main factor determining the hostility of the HPA, the sensitivity of both the
44
45 X-OFDM and DFT-OFDM systems are increased as the IBO is reduced to 3dB as shown in Figs. 9 and
46
47 10. However, our proposed system still show much better performance and low sensitivity to non-linear
48
49 distortion in comparison with the conventional DFT-OFDM counterpart.
50
51
52

53
54 3) *In the Presence of CFO:* In this section, the BER performances of the proposed X-OFDM system
55
56 in the presence of CFO is investigated and compared with that of the DFT-OFDM system. The sensitivity
57
58 to the CFO is demonstrated when no synchronization algorithm is used and when $M\&M$ [22] algorithm
59
60

1
2 for CFO estimation is utilized. Fig. 11 shows the BER performance of the proposed X-OFDM, and
3 the DFT-OFDM systems when no CFO estimation algorithm is applied and for different values of the
4 normalized CFO (ϵ) ($\epsilon = 0.02, 0.05, 0.07$ and 0.1). It is evident that the proposed system is superior to
5 the others for small ϵ around 0.03 while it has a worse BER for ϵ around 0.05 , this can be considered as
6 an advantage for DFT-OFDM system over the X-OFDM system. However, it is also evident that all of
7 the aforementioned systems will completely lose their orthogonality when ϵ is above 0.1 . Fig. 12 shows
8 the BER performance when the *M&M* [22] algorithm for CFO estimation is employed in this simulation.
9 Where the number of subcarriers are $N = 1024$, iterative data $L_i = 8$, $\epsilon = 3.42$ and (E_b/N_0) is set to
10 be 25 dB in order to get a precise estimation. It is clearly shown that the proposed X-OFDM system
11 outperforms the conventional DFT-OFDM system by approximately 14 dB (E_b/N_0) at 10^{-4} BER when
12 a 16 QAM constellation is used.
13
14
15
16
17
18
19
20
21
22
23
24
25
26

27 IX. CONCLUSION

28
29 In this paper, a new very low complexity **X** transform that combines the effects of the DHT and DFT
30 transforms has been presented. The transform analysis and complexity calculations were also demonstrated
31 in this work and compared with those of the FFT and the DHT-FFT transforms illustrating that the proposed
32 **X** transform has the lowest complexity. Transform application in OFDM system to produce new X-OFDM
33 system with cyclic prefix has been investigated and compared with that of the multi-carrier DFT-OFDM
34 system. BER performance over ITU pedestrian and vehicular channel models were evaluated theoretically
35 and by simulation for the QPSK and 16 QAM modulation formats showing that the proposed X-OFDM
36 is superior to the DFT-OFDM system by about 15 dB E_b/N_0 at 10^{-4} BER. Furthermore, the proposed
37 scheme was found to achieve an inherent reduction of about 6 dB in the PAPR in comparison with the
38 conventional DFT-OFDM system, as it reduces the number of symbols superposition to produce each
39 X-OFDM output sample. The BER performance investigation has also been carried out in the presence of
40 HPA and the proposed system has been proved to be superior to the DFT-OFDM system for a diversity of
41 IBO, channel models and modulation formats. Finally, the sensitivity of the proposed X-OFDM system to
42 the CFO was investigated revealing that the proposed scheme can retain its superiority when a frequency
43
44
45
46
47
48
49
50
51
52
53
54
55
56
57
58
59
60

synchronization algorithm is utilized. The applications of the proposed scheme can be extended to multiple access technique (OFDMA), multiple input-multiple output (MIMO) and for wire-line communication such as discrete multi-tone (DMT) modulation.

REFERENCES

- [1] W. Zhendao and G. B. Giannakis, "Wireless multicarrier communications," *Signal Processing Magazine, IEEE*, vol. 17, pp. 29-48, 2000.
- [2] X. Xiang-Gen, "Precoded OFDM systems robust to spectral null channels and vector OFDM systems with reduced cyclic prefix length," in *Communications, 2000. ICC 2000. 2000 IEEE International Conference on*, 2000, pp. 1110-1114 vol.2.
- [3] Y. Hen-Geul and C. C. Wang, "New parallel algorithm for mitigating the frequency offset of OFDM systems," in *Vehicular Technology Conference, 2004. VTC2004-Fall. 2004 IEEE 60th*, 2004, pp. 2087-2091 Vol. 3.
- [4] X. Hai and Y. Shiyuan, "A loosely synchronous-coded OFDM system for power-line communications in home networks," *Power Delivery, IEEE Transactions on*, vol. 21, pp. 1912-1918, 2006.
- [5] A. M. Tonello, S. D'Alessandro, and L. Lampe, "Cyclic Prefix Design and Allocation in Bit-Loaded OFDM over Power Line Communication Channels," *Communications, IEEE Transactions on*, vol. 58, pp. 3265-3276, 2010.
- [6] A. Czyliw, "Comparison between adaptive OFDM and single carrier modulation with frequency domain equalization," in *Vehicular Technology Conference, 1997. IEEE 47th*, 1997, pp. 865-869 vol.2.
- [7] H. Sari, et al., "An analysis of orthogonal frequency-division multiplexing for mobile radio applications," in *Vehicular Technology Conference, 1994 IEEE 44th*, 1994, pp. 1635-1639 vol.3.
- [8] A. Alavi, C. Tellambura, and I. Fair, "PAPR reduction of OFDM signals using partial transmit sequence: an optimal approach using sphere decoding," *Communications Letters, IEEE*, vol. 9, pp. 982-984, 2005.
- [9] Y. Jie, C. Lei, and M. Wei, "A Modified Selected Mapping Technique to Reduce the Peak-to-Average Power Ratio of OFDM Signal," in *Consumer Electronics, 2007. ICCE 2007. Digest of Technical Papers. International Conference on*, 2007, pp. 1-2.
- [10] J. Chin-Kuo, L. Syu-Siang, and S. Muh-Tian, "On the DHT-based multicarrier transceiver over multipath fading channel," in *Personal, Indoor and Mobile Radio Communications, 2009 IEEE 20th International Symposium on*, 2009, pp. 1662-1666.
- [11] W. Dejiang, L. Danpu, L. Fang, and Y. Guangxin, "A novel DHT-based ultra-wideband system," in *Communications and Information Technology, 2005. ISIT 2005. IEEE International Symposium on*, 2005, pp. 672-675.
- [12] R. Merched, "On OFDM and single-carrier frequency-domain systems based on trigonometric transforms," *Signal Processing Letters, IEEE*, vol. 13, pp. 473-476, 2006.
- [13] P. S. Chen, C. K. Jao, and M. T. Shiu, "A low complexity real-valued kernel DHT-based OFDM modulator/demodulator design," in *Proceedings - IEEE International Symposium on Circuits and Systems, Taipei, 2009*, pp. 1529-1532.
- [14] J. Chin-Kuo, L. Syu-Siang, and S. Muh-Tian, "DHT-Based OFDM System for Passband Transmission Over Frequency-Selective Channel," *Signal Processing Letters, IEEE*, vol. 17, pp. 699-702, 2010.
- [15] G. D. Mandyam, "Sinusoidal transforms in OFDM systems," *Broadcasting, IEEE Transactions on*, vol. 50, No.2, pp. 172-184, 2004.
- [16] N. Al-Dhahir, M. Hlaing, and S. Satish, "Optimum DCT-based multicarrier transceivers for frequency-selective channels," *Communications, IEEE Transactions on*, vol. 54, pp. 911-921, 2006.
- [17] N. C. B. a. P. Tan, "Systems and methods for OFDM Transmission and Reception," U.S. Patent 0095267 A1 2008.
- [18] T. Peng and N. C. Beaulieu, "A Comparison of DCT-Based OFDM and DFT-Based OFDM in Frequency Offset and Fading Channels," *Communications, IEEE Transactions on*, vol. 54, pp. 2113-2125, 2006.
- [19] L. Yuan-Pei and P. See-May, "BER minimized OFDM systems with channel independent precoders," *Signal Processing, IEEE Transactions on*, vol. 51, pp. 2369-2380, 2003.
- [20] Z. Dlugaszewski and K. Wesolowski, "WHT/OFDM - an improved OFDM transmission method for selective fading channels," in *Communications and Vehicular Technology, 2000. SCVT-200.Symposium on*, 2000, pp. 144-149.
- [21] A. Zolghadrasli and M. H. Ghamat, "PAPR reduction in OFDM system by using hadamard transform in BSLM techniques," in *Signal Processing and Its Applications, 2007. ISSPA 2007. 9th International Symposium on*, 2007, pp. 1-4.
- [22] M. Morelli and U. Mengali, "An improved frequency offset estimator for OFDM applications," in *Communication Theory Mini-Conference, 1999, 1999*, pp. 106-109.
- [23] D. Yanwu, et al., "Minimum BER block precoders for zero-forcing equalization," *Signal Processing, IEEE Transactions on*, vol. 51, pp. 2410-2423, 2003.
- [24] J. G. Proakis and M. Salehi, "Digital Communications", McGraw-Hill Companies, Inc, 1221 Avenue of the Americas, New York, 2008.
- [25] R. Corvaja, E. Costa, and S. Pupolin, "Analysis of M-QAM-OFDM Transmission System Performance in the Presence of Phase Noise and Nonlinear Amplifiers," in *Microwave Conference, 1998. 28th European*, 1998, pp. 481-486.
- [26] E. Costa and S. Pupolin, "M-QAM-OFDM system performance in the presence of a nonlinear amplifier and phase noise," *Communications, IEEE Transactions on*, vol. 50, pp. 462-472, 2002.
- [27] J. Tao and W. Yiyan, "An Overview: Peak-to-Average Power Ratio Reduction Techniques for OFDM Signals," *Broadcasting, IEEE Transactions on*, vol. 54, pp. 257-268, 2008.

1
2
3
4
5
6
7
8
9
10
11
12
13
14
15
16
17
18
19
20
21
22
23
24
25
26
27
28
29
30
31
32
33
34
35
36
37
38
39
40
41
42
43
44
45
46
47
48
49
50
51
52
53
54
55
56
57
58
59
60

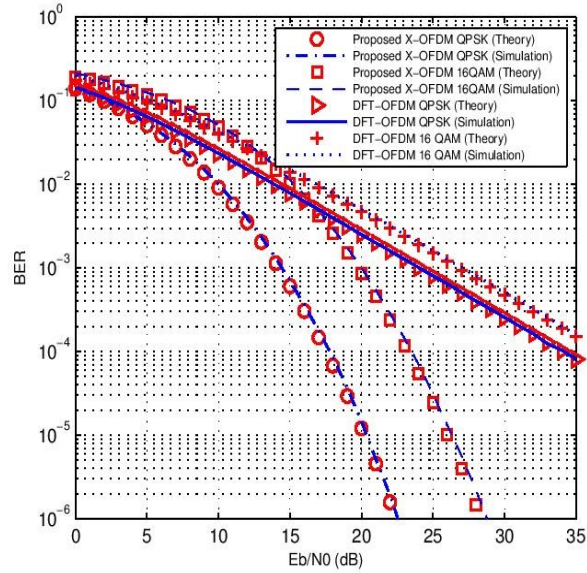


Fig. 3. BER performance of the proposed X-OFDM and the DFT-OFDM systems for QPSK and 16 QAM modulation formats over ITU Pedestrian B channel and MMSE detection.

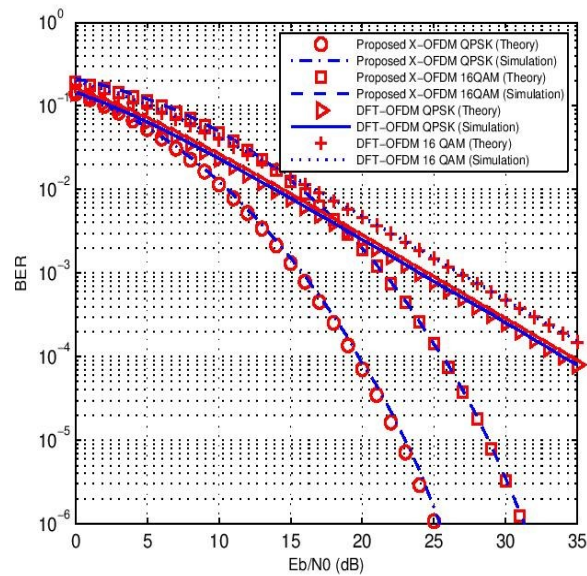


Fig. 4. BER performance of the proposed X-OFDM and the DFT-OFDM systems for QPSK and 16 QAM modulation formats over ITU Vehicular A channel and MMSE detection.

1
2
3
4
5
6
7
8
9
10
11
12
13
14
15
16
17
18
19
20
21
22
23
24
25
26
27
28
29
30
31
32
33
34
35
36
37
38
39
40
41
42
43
44
45
46
47
48
49
50
51
52
53
54
55
56
57
58
59
60

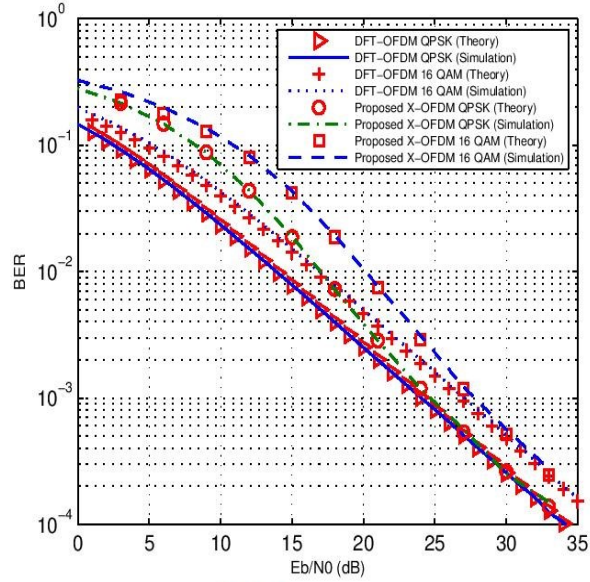


Fig. 5. BER performance of the proposed X-OFDM and the DFT-OFDM systems for QPSK and 16 QAM modulation formats over ITU Pedestrian B channel and ZF detection.

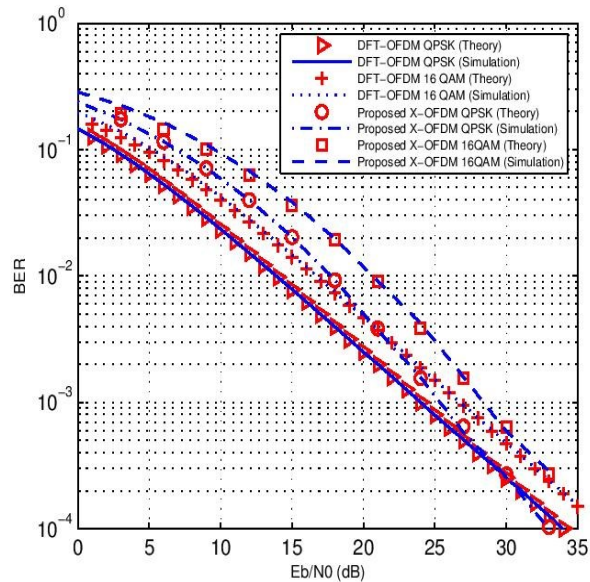


Fig. 6. BER performance of the proposed X-OFDM and the DFT-OFDM systems for QPSK and 16 QAM modulation formats over ITU Vehicular A channel and ZF detection.

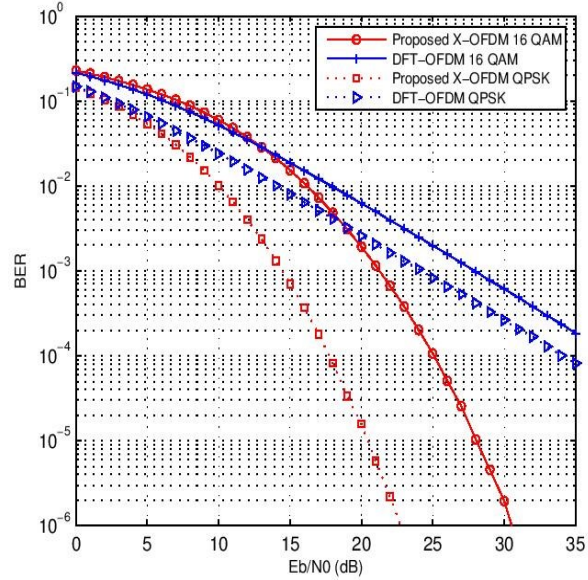


Fig. 7. BER performance of the proposed X-OFDM and the DFT-OFDM systems of QPSK and 16 QAM modulation formats with HPA (IBO=5dB) over ITU Pedestrian B channel.

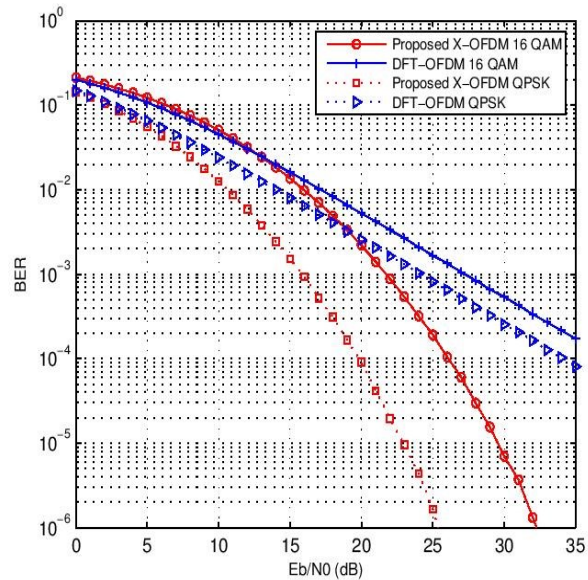


Fig. 8. BER performance of the proposed X-OFDM and the DFT-OFDM systems of QPSK and 16 QAM modulation formats with HPA (IBO=5dB) over ITU Vehicular A channel.

1
2
3
4
5
6
7
8
9
10
11
12
13
14
15
16
17
18
19
20
21
22
23
24
25
26
27
28
29
30
31
32
33
34
35
36
37
38
39
40
41
42
43
44
45
46
47
48
49
50
51
52
53
54
55
56
57
58
59
60

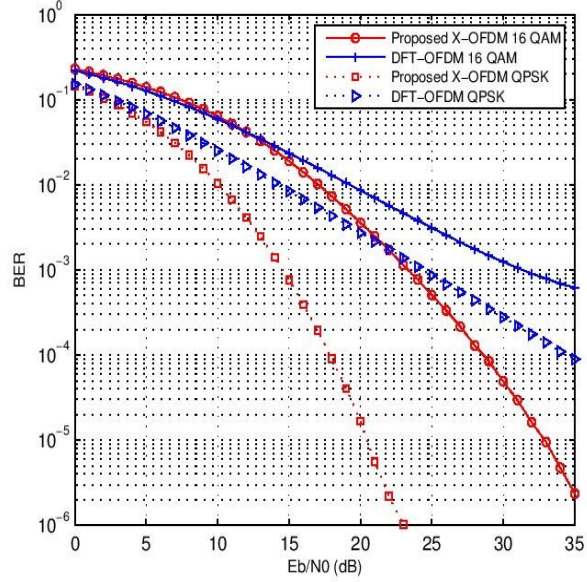


Fig. 9. BER performance of the proposed X-OFDM and the DFT-OFDM systems of QPSK and 16 QAM modulation formats with HPA (IBO=3dB) over ITU Pedestrian B channel.

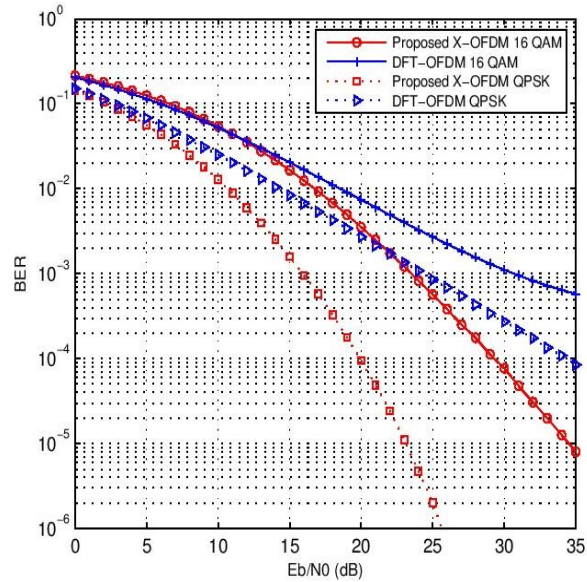


Fig. 10. BER performance of the proposed X-OFDM and the DFT-OFDM systems of QPSK and 16 QAM modulation formats with HPA (IBO=3dB) over ITU Vehicular A channel.

1
2
3
4
5
6
7
8
9
10
11
12
13
14
15
16
17
18
19
20
21
22
23
24
25
26
27
28
29
30
31
32
33
34
35
36
37
38
39
40
41
42
43
44
45
46
47
48
49
50
51
52
53
54
55
56
57
58
59
60

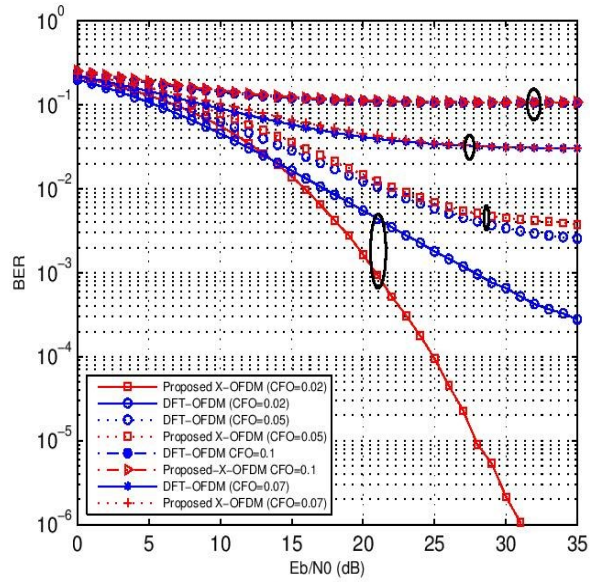


Fig. 11. BER performance for the proposed X-OFDM and the DFT-OFDM system over ITU pedestrian class B channel and CFO=0.02, 0.05, 0.07 and 0.1 and 16 QAM modulation format

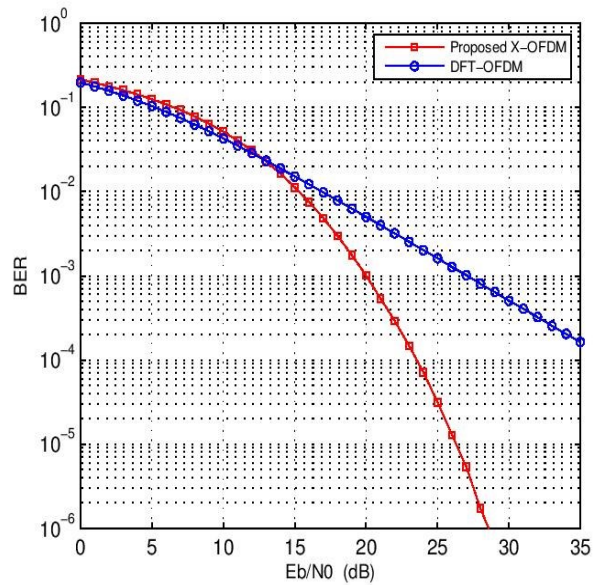


Fig. 12. BER performance for the proposed X-OFDM and the DFT-OFDM system over ITU pedestrian class B channel and CFO=3.42 when 16 QAM modulation format and $M\&M$ synchronization algorithm are employed

References

- [1] R. Chang, “Orthogonal frequency multiplex data transmission system,” *USA U.S. Patent 3,488,445*, 1966.
- [2] J. Bingham, “Multicarrier modulation for data transmission: An idea whose time has come,” *IEEE Commun. Mag.*, vol. 28, pp. 5–14, 1990.
- [3] S. Weinstein and P. Ebert, “Data transmission by frequency-division multiplexing using the discrete fourier transform,” *IEEE Trans on communication Technology*, vol. 19, pp. 628–634, Oct. 1971.
- [4] A. Peled and A. Ruiz, “Frequency domain data transmission using reduced computational complexity algorithms,” in *In Proc. IEEE Int. Conf. Acoust., Speech, Signal processing*, 1980, pp. 964–967.
- [5] L. Cimini and Jr., “Analysis and simulation of a digital mobile channel using orthogonal frequency division multiplexing,” *IEEE Trans. Commun.*, vol. 33, pp. 665–675, July 1985.
- [6] Alard, Michel, Lassalle, and Roselyne, “Principles of modulation and channel coding for digital broadcasting for mobile receivers,” *EBU Technical Review*, no. 224, pp. 168–190, 1987.
- [7] H. Z. H, G. Wang, and L. Mingying, “Analysis and implementation of digital automatic gain control for DAB baseband decoder,” *IEEE Trans. Consum. Electron.*, vol. 57, pp. 327–334, May 2011.
- [8] M. Kornfeld and G. May, “DVB-H and ip datacastbroadcast to handheld devices,” *IEEE Trans. Broadcast.*, vol. 53, pp. 161–170, Mar. 2007.
- [9] J. Chow, J. Tu, and J. Cioffi, “A discrete multitone transceiver system for hdsl applications,” *IEEE J. Sel. Areas Commun.*, vol. 9, pp. 895–908, 1991.

-
- [10] I. Telatar and R. Gallager, "Combining queueing theory with information theory for multiaccess," *IEEE J. Sel. Areas Commun.*, vol. 13, pp. 963–969, Aug. 1995.
- [11] H. Rongqing, "XPM and FWM in OFDM optical systems," in *IEEE 14th Annual Meeting of Lasers and Electro-Optics Society (LEOS)*, 2001.
- [12] O. Gonzalez, R. Perez-Jimenez, S. Rodriguez, J. Rabadan, and A. Ayala, "Adaptive OFDM system for communications over the indoor wireless optical channel," *IEE Proc. on Optoelectron*, vol. 153, p. 139144, Aug. 2006.
- [13] O. Gonzalez, R. Perez-Jimenez, S. Rodriguez, J. Rabadan, and A. Ayala, "OFDM over indoor wireless optical channel," *IEE Proc. on Optoelectronics*, vol. 152, pp. 199–204, Aug. 2005.
- [14] B. Schmidt, A. Lowery, and J. Armstrong, "Experimental demonstrations of electronic dispersion compensation for long-haul transmission using direct-detection optical OFDM," vol. 26, pp. 196–203, Jan. 2008.
- [15] S. Jansen, I. Morita, T. Schenk, N. Takeda, and H. Tanaka, "Coherent optical 25.8-gb/s OFDM transmission over 4160-km ssmf," vol. 26, pp. 6–15, 2008.
- [16] A. Lowery and J. Armstrong, "10 gbit/s multimode fiber link using power-efficient orthogonal-frequency-division multiplexing," *Optics Expr.*, vol. 13, pp. 1–7, 2005.
- [17] S. Lee, F. Breyer, S. Randel, M. Schuster, J. Zeng, F. Huiskens, H. van den Boom, A. Koonen, and N. Hanik, "24-gb/s transmission over 730 m of multimode fiber by direct modulation of 850-nm vcsel using discrete multi-tone modulation," *presented at the Proc. OFC/NFOEC, Anaheim, CA*, p. Paper PDP6, Mar. 2529, 2007.
- [18] S. Lee, F. Breyer, S. Randel, O. Ziemann, H. van den Boom, and A. Koonen, "Low-cost and robust 1-gbit/s plastic optical fiber link based on light-emitting diode technology," in *Optical Fiber communication/National Fiber Optic Engineers Conference, 2008. OFC/NFOEC 2008. Conference on*, Feb. 2008, pp. 1–3.

-
- [19] C. Esli, B. Ozgul, and H. Delic, "Space-frequency coded HIPERLAN/2," *IEEE Trans. Consum. Electron.*, vol. 50, pp. 1162–1168, Nov. 2004.
- [20] J. G. Andrews, A. Ghosh, and R. Muhamed, *Fundamentals of WiMAX: Understanding Broadband Wireless Networking*. Prentice Hall; 1 edition (March 9, 2007), 2007.
- [21] F. Wang, A. Ghosh, C. Sankaran, P. Fleming, F. Hsieh, and S. Benes, "Mobile WiMAX systems: performance and evolution," *IEEE Commun. Mag.*, vol. 46, pp. 41–49, Oct. 2008.
- [22] S. Edinger, C. Bauer, and N. Fliege, "DMT transmission in the context of industrial telecontrol applications," *Advances in Radio Science*, vol. 4, pp. 155–160, 4-9-2006.
- [23] O. Krajsa, P. Silhavy, and P. Sysel, "Filterbank modulation techniques and its utilization in adsl systems," in *IEEE 34th International Conference on Telecommunications and Signal Processing (TSP)*, Aug. 2011, pp. 514–517.
- [24] K. Yong-Hwa and L. Jong-Ho, "Comparison of passband and baseband transmission schemes for power-line communication OFDM systems," vol. 26, no. 4, pp. 2466–2475, Oct. 2011.
- [25] J. Chow, J. Tu, and J. Cioffi, "A discrete multitone transceiver system for HDSL applications," *IEEE J. Sel. Areas Commun.*, vol. 9, pp. 895–908, Aug. 1991.
- [26] A. Al-Habashna, O. Dobre, R. Venkatesan, and D. Popescu, "Second-order cyclostationarity of mobile WiMAX and LTE OFDM signals and application to spectrum awareness in cognitive radio systems," *IEEE Journal of Selected Topics in Signal Processing*, vol. 6, no. 1, pp. 26–42, Feb. 2012.
- [27] P. Siohan, C. Siclet, and N. Lacaille, "Analysis and design of OFDM/OQAM systems based on filterbank theory," *IEEE Trans. Signal Process.*, vol. 50, pp. 1170–1183, May 2002.
- [28] W. Luqing and C. Tellambura, "Cross-entropy-based sign-selection algorithms for peak-to-average power ratio reduction of OFDM systems," *IEEE Trans. Signal Process.*, vol. 56, no. 10, pp. 4990–4994, Oct. 2008.

-
- [29] G. Mandyam, "Sinusoidal transforms in OFDM systems," *IEEE Trans. Broadcast.*, vol. 50, no. 2, pp. 172–184, June 2004.
- [30] N. Beaulieu and P. Tan, "Systems and methods for OFDM transmission and reception," *USA U.S. Patent 0095267 A1*, 2008.
- [31] T. Peng and N. Beaulieu, "A comparison of DCT-Based OFDM and DFT-Based OFDM in frequency offset and fading channels," *IEEE Trans. Commun.*, vol. 54, pp. 2113–2125, 2006.
- [32] G. Feifei, C. Tao, A. Nallanathan, and C. Tellambura, "Maximum likelihood based estimation of frequency and phase offset in DCT-OFDM systems under non-circular transmissions: algorithms, analysis and comparisons," *IEEE Trans. Commun.*, vol. 56, pp. 1425–1429, Sep. 2008.
- [33] T. Peng and N. Beaulieu, "Precise bit error probability analysis of DCT-OFDM in the presence of carrier frequency offset on AWGN channels," in *IEEE Proc. Globecom Conference*, 2005.
- [34] A. Rushdi and J. Tuqan, "PAPR reduction in trigonometric-based OFDM systems," in *41st Conference Record of the Asilomar Conference on Signals, Systems and Computers (ACSSC)*, 2007, pp. 1747–1751.
- [35] N. Al-Dhahir, M. Hlaing, and S. Satish, "Optimum DCT-based multicarrier transceivers for frequency-selective channels," *IEEE Trans. Commun.*, vol. 54, no. 4, pp. 911–921, April 2006.
- [36] M. Elhadad, S. El-Dolil, and Y. Albagory, "Application of trigonometric transforms in discrete multi tone systems," in *International Conference on Computer Engineering Systems (ICCES)*, Dec. 2009, pp. 171–176.
- [37] L. Yuan-Pei and P. See-May, "BER minimized OFDM systems with channel independent precoders," *IEEE Trans. Signal Process.*, vol. 51, pp. 2369–2380, Sep. 2003.
- [38] J. Ortin, P. Garcia, F. Gutierrez, and A. Valdovinos, "Channel independent precoder for OFDM-based systems over fading channels," *IEEE Trans. Broadcast.*, vol. 55, no. 4, pp. 818–825, Dec. 2009.

-
- [39] Z. Dlugaszewski and K. Wesolowski, "WHT/OFDM-an improved OFDM transmission method for selective fading channels," in *Symposium on Communications and Vehicular Technology (SCVT)*, 2000, pp. 144–149.
- [40] A. Zolghadrasli and M. Ghamat, "PAPR reduction in OFDM system by using hadamard transform in bslm techniques," in *9th International Symposium on Signal Processing and Its Applications ISSPA*, 2007, pp. 1–4.
- [41] W. Zhendao and G. Giannakis, "Wireless multicarrier communications," *IEEE Signal Process. Mag.*, vol. 17, pp. 29–48, Oct. 2000.
- [42] Y. Hen-Geul and C. Wang, "New parallel algorithm for mitigating the frequency offset of OFDM systems," in *IEEE 60th Vehicular Technology Conference (VTC2004-Fall)*, 2004, pp. 2087–2091.
- [43] X. Hai and Y. Shiyuan, "A loosely synchronous-coded OFDM system for power-line communications in home networks," *IEEE Trans. Power Del.*, vol. 21, pp. 1912–1918, 2006.
- [44] A. Tonello, S. D'Alessandro, and L. Lampe, "Cyclic prefix design and allocation in bit-loaded OFDM over power line communication channels," *IEEE Trans. Commun.*, vol. 58, pp. 3265–3276, Jan. 2010.
- [45] A. Czylik, "Comparison between adaptive OFDM and single carrier modulation with frequency domain equalization," in *IEEE 47th Vehicular Technology Conference*, Denver, USA, June 1997, pp. 865–869.
- [46] H. Sari, G. Karam, and I. Jeanclaude, "An analysis of orthogonal frequency-division multiplexing for mobile radio applications," in *IEEE 44th Vehicular Technology Conference (VTC)*, June 1994, pp. 1635–1639.
- [47] A. Alavi, C. Tellambura, and I. Fair, "PAPR reduction of OFDM signals using partial transmit sequence: an optimal approach using sphere decoding," *IEEE Commun. Lett.*, vol. 9, pp. 982–984, Nov. 2005.
- [48] Y. Jie, C. Lei, and M. Wei, "A modified selected mapping technique to reduce the peak-to-average power ratio of OFDM signal," in *International Conference on Consumer Electronics (ICCE), digest of Technical Papers*, 2007.

-
- [49] J. Chin-Kuo, L. Syu-Siang, and S. Muh-Tian, "On the DHT-based multicarrier transceiver over multipath fading channel," in *IEEE 20th International Symposium on Personal, Indoor and Mobile Radio Communications*, 2009, pp. 1662–1666.
- [50] P. Chen, C. Jao, and M. Shiue, "A low complexity real-valued kernel DHT-based OFDM modulator/demodulator design," in *IEEE Proc. International Symposium on Circuits and Systems, Taipei*, 2009, pp. 1529–1532.
- [51] R. Merched, "On OFDM and single-carrier frequency-domain systems based on trigonometric transforms," *IEEE Signal Process. Lett.*, vol. 13, pp. 699–702, 2006.
- [52] W. Deqiang, L. Danpu, L. Fang, and Y. Guangxin, "A novel DHT-based ultra-wideband system," in *IEEE International Symposium on Communications and Information Technology (ISCIT)*, 2005, pp. 672–675.
- [53] J. Chin-Kuo, L. Syu-Siang, and S. Muh-Tian, "DHT-based OFDM system for passband transmission over frequency-selective channel," *IEEE Signal Process. Lett.*, vol. 17, pp. 182–197, 2010.
- [54] G. Mandyam, "On the discrete cosine transform and OFDM systems," in *Proc. IEEE Acoustics, Speech, and Signal Processing (ICASSP)*, vol. 4, April 2003, pp. 1–4.
- [55] M. Ahmed, S. Boussakta, B. Sharif, and C. Tsimenidis, "OFDM based on low complexity transform to increase multipath resilience and reduce PAPR," *IEEE Trans. Signal Process.*, vol. 59, no. 12, pp. 5994–6007, Dec. 2011.
- [56] L. Deneire, B. Gyselinckx, and M. Engels, "Training sequence versus cyclic prefix—a new look on single carrier communication," *IEEE Commun. Lett.*, vol. 5, pp. 292–294, July 2001.
- [57] N. Y. Hoe and C. T. Chee, "Single-carrier cyclic prefix-assisted PLC systems with frequency-domain equalization for High-Data-Rate Transmission," *IEEE Trans. Power Del.*, vol. 25, pp. 1450–1457, July 2010.

-
- [58] W. Yang, Y. Cai, and B. Zheng, "Distributed space-time-frequency coding for broadband wireless relay networks," *IEEE Trans. Veh. Technol.*, vol. 61, no. 1, pp. 15–21, Jan. 2012.
- [59] Al-Nahari, A. Seddik, K. Dessouky, M. El-Samie, and F.E.A., "Distributed space-frequency coding for cooperative diversity over broadband relay channels with DF relaying," *IEEE Trans. Veh. Technol.*, vol. 61, no.7, pp. 3266–3272, Sep. 2012.
- [60] K. Wen-Yi and M. Fitz, "Design and analysis of transmitter diversity using intentional frequency offset for wireless communications," *IEEE Trans. Veh. Technol.*, vol. 46, pp. 871–881, Nov. 1997.
- [61] D. Dao and C. Tellambura, "Optimal rotations for quasi-orthogonal STBC with two-dimensional constellations," in *IEEE Global Telecommunications Conference (GLOBECOM)*, vol. 4, Dec. 2005, pp. 1–5.
- [62] D. Senaratne and C. Tellambura, "Spatial multipath resolution with space time block codes," *IEEE Wireless Commun. Lett.*, vol. 1, pp. 249–252, Mar. 2012.
- [63] S. Alamouti, "A simple transmit diversity technique for wireless communications," *IEEE J. Sel. Areas Commun.*, vol. 16, pp. 1451–1458, Oct. 1998.
- [64] N. Al-Dhahir, "Overview and comparison of equalization schemes for space-time-coded signals with application to EDGE," *IEEE Trans. Signal Process.*, vol. 50, no. 10, pp. 2477–2488, Oct. 2002.
- [65] Y. You, W. Jeon, and J.H.Paik, "Investigation of peak-to-average power ratio in STBC-OFDM," *Electronics Letters*, vol. 39, no. 13, pp. 1010–1011, June 2003.
- [66] K. Eunseok and H. Daesik, "A robust STBC-Based transmit diversity scheme for OFDM systems over spatially transmit correlated fading channels," *IEEE Trans. Veh. Technol.*, vol. 56, pp. 984–991, Mar. 2007.
- [67] H. Suraweera and J. Armstrong, "Alamouti coded OFDM in rayleigh fast fading channels-receiver performance analysis," in *IEEE Region 10 TENCON*, 2005, pp. 1–5.

-
- [68] L. Jong-Ho and K. Seong-Cheol, "Efficient ISI cancellation for STBC-OFDM systems using successive interference cancellation," *IEEE Commun. Lett.*, vol. 10, pp. 629–631, 2006.
- [69] D. Palomar, J. Cioffi, and M. Lagunas, "Joint Tx-Rx beamforming design for multicarrier MIMO channels: a unified framework for convex optimization," *IEEE Trans. Signal Process.*, vol. 51, no. 9, pp. 2381–2401, Sep. 2003.
- [70] A. Punctihewa, V. Bhargava, and C. Despins, "Linear precoding for orthogonal space-time block coded MIMO-OFDM cognitive radio," *IEEE Trans. Commun.*, vol. 59, no. 3, pp. 767–779, Mar. 2011.
- [71] A. Scaglione, P. Stocia, S. Barbarossa, G. Giannakis, and H. Sampath, "Optimal designs for space-time linear precoders and decoders," *IEEE Trans. Signal Process.*, vol. 50, no. 5, pp. 1051–1064, May 2002.
- [72] C. Jihoon, R. Heath, and Jr., "Interpolation based unitary precoding for spatial multiplexing MIMO-OFDM with limited feedback," in *IEEE Global Telecommunications Conference (GLOBECOM)*, 2004, pp. 214–218.
- [73] F. Yu, W. Krzymien, and C. Tellambura, "Precoding for orthogonal Space-Time-Block-Coded OFDM Downlink: Mean or covariance feedback?" *IEEE Trans. Veh. Technol.*, vol. 58, no. 7, pp. 3263–3270, Sep. 2009.
- [74] X. Xiang-Gren, S. Weifeng, and L. Hui, "Filterbank precoders for blind equalization: polynomial ambiguity resistant precoders (PARP)," *IEEE Transactions on circuits and Systems I: Fundamental Theory and Applications*, vol. 48, no. 2, pp. 193–209, Feb. 2001.
- [75] C. Yuan-Hwui and P. See-May, "Unitary precoders for ST-OFDM systems using alamouti STBC," *IEEE Transactions on circuits and Systems I: Regular Papers*, vol. 55, pp. 2860–2869, 2008.
- [76] J. Tao and W. Yiyan, "An overview: Peak-to-average power ratio reduction techniques for OFDM signals," *IEEE Trans. Broadcast.*, vol. 54, pp. 257–268, June 2008.

-
- [77] E. Costa and S. Pupolin, "M-QAM-OFDM system performance in the presence of a nonlinear amplifier and phase noise," *IEEE Trans. Commun.*, vol. 50, no. 3, pp. 462–472, Mar. 2002.
- [78] I. Baig and V. Jeoti, "DCT precoded SLM technique for PAPR reduction in OFDM systems," in *Intelligent and Advanced Systems International Conference*, June 2010, pp. 1–6.
- [79] Imran Baig and Varun Jeoti, "PAPR analysis of DHT-precoded OFDM system for M-QAM," in *International Conference on Intelligent and Advanced Systems (ICIAS)*, June 2010, pp. 1–4.
- [80] X. Zhu, G. Zhu, and T. Jiang, "Reducing the peak-to-average power ratio using unitary matrix transformation," *IET in Communications*, vol. 3, pp. 161–171, Feb. 2009.
- [81] E. Al-Dalakta, A. Al-Dweik, A. Hazmi, C. Tsimendis, and B. Sharif, "Efficient BER reduction technique for nonlinear OFDM transmission using distortion prediction," *IEEE Trans. Veh. Technol.*, vol. 50, no. 5, pp. 2330–2336, June 2012.
- [82] H. A. Leftah and S. Boussakta, "Precoded DCT-OFDM system for baseband and wireless transmission: Performance analysis and evaluation," in *Wireless Telecommunications Symposium (WTS), 2012*, April 2012, pp. 1–6.
- [83] D. Hein and N. Ahmed, "On a real-time WalshHadamard/cosine transform image processor," *IEEE Trans. Electromagn. Compat.*, vol. 147, No. 1, p. 453457, Oct. 1978.
- [84] H. A. Leftah and S. Boussakta, "Efficient OFDM system based on new transform for PAPR reduction and diversity enhancement," *submitted to IEEE trans. on Communication (Manuscript ID:TCOM-TPS-11-0770)*, 15 Nov. 2011.
- [85] —, "Efficient modulation scheme for OFDM system with ZP and MMSE equalizer," in *IEEE International Conference on Communications (ICC)*, June 2013, pp. 1–5.

-
- [86] —, “Efficient coded DCT-OFDM system utilizing walsh-hadamard transform,” in *Wireless Telecommunications Symposium (WTS), 2012*, April 2012, pp. 1–5.
- [87] Y. Ma, P. So, and E. Gunawan, “Performance analysis of OFDM systems for broadband power line communications under impulsive noise and multipath effects,” *IEEE Trans. Power Del.*, vol. 20, no.2, pp. 674–682, April 2005.
- [88] Y. Ding, T. N. Davidson, Z.-Q. Luo, and K. M. Wong, “Minimum ber block precoders for zero-forcing equalization,” *IEEE Trans. Signal Process.*, vol. 9, pp. 2410–2423, Sep. 2003.
- [89] B. Muquet, W. Zhengdao, G. B. Giannakis, M. de Courville, and P. Duhamel, “Cyclic prefixing or zero padding for wireless multicarrier transmissions?” *IEEE Trans. Commun.*, vol. 50, pp. 2136–2148, Dec. 2002.
- [90] P. Tan and N. Beaulieu, “An improved DCT-based OFDM data transmission scheme,” in *IEEE 16th International Symposium on Personal, Indoor and Mobile Radio Communications (PIMRC)*, Vol 2 2005, pp. 745–749.
- [91] D. Yanwu, T. Davidson, L. Zhi-Quan, and W. K. Max, “Minimum BER block precoders for zero-forcing equalization,” *IEEE Trans. Signal Process.*, vol. 51, no. May, pp. 2410–2423, 2008.
- [92] J. Proakis and M. Salehi, *Digital Communications*. McGraw-Hill Companies, Inc, 1221 Avenue of the Americas, New York, 2008.
- [93] G. E. Bottomley, *Channel equalization for wireless communications: from concepts to detailed mathematics*. A John Wiley and sons, Inc., publication, 2011.
- [94] van de Beek, J.J, M. Sandell, and P. Borjesson, “ML estimation of time and frequency offset in OFDM systems,” *IEEE Trans. Signal Process.*, vol. 45, no. 7, pp. 1800–1805, July 1997.
- [95] U. Tureli, P. Honan, and L. Hui, “Low-complexity nonlinear least squares carrier offset estimator for OFDM: identifiability, diversity and performance,” *IEEE Trans. Signal Process.*, vol. 52, no. 9, pp. 2441–2452, Sep. 2004.

-
- [96] Y. Tanabe, Y. Egashira, and K. Sato, "A novel IQ imbalance estimation scheme using transient local frequency for OFDM systems," in *IEEE 18th International Symposium on Personal, Indoor and Mobile Radio Communications (PIMRC)*, Sep. 2007, pp. 1–5.
- [97] C. Yang-Seok, P. Voltz, and F. Cassara, "On channel estimation and detection for multicarrier signals in fast and selective rayleigh fading channels," *IEEE Trans. Commun.*, vol. 49, pp. 1375–1387, Aug. 2001.
- [98] M. Sharif and B. Hassibi, "On multicarrier signals where the PMEPR of a random codeword is asymptotically logn," *IEEE Trans. Inf. Theory*, vol. 50, pp. 895–903, May, 2004.
- [99] S. Litsyn and G. Wunder, "Generalized bounds on the crest-factor distribution of OFDM signals with applications to code design," *IEEE Trans. Inf. Theory*, vol. 52, pp. 992–1006, Mar. 2006.
- [100] M. Morelli and U. Mengali, "An improved frequency offset estimator for OFDM applications," *IEEE Commun. Lett.*, vol. 3, no. 3, pp. 75–77, Mar. 1999.
- [101] V. Britanak, P. Yip, and K. Rao, *Discrete cosine and sine transforms: General properties, fast algorithms and integer approximations*. Amsterdam: Academic, 2007.
- [102] S. Sun, C. Hou, L. Yan, and J. Fu, "A novel method based DCT to reduce PAPR of OFDM systems," in *IEEE 4th Wireless Communications, Networking and Mobile Computing International Conference (WiCOM)*, Oct. 2008, pp. 1–5.
- [103] P. Banelli and S. Cacopardi, "Theoretical analysis and performance of OFDM signals in nonlinear AWGN channels," *IEEE Trans. Commun.*, vol. 48, no. 3, pp. 430–441, Mar. 2000.